Vol. 135 No. 1, February 1, 1982 ISSN 0003-2670

ANALYTICA CHIMICA ACTA

International journal devoted to all branches of analytical chemistry

ELSEVIER SCIENTIFIC PUBLISHING COMPANY

ANALYTICA CHIMICA ACTA

International journal devoted to all branches of analytical chemistry
Revue internationale consacrée à tous les domaines de la chimie analytique
Internationale Zeitschrift für alle Gebiete der analytischen Chemie

PUBLICATION SCHEDULE FOR 1982

	J	F	M	A	M	J	J	A	S	O	N	D
Analytica Chimica Acta	134	135/1	135/2	136	137	138	139	140	141	142	143	144

Scope. *Analytica Chimica Acta* publishes original papers, short communications, and reviews dealing with every aspect of modern chemical analysis, both fundamental and applied.

Submission of Papers. Manuscripts (three copies) should be submitted as designated below for rapid and efficient handling:

Papers from the Americas to: Professor Harry L. Pardue, Department of Chemistry, Purdue University, West Lafayette, IN 47907, U.S.A.

Papers from all other countries to: Dr. A. M. G. Macdonald, Department of Chemistry, The University, P.O. Box 363, Birmingham B15 2TT, England. Papers dealing particularly with computer techniques to: Professor J. T. Clerc, Universität Bern, Pharmazeutisches Institut, Sahlistrasse 10, CH-3012 Bern, Switzerland.

Submission of an article is understood to imply that the article is original and unpublished and is not being considered for publication elsewhere. Upon acceptance of an article by the journal, authors resident in the U.S.A. will be asked to transfer the copyright of the article to the publisher. This transfer will ensure the widest dissemination of information under the U.S. Copyright Law.

Information for Authors. Papers in English, French and German are published. There are no page charges. Manuscripts should conform in layout and style to the papers published in this Volume. Authors should consult Vol. 132, p. 239 for detailed information. Reprints of this information are available from the Editors or from: Elsevier Editorial Services Ltd., Mayfield House, 256 Banbury Road, Oxford OX2 7DH (Great Britain).

Reprints. Fifty reprints will be supplied free of charge. Additional reprints (minimum 100) can be ordered. An order form containing price quotations will be sent to the authors together with the proofs of their article.

Advertisements. Advertisement rates are available from the publisher.

Subscriptions. Subscriptions should be sent to: Elsevier Scientific Publishing Company, P.O. Box 211, 1000 AE Amsterdam, The Netherlands.

Publication. *Analytica Chimica Acta* appears in 11 volumes in 1982. The subscription for 1982 (Vols. 134–144) is Dfl. 1815.00 plus Dfl. 220.000 (postage) (total approx. U.S. $814.00). Journals are sent automatically by airmail to the U.S.A. and Canada at no extra cost and to Japan, Australia and New Zealand for a small additional postal charge. All earlier volumes (Vols. 1–133) except Vols. 23 and 28 are available at Dfl. 164.00 (U.S. $66.00), plus Dfl. 13.00 (U.S. $5.20) postage and handling, per volume.

Claims for issues not received should be made within three months of publication of the issue, otherwise they cannot be honoured free of charge.

Customers in the U.S.A. and Canada who wish to obtain additional bibliographic information on this and other Elsevier journals should contact Elsevier/North Holland Inc., Journal Information Center, 52 Vanderbilt Avenue, New York, NY 10017. Tel: (212) 867-9040.

FOUR NEW BOOKS

Electron Capture – Theory and Practice in Chromatography

edited by A. ZLATKIS, *Houston, TX, USA, and* C. F. POOLE, *Detroit, MI, USA*

JOURNAL OF CHROMATOGRAPHY LIBRARY – Volume 20

This comprehensive coverage of all aspects of the theory, design, operation and applications of the electron-capture detector in chromatography contains solutions to instrumental and technical problems which can arise during practice. It includes an extensive tabulation of all pertinent data concerning the use of this technique in gas and liquid chromatography. Each chapter has been prepared by experts in their fields and contains in-depth coverage of its topic.

Sept. 1981 viii + 376 pages
Price: US $76.50/Dfl. 180.00
ISBN 0-444-41954-3

Affinity Chromatography and Related Techniques

edited by T. C. J. GRIBNAU, *Oss,* J. VISSER, *Wageningen, and* R. J. F. NIVARD, *Nijmegen, The Netherlands*

ANALYTICAL CHEMISTRY SYMPOSIA SERIES – Volume 9

The 45 papers in this Proceedings volume cover the theoretical aspects of affinity chromatography, review the preparation and properties of polymeric matrices and methods for ligand immobilization, and illustrate the increasing importance of affinity techniques in industrial and biomedical/diagnostic applications. A wide variety of the applications of organic dyes are included, as well as information on the application of affinity techniques in high-performance liquid chromatography.

Nov. 1981 xviii + 584 pages
Price: US $83.00/Dfl. 195.00
ISBN 0-444-42031-2

Drugs of Abuse

by L. FISHBEIN, *Jefferson, AR, USA*

CHROMATOGRAPHY OF ENVIRONMENTAL HAZARDS 4

This is both a practical text and a literature reference source for chromatographic procedures used in the separation, detection and quantification of a spectrum of commonly abused drugs from biological, licit and illicit samples. These procedures are primarily useful in therapeutic monitoring, pharmacokinetic studies, emergency, clinical, forensic and toxicological analyses, and monitoring in drug abuse screening programs. It is the final volume in this series which also covers carcinogens, mutagens and teratogens, metals, gaseous and industrial pollutants, and pesticides.

Oct. 1981 x + 490 pages
Price: US $95.75/Dfl. 225.00
ISBN 0-444-42024-X

Mass Spectrometry in Biochemistry, Medicine and Environmental Research, 7

Proceedings of the 7th International Symposium on Mass Spectrometry in Biochemistry, Medicine and Environmental Research, Milan, Italy, 16-18 June 1980

edited by A. FRIGERIO, *Milan, Italy*

ANALYTICAL CHEMISTRY SYMPOSIA SERIES – Volume 7

The main topics covered in the 32 papers presented at this symposium are the applications of mass spectrometric techniques in drug metabolism, metabolism of other substances, the identification and/or quantitation of endogenous compounds, studies involving respiratory gases, and environmental studies. Advances in methodology are also included.

Oct. 1981 x + 360 pages
Price: US $72.50/Dfl. 170.00
ISBN 0-444-42029-0

Order from your bookseller or directly from

ELSEVIER SCIENTIFIC PUBLISHING COMPANY
P.O. Box 211,
1000 AE Amsterdam,
The Netherlands

ELSEVIER
NORTH-HOLLAND INC.
52 Vanderbilt Ave.,
New York, NY 10017

Prepaid orders are supplied postfree.

The Dutch guilder price is definitive. US $ prices are subject to exchange rate fluctuations.

Electrodes of Conductive Metal Oxides

edited by SERGIO TRASATTI, *Laboratory of Electrochemistry, University of Milan, Italy.*

STUDIES IN PHYSICAL AND THEORETICAL CHEMISTRY 11.

This two-part work provides a general unifying introduction plus a state-of-the-art review of the physicochemical properties and electrochemical behaviour of conductive oxide electrodes (DSA). The text has been divided into two volumes – Part A dealing mainly with structural and thermodynamic properties and Part B dealing with kinetic and electrocatalytic aspects. This division came about due to the large amount of material to be treated and also because, in a rapidly developing field, difficulties arise in collecting all relevant material at one given moment.

The editor approaches the subject from a multidisciplinary angle, for example, the electrochemical behaviour of oxide electrodes is presented and discussed in the context of a variety of physicochemical properties – electronic structure, nonstoichiometry, crystal structure, surface structure, morphology and adsorption properties. For the first time the different groups of oxides are treated together in order to emphasise their similarities and differences.

This major reference work is mainly directed to electrochemists and those working on catalysis. It will also be useful to those in the fields of materials science, physical chemistry, surface and colloid chemistry and in areas where oxide surfaces may play a major role as in chromatography and photochemistry.

CONTENTS: Chapters. 1. Electronic Band Structure of Oxides with Metallic or Semiconducting Characteristics *(J. M. Honig)*. 2. Chemisorption and Catalysis on Metal Oxides *(A. Cimino and S. Carrà)*. 3. Oxide Growth and Oxygen Evolution on Noble Metals *(L. D. Burke)*. 4. Electrochemistry of Lead Dioxide *(J. P. Pohl and H. Rickert)*. 5. Properties of Spinel-Type Oxide Electrodes *(M. R. Tarasevich and B. N. Efremov)*. 6. Physicochemical and Electrochemical Properties of Perovskite Oxides *(H. Tamura, Y. Yoneyama and Y. Matsumoto)*. 7. Properties of Conductive Transition Metal Oxides with Rutile-Type Structure *(S. Trasatti and G. Lodi)*. 8. Fundamental Properties of the Oxide/Aqueous Solution Interface *(D. N. Furlong, D. E. Yates and T. W. Healy)*. 9. Reactions of Hydrogen and Organic Substances with and at Anodic Oxide Films at Electrodes *(B. E. Conway)*. 10. Oxygen and Chlorine Evolution at Conductive Metallic Oxide Anodes *(S. Trasatti and G. Lodi)*. 11. Technological Impact of Metallic Oxides as Anodes *(A. Nidola)*.

Part A:
1980 xvi + 366 pages.
US $72.25/Dfl. 170.00.
ISBN 0-444-41912-8.

Part B:
1981 xiv + 336 pages.
US $72.25/Dfl. 170.00.
ISBN 0-444-41988-8.

ELSEVIER

P.O. Box 211
1000 AE Amsterdam
The Netherlands

52 Vanderbilt Avenue,
New York, N.Y. 10017

The Dutch guilder price is definitive. US $ prices are subject to exchange rate fluctuations.

ANALYTICA CHIMICA ACTA
VOL. 135 (1982)

ANALYTICA CHIMICA ACTA

International journal devoted to all branches of analytical chemistry

ELSEVIER SCIENTIFIC PUBLISHING COMPANY

Analytica Chimica Acta, 135 (1982) 1
Elsevier Scientific Publishing Company, Amsterdam — Printed in The Netherlands

Guest Editorial

TRIPLE A

Every skilful analyst likes his chauffeur to polish his AAA (American Automobile Association) on the front of his RR (Rolls Royce). At the recent Euroanalysis IV conference, I gave a plenary lecture on AAA (Arctic Automatic Analysis). In introducing my talk, Professor Osmo Mäkitie was tempted to state that he thought I was going to speak about AAA (Anti-Alcohol Analysis); he resisted this temptation. In the 6th edition of "Acronyms, Initialisms & Abbreviations Dictionary" there are listed 50 meanings of triple A. Every analyst who knows something about computerization likes to show off by speaking about his IC's (Integrated circuits) and his "I triple E four double eight bus", knowing for sure that his less learned colleagues are unaware that IEEE stands for Institute of Electrical and Electronic Engineers and that the 488 bus is a GPIB (general-purpose interface bus that stops neither at Waterloo nor at Grand Central). In articles on the hydration of silicon dioxide, SiO_2 and $Si(OH)_4$ are normally used, but if the i is dropped (SO_2) or exchanged for an e (SeO_2) upon typesetting, the reader most likely gets very confused.

English is preferred among abbreviators or acronymphs. For Scandinavians who, for example, use f instead of ph, this sometimes causes moments of confusion. TBP is well known to all solvent extraction chemists and you can extract uranium with the aid of TBP (tributylphosphate) and cesium with TPB (tetraphenylborate, where it is found under TPB in the book on Acronyms, loc. cit.). For non-chemists TBP means to be provided, and for lovers TBP is no two-body problem. Likewise PTO stands for please turn over and PTA for Parents Teachers Association and not for any oxide or acid containing phosphorus, phenyl, pyridine, poly, tri or tetra something or thiol. Recently I attended a meeting where the speakers used either PAH (polyaromatic hydrocarbons) or PNA (polynuclear aromatics), but were speaking about the same compounds. The NPD ratio (naphthalene/phenanthrene/dibenzothiophene) was then important to the environment.

If the purpose of your talk or paper is to communicate with other scientists with different training and language backgrounds, different priorities and different sets of initialisms and similar condensed appellations, then you should be careful with your acronyms. They may have an entirely different meaning for your listeners or readers or no meaning at all. ACA has over 70 meanings. Look on your ticket to Acapulco or on your automatic clinical analyzer, but for many of us it only means our dear international journal devoted to all branches of analytical chemistry.

David Dyrssen

Analytica Chimica Acta, 135 (1982) 3—49
Elsevier Scientific Publishing Company, Amsterdam — Printed in The Netherlands

Special Report

PHYSICS AND CHEMISTRY OF THE SHROUD OF TURIN
A Summary of the 1978 Investigation[a]

L. A. SCHWALBE* and R. N. ROGERS

Los Alamos National Laboratory, P.O. Box 1663; Mail Stop 912, Los Alamos, NM 87545 (U.S.A.)

(Received 3rd August 1981)

SUMMARY

This report reviews and correlates results obtained from tests conducted on the Shroud of Turin during the October 1978 investigation. Several image formation hypotheses are addressed. Although no single theory adequately accounts for all of the observations, it is concluded that the image is the result of some cellulose oxidation—dehydration reaction rather than an applied pigment. The application or transfer mechanism of the image onto the cloth is still not known. Because many proposed mechanisms of image formation strongly depend upon historical considerations, a determination of the age of the Shroud by radiocarbon dating is necessary for further hypothesis testing. Available data from the "blood" areas are considered and the results show these to be blood stains.

The Shroud of Turin, believed by many to be the burial cloth of Jesus, has generated considerable controversy, but unlike some other controversial subjects (e.g. flying saucers and ghosts), the Shroud exists as a material object. It can be observed directly and objectively. The results of studies can be analyzed by scientific methods.

The 1898 photographs by Secondo Pia stirred initial scientific interest in the Shroud. These and subsequent studies prior to 1978 are described in both popular [1—4] and technical accounts [5, 6]. The most recent observations were initiated during a five-day examination in October 1978 by the Shroud of Turin Research Project [7], two members associated with the International Center of Sindonology (Shroud studies) in Turin, and three other investigators. The description and results of the tests conducted at that time have appeared in separate publications [8—14]. The purpose here is to present as comprehensively as possible our current understanding and interpretation of available data.

Two views of the 4.3 × 1.1-m linen cloth are shown in Figs. 1 and 2. The most significant aspect of the Shroud is the visible frontal and dorsal image on the fabric surface. The greater part of this discussion is, therefore, given

[a]Further information available from: The Shroud of Turin Research Project, P.O. Box 7, Amston, CT 06231, U.S.A.

0003-2670/82/0000-0000/$11.75

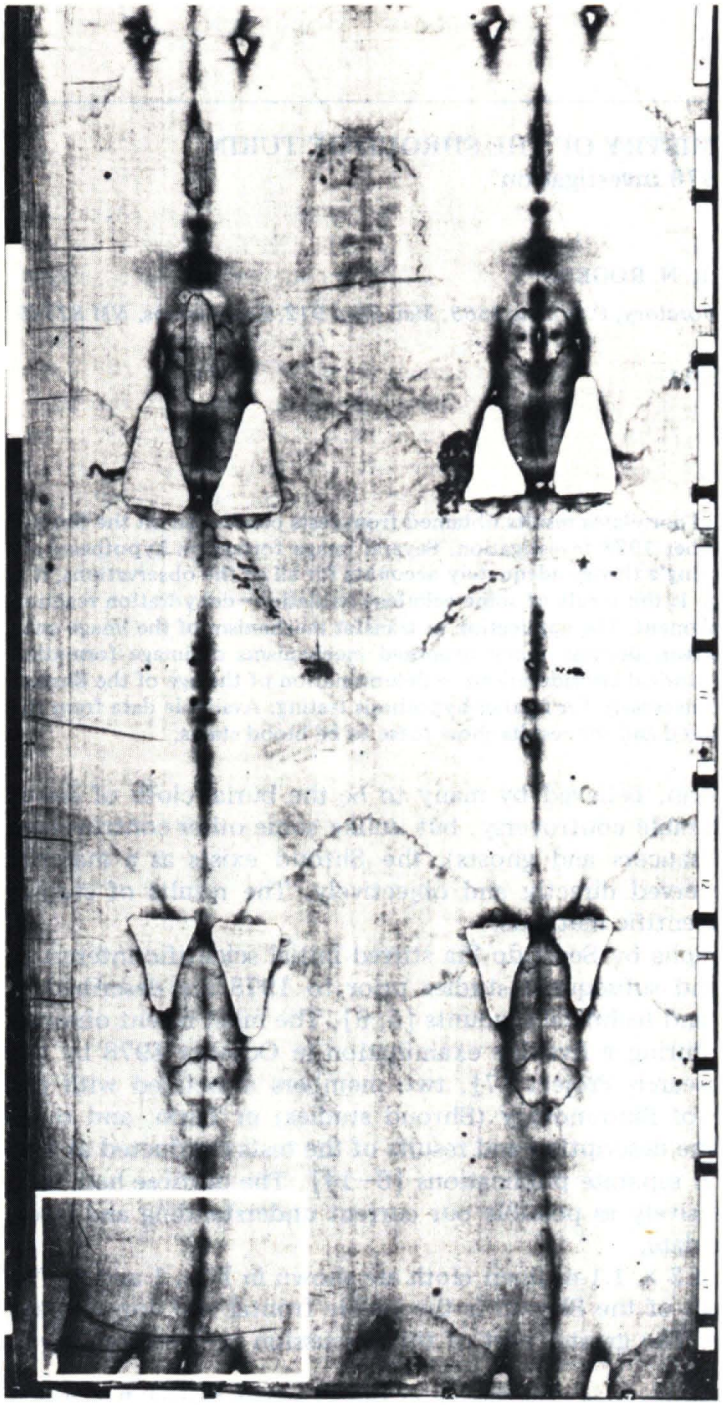

Fig. 1. Photograph of the Shroud area containing the full frontal image. A radiograph of the region indicated at the bottom of the figure is presented in Fig. 7.

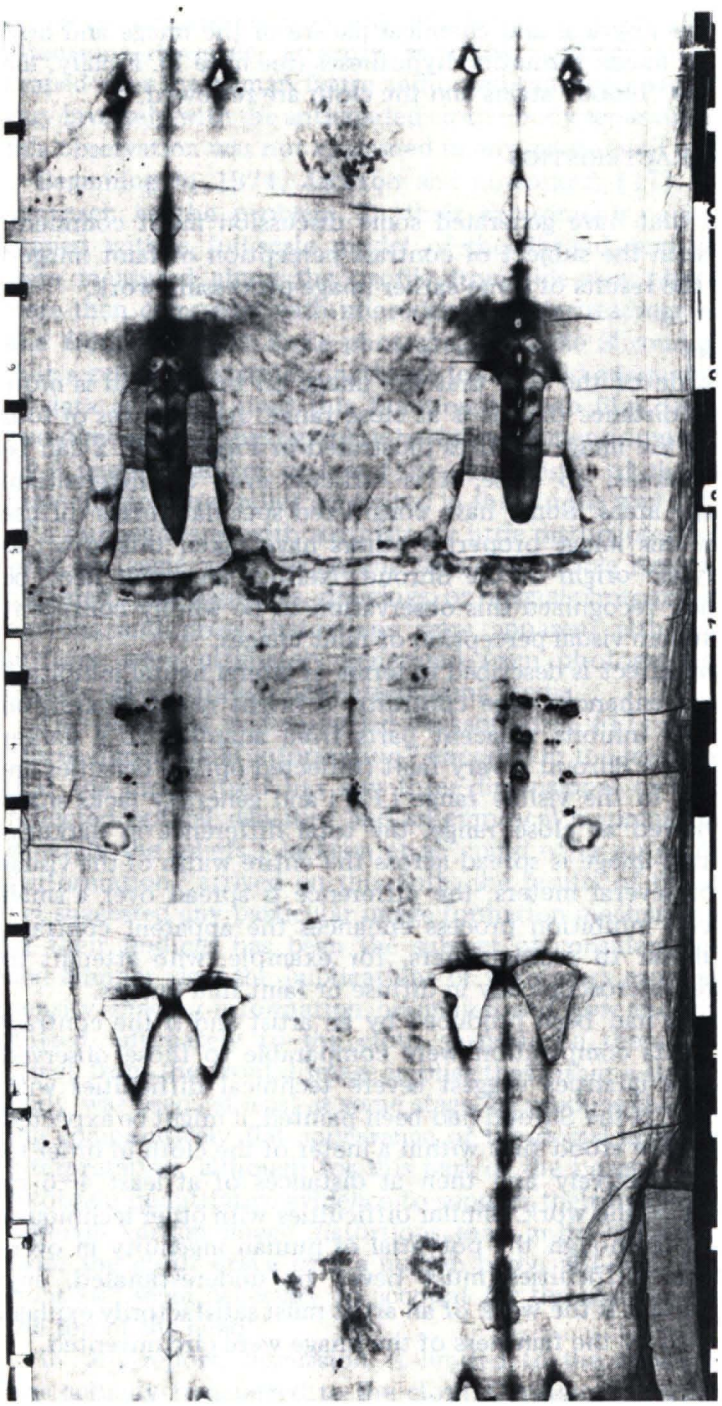

Fig. 2. Photograph of the Shroud area containing the full dorsal image.

to observations of the physical and chemical nature of the image and how these relate to various image formation hypotheses (see note 1). Finally, the data obtained from the "blood" stains and the cloth are reviewed.

GENERAL IMAGE CHARACTERISTICS

Two observations that have generated some discussion merit comment. The first has to do with the subject of contrast perception of faint images; the second concerns the results of some earlier image-processing work.

Faint image properties

Much has been made of the fact that the image on the Shroud is more readily perceived at a distance than it is at close range. At distances of four to five meters, all of the image features illustrated in Figs. 1 and 2 can be easily recognized; whereas, up close, it is difficult even to differentiate image from non-image areas. Some have considered specular versus diffuse reflection to explain this image property; others have taken this effect as evidence for the mystic origin of the Shroud. Neither argument need be invoked. D. H. Janney recognized this observation to be wholly consistent with the process of human visual perception of faint images.

Physiologically, the effect is described in terms of lateral neural inhibition [15]. The human eye enhances edge contrasts. A bright region imaged on one part of the retina inhibits adjacent parts from adapting to a darker region. The image on the Shroud is very faint (reflected optical densities are typically less than 0.1 in the visible range [12]) and generally lacks sharp boundaries. When viewed at close range, the total difference in darkness between image and non-image is spread across the entire width of the visual field. At distances of several meters, the difference is spread over a small region, and the lateral inhibition process enhances the apparent contrast. Such effects are familiar to radiographers, for example, who attempt to examine small features microscopically in diffuse or faint film images.

If the Shroud image had been produced by an artist and if the contrast values at the time of its composition were comparable to those observed today, the faint image qualities suggest severe technical difficulties with execution. For example, if the Shroud had been painted, it might be expected that the artist would have stood first within a meter of the cloth in order to control the medium effectively and then at distances of at least 4—5 m to observe the progress of the work. Similar difficulties with other techniques can also be envisaged. Although the potential of human ingenuity in overcoming such technical difficulties must never be underestimated, any hypothesis that the Shroud is the work of an artist must satisfactorily explain how the problems posed by the faintness of the image were circumvented.

Density shading and color properties

The density shading properties of the image have been a subject of scientific interest for over 80 years. During this time, the apparent negative image

characteristics, revealed in the 1898 Pia photographs, have received the most attention. However, as early as 1902, Vignon [16] imagined the cloth draped over the human figure and noted that the image densities appeared to vary inversely with the anticipated cloth—body separations. To our knowledge, this observation was not examined in any great detail until much later.

Beginning in 1974, Jackson and coworkers [17] took a more analytic approach to the problem. In their experiments, a human volunteer was draped with a full-scale model of the Shroud, and cloth—body distances were measured along the profile from side-view photographs. The results were then compared with microdensitometer readings along a corresponding line from the 1931 Enrie photographs of the Shroud. Jackson et al. found that a relatively simple functional form could adequately relate the two sets of data and then used this function to map film densities from the entire two-dimensional photograph into a three-dimensional surface with a modified VP-8 image analyzer system [18]. The result of the exercise was that the three-dimensional relief generated in this simple way strongly resembled that of a human figure with surprisingly little distortion. They further illustrated with the same video technique that comparable results were not ordinarily obtained from paintings, drawings, or normal photographs. In almost all cases, obvious and gross distortions were apparent although satisfactory relief surfaces were ultimately generated from photographs of phosphorescent objects taken through light-attenuating media.

The results of this study led Jackson et al. [17] to conclude that there is "three-dimensional information" encoded in the image. (This is not to imply that the image itself has any three-dimensional or layered structure; only reflected optical densities and an empirical mapping function were used to generate the reliefs.) Jackson et al. could offer no explanation for how this "information" arrived on the cloth; the results of this experiment have not yet suggested any particular image formation mechanism. Yet the significance of their findings has been the subject of considerable discussion. Jackson and Jumper view the implications of their work more in terms of where this density shading information originated and how the information was transmitted, ultimately to the cloth surface. To them, the three-dimensional effect from the frontal image implies that either a statue or an actual human body was used, at least at some stage, to produce the image. They argue that the comparatively flat appearance of the dorsal image is consistent with this interpretation, although for this part of the image, it is much more difficult to obtain quantitative evidence to support their hypothesis. Jackson similarly observes certain image distortions that, in his opinion, might have resulted from the cloth drape over a human body, although certain special assumptions still seem necessary to account for the absence of the "imprint" from the top of the head.

In this report, discussion is limited to the question of how the image was actually transferred to the cloth. Considerations of the image resolution and the density shading characteristics bear on this discussion only insofar as

they examine various physical processes and their potentials for generating or preserving these characteristics. In this context, the VP-8 results do not prove that a three-dimensional object was used directly in the image formation process. That is, it may still be appropriate to consider image transfer mechanisms from flat models (paintings, etchings, or shallow bas reliefs, for example) which themselves may contain the information that gave rise to the contour shading properties of the image. For this discussion, the most significant result of the VP-8 study is the apparent global consistency of the three-dimensional reconstruction. To us, this implies the existence of a simple function that maps Shroud image densities to cloth—body distances in a global sense. This is potentially important because it would establish a condition that must be satisfied by any seriously considered image transfer mechanism.

LaRue [19] has expressed caution concerning the use of the Enrie photographs for further three-dimensional studies. The 1969 photographs of Judica Cordiglia [20] show that Enrie's use of orthochromatic emulsions introduced tonal distortions especially for the reds that might critically affect results. These difficulties have now been overcome. The work by Judica Cordiglia and the more recent high-resolution photographs by Miller were taken and developed under controlled and recorded conditions. The latter include panchromatic and multispectral narrow-band mosaics at 5.6:1 and 22:1 reductions of the entire cloth surface. For the multispectral photography, Miller used a liquid filter to isolate the 335—375-nm ultraviolet band and a subtractive set of filters: B (370—500 nm), G (500—575 nm), and R (585—750 nm) for the visible range.

Preliminary VP-8 analyses of these latest photographs have shown results that are quite similar to those obtained from the original studies; the frontal images yield rather impressive three-dimensional relief figures whereas the dorsal images remain comparatively flat in appearance. The effect, therefore, does not seem to arise from some peculiarity of the Enrie photographs but appears to be a genuine property of the image. Jackson and Jumper are presently continuing work with the 1978 photographs to establish more accurate limits for the mapping function. Considerable uncertainty exists in the analytic form of their original function because it was chosen somewhat arbitrarily to represent the relatively imprecise correlation of data over a limited region. Further refinements are constrained somewhat by the resolution of the image, but most severely by the assumed cloth drape and the expected uncertainties in the detailed appearance of the reconstructed three-dimensional model [21]. Nevertheless, it is useful to define the mapping function as accurately as possible for comparison with predictions from image-transfer models and empirical results.

Preliminary studies of other aspects of the image analysis problem have also been reported [22—25]; yet an abundance of work remains to be done in this area. For example, film density differences or ratios among the multispectral photographs at all locations could provide further information about

spatially-dependent color variations. Thus far, only limited image analysis work has been done with the 1978 photographs.

HYPOTHESES ON BODY-IMAGE FORMATION

The image on the Shroud is most intriguing because it is not immediately obvious how it was produced. The primary goal of the 1978 investigation was to apply a series of nondestructive tests to determine the physical and chemical characteristics of the image more exactly. Various hypotheses about the image formation can now be tested with these data. Unfortunately, the years of controversy have generated a large number of arguments about how the image may have been formed. Each of these hypotheses cannot be tested individually, but the discussion in this section has been organized, according to Fig. 3, to consider rather broad categories.

In most cases, the available data are insufficient to allow individual hypotheses or entire categories to be discarded, but these deficiencies serve to direct efforts in continuing research. It is emphasized that this article is a status report, and specific problems are mentioned as they arise. Interest from specialists in areas (art history and techniques, textiles, etc.) outside our range of technical expertise is encouraged.

Hypothesis: The image is an artifact

When first introduced to the subject of the Shroud, many suspect that the image was produced by human skill and ingenuity. Indeed the hypothesis

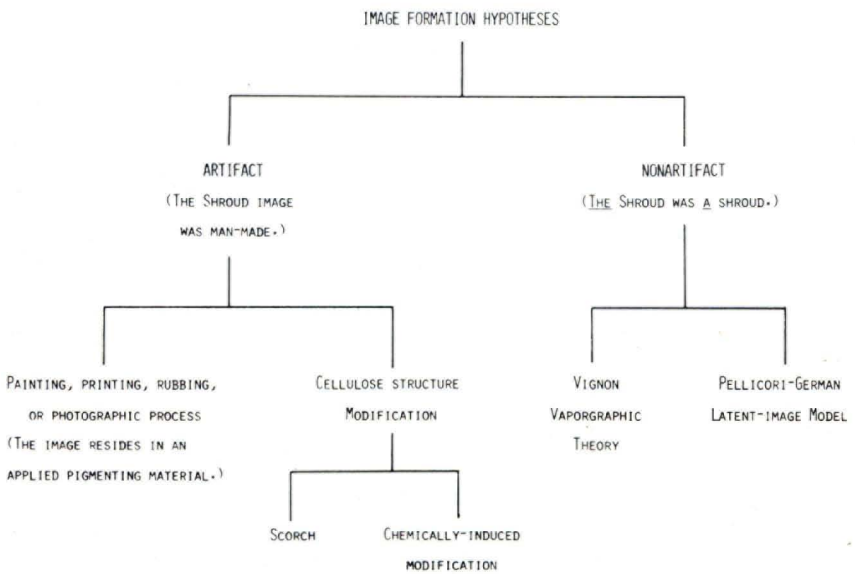

Fig. 3. Schematic representation of the logical structure of the section dealing with hypotheses on image formation.

that the image is a medieval artifact is at least 600 years old. A letter [26] written in 1389 by Pierre d'Arcis, Bishop of Troyes, refers to an investigation by his predecessor that allegedly exposed the artist who had painted it. The controversy was revitalized in this century when Chevalier [27] based his own opinion on this historical evidence.

Unfortunately, the materials and painting method were not specified in the bishop's statement, leaving us with an open-ended problem. We are left to consider all possible materials and methods that could have been used to produce an image on cloth through human skill or cunning. This situation results in the fact that elimination of all known methods does not prove that a clever artist or hoaxer did not use a method currently unknown. However, the elimination of historically known (and unknown but technologically feasible) methods would make image production by willful human action appear less probable. If the Shroud image is an artifact, few presuppositions about the time and place of its origin can be held. It could have been produced in Europe during the 14th century or somewhere else before that time; even remote possibilities cannot be discounted [28, 29] (see note 2). In any case, it is reasonable to suppose that if an artist produced the image, it would have been necessary to have either added a colored material to the cloth or changed the composition of the cloth to produce a color. Different observations are required to test these two corollaries.

Corollary: The image is an applied pigment

If the image were produced by painting (using the normal dictionary definition), block printing [29], transfer-rubbing over a bas relief [30, 31], spray painting, or some unreported photographic-like process [32], a foreign material would have been added to the cloth. The foreign material would cause changes in relative density, chemical composition, spectral reflectance characteristics, mechanical properties, and/or microstructure.

Within the limitations imposed by time, expense, and damage to the Shroud, tests and observations that have been made include (1) direct microscopic observations and photomicrographs [8], (2) x-ray fluorescence spectrometry [9] to observe discontinuities in elemental composition, (3) low-energy x-radiography [10] to observe areal density discontinuities, (4) infrared, visible, and ultraviolet reflectance spectra [11—13], (5) photoelectric [12] and photographic [14] fluorescence, (6) direct macroscopic visual observations and photographic images in different, known wavelength regions, and (7) thermal emission images [11] in different wavelength regions. Visible transmission, side-lit, and glancing-angle photographs of the Shroud were also taken. Riggi examined vacuumed material from the cloth and its repository by electron microscopy and microprobe. Finally, surface-transfer samples were taken on specially prepared, pure hydrocarbon adhesive tape for later microscopic and chemical examination and various microchemical and instrumental techniques.

Microscopy

The most important observations for testing the painting hypothesis are those made by direct microscopy. The Shroud threads (nominally 0.15 mm in diameter [10]) are composed of linen fibers of 10—15 μm diameter. What the eye sees as the image is caused by a discontinuous translucent-yellow discoloration of these fibers. In pure image areas, the colored fibers appear only on the topmost segments of the threads [33], and coloration extends only 2 or 3 fibers deep into the thread structure.

The image has a half-tone quality; its density or darkness is determined by the number of colored fibers per unit area. The hue of discolored fibers is the same on light and dark density areas. The front and rear images of the body show the same distribution of fiber coloration and maximum image densities [33]. Color does not penetrate the cloth in any image area [33] (see note 3) nor is there any evidence for cementation between fibers or capillary flow of liquids. Fibers from the image area have a "frosty" appearance; that is, their surfaces show a more diffuse light reflectance than do the non-image fibers. No pigment particles can be resolved at 50X magnification in image areas. The image does not look like a painting by direct microscopic examination.

In 1973, Frei [34] used sticky tape to remove samples of surface debris for subsequent pollen studies. The same technique was also used in 1978 by Rogers and Dinegar who took and documented a total of 32 samples from the Shroud image, "blood" stain, scorch, water stain, and background areas. The tape samples, each about 5 cm^2 in area, were applied with a specially designed roller and then carefully pulled from the cloth surface. Rogers noted immediately that the sticky tape surfaces retained a wide diversity of materials but that the amounts of material varied from sample to sample and in some cases appeared to depend upon the thread lot associated with the sampled area. He also observed that the image-area tapes "lifted" more easily than non-image tapes suggesting that the topmost fibers in the image area were somehow weakened.

Later, McCrone and Skirius [35], McCrone [36], and Heller and Adler [37] examined the tapes by light microscopy. Heller and Adler documented and classified the observed materials into two general categories. The first included "occasional" materials such as insect parts, pollen (see note 4), wax, wool, red silk, and modern synthetic fibers. The second category included the more consistently occurring materials: linen fibrils (or fiber fragments) and several types of red and less frequent black particles.

McCrone and Skirius [35], who first examined the samples, found two types of linen fibrils present, some clear and others uniformly colored yellow to faint yellow. Their study showed that significantly greater ratios of yellow to clear fibrils were present on the tapes from the image area than on those from the non-image areas. The yellow fibrils are considered to be the most important direct observations of the Shroud and subsequent photomicroscopic examinations indicate that they represent the dominant and probably sole visible image element.

In addition, McCrone and Skirius reported that eighteen of the tapes showed significant amounts of submicrometer-sized red particles which they identified as Fe_2O_3 of varying degrees of hydration. According to their report, most of the particles appeared to be "well dispersed" and, of these, the majority were intimately associated with the linen fibril surfaces. Smaller quantities of the particles were seen to be clustered and perhaps bound into larger (20—30 μm diameter) aggregates especially in the "blood" area samples. In a further examination, the tapes were separated into two groups depending on the microscopically observed presence or absence of red particles but without prior knowledge of the sample location on the Shroud. The results showed that none of the control samples (those with no image) contained red particles whereas all the samples from the "blood" area and two-thirds of the samples from the body-image area showed significant amounts of the material. They concluded that a direct correlation exists between Fe_2O_3 particle concentrations and the image areas and postulated that this material may have been used to enhance the image contrast. The well-dispersed particle distribution suggested to them that the "red pigment" may have been applied as a very dilute particle—liquid suspension. In particular, they state that the fiber discoloration may have resulted from a paint medium that had yellowed with age.

The postulated identification of fiber discoloration with a pigment vehicle offers an hypothesis that can be tested. There are several media that could have been used by a medieval painter. Thompson [38] lists glair (egg white), size (animal collagen or gelatin and fish glue), and plant gums (arabic, tragacanth) as several commonly used pigment vehicles in the 14th century. These vehicles were taken separately or in combinations depending on the particular application. Honey, sugar, egg yolk, and even ear wax were occasionally added to obtain certain desired effects. Drying oils such as linseed, hempseed, walnut, and possibly poppyseed were known and used in painting although the extent of their application has been debated. Gettens and Stout [39] suggest casein, starch, and waxes as further but less likely possibilities. Although, once again, the possibility remains that some other vehicle was employed, there is no evidence to support the contention that any of the above media produced the yellow fiber discoloration.

One general problem has to do with the observed fibril structure. Linen fibers consist of plant cells joined end-to-end. Microscopically they have a bamboo-like appearance; the joints are seen as well-defined circumferential structures. Our observations of both clear and colored fibrils from a pure-image area showed no obvious evidence for a coating of paint medium. The growth joints are clear and sharp with no evident meniscus marks. (Phase microscopic examinations [37] of fibrils from a pure-image area also showed well-defined surface erosion features which, we believe, give rise to the general "frosty" appearance of the image fibers in the photomicrographs.) It could be supposed that a sufficiently non-viscous or diluted tempera vehicle was used; however, it is then difficult to explain the absence of either

discoloration or liquid capillary flow into the deeper portions of the threads without, at the same time, postulating some unusual mechanism of application.

Even if this possibility is accepted, there is another problem that has to do with the chemical nature of the discoloration. Heller and Adler [37] applied a series of microchemical tests to the various types of fibrils. Among these were several protein tests including the biuret/Lowry, coomassie blue, bromothymol blue, amido black, bromocresol green and fluorescamine tests and various controls including several types of protease digestions. With these, they found that positive protein tests could only be obtained from fibrils associated with the "blood" areas. McCrone [36] similarly obtained positive results in the amido-black test for samples 3-CB (right side wound) and 1-AB (back of right foot), both nominal "blood" areas.

The results are interesting for several reasons. First, they indicate that minute quantities of aged protein materials can be detected by microchemical techniques. (Heller and Adler have confirmed that the fluorescamine test is sensitive to protein under these conditions at the 1—10 nanogram level.) Although the presence of protein in the "blood" may suggest that a pigment vehicle was used there, the result is most interesting in connection with certain independent evidence for the presence of blood in these stains [40]. In this case, positive protein tests would actually be expected. In contrast, negative tests on yellow fibrils from pure-image areas would effectively eliminate all protein-based vehicles including glair, egg yolk, size, and casein.

McCrone's opposite conclusion [36] is not well supported because his positive amido-black tests were observed in "blood" areas only and cannot be taken as evidence for the presence of a protein-based tempera vehicle for the image areas generally. In our view, McCrone's inference has two problems: first, no protein has been observed by any method in pure-image areas as distinguished from "blood" areas; second, a more selective test must be employed, because amido black stains cellulose easily, making false positive results probable.

Heller and Adler [37] conducted further tests on the fibrils to detect inorganic compounds. These results were consistently positive for iron and calcium but negative for manganese, cobalt, nickel, aluminum, arsenic, tin, lead, magnesium, and silver. Although these tests were not sufficiently sensitive to detect siccative (oil drying) compounds, they show that the yellow fibril discoloration does not result from any likely (non-ferrous) inorganic or lake pigmentation (see note 5).

Additional tests for organic dyes and stains gave similar results. Heller and Adler could not extract the yellow color with strong acids, strong bases, or a variety of organic solvents including ethanol, methanol, carbon tetrachloride, benzene, pyridine, ethyl acetate, and acetone. Moreover, the color could not be bleached by strong oxidants (e.g., hydrogen peroxide) or by treatment with standard addition reagents such as iodine in the Hanus, and Wijs methods. However, they found that strong reductants, diimide and

hydrazine (though at a slower rate), could bleach the color of image fibrils. Tests for the presence of nitro groups, phenol groups, steroids, and lignin were negative, but the fibrils did show positive tests for aldehyde and carboxyl groups. Semi-quantitative tests indicated the greatest aldehyde and carboxyl concentrations for scorch-area fibrils, with lesser relative quantities for image and least for non-image fibrils.

Shroud samples from the tapes and excised threads [41] were examined by both laser-microprobe Raman spectroscopy and mass spectrometry. Results from the Shroud samples were compared with those obtained from modern samples of linen prepared by primitive techniques. No quantitatively significant Raman spectra could be obtained from any of the samples. The only unequivocal spectrum that could be obtained was that of the Mylar backing of the tape. There was no evidence for Saponaria or any other coating on the excised threads or image fibrils.

Mass spectrometry was run by pyrolysis of the samples within the source unit of the instrument. Mass spectrometry should provide the most sensitive and general method for the detection of foreign organic materials. (The system was sufficiently sensitive to detect traces of polyethylene that had been transferred to an excised thread by contact with its wrapping material, for example.) Although these data have not yet been fully evaluated, some conclusions have been drawn. There is a significant difference between the Shroud and the modern-primitive samples. The latter were found to contain lignin. This result was not entirely unexpected, because independent microscopic examinations of the modern-primitive samples had revealed lignin with the phloroglucinol/hydrochloric acid test, although the same test showed none on the Shroud samples. The mass spectrometric measurements detected no foreign materials on the image fibrils. Neither did mass spectrometry show any significant difference between the pyrolysis products observed from control areas and image areas at the level of data analysis that is now available.

The results of these studies lead toward some interesting conclusions. If any of the expected dyes, stains, pigments, or painting media had been present in the image, there should have been some indication from the microscopic, chemical laser microprobe, or mass spectrometric examinations. Subjects of earlier speculation, which involve the presence of burial spices (aloes, myrrh), oils (skin secretions), or saponins [3], likewise receive no support. By contrast, the chemistry of the fibrils does indicate a difference in the degree of oxidation and dehydration of the cellulose structure between image and non-image fibrils. The microscopic and chemical data, therefore, suggest the image to be the result of some cellulose degradation effect rather than an applied pigment. However, before this conclusion is accepted, the hypothesis must be subjected to the remaining evidence. More discussion of "painting hypotheses" will follow in later sections.

First, the presence of iron oxide and its suspected correlation with image areas requires some comment. Thus far, only the possibility that it represents

an artist's attempt to enhance the image has been mentioned, but there have been other suggestions. Riggi, for example, postulated that the Shroud may have been contaminated with some remnant of a jeweler's rouge polishing agent by inadvertent contact with one or more of the protective glass plates used in earlier exhibits.

As another possibility, Heller and Adler [37] observed that the appearance of the particles, and especially their occasional occurrence within the fibril medulla, are identical to those produced by an iron salt, alkaline precipitation, and dehydration reaction which were formerly used in khaki manufacture. They state that such reactions are known to occur naturally during the linen retting process. Detection of iron and calcium bound by ion exchange on both the image and non-image fibrils supports this hypothesis. The observed Fe_2O_3 particles could have been produced during the original retting or, also, at the "dousing" of the 1532 fire, by a chromatographic concentration mechanism similar to the khaki-type process. Heller and Adler observed Fe_2O_3-coated fibrils most frequently in the samples from the margins of the water stains and consider the latter process to be the major source of this type of artifact. Although the ultraviolet and x-radiographic data, described at greater length in later sections, tentatively support this conclusion, future x-ray fluorescence examination of the water-stain margins should provide more conclusive evidence.

In addition to Fe_2O_3, Heller and Adler [37] found "blood sherds" and "blood flakes" on many of the samples. The "blood flakes" are nearly indistinguishable from the comparably-sized Fe_2O_3 particles by the usual optical techniques. However, the two materials may be differentiated by the solubility of the "blood flakes" in hydrazine and the acid solution properties of Fe_2O_3. (The "blood sherds", which they found to be detached fiber-coatings of blood, are similarly distinguished from the identically appearing scorched fibrils by the "sherd" solubility in hydrazine.)

McCrone and Skirius [35] reported large concentrations of Fe_2O_3 particles for the "blood" areas, but Heller and Adler found most of these red particles to be "blood flakes" and not Fe_2O_3. It is, therefore, possible that the "Fe_2O_3" particle correlation with image areas reported by McCrone and Skirius is in fact a "blood flake" correlation obtained by translocation in the cloth folding. Jackson has experimentally tested the translocation hypothesis. From the sizes and positions of the burned holes, he has reconstructed the folded configuration of the Shroud at the time of the 1532 fire. Using these results, he then demonstrated that if the "blood" stain regions are assumed to contain substantial amounts of submicrometer-sized particulate material, a correlation almost identical to McCrone's is obtained by simple contact transfer in folding and unfolding the cloth several times.

The chemical composition of the true Fe_2O_3 particles may ultimately identify their origin. Heller and Adler [37] noted that iron found in hematite, ochers, and earth pigments is invariably contaminated with manganese, nickel, cobalt, or aluminum. They conducted a series of spot tests on the

various particles. After acid digestion, all but one of the red particles gave positive tests for iron although no traces for manganese, cobalt, nickel, aluminum, arsenic, copper, lead, or magnesium were detected above the estimated detection level of 1% (by weight). These results suggested to them that the iron oxide was of either hydrologic or biologic origin. The one exceptional red particle, which was found on the non-sticky side of one tape and tested positively for mercury and negatively for iron, was identified as mercury(II) sulfide. The black particles were generally found to contain iron although occasionally some of these near the scorch areas contained silver and not iron. Heller and Adler suggested that the silver may represent molten debris from the casket, that was deposited onto the cloth in the 1532 fire. The black (iron-containing) particles might similarly be postulated as Fe_3O_4 that formed either from Fe_2O_3 or the "blood" during the fire.

McCrone and Skirius [35] also reported seeing a few particles of orpiment, ultramarine, azurite, wood charcoal, madder rose, and larger quantities of vermillion. Although these observations have not been confirmed independently, Heller and Adler note that the occasional occurrence of such materials may not be unexpected because the Shroud is known to have been reproduced by artists and was, therefore, probably exposed to pigment-contaminating environments. Most recently, McCrone [42] detected the presence of minute amounts of mercury(II) sulfide in several material agglomerates tested from a single tape taken from the area of the side wound. The observation may warrant more precise x-ray fluorescence measurements there in the future; however, the data of Morris et al. [9] suggest that mercury is present nowhere in amounts greater than about 10 $\mu g\ cm^{-2}$.

X-ray fluorescence

Prior to the 1978 investigation, there was little information about the Shroud image beyond that provided by rather qualitative descriptions of its color and superficial distribution. In view of the vague historical references to a painted image, operations in the Shroud of Turin Research Project were planned to test this hypothesis thoroughly. In the 14th century, there were several pigments that might have been used to produce an image (see note 5). The most important nondestructive test applied to detect inorganic pigments specifically was x-ray fluorescence. With this technique, a painting produced from an iron, arsenic, lead, or other heavy-metal compound would be expected to reveal its presence as a discontinuous element distribution between image and background areas.

Morris et al. [9] reported results of the x-ray fluorescence studies. Their system excitation source consisted of an x-ray tube and tin secondary emitter that produced a nearly monochromatic beam of 25.5-keV Sn—K_α x-rays incident to the sampled area. A nominal 160-eV Si(Li) detector and energy-dispersive instrumentation were used to detect and process fluorescent x-rays in the range 1.5—22.0 keV. This system allowed detection of elements with atomic number greater than 16 with varying degrees of efficiency.

(The technique cannot be applied directly to detect low-atomic-number organic dyes or tempera vehicles.)

Generally, the x-ray fluorescence results showed no evidence for a painted image. Within the detection and precision limits of the data, there were no detectable differences in the heavy-element concentrations between image and non-image areas. Unfortunately, because of time constraints and the desire to examine as many different areas as possible, the precision levels of the measurements were rather limited. For example, Morris et al. estimated a detection limit to changes in iron concentrations of 5 $\mu g\ cm^{-2}$; longer counting times could have improved overall data precision. Despite these and other difficulties, the x-ray fluorescence results were sufficient to establish weight concentration limits for most elements of potential interest; however, in the absence of microscopic evidence for the presence of inorganic pigments (with the exception of Fe_2O_3 discussed below), there seemed little need to relate these numbers to corresponding pigment concentration levels.

Morris et al. reported relatively uniform concentrations of calcium and strontium in all of their spectra (see note 6). The large quantities of calcium ($200 \pm 50\ \mu g\ cm^{-2}$) and traces of strontium ($2.5 \pm 1.0\ \mu g\ cm^{-2}$) were tentatively interpreted as dust accumulations, probably natural calcium carbonate, on the Shroud. Riggi similarly observed substantial quantities of calcium compounds in the samples that he vacuumed from the back-side of the cloth. Although Riggi's observation tends to support Morris' interpretation, subsequent microscopic examination of the tapes showed little or no calcium compound debris from the Shroud image surface. Heller and Adler [37] have since postulated that the calcium and strontium were absorbed into the linen during the retting process (in which case the elements would be detectable with x-rays but not with the tape surface samples). They draw support for this hypothesis from both an experimental demonstration of the ion-exchange process and the observed presence of iron and calcium in several other antique linen samples.

In addition to calcium and strontium, small concentrations of iron were also detected in the non-"blood" areas. Quantities of about 30 $\mu g\ cm^{-2}$ were reported for the (non-image/water stain) foot scan and 10 $\mu g\ cm^{-2}$ for the (image) face scan regions. These results are generally consistent with microscopic observations, made during the period of direct examination, of particulate material throughout the Shroud. Pellicori and Evans [8] noted significantly higher concentrations of particulates in the nose and foot regions of the image. In these areas, x-ray fluorescence indicated statistically significant excesses of iron above background levels.

The data of Morris et al. [9] have provided some information to supplement the results of the tape study discussed above. McCrone and Skirius [35] postulated in their work that iron oxide contributes to the coloration of the image, but they gave no quantitative estimates either for the number densities of particles adhering to the fibrils or for macroscopic areal weight

concentrations of the material. Morris et al. measured changes of 0.01 in neutral reflected optical density for 1 μg cm^{-2} changes in iron concentrations of (anhydrous) Fe_2O_3 at low densities. A minimum visually-detectable quantity of this material is, therefore, about 2 μg Fe cm^{-2}, which is a result that has been confirmed by Pellicori [13]. If an artist deliberately used a hematite pigment to produce a visual effect on the image, then he must have applied at least this amount.

This hypothesis can be followed further. If an Fe_2O_3-enhancement implies an intentional darkening of faintly dark image areas, then one would expect to see some direct correlation of iron concentration with image density. Morris et al. [9] presented results of their x-ray fluorescence scan of the facial region indicated by the enclosed area in Fig. 4. The measurements were taken over roughly 1-cm^2 areas at 1-cm intervals along a scan line from the tip of the nose out to the "blood" trickle in the hair. It can be observed from the figure that the image density varies visibly along this scan, yet, except for the end points, the x-ray fluorescence showed no statistically significant variations in element density along the scan. Although the areal-concentration data for iron qualitatively suggest a correlation, these variations are smaller than the ± 2.5 μg Fe cm^{-2} precision limits of the measurements.

This data precision is, therefore, insufficient to test the hypothesis of image enhancement with Fe_2O_3 definitively, but the results do place rather narrow limits, 2—5 μg cm^{-2}, on whatever areal weight concentrations such an hypothesis might imply for hematite. (Hematite or anhydrous Fe_2O_3 would represent a "worst case" because the hydrous forms are less potent coloring agents. Thus, for an equivalent darkening, hydrated Fe_2O_3 would require greater relative iron concentrations than the hydrous compound and would, therefore, be more readily detected with the x-ray fluorescence.) A more precise x-ray fluorescence study could be made in some future attempt to improve on the present results. However, variations in a large but visually undetectable background quantity of iron may preclude any more definite conclusions than those drawn here.

Low-energy radiography

Mottern et al. [10] radiographed the entire Shroud with a Baltograph 5-50 x-ray unit operated at 15 (peak) kV and 10 mA for 10 min. The tungsten tube had a focal spot 1.5-mm square and inherent filtration of 1.0-mm beryllium. Mottern used Class I films (Kodak Types DR and M) with a source to object/film distance of 1 m.

Ordinarily, x-radiographic techniques are well suited for observations of paintings produced with heavy-metal pigments laid on at appreciable thickness, but the Shroud image is certainly not in that category. No density discontinuities that correspond to visible body image could be observed anywhere, although the weave structures and cloth density variations are easily visible in all of the radiographs. The water-stain margins are also seen as high-density structures, but in the absence of x-ray fluorescence data, the

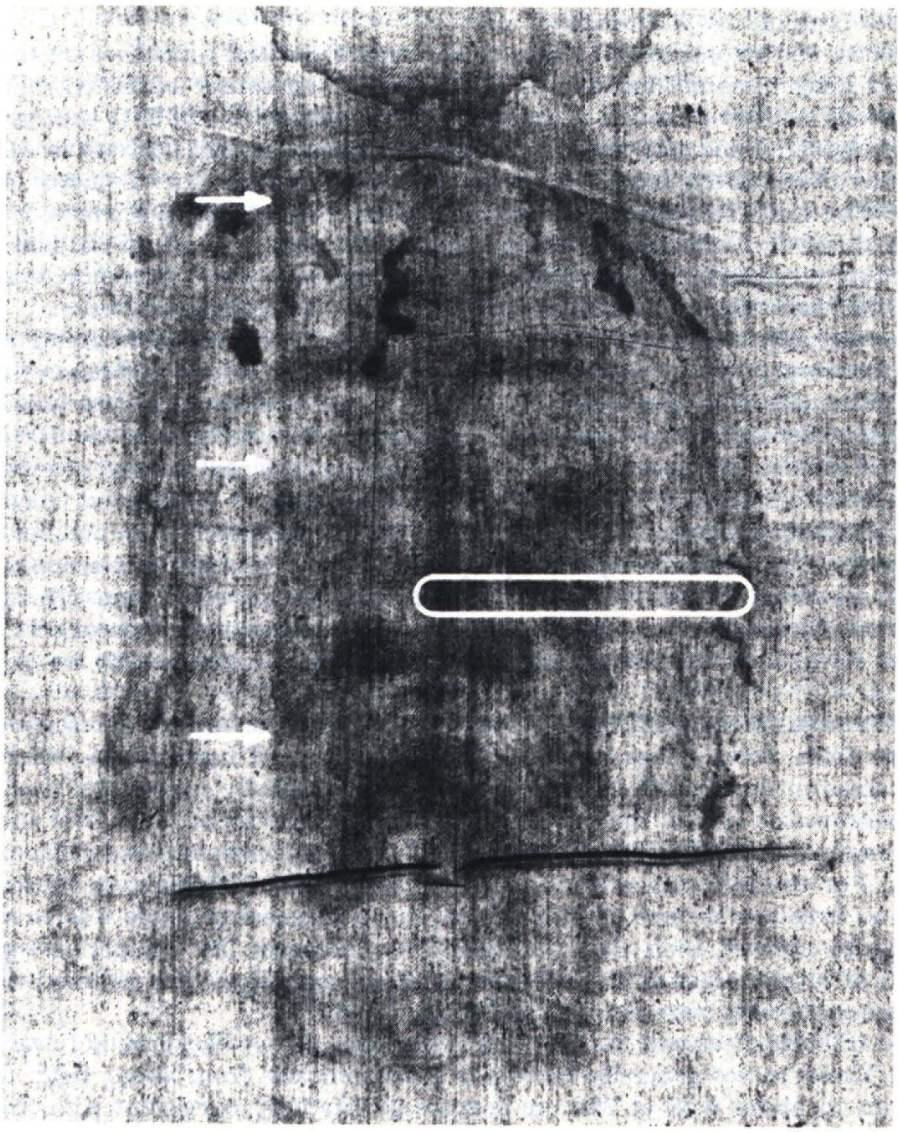

Fig. 4. Slightly contrast-enhanced photograph of the frontal-image face region. The enclosed region in the figure roughly indicates the area examined by x-ray fluorescence. The arrows point out the position of an abrupt change in the image density at the side of the face.

elemental composition of these deposits remains unknown. Mottern et al. [10] estimated the radiographic sensitivities to be about 5% for changes in areal cloth density. They used effective-energy considerations to estimate radiographic sensitivities to Fe_2O_3 and other high-Z pigments and found that these were roughly an order of magnitude less than the sensitivities reported for the x-ray fluorescence studies.

Photoelectric spectrophotometry

Accetta and Baumgart [11] measured infrared spectral reflectives on the Shroud image, scorch, and background areas. Their source consisted of a black-body emitter operated at ca. 1250 K (11.5 μm) with a 500-Hz chopper (for background and self-emission component rejection) and $f/1$ NaCl lenses to focus the incident beam onto a target spot with a nominal diameter of 2 cm. The HgCdTe detector and circular variable filter system scanned the 3—5 μm and 8—14 μm ranges with a spectral resolution, $\lambda/(\Delta\lambda)$, of 60. Their procedure consisted of alternately measuring the sample and reference standard (flat-black enamel on 240-grit sandpaper) in identical geometries.

Accetta and Baumgart [11] noted that their single-beam configuration was quite susceptible to instabilities. They found, for example, that relatively large fluctuations in atmospheric absorption and system noise precluded absolute reflectance measurements. The inherent low reflectance (5—10%) of the cloth also added to the uncertainty. Although their experiment showed an impressive similarity between the spectral features of the Shroud image and scorches, the results were judged to be inconclusive. In subsequent laboratory studies, similar spectral properties of linen, cotton, and scorches of varying visual intensity suggested to them that surface effects most likely dominate chemical or composition differences. Limited instrumental sensitivities have, thus far, largely precluded definitive infrared results for the Shroud.

Gilbert and Gilbert [12] measured u.v.—visible reflectance and fluorescence spectra from body image, scorch, "blood" stain, and background (clear) cloth areas on the Shroud. Their instrument was a specially constructed dual-monochromator system that allowed continuous scans to be made over the wavelength range 250—750 nm with an effective instrumental bandwidth of 5 nm. For the reflectance measurements, they used a 150-W xenon source lamp to irradiate an area of 6 × 3 mm and a magnesium oxide reference surface to convert their data to absolute reflectances. By comparing the results of several scans at single locations, they established that their individual measurements were reproducible to about ±3%.

The Gilberts measured the absolute reflectance of five background (clear) areas. These curves generally increased monotonically from about 0.08 at 250 nm to about 0.50 at 750 nm and are qualitatively consistent with the expected reflectance behavior of old linen material. Cellulose aging is evidenced by yellowing and loss of strength [43]. Chemically, the aged cellulose chain contains carboxyl and carbonyl groups, free radicals, and double bonds of varying degrees of conjugation [44]. These groups absorb light increasingly toward shorter wavelengths to produce the observed discoloration. The individual spectra in the background series were offset by as much as 7% from their mean curve. These differences are probably not excessive in view of the weave structure interference and the diffusely mottled visual appearance of the cloth background. It is assumed that the mottling results either from unevenly deposited pyrolysis products from the 1532 fire or from varying extents of cellulose degradation in these areas.

Reflectance measurements of the body image were made in eight different locations. The Gilberts referenced these data to the same mean clear-area spectrum and presented the results of four typical reflectance scans in their report. Generally, the relative reflectance of the image increases with increasing wavelength although there are noticeable differences among the individual measurements. For example, the Gilberts observed rather large and nominally constant offsets among the spectra; some of these appear to be as large as 40% to 50%. These offsets probably result from the different image densities in the different sampled areas and their magnitudes do not seem unreasonable.

Besides these, there are obvious non-uniformities in the detailed functional behavior of the individual scans, variations that are occasionally beyond the limits established for the maximum probable variance of the measurements. These variations are believed to represent actual signal variations rather than instrumental noise, but they cannot be immediately attributed to corresponding changes in the image density. The Gilberts suggested that they most likely arise from non-uniformities in the local background reflectances. This unavoidable difficulty prevents each of the measurements from being interpreted individually; however, we have compared possible fine-structure variations and have found none common to the spectra in this series.

Figure 5 illustrates that none of the spectral characteristics expected from normal dyes, stains, and pigments are observed. Included in the plot are the results obtained from a scan of (anhydrous) Fe_2O_3. The steep slope in the data over the approximate range 550—600 nm exemplifies a rather characteristic

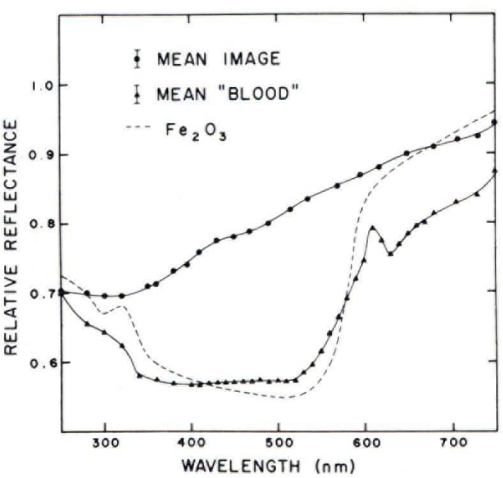

Fig. 5. Plots of the mean relative reflectance (referenced to the same mean "clear"-area spectrum) of five body-image and four "blood"-stain areas [12]. The Gilberts' scans were continuous. The points indicated in the plots do not represent individual measurements but values obtained from manually averaging the individual relative reflectance spectra. Error bars in the legend represent estimated maximum probable variances for the respective curves. Also included are results obtained from a scan of (anhydrous) Fe_2O_3.

behavior of pigments, stains, and dyes. Pellicori [13] suggested that the absence of a corresponding discontinuity in the image-area data places an upper limit of roughly 5 μg Fe cm^{-2} for hematite there, and that this material does not contribute significantly to the coloration of the image.

Pellicori [13] reported results of similar Shroud measurements on six samples of each type of stain and clear background. In his system, a 500-W tungsten source illuminated a 1-cm^2 sample area. This sample area is about 4.4 times that of the Gilbert measurements and presumably allowed Pellicori to integrate more effectively over local inhomogeneities such as the cloth weave. Pellicori reported an approximate ±1% repeatability for the measurements and a spectral resolution of 17 nm (FWHM). Whereas the Gilberts' scans were continuous, Pellicori's signals were read out digitally at 20-nm intervals in the wavelength range 440—700 nm. The results of the two independent reflectometry systems in Turin reportedly agreed within 5% on an absolute scale [13].

The photographic results are qualitatively consistent with the spectral reflectance data obtained. The multispectral narrow-band photographs of Miller show decreasing image contrast from the near ultraviolet to the red-visible. The Gilberts' plot of the average image density as a function of wavelength showed a broad maximum of about 0.15 near 300 nm and a general monotonic decrease to about 0.02 at 750 nm.

Photoelectric and photographic fluorescence

For their optical fluorescence measurements, the Gilberts used a 200-W mercury arc lamp with the source monochromator set at 365 nm. They also placed a u.v.-transmitting/visible-absorbing filter in the source beam to eliminate visible radiation incident to the target. The detector monochromator was then scanned continuously from 390 to 700 nm. In this configuration, the instrument had an effective bandwidth of 8 nm. The Gilberts' results showed that background cloth areas fluoresce in a broad band with a maximum near 435 nm. Pure cellulose fluoresces weakly, if at all. For comparison, they showed that a reference sample of Whatman 42 (ashless filter paper) produced a peak fluorescence at 435 nm which was only 0.28 times that from the clearest tested area on the Shroud.

The image itself did not fluoresce measurably. (Although the data suggested low-level fluorescence signals in the 600—700 nm region, the observation can be accepted only tentatively because the signals were of approximately the same magnitude as the stated maximum probable data variance.) The Gilberts observed that the image reduced the fluorescence of the underlying background and shifted the maximum slightly to longer wavelengths. They also found that this fluorescence reduction and maximum shift is produced by the scorches and to some extent by the mottling in the background areas.

The fluorescence reduction is probably a combined result of several factors. A decrease in the areal density of fluorescent material would contribute,

as would an attenuation of both incident excitation and emitted fluorescent radiation through the scorches and image. The Gilberts' data show that, within a given series of sampled areas (scorches, image, or background), as the reflectance is reduced, the fluorescence is also reduced. This observation is consistent with any of the proposed mechanisms, but the shift of the background fluorescence peak to longer wavelengths suggests that an attenuation of the emitted background fluorescent radiation is a contributing factor.

Miller and Pellicori [14] photographed the visible light emitted from the Shroud as it fluoresced under ultraviolet (335—375 nm) radiation. The u.v.-source lamps were filtered to eliminate any visible light, and the camera was filtered to eliminate any ultraviolet contribution to the image on the film. Their photographs illustrate the effect observed in the spectrophotometric data; the image appears to attenuate the fluorescence of the underlying cloth.

These u.v.-fluorescence results may serve as an independent test for the hypothesis that a paint vehicle based on animal collagen was used on the cloth. However, preliminary results on modern collagen indicated that both Knox gelatin (which, incidentally, is used in photographic emulsions!) and gelatin extracted from a laboratory rat's tail fluoresced noticeably in the visible under ultraviolet illumination. The test samples evidently contained significant quantities of aromatic amino acids or other fluorescent compounds. If a collagen-binder hypothesis were valid, it must be assumed that the vehicle either contained no fluorescent compounds or that their fluorescent properties disappeared uniformly with time or in the heat of the 1532 fire.

Heller pointed out that a yellow animal collagen should contain aromatic amino acids and, therefore, should fluoresce. Miller has examined a 13—14th century Bible and found that both the page binding material and the manuscript illuminations fluoresced visibly under ultraviolet radiation. An interesting study might be to examine the fluorescent properties of known 14th-century animal-tempera paintings.

Photographic and direct macroscopic visual observations

Direct observation of the Shroud shows that it was subjected to very steep thermal gradients at the time of the 1532 fire, and a number of locations can be identified where scorches intersect image areas. Those parts of the image that intersect scorches were observed to have identical color tone and density as the image areas at the farthest (as folded) distance from scorches. This can be taken to indicate that neither the color nor density of the image changed as a result of either heating or reactive pyrolysis products from the scorching cloth. Organic dyes and stains, inorganic pigments, and painting media can be tested against this observation.

Pure silver melts at 960°C, but because of suspected alloy contaminants, the silver casket in which the Shroud was stored in 1532 would probably have melted at 820—850°C. (Pure cellulose begins to produce gaseous

products at an appreciable rate at about 310°C [44].) Few organic dyes or stains could survive the scorching conditions, and most of the inorganic pigments available during the 14th century would have suffered some change. Hydrated iron oxides, the ochers and siennas for instance, change color on heating to become their "burnt" equivalents, and even Fe_2O_3 tends to be reduced to black Fe_3O_4. Sulfide pigments (orpiment, realgar, etc.) would be converted to salts, many of which would be water-soluble and all of which would be a different color. If the image had been painted with a proteinaceous, plant-gum-, or starch-based vehicle, the medium would have scorched more rapidly than the cellulose of the linen. No evidence for a scorched medium can be seen.

The water used to extinguish the fire in 1532 migrated through the cloth in both scorched and unscorched image areas. No evidence has been found that any part of the image was water-soluble either before or after scorching. Any hydrophobic medium (oils, waxes, etc.) that migrated through the cloth would retard water migration. It can be seen that water migration through the cloth was not inhibited by the presence of the image, although it was retarded by several "blood" stains including that at the side wound, for example.

There is no apparent evidence of brush marks that might suggest a painting. Neither is there any general non-uniform image fading or variation of color with position. Infrared thermographic images [11] likewise showed no evident anomalies in the investigated areas (face, back of head, hands, foot, and side wound areas). However, any good photograph of the Shroud does show that the relative density of the image changes abruptly across a single thread in many places. These density changes correlate with thread overlaps where they can be observed in weft locations. That is, the image density changes at a location where the material used to weave the cloth changes.

An abrupt change in the image density can be seen in Fig. 4 at a single warp thread at the side of the face. The effect at this location has been mistakenly taken as evidence for a chin band [45, 46]. Such a change in density would not occur if the material had been brushed or sprayed, but it might be observed from a block print or rubbing where thread-lot thickness or surface discontinuities affected the amount of material transferred in the process. In this particular region, the radiographs show no discontinuity in the cloth areal density; it can, therefore, be concluded that adjacent warp-thread-lots differed either in their surface or chemical characteristics.

Corollary: The image results from chemical changes of the cloth

We have reviewed the experimental results of the Shroud of Turin Research Project and have found no evidence to suggest that the Shroud image consists of a colored foreign material on the cloth. The only alternative seems to be that the chemical composition of the cellulose fabric was somehow altered to produce the effect. In the following discussion, the processes that may

have accomplished this are grouped into two categories. The first of these involves simply scorching or burning the material either by direct contact or radiant energy transfer. The second category includes mechanisms in which the cloth is treated locally by some applied reagent. In this case, a dehydrating agent, such as an acid, may produce the image directly, or a catalyst may sensitize the cloth to produce a latent image which is then developed either by a direct application of heat, radiant energy, or by aging.

Scorch hypotheses

In 1966, Ashe [47] suggested that the image was a surface scorch and produced experimental images on cloth by using a heated brass ornament. This hypothesis has become particularly interesting because the Shroud image appears to have many of the physical and chemical properties of a light scorch. With properly controlled heat and timing, superficial scorches can be produced on cloth without affecting the gross mechanical properties of the fabric. Generally, scorches do not fade with time and are stable to further heating up to temperatures and times that will produce an equivalent scorch in the base material. Scorches do not move as water percolates through them nor do they impede water flow. The chemical components of scorches are not soluble in acetic acid, organic or redox solvents. The fibers in lightly scorched areas are translucent and closely resemble the observed image-area fibril color.

Unfortunately, the term "cellulose scorching" does not describe a unique or simple set of chemical reactions. Conditions of time and temperature determine whether or not a visible scorch is produced and the chemical nature of the color. The mechanisms of scorching processes are extremely complex [44], and the phenomena cannot be described here in any great detail. However, it can be stated that dehydration is the main reaction at moderate temperatures (less than 280°C). Dehydration produces unsaturation and conjugated double bonds with different degrees of conjugation which absorb light at specific wavelengths. If the wavelengths absorbed are in the visible region of the spectrum, the transmitted or reflected light appears colored. Higher temperatures can produce color in shorter times, but the colored products may be much different at different temperatures. Free radicals, multiple carbonyl groups, and free carbon can be involved in the observed color as well as conjugated double bonds.

The strongest supporting evidence for the scorch hypothesis is found from the spectrophotometric work of Gilbert and Gilbert [12]. Their report includes relative spectral reflectance curves for both image areas and scorches of different densities. Whereas the deepest scorches were found to absorb strongly and broadly near 375 nm, the lighter ones exhibited a more nearly monotonic behavior which is qualitatively consistent with the expected absorption behavior of dehydrated cellulose. Figure 6 compares the mean reflected density from three light scorches with that of five image areas;

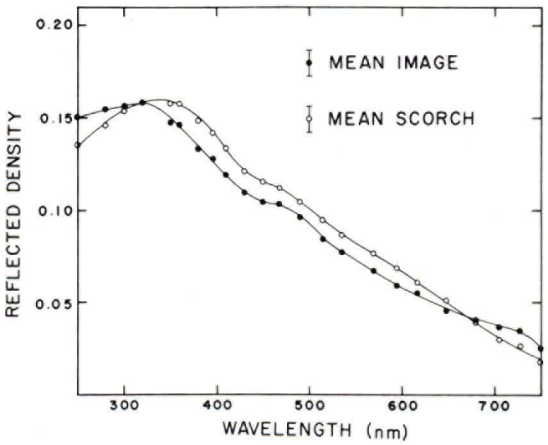

Fig. 6. Plots of mean reflected densities from the image and from scorch [12]. These results were obtained by averaging continuous relative reflectance spectra from five body-image and three light-scorch areas. The points in the plot do not represent individual measurements but the values obtained from averaging these data. Error bars in the legend represent estimated maximum probable variances for the curves.

the two curves agree within experimental error. The Gilberts also reported that image and the light scorch-areas reduce the background fluorescence in a similar way.

Despite this correlation, there has been some disagreement about the visual similarity of the image and scorches on the Shroud. In Pellicori's opinion, the resemblance is only superficial. He perceives the scorches on the Shroud to be visually redder than the body image [8], and notes their different characteristics in the u.v.-fluorescence photographs [14]. (The Gilberts' spectra likewise suggest that the scorches fluoresce more strongly than the image in the 600—700-nm region, but again, these were both very weak responses and no quantitative evaluations can be made.)

If the Shroud image is a scorch, the slight differences between it and the known scorches from the fire may be attributed to different ambient conditions during the two processes. It is known that in 1532, the Shroud was burned while it was inside a metal box [1] and may be supposed that the oxygen in this environment was rapidly consumed. As the temperature increased in the scorching zones, several fluorescent or reactive pyrolysis products would have been produced, including furfural, formaldehyde, formic acid, and levulinic acid, for example. Miller and Pellicori [14] demonstrated experimentally that pure cellulose heated in an oxygen-depleted environment produced pyrolysis products that fluoresced faintly red in the same manner as those Shroud areas damaged in the 1532 fire. In those areas of previous fire damage, which Wilson [1] has speculated to be hot-poker holes (see note 7), no fluorescence is observed. These results suggest that the earlier burns and perhaps also the Shroud image, if it is a scorch, occurred in the presence of oxygen.

Pellicori has raised some questions about the latter hypothesis. Miller and Pellicori [14] produced light sources on modern linen in an atmospheric environment with a hot soldering iron. They found that scorches produced at various temperatures on both dampened and dry cloth all fluoresced yellow—green under ultraviolet radiation. Further experiments showed that the fluorescent compounds were quite water-soluble, although even after repeated rinsing, the scorched areas retained their fluorescent properties. In addition, they demonstrated the stability of the fluorescent compounds by baking the samples at 145°C for six hours. Pellicori recalls that the Shroud image itself does not fluoresce measurably. In view of the results of these scorch studies, he feels that it is unlikely that the image was produced by scorching, for otherwise there should have been some characteristic fluorescent behavior observed.

These results draw the "air" scorch hypothesis into serious question; however, it was chosen to leave the matter as an open question for now. Before the non-fluorescent property of the image is taken as conclusive evidence against scorch hypotheses generally, the conditions and reactions that are involved in the formation of these compounds must be better understood. Future studies should include many of Miller and Pellicori's original experiments on actual Shroud threads.

There has been some speculation that a short burst of high-intensity radiation might produce effects on cloth that resemble the Shroud image [3]. Direct photolysis of cellulose occurs at wavelengths shorter than about 340 nm [44]. At longer wavelengths, energy absorption can allow similar reactions to proceed indirectly. However, our own experiments with intense flash lamps, and ultraviolet, visible, and infrared lasers have not successfully reproduced the color density and distribution observed on the Shroud. Although very short flashes are required to obtain a superficial discoloration, these radiant energy sources produced different relative amounts of products and, therefore, different colors. These studies also showed that high radiant-energy flux tends to cause surface explosions and damage that was not observed on the Shroud image. The results suggest that so-called "flash-of-light" hypotheses are difficult to support.

At this time, the most likely scorch hypothesis is that the Shroud image is a light "air" scorch produced at temperatures lower than those sufficient to carbonize the material. While some data support this hypothesis, they do not prove its validity nor do they suggest what scorching technique may have been used. Any complete hypothesis must also account consistently for the observed density shading characteristics of the image.

Following Ashe [47] and in direct response to the article by Culliton [4], there has been increased speculation about the so-called "hot-statue" hypotheses [48, 49]. Generally these arguments are based on the known 14th-century existence of full-sized statues in either stone or metal. They postulate that one of these statues was heated and then pressed or tented with the cloth. Hot-statue hypotheses have the image scorched by radiant energy and

the contour information recorded on the cloth as different scorch densities in different locations depending upon the respective distances from the cloth to the heated statue surface.

Jackson has done both theoretical [50] and experimental work to address three-dimensional hot-statue hypotheses. He found that a simple isotropic radiation source could not yield the observed Shroud-image shading and resolution (see note 8) although it could be obtained if emission (or cloth absorption) anisotropies were assumed or if significant attenuation were present in the intervening medium. However, in these cases the resulting directionality of the radiation normal to the surface of the hot statue would introduce an unacceptable distortion of the image on the cloth. Moreover, at cloth-contact points one would expect to see "hot spots" or well-defined regions of enhanced image density that result from thermal conduction. No evidence for "hot spots" in the Shroud image has been found.

Because Jackson's studies have shown that three-dimensional hot-statue hypotheses are rather unlikely, we suggest that perhaps an etched or scribed flat-plate may have been used. In this case, either the differing directional or radiant intensity characteristics of metallic and insulator materials [51] might be used to produce the observed image. So far, no experimental work has been done to test this hypothesis, but there would be potential problems, particularly with controlling the temperature distribution within a 1 × 2-m metal plate. At present, we are aware of no scorching technique that satisfactorily accounts for the observed image density characteristics.

Hypotheses on chemically-induced cellulose degradation

It has been shown that light surface-scorches have many important Shroud-image characteristics, but stains produced by the action of certain locally applied reagents can have similar properties. Concentrated sulfuric acid, for example, dehydrates cellulose to produce a convincing yellow discoloration; however, attempts to create an image with acid were rather disappointing. In particular, it proved quite difficult to control the depth penetration and densities of the stains. Also, unless the acid is properly neutralized, the continuing reaction can cause disastrous effects. Mainly because of these problems, an "acid-painting" hypothesis seems rather unlikely, although the possibility cannot be strictly ruled out.

Pellicori has developed a slightly different technique that has shown more promising results. A previous section briefly mentioned the effects of cellulose aging. Pellicori [13] described laboratory simulations of these changes in which he used a baking technique that is similar to that employed in paper and textile research. The results obtained after baking for about 7.5 h at about 150°C qualitatively reproduced the spectral reflectance and fluorescence characteristics of the Shroud background areas. In addition to this, he applied thin, invisible coatings of skin secretions (perspiration plus oils), myrrh, and olive oil to different areas of his linen samples. After baking in air at 140°C for 3.5 h, these treated areas attained a yellow density

in excess of the observed background discoloration. (The reaction is apparently limited because continued baking of the samples did not darken them further.) Similar discoloration was produced at 125°C, but longer times were required. Although the materials used to catalyze the stains showed either no fluorescence or very faint emission (olive oil: neutral to reddish), the spectrophotometric character of the treated areas (and of myrrh, in particular) after baking closely matched that of the Shroud image.

Pellicori observed that the specific foreign material responsible for locally advancing the degradation of the cellulose is not of prime importance. It need only satisfy the requirement of greater optical absorption for blue light than red in the case of photosensitization [43], or of some property like a reduction of the cellulose crystallinity or the improved thermal impedance matching for the surface reaction involved. Although no traces of sensitizing materials were observed on the Shroud, these may have been lost in time by chemical transformation, evaporation, or washing.

The results of experiments with chemically-induced cellulose degradation have, so far, provided the closest approximation to the observed image characteristics; however, the approach has some difficulties. The problem of controlling depth penetration of the applied materials has already been mentioned. (The Shroud image coloration extends no deeper than a few fiber thicknesses and generally does not follow the dips of the threads.) Depth penetration can depend not only on the fluid properties of the foreign materials but also on the surface and absorption characteristics of the linen fibers. Simulated image stains, to date, have been fairly successful, but more work is necessary. It may be suggested that future studies account for other possibly significant factors. For example, the moisture absorptivity of the fibers, the foreign material composition, and the ambient atmosphere are but a few potentially influential parameters. Pretreatment of the linen may also be significant. Druzik suggested that if the large calcium concentrations [9] had been present in the cloth before the image was formed, it might be expected that it would have buffered certain types of reactions and, thereby, assisted in confining the discoloration to the tops of the thread crowns.

Another problem is that a detailed mechanism for the application of the image has not yet been formulated, although it appears, in the present context, that some direct-contact material transfer must be involved. Vapor diffusion of the sensitizing materials from a three-dimensional model seems unlikely, because the image appears only on the thread crowns and not in the lower weave structure. Moreover, a material distributed by diffusion would be essentially isotropic ($1/r^2$ density) and susceptible to convective fluctuations, and, therefore, would not preserve the shading and resolution according to Jackson's arguments [50].

If the image were the result of cellulose degradation processes, the possibility cannot be discounted that the Shroud was artificially imprinted with a cloth-sensitizing material and the image subsequently developed,

perhaps by baking as Pellicori has described. Although the spatial gradation of image density, which has been correlated with vertical cloth-body separation, does not result in an obvious manner from simple contact models, there may be some possibilities.

Smith [52] suggested that a latent image transfer may have occurred as the cloth contacted an existing flat painting, perhaps during storage. In this case, loose pigment particles may have been transferred to the cloth surface, or slightly volatile organic components from a painting medium may have diffused there. In a damp environment, water-soluble materials might have been adsorbed onto the surface fibers. Smith argued that foreign materials could locally modify the darkening of the fabric with age even if their presence could not be detected visually. To support this hypothesis, he noted that such transfer effects can be seen in many old books that contain color illustrations. So far, there has been no experimental work done to test the feasibility of Smith's general model.

As another possibility, Nickell [30, 31] described several contact transfer mechanisms that might produce the observed contour density effects. His latest technique [31] involves molding a wetted cloth to conform to the surface contours of a "suitable" bas relief model. The cloth is permitted to dry, and powdered pigment is applied with a cotton or cloth dauber. Although microscopic examination of the Shroud shows that the image does not consist of powdered pigments, any of a number of cellulose-sensitizing materials could have been used instead. One may postulate that the image was developed as the deformed cloth material was ironed flat, baked, or exposed to the sun for some period of time.

There seems to be no historical evidence to suggest that any such technique was used before the 19th century. Thus Nickell's method, "using only 14th century technology", may at best represent a unique and subsequently forgotten innovation. Some have questioned the possibility of preserving the global precision of the Shroud image with this technique. (Jackson has analyzed some of Nickell's images with the VP-8 system, but the results have been quite disappointing.) Nevertheless, these and further ideas are to be encouraged. It must be stressed, however, that hypotheses can only be meaningfully evaluated from detailed quantitative comparisons of test results to actual Shroud data.

Conclusions

The only existing evidence that the Shroud of Turin is an artifact is the letter written by Pierre d'Arcis in 1389 that simply states it as a fact. Although this historical reference is not subject to verification, it deserves serious consideration. Humber [2] wrote that in medieval Europe there were at least forty-three "True Shrouds", some with and some without figures. Shroud-image forgeries, and most likely very good ones, existed. Eastlake [53] noted that tempera and watercolor paintings on linen were common in

England and Germany in the 14th century. Unfortunately, we have not examined any of these and have no basis for comparison with the Shroud image. Our conclusions are based mainly on direct observations and the results of other follow-up studies.

There has been no evidence found to suggest that the visible image results from a colored foreign material on the cloth. In this regard, the data are quite internally consistent. Microscopic studies have revealed the image to be highly superficial; the image resides in the topmost fibers of the woven material as a translucent yellow discoloration. No pigment particles can be resolved by direct Shroud observation at 50X magnification, nor can unambiguously identified pigment particles be found on the tape samples at 1000X. Microchemical studies of yellow fibrils taken from tape samples of the pure-image area have shown no indication for the presence of dyes, stains, inorganic pigments, or protein-, starch-, or wax-based painting media. X-ray fluorescence shows no detectable difference in elemental composition between image and non-image areas. Spectrophotometric reflectance reveals none of the characteristic spectral features of pigments or dyes. Ultraviolet fluorescence shows no indication of aromatic dyes or aromatic amino acids that might be expected from animal-collagen pigment binders. Direct visual observations of image areas that intersect scorch and water stains reveal nothing that might suggest the presence of organic dyes or water-, protein-, or starch-based painting media.

The possible correlation of submicrometer-sized Fe_2O_3 particles with image areas has been discussed. One interpretation of this observation has been that it represents an artist's attempt to enhance a pre-existing image. However, the observation of red particles from the tape samples has provided only limited, qualitative information. The results of independent tests have not supported the image-enhancement hypothesis. Spectrophotometric reflectance and x-ray fluorescence data have established rather severe limits for whatever iron-oxide areal concentrations that such an interpretation might imply. Indeed there is some doubt that the original identification of this material is valid. The red particles are most likely "blood flakes" distributed by cloth folding from the "blood" areas. In view of the small amounts of this material present and the alternative hypotheses that have been proposed to explain its appearance and distribution, this evidence is judged to be irrelevant to the image-formation problem.

The reflectance and fluorescence characteristics, as well as the apparent chemical nature and microscopic appearance of the image, suggest more strongly that it is an effect of cellulose structure modification. Within the context of the present category of hypotheses, it has not been definitely determined whether the image was scorched at moderate temperatures or treated chemically and subsequently developed. If scorched, there was probably no structurally three-dimensional model used. If treated chemically, a direct-contact transfer was probably employed. In either case, there remains the unanswered question of how the apparent global precision and

resolution of the image was maintained. Certainly more work is necessary; further research might also include investigations of sequential processes which have so far received little attention.

Hypothesis: The image is not an artifact

This class of hypotheses includes natural processes not involving direct, willful human intervention. These hypotheses are based exclusively on the assumption that the Shroud was actually a burial shroud and that the image was formed or initiated by some unaided natural mechanism. (With the possible exception of Smith's contact model, which involves an existing painting [52], no other "natural" processes have been examined that might have produced such a detailed and anatomically correct image on cloth without the presence of a human body.) This discussion will, therefore, be limited to the physical evidence as it pertains to the question of whether the Shroud was a shroud without considerations given to the time or place of origin.

Vignon vaporgraphic theory

Vignon [16, 54] documented the first scientifically based hypothesis to account for the apparent negative image characteristics, revealed in the Pia photographs, in terms of physical and chemical processes. He knew that a body in pain perspires and that the perspiration contains urea. Under certain conditions, fermentation may convert the urea into carbon dioxide and ammonia. Vignon assumed that the burial cloth was soaked in aloetine, an embalming formula consisting of aloes and olive oil, and that the ammonia diffused from the corpse to the cloth where it reacted with the aloetine to produce the observed brown stains. He reasoned that those cloth areas nearest the body would stain darker because of their shorter diffusion path length, and a negative body image would result.

The resolution limitations involved with the diffusion transfer mechanism have already been discussed. Vignon's theory presents additional problems. A necessary condition for the hypothesized chemical reaction to proceed is that the cloth be damp. Vignon himself realized that a damp cloth would cling to the body in various locations and cause image saturation and distortions; these effects are not observed on the Shroud image [55]. A more compelling argument is that ammonia or, at contact points, low-molecular-weight fatty acids from the body and essential oils from spices should permeate the fabric. The image, as noted above, is characteristically superficial and cannot be seen on the reverse side of the cloth as Vignon had thought. Yet another problem is that the amount of ammonia needed to produce a satisfactorily intense image is greater than might be expected from the natural reactions described above [31].

Judica Cordiglia, Romanese, and Scotti have experimented with related techniques [56], but these have all generally involved the same materials and chemical reactions as in Vignon's model. Sebaceous secretions from a body

should be about 65% fatty-acid esters of glycerol, sterols, and wax alcohols with about 30% unsaponifiable materials [57]. The chemical properties of these natural products eliminate them from consideration. Few are thermally stable; many are surface-active on water. Formaldehyde, as would have been produced during the 1532 fire, denatures proteins, reacts with amines, couples with phenolic compounds, reacts with alcohols and sterols, and acts as a potent reducing agent. Steam and acids hydrolyze esters, and many fractions would volatilize [58]. If unstable natural-product systems were responsible for the image, they should have decomposed, changed color, or volatilized at different rates depending on their distances from high-temperature zones during the fire. No such changes have been observed using available photographs or by direct observation of the Shroud. In addition, no foreign materials have been detected spectrophotometrically, chemically, or microscopically in the image areas on the cloth.

Latent-image hypothesis

Certain details of Pellicori's latent-image process have already been described under the artifact category of hypotheses. His work involved sensitizing materials that might be found on an interred human corpse; it is therefore appropriate that his arguments be reconsidered within the context of natural mechanisms. Pellicori's hypothesis is that the burial cloth was sensitized by adsorbed materials transferred from the corpse by direct contact and that the latent image developed in time by a gradual process of locally-catalyzed cellulose degradation [8]. He demonstrated that linen stains, having many of the chemical and physical properties observed for the Shroud image, can be produced by treating the cloth with thin coatings of perspiration, olive oil, myrrh, or aloes and then baking.

There has been some discussion about the baking technique and its postulated equivalence to aging on an accelerated time scale. At moderate temperatures, the dominant cellulose degrading reactions are oxidation and dehydration. However, at the elevated temperatures (125—150°C) used in the baking experiments, it might be expected that greater relative concentrations of more complex pyrolytic products would be observed, because their respective activation energies form a nearly continuous distribution in the energy-equivalent temperature range below 230°C. Pellicori argues that these effects contribute negligibly to his results. Many of these additional products would be colored or fluorescent, but neither fluorescence nor spectrophotometric data from his simulations show any appreciable concentrations of these more complex structures. The equivalence of baking to accelerated aging has been fairly well established, but there are still some questions about the detailed effects resulting from differential reaction kinetics between amorphous and crystalline cellulose phases. Work in this area is continuing.

It was noted above that Pellicori's latent image process has provided the closest approximation to the color and chemical properties of the image.

However, the process, by itself, provides no description for the well-characterized density distributions of the image. Some additional physical mechanism that may have generated (or preserved) the observing shading must be postulated. Earlier, there were some possible ways suggested by which an artist may have accomplished this; here image-transfer mechanisms that may have operated by "accident" rather than by human design must be considered.

If the Shroud were a burial shroud and if the image were recorded by a latent-image type process, the transfer of sensitizing material must have taken place either by direct contact or vapor diffusion from the corpse. Pellicori believes that direct contact is the more likely of the two and cites some positive evidence to suggest that a cloth—body contact did occur. Miller and Pellicori [14] pointed out that, in visible reflected light, the so-called scourge marks have the appearance of diffuse "blood"-red dumbell shapes, but in fluorescence they show more sharply defined structure. (In several areas, including the right dorsal calf image in particular, the scourges are resolved into fine scratches. Three, and in some cases four, parallel scratches can be distinguished.) The scourge marks appear to have been directly imprinted onto the linen because their high-resolution fluorescence characteristics would not otherwise have been preserved. Total cloth—body contact is suggested by the fact that scourge marks with these characteristics are to be found over nearly the entire image area.

The one major deficiency seems to be just how a contact mechanism could have operated to produce the peculiar density gradations. German proposed a model to account for this by postulating the Shroud as originally somewhat stiff either from pressing or possibly starching. When it was laid over the body, it initially contacted only the high points of the profile. During the course of some time, water vapor either from the body tissues or from the damp atmosphere of a tomb, was slowly absorbed into the cloth causing it gradually to lose its stiffness and droop, much like a starched shirt on a damp day. Eventually, the cloth touched all of the body where image is observed.

German suggested that acceptable contour-shading qualities might be generated if the recording mechanism were to permit the image density to vary in proportion to the time of cloth—body contact. According to this argument, longer periods of cloth contact with higher portions of the profile would yield a darker image and the global mapping function, suggested by the earlier work of Jackson et al. [17], would be readily explained. Although Pellicori's latent-image process has not yet specifically allowed for an explicit time-dependence for material transfer, satisfactory density gradations might ultimately be generated with this composite mechanism.

In the meantime, several difficulties with the German model must be resolved. Although this contact transfer may avoid the resolution limitations inherent to Vignon's theory [16], it provides no constraints against diffusion of the sensitizing material into the damp cloth. Moreover, as Jumper noted,

particularly for the facial region, there are no absences (drop outs) in density. (The face is an ideal area to test such a theory, because it is expected to contain the highest contour gradients.) This would imply that the cloth must have become flexible enough to contact every point on the face. Evidently, for the mechanism to have worked, the face contours would either have been much shallower than those typically assumed, or the cloth would have had to have been much more flexible than the Shroud appeared to be.

Another point is that the face shows no evidence of image saturation [55]; that is, with the possible exception of the eyes, the three-dimensional reconstructions show no plateaus [17]. This constraint would require the time-dependence of the German model to be extremely sensitive. The overall superficial nature of the image and the fact that densities at presumed contact points along the profile ridgeline region [17] are not all identical suggest rather severe limits for the assumed distribution of the sensitizing material over the body. Further special assumptions would seem necessary to account for the appearance of the hair.

This entire category of hypotheses is predicated on the assumption that the Shroud was a burial shroud and that the image was formed by some unaided natural mechanism. If the image had been caused by the catalytic action of materials present on the corpse, direct contact of the body with the cloth seems to be the only likely material transfer mechanism. A general problem now becomes apparent. It would seem to follow that the dorsal image area was influenced by the weight of the body whereas the frontal image was imprinted only by the lesser weight of the covering cloth. Recall, however, that the densities at presumed contact points on both frontal and dorsal images do not differ significantly. These characteristics along with the superficial nature of the image would suggest that the contact transfer mechanism is pressure-independent. This apparent contradiction challenges not only the Pellicori—German model but most other hypotheses in this category.

Conclusions

The evidence seems to be quite conclusive for ruling out the Vignon vaporgraphic theory as an image formation hypothesis. Vignon's theory [16] suffers two major problems. First, it has the image residing in chemically transformed (darkened) foreign materials on the cloth, but none of the physical or chemical properties expected for any of the suggested materials has been observed. The second problem is the inadequacy of diffusion transfer to explain the superficial nature of the image or to preserve the observed resolution.

Recent work has attempted to avoid these two difficulties. Pellicori's latent-image recipe [8, 13] adequately accounts for many of the observed image characteristics; it has the image residing in the chemically-transformed cellulose material in the cloth itself. Although Pellicori similarly postulates

the addition of foreign materials, these are assumed to have acted only as catalysts and need no longer be present on the cloth at all. The idea appears promising, but the question remains how the image transfer occurred.

German's time-dependent, direct-contact model would seem to avoid several obvious deficiencies of Vignon's diffusion mechanism. However, it too has met with considerable objections; to produce the qualities observed on the Shroud image, too many special conditions seem necessary. At this time, the image has not been explained completely by the latent image hypothesis chiefly because a satisfactory image-transfer mechanism has not yet been formulated.

"BLOOD"-STAIN COMPOSITION

The discussion thus far has mainly concerned the physical and chemical properties of the body image areas and the question of how the image was formed. Generally, the "blood"-stain observations have little relevance to this problem. The chemical composition of the "blood" provides only circumstantial evidence bearing on the question of the origin of the Shroud. A forger could have used blood to produce the stains, or a genuine shroud, containing an image only, could have been touched up with red paint by someone who was impressed but dissatisfied with the overall effect. Nevertheless, the "blood"-stain composition poses an interesting problem in itself, and the observations may ultimately give some clues to help us understand how the image was formed. For example, one important question that might be answered is whether the "blood" or the image was applied first.

Wilson [1] and Humber [2] have provided qualitative descriptions of the "blood" areas on the Shroud. Frache et al. [59] and Filogamo and Zina [60] documented in more detail the results of their earlier studies on materials removed from a few of these stains. One of the goals of the 1978 investigation was to characterize the "blood" areas further. All of the tests that were performed on the body image, scorches, and background cloth were also applied to the "blood".

Microscopy and photomicrography

Even superficially, the "blood" and image areas appear to be quite different in their color, texture, and composition [33]. At 50X magnification the "blood" looks as if it were applied as a viscous fluid which then flowed around the threads [41, 59] and soaked through to the opposite side of the cloth where it is also visible. The meniscus characteristics of viscous fluids can be seen throughout the "blood" areas. Thread fibers are matted and cemented together. The stains appear brownish-red in reflected white light and crimson in transmission.

The earlier microscopic investigations of Frache et al. [59] revealed the "blood" threads to have slanting or diagonal bands of "granulation" that ranged in color from yellow to red. Filogamo and Zina [60] similarly reported

seeing granular particulates but apparently nothing resembling red corpuscles. Photomicrographs [8] of the "blood" stains reveal amorphous red—orange encrustations between the fibers and in the crevices, with higher concentrations in the valleys at the intersections of warp and weft threads. In some areas it appears as if similar material once on the crowns of the threads had either fallen away or had been mechanically eroded to leave exposed the red—orange stained fibers that are now seen. The color of the individual "blood"-stained fibers is not strictly uniform; colors range from orange—red to yellow—orange.

Heller and Adler [40] reported that under 250—1000× magnification the "blood"-stained fibrils on the tape samples appear either garnet red or brown in color depending on the light source and whether they are observed by reflection or transmission. Generally, the stain appears to surround or coat the fibrils; in some cases, the coatings have become detached and appear as "blood sherds". Heller and Adler examined one of the tape samples, which contained a small, brown crystallite in addition to the "blood"-stained fibrils, by microspectrophotometry in the visible range (400—650 nm). They reported that the crystallite and stained fibrils showed intense Soret absorption (400—450 nm), which indicates the presence of a porphyrinic material.

No more definite material identification was made from these measurements. Characteristic visible band features can be obscured by scattering and absorption processes in both the stain and the cellulose substrate material. The data do suggest the presence of hemoglobin, however. To test this hypothesis, they treated the samples first with a strong reducing agent (97% hydrazine vapor) to reduce the iron to the iron(II) state and then with a strong acid (97% formic acid vapor) to displace the iron. Under near-u.v. radiation, the treated sample "blood" fibrils were seen to fluoresce in the red, confirming the suspected presence of porphyrin and, therefore, also blood in the "blood" areas. Recently, Heller and Adler [37] have also detected bilirubin with a modified Jendrassik method and albumin with bromocresol green; both findings corroborate their earlier conclusion.

It was mentioned earlier that yellow fibrils were observed on tape samples from both "blood"- and pure-image areas. It is important to reiterate here that the respective yellow discolorations differ in several respects. First, those from "blood" areas exhibit a deeper yellow discoloration. (It is probable but not entirely certain that this corresponds to the "shiny honey-yellow" color that Frache et al. [59] reported for the interior fibers of the "blood" threads.) Second, the yellow color in the "blood" areas is clearly a coating that yields positive tests for protein whereas the yellow body-image fibrils do not. The evidence would imply different origins for the two yellow discolorations. It would seem that the yellow material in the "blood" areas derives from blood serum directly.

Radiography and x-ray fluorescence

The radiographs [10] revealed no readily apparent high-density structures that might correspond to the visible "blood" stains. However, the x-ray

fluorescence studies [9] indicated iron concentrations 20—40 $\mu g\ cm^{-2}$ above measured or inferred background levels in the "blood" areas. Morris et al. [9] found these numbers to be generally consistent with the expected quantities of iron in comparable blood stains; however, their measurements could not differentiate between actual blood and iron-based pigments because x-ray fluorescence detects only element concentrations without regard to molecular arrangement.

The excess "blood" iron was the only detectable spectral characteristic that clearly differentiated these stains from the non-"blood" areas. In particular, Morris et al. noted that no potassium signals could be found in any of the "blood" area data. In whole blood, the potassium K_α peaks are typically an order of magnitude smaller than the iron K_α peaks. They are still smaller for blood soaked into a cellulose substrate. Therefore, even if potassium signals were present, they would probably have remained undetected within the substantial noise level in the low-energy range of the x-ray fluorescence spectrum. Heller has suggested that because potassium compounds in blood are quite soluble, they may have been dispersed in the presence of moisture. The failure to detect potassium, therefore, is felt to have no significant bearing on the question of whether the "blood" stains contain blood.

Photoelectric spectrophotometry

Gilbert and Gilbert [12] presented reflectance and fluorescence results from four different "blood"-stain areas. Their relative reflectance data, referenced to the same mean clear-area spectrum, show moderately strong absorption in the wavelength range 320—550 nm. A reflected-density curve was calculated from an average of these relative-reflectance spectra. The averaged density appears to be quite uniform in this short wavelength range, which suggests that no identifiable structures are common to the rather noisy individual spectra. The absorption is weaker at longer wavelengths, but there is a rather interesting reproducible feature at 600—630 nm.

Pellicori [13] has examined the absorption characteristics of whole blood with a Cary 14 spectrophotometer to compare with the Turin results. He found a strong absorption band at 400—420 nm that corresponds to the Soret band, and weaker bands at 530—580 and 625 nm. These effects are far more pronounced in transmission than in reflection; only the weakest band at 625 nm could conceivably correspond to the small structure seen in the Turin data. He also measured absorption spectra for Fe_2O_3 and blood after baking at 60°C for 7.5 h to simulate aging. None of these data resembles the Gilberts' Shroud "blood" absorption spectra in detail, but that of Fe_2O_3 approximates them most nearly. The Gilbert "blood" spectrum is shown along with that for Fe_2O_3 in Fig. 5; the two reflectance curves are quite similar over the greater part of the wavelength range, although the curious "blood"-stain feature at about 630 nm is not observed for Fe_2O_3.

Heller and Adler [40] have noted that there is no specific spectrum for blood per se: the spectral characteristics depend on the chemical state (coordination and decomposition) of the hemoglobin and also on its state of aggregation. They pointed out the strong resemblance of the Gilberts' "blood" data to those for "perturbed" acid methemoglobin, which is a chemical state of blood in which the iron in the hemoglobin has been oxidized [61]. Cameron and George [62] have published absorption spectra for acid methemoglobin in the range 480—640 nm. These data strongly resemble the Gilberts' curves and even include the small absorption structure at about 630 nm. Recent microchemical tests [37] reveal the presence of bile pigments (i.e., decomposition products of porphyrin) in some of the "blood" artifacts. Their presence could account for some of the non-heme peaks seen in the spectral data. Independent measurements on methemoglobin samples by both Adler and Pellicori have shown strong Soret absorption, an observation that is in agreement with the microspectrophotometric results. Pellicori [13] feels that the absence of the Soret peak in the Gilbert reflectance data was due to low signal-to-noise ratios in this wavelength range.

Photoelectric and photographic fluorescence

The Gilberts' spectra show no detectable "blood"-stain fluorescence. The "blood", like the other stains, reduces the background fluorescence but apparently without shifting the maximum to longer wavelengths as observed for image and scorch areas. (According to our earlier interpretation of this effect, the absence of a shift in the fluorescence peak is consistent with the nearly constant absorption characteristics of the "blood" in the 400—600-nm range.) Although the photoelectric fluorescence results are consistent with the nonfluorescent properties of hemoglobin, they have given little specific information about the "blood"-stain composition.

The u.v.-fluorescence photographs of Miller and Pellicori [14] reveal an interesting effect in several nominal image areas where "blood" flows are present: the dark "blood" regions are partially surrounded by margins that appear to fluoresce as intensely as do the non-image background areas. Weaver [3] has published four of these photographs along with drawings to illustrate the "light-colored" margin locations at the side wound, the "nail" wound in the wrist, and the "blood" flow at the right foot on the dorsal image. (At other "blood" locations, such as the flow across the back and the left dorsal foot region, no fluorescent margins are seen.) This unexpected effect is most clearly visible under the special conditions described above, and it is unfortunate that this observation was made only after the direct examination period. Neither photomicrographs, spectral reflectance, nor quantitative fluorescence data are available from these regions to aid our interpretation. Multispectral analysis of these areas has not yet been done.

There are several possible explanations for these light areas. They could represent a direct attempt by an artist to represent blood serum and were perhaps more recognizable at the time the image was produced. A second

possibility is that the effect was accidental; the light areas could have resulted either from a non-pigmented vehicle in the paint used to represent blood or from actual blood serum flowing into the cloth ahead of the red cells or away from them in the case of clot retraction. Miller and Pellicori [14] suggested that the non-pigmented fluid itself may be fluorescing; they demonstrated that blood serum on linen does fluoresce moderately.

Another suggestion is that image is not present in these areas and that background fluorescence is being observed. If this is the case, the non-pigmented flow may have eradicated an existing image or it may have reduced or altogether prevented image formation. Heller considers the first possibility to be rather unlikely. In view of the conclusions that the "blood" is blood and that the image is a cellulose degradation effect, there seem to be no likely reactions capable of eradicating the image in any way resembling the spot tests with strong reductant mentioned earlier. The second possibility is more plausible and all the more interesting because it is difficult to reconcile with the image as an artistic production. It would be quite difficult to paint blood onto a cloth before image production with sufficient accuracy to index with every desired image location after image production. It seems more logical that an artist would have superimposed the blood on an existing image.

At this time, the fluorescent blood-margins are not well understood, but it would seem that they derive in some way from blood serum that had been isolated by clot retraction, probably before it was applied to the cloth. The "blood" areas, particularly in these peripheral regions, should be a subject of considerable interest in future studies.

Conclusions

The evidence seems to be sufficient to conclude that the Shroud "blood" areas are blood. The presence of protein, bilirubin, and albumin, the optical absorption and fluorescence characteristics of individual fibrils, and the iron concentrations determined by x-ray fluorescence, all support this hypothesis. This contradicts earlier tentative conclusions [59, 60] that were drawn mainly from the negative results of less sensitive tests.

At this time, the most interesting unanswered question is whether the blood or the image was applied first. So far, the results of most tests have provided little information pertaining to this problem. Conclusions have been drawn only for rather specific instances. For example, if the blood had been applied initially and the image then scorched, there might be burnt blood similar to that seen near burned areas from the 1532 fire. The fact that the blood areas are not obviously scorched argues against this particular hypothesis. Future studies should be directed at this problem.

CLOTH CHARACTERISTICS

There are two objectives in our attempt to establish a broad scientific data base for the Shroud. The first is to learn about the origin of the cloth

and how the image was created. The second and perhaps more important objective is to evaluate the current physical condition of the Shroud and to support valid recommendations for its preservation.

Although the first of these has been dealt with, concern over proper and immediate conservation measures is justified. In 1978, the backing cloth was partially removed from the Shroud in the vicinity of the dorsal foot region. The reverse side of the Shroud appeared whiter than the image side. Evidently, the topside has darkened, and there is some fear that progressive deterioration and soiling will decrease the relative contrast between the image and background. Riggi found both fungi and spores in his vacuumed-material samples. Also, the atmospheric conditions of the urban environment in Turin could be particularly damaging to the image and fabric. To our knowledge, only Curto [33] and Pellicori [13] have published any specific recommendations toward conservation. Members of the Shroud of Turin Research Project hope that their contributions will aid and interest textile conservators and others qualified to address the problem.

Observations on fabric and thread

The following discussion concerns specific observations of the fabric and threads. The 4.3 × 1.1 m Shroud appears to consist of two panels of visually identical linen material joined together lengthwise by a seam which is 4—5 mm wide. The image is located wholly on the larger "main" section of the cloth. Apparently sewn to this main section is the so-called side strip that varies in width between 7.8 and 8.4 cm. The 1973 Turin Commission Report [5] contains some documentation on the cloth. Delorenzi [63] recorded visual observations of the patch and repair stitching, and Raes [64] reported his work on samples of extracted material.

Raes examined two threads (1 warp and 1 weft) from the main portion of the cloth and a triangular-shaped sample (about 40 mm wide × 42 mm high) of the fabric that had been removed from one end of the Shroud along the edge (see Figs. 1 and 7). The triangular-shaped sample evidently consisted of two pieces: one from the main section and one from the side strip. Raes reported both pieces to have the same herringbone 3:1 twill weave but, because this type of weave is not particularly distinctive, could not determine where or when the cloth had originated. Weft threads from the two pieces were found to differ somewhat in diameter although the number of weft threads per centimeter were virtually identical. Raes was unable to tell whether or not the main cloth and side strip were of different manufacture because of the short thread lengths that were available to him.

More recent data have provided supplementary information. The radiograph, shown in Fig. 7, suggests that the side strip either is, or at least was, at one time an integral portion of the full cloth. In this particular area, there are alternating high- and low-material-density "bands" that evidently correspond to weft lots of different weight used in the weaving. (The visible-light transmission photographs of Schwortz also clearly show these struc-

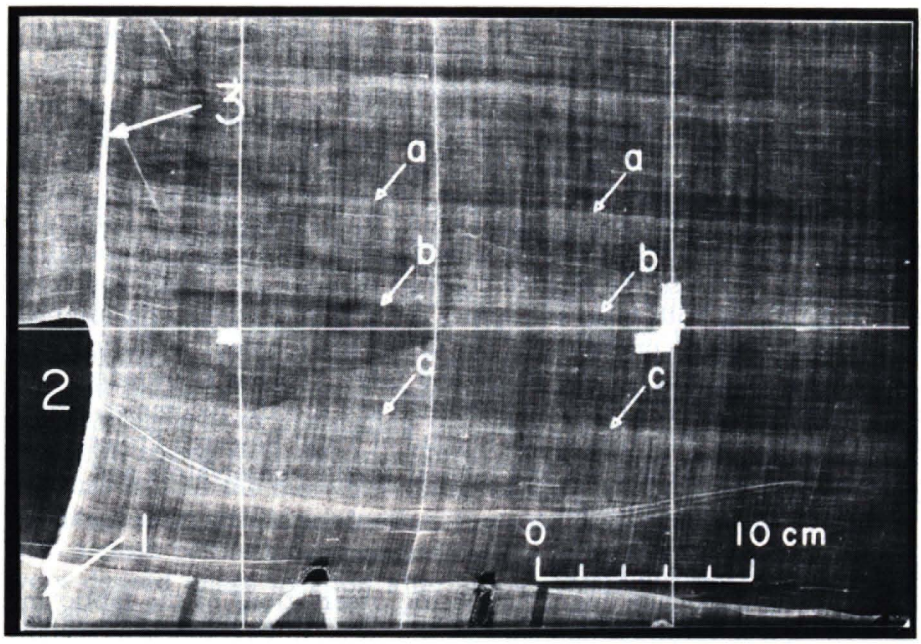

Fig. 7. Radiograph of the Shroud area indicated at the bottom of Fig. 1. The area labeled 1 in this figure is where the Raes [64] fabric sample was taken. The area labeled 2 designates a cutout portion of the Shroud where only the backing cloth is present. Alternating high- and low-density bands, orientated horizontally in this figure (three boundaries are indicated by the arrow sets labeled a, b and c), are continuous through the seam (3) and suggest that the so-called side strip either is or was at one time an integral part of the main section of the Shroud.

tures.) The density variations of the material are apparently associated with the Shroud, because they are not visible in the cut-out portion in which only the backing cloth is present. The distinct weft structure is continuous across the seam joining the two panels and strongly suggests that the side strip and the main section were of a single manufacture. A more careful examination of the seam needs to be made to determine whether the side strip was actually detached.

The Raes report contained two further, rather interesting findings that have been confirmed by J. L. Janney and other members of the Project team. First, the Shroud threads were spun in the Z-direction, which is apparently somewhat unusual. Egyptian linen, for example, was typically spun in the S-direction to conform to the natural twist that flax assumes upon drying [65]. (Raes observed that the linen thread used to sew together the two pieces of his fabric sample was spun in the S-direction.) Second, Raes found small traces of cotton fibers included in both warp and weft threads from the main-cloth section. He was able to identify these from the number of reversals per centimeter as *G. herbaceum*, a common Middle East variety.

The small quantities of cotton present suggested to him that perhaps the Shroud linen had been spun with the same equipment used previously for cotton. The observation of cotton-fiber inclusions is particularly interesting, because it would suggest a Middle-East manufacture. Beyond this, however, neither observation is sufficient to locate the Shroud's origin unambiguously.

Carbon-14 and areal cloth densities

It is clear that none of the available data provide any substantial clues to the actual age of the Shroud. Lack of this fundamental information has, in fact, been the greatest obstacle in interpreting the results fully. The only universally accepted technique for obtaining a satisfactory age for objects of this sort is the carbon-14 method. However, Shroud custodians have been reluctant to sacrifice the rather large amounts of material required for conventional ^{14}C testing. Earlier recommendations and decisions to postpone these tests were quite justified at the time.

In recent years, however, new methods have been developed that require only minute samples. Purser et al. [66] have provided an excellent review of the latest ultra-sensitive particle identification techniques and their capabilities. In particular, they described the Rochester tandem Van de Graaff system that operates on essentially the same principle as conventional mass spectrometers. The advantage of this system is that negative ions are accelerated to MeV/amu energies and can provide high resolution and transmission with exceedingly low background levels. Accelerator carbon-dating techniques have demonstrated accuracies (±150 years for 2000-year-old samples) that are similar to those of the more familiar radioactive counting methods but are orders of magnitude more sensitive. Purser et al. quote sensitivities of $1:3 \times 10^{15}$ for ^{14}C in natural carbon and can date milligram-weight samples in a few hours. Measurements on a 2000-year-old Egyptian bull mummy cloth have given accurate results [67] and demonstrate that this technique could be readily applied to similar samples from the Shroud.

Given that milligram-weight carbon samples are sufficient for reliable dating measurements, these numbers are now related to areal cloth dimensions. An indirect estimate of the areal weight density of the Shroud can be made by measuring those of modern linen with comparable thickness, weave density, and thread diameters. These data are available. Jackson and Rogers measured the fabric thickness of the Shroud at three widely separated points and found it to be 345 ± 22 μm. (Measurements of the Shroud plus backing cloth together yielded 615 ± 29 μm.) Raes [64] quoted 38.6 cm^{-1} and 25.5 cm^{-1} respectively for the number of warp and weft threads in the weave of the sample taken from the main cloth. Mottern et al. [10] estimated thread diameters to be nominally 0.15 mm. Edgerton prepared samples of linen cloth to conform to the most recent Shroud data (although her thread diameters were larger) and found an areal density of 23.7 mg cm^{-2}. Edgerton's result agrees remarkably well with the value 23.4 mg cm^{-2} that Timossi [68] derived earlier using essentially this same approach.

Other indirect estimates can be made from the 1978 data. Morris et al. [9] measured peak intensities for Compton scatter from the Shroud and backing cloth together. These results gave combined cloth areal densities between 30 and 40 mg cm^{-2} at various locations and an average value of about 35 mg cm^{-2} (see note 9). If this average composite value is multiplied by the ratio of the Shroud to total cloth thickness values quoted above, a Shroud density of 20 ± 5 mg cm^{-2} is found. However, this figure is believed to be low because of the comparatively open weave structure of the backing cloth. Cloth-density ratios derived from the radiographic data combined with the double-cloth values of Morris et al. place Shroud areal densities between 25 and 30 mg cm^{-2} (see note 10). Even allowing for a weight recovery of 20% carbon from a given sample, the estimates show that a radiocarbon date can be easily made with the equivalent of about 1 cm^2 of Shroud material. This amount of fabric has already been removed from the Shroud [41]. While some may argue that intact material should be saved for further non-destructive testing, large amounts of material could be removed from beneath the patches. Mottern et al. presented a radiograph of one of the patched-hole areas that reveals some of the Shroud material that could be recovered; a total Shroud area of approximately 400 cm^2 lies concealed beneath all of the patch work. This is sufficient for literally hundreds of carbon-14 tests with the latest techniques. Any of this material could be removed without affecting the visual appearance of the Shroud or damaging the fabric structure. (Indeed, as a conservation measure, this charred material should be removed to prevent further irreversible soil-contamination of the cloth.)

CONCLUSION

The purpose of this report has been to review the rather substantial collection of available scientific observations on the Shroud of Turin. These are now sufficient to allow some evaluation of selected hypotheses on image formation. Properties of the faint image and its peculiar density shading were noted as the outset. Three-dimensional profiles, generated from the frontal image densities, strongly resemble the human form and suggest that a simple global mapping function may relate the two. Unfortunately these phenomenological studies have implied nothing more definite about the image-transfer process. The faint and apparently negative image characteristics have likewise proven little, although the combined evidence does suggest that rather severe difficulties would have been encountered with conventional painting techniques.

The primary conclusion is that the image does not reside in an applied pigment. The reflectance, fluorescence, and chemical characteristics of the Shroud image indicate rather that the image recording mechanism involved some cellulose oxidation/dehydration process. It is not possible yet to say definitely whether these chemical modifications were produced by scorching

or by some sensitized thermal or photochemical reaction. The fluorescent properties of scorches may eliminate them from consideration, but more detailed investigations are required to rule out scorch hypotheses generally.

Much has been learned about the density shading and chemical properties of the image, but, so far, there are no firm ideas about how the image may have been applied to the cloth. Again, Jackson's three-dimensional studies and the global consistency of the image suggest that some global mechanism was involved; however, nothing more specific can be concluded. Nonetheless, the choices are narrowed somewhat. Resolution considerations and the lack of gross distortion of the image in high profile-gradient regions argue against three-dimensional "hot-statue" hypotheses, although the remote possibility of contact or radiant thermal energy transfer from a flat model cannot yet be dismissed. If the image proves to be a chemically-induced cellulose modification instead of a scorch, it would be seen that the material transfer must have been accomplished by direct contact. (The superficial nature of the image eliminates a vapor diffusion mechanism.) Several contact-transfer models were considered, but none seems totally practical or convincing.

Several important questions about the Shroud have been answered to our satisfaction. For example, it is believed that the "blood" stains are indeed blood. Yet many questions remain. Some of these can be addressed with currently available data (especially in the areas of computer analysis of the image and forensic pathology [69]); others must await the results of future testing. The most important outstanding problems pertain to the image transfer mechanism. Briefly stated, we seem to know what the image is chemically, but how it got there remains a mystery. The dilemma is not one of choosing from among a variety of likely transfer mechanisms but rather that no technologically-credible process has been postulated that satisfies all the characteristics of the existing image.

With all of the questions concerning variations of contrast with time, latent images, artistic styles and techniques, few further definite conclusions are possible without information about the age of the cloth. Given the unique nature and complexity of the problem, the only unambiguous means to establish this is by the carbon-14 method. An objective date, even to within a century or two, is essential for judging the relative likelihood of the many image hypotheses considered here. The additional information will also greatly aid in taking proper conservation measures and in planning future research.

The Shroud of Turin Research Project is a non-profit organization supported solely by contributions from private individuals. This research is a product of volunteer efforts by all the project members. Most of the material used in this article has been drawn from the published scientific literature, although unpublished data and ideas from other members of the project are also included. The following members, in particular, contributed significantly to the present work through their discussion and critical reading of the

manuscript: J. S. Accetta, Lockheed Corp.; A. D. Adler, West Connecticut State College; J. D. German, U. S. Air Force Weapons Laboratory; V. D. Miller, Brooks Institute; R. H. Dinegar, D. H. Janney, J. L. Janney, J. R. London, R. A. Morris, and D. M. Soran, Los Alamos National Laboratory; T. F. D'Muhala and G. Markowski, Nuclear Technology Corporation; R. Gilbert and M. Gilbert, Oriel Corporation; J. H. Heller, New England Institute; J. P. Jackson, University of Colorado; R. D. LaRue Jr., U.S. Air Force Academy; E. J. Jumper, Wright-Patterson Air Force Base; D. J. Lynn and J. J. Lorre, Jet Propulsion Laboratory; R. W. Mottern, Sandia National Laboratory; S. F. Pellicori, Santa Barbara Research Center; G. Riggi, Societa Progettazione Riggi; B. M. Schwortz, Barrie M. Schwortz Photography; K. Stevenson, IBM.

The authors thank B. M. Schwortz for providing some of the photographs used in this article, H. W. Johnson for the remaining photographic and overlay work, J. Druzik of the Los Angeles County Museum of Art for many helpful suggestions, Alan Wreigard of 3M Corporation for providing the tape used in these studies, the personnel of Instruments S. A., Metuchen, NJ, for providing the laser-microprobe Raman results, the personnel of the Midwest Center for Mass Spectrometry at the University of Nebraska, Lincoln, NE 68588, for providing the mass spectrometric results, K. Edgerton for providing the "modern/primitive" samples, and the Italian authorities for lending us the thread samples for nondestructive testing.

NOTES

1. The term "image formation" is used here to describe the composite process of image transfer and recording, where "transfer" refers specifically to application mechanisms such as direct contact, diffusion, or radiation, and "recording" phenomena generally pertain to the visible element of the image, i.e., its material composition, whether it be a pigment or an altered cellulose structure on the cloth surface. The latter term will also be used in reference to chemical processes involved in cellulose transformation.

2. For example, Wilson [28] recalled the rumor in 1532 that the Shroud had been completely destroyed in the fire. If this were true, the object we observe today may have been produced sometime before its "reappearance" in 1534 by some Italian Renaissance craftsman. We have neither physical nor chemical evidence to support this rumor. Indeed, the observations of silver fragments and burnt blood [37] as well as the red fluorescence of the pyrolyzed cloth areas [14] are in full accord with the historical documentation of the fire. As another possibility, Gabrielli [29] suspected that the image was produced by some printing technique in the late 15th or early 16th century but before the 1532 fire.

3. This is deduced from direct observations of the underside of the cloth near the dorsal foot region. Gonella has questioned this conclusion on the basis of the discussion presented under the faint image properties because the observation could only be made at close range. However, we were looking specifically for surface discolorations on underside cloth areas that directly correspond to the "top" surface image. Even so, the observation that image discoloration resides only on the top few fiber thicknesses testifies far more strongly to the superficial nature of the image.

4. In 1973, Frei [34] took similar sticky-tape samples, and found and identified pollen from 48 different plants. He stated that some of these plant species are native to central Europe, although others are indigenous only to Palestine and still others to Asia Minor

and the region about Constantinople. Frei takes this as evidence for the Shroud having been in each of these regions during its history and exposed to the environment. Very few pollen were observed on the tape samples taken in the present Project, and no effort was made to identify them.

5. According to Thompson [38], the most important yellow in medieval painting was gold metal. One of the most important services provided by other yellow pigments was to imitate gold and to modify greens and reds. Their least important function was to represent yellow things! Some of the inorganic pigments that were commonly used in the 14th century are yellow ocher (hydrated Fe_2O_3), orpiment (As_2S_3), realgar (As_2S_2), giallulinum (possibly Naples Yellow $Pb_3[SbO_4]$ or massicot PbO), and mosaic gold (SnS_2). Organic dyes include saffron which was often mixed with glair and varnishes. Bile yellows, buckthorn, and weld were used as lake pigments.

6. Morris et al. [9] were concerned that the detected trace elements may not have been uniquely associated with the Shroud. The ambiguity arose because the Holland backing cloth could not be removed from the Shroud for the measurements; technically, their data pertain to the double-cloth system. However, thirteen threads, removed from non-image, non-blood areas of the Shroud in November 1973 [41], were brought to America following the Turin study. X-ray fluorescence measurements were made on these with isotope sources of ^{55}Fe, ^{109}Cd, ^{145}Sm, and ^{57}Co for counting periods of 500—1000 min. These results showed roughly the same relative concentrations of calcium, strontium, and iron that were observed in the original 1978 Turin data. In addition, they showed smaller traces of potassium, chlorine, and possibly lead. The small sizes of the thread samples precluded quantitative estimates for these traces, but the later results suggest that the reported Turin measurements do pertain to the Shroud.

7. The hypothesis that these holes were burned through with a hot poker is probably incorrect. Close inspection of the peripheral areas reveals a foreign material there, resembling pitch. The radiographs also show high density structures that support this observation. This earlier damage may have resulted from burning pitch that perhaps fell onto the Shroud from a torch.

8. Definition on this point is admittedly vague. Certainly, the resolution of the image on the cloth is ultimately limited to about 0.02 cm by the weave structure. However, when the term "resolution" is used here we assume the existence of a uniquely defined parameter that is characteristic of a mechanism of image formation, as yet unknown. Given this assumption, the "resolution" can only be inferred by measuring distances between closely spaced but visually distinct image features; typically the lips have been taken for this estimate. Pellicori [13] quoted 0.5 cm for the minimum resolvable feature; Jackson [50] used 0.6 cm in his theoretical studies. Later, Jackson suggested a parameter that pertains strictly to a model that involves a cloth-draped three-dimensional human figure: d/D where d is the cloth—body distance and D is the distance between two marginally resolved points. He estimates this ratio to be about 1.6 ± 0.8 for the lips. All of these values should be understood as lower bounds; until the image formation mechanism is known, the resolution limit cannot be determined exactly.

9. For the Shroud and backing cloth, Mottern et al. [10] estimated a total density of 66 mg cm^{-2} which is too large. The average density of 35 mg cm^{-2}, quoted here, yields a total weight of 1.66 kg which is more nearly consistent with the value 2.47 kg measured directly by Gonella. The 810-g difference may be attributed to additional, appended material. The Shroud and Holland cloth are surrounded by a blue fabric border. Sewn to this along the length is a piece of red silk (ca. 4.3×1.0 m) that is intended to protect the image surface while the Shroud is stored in its rolled configuration.

10. The film densities of both the backing cloth (through 38 existing holes in the Shroud) and adjacent double-cloth areas were measured from the set of DR films of Mottern et al. [10]. The film density differences, which represent the attenuation caused only by the Shroud material, were typically in the range 0.4—0.5. We then assembled a Balteau radiograph system to duplicate the geometry, inherent beryllium-window filtration,

and atmospheric pressure conditions in Turin. Several calibration curves of DR film density versus cellulose areal density were generated to match nominal film densities (1.8—2.3) of the Turin radiographs at double cloth thicknesses to the corresponding double-cloth weight densities (30—40 mg cm^{-2}) reported by Morris et al. [9]. These combined data then showed the Shroud areal density to be about 25—30 mg cm^{-2}. The close correspondence of these results to those obtained indirectly corroborates the validity of the quantitative elemental concentrations published by Morris et al.

REFERENCES

1 I. Wilson, The Shroud of Turin, Doubleday, New York, 1978.
2 T. Humber, The Sacred Shroud, Pocket Books, New York, 1977.
3 K. F. Weaver, Nat. Geogr. Mag., 157 (1980) 730.
4 B. J. Culliton, Science, 201 (1978) 235.
5 Report of the Turin Commission on the Holy Shroud, Screenpro Films, 5 Meard St., London W1V 3HQ, 1976.
6 K. Stevenson (Ed.), Proceedings of the 1977 United States Conference of Research on the Shroud of Turin, Holy Shroud Guild, 294 East 150 St., Bronx, NY 10451, 1977.
7 E. J. Jumper and R. W. Mottern, Appl. Opt., 19 (1980) 1909.
8 S. F. Pellicori and M. S. Evans, Archeology, 34 (1981) 34.
9 R. A. Morris, L. A. Schwalbe and J. E. London, X-Ray Spectrom., 9 (1980) 40.
10 R. W. Mottern, J. R. London and R. A. Morris, Mater. Eval., 38 (1980) 39.
11 J. S. Accetta and J. S. Baumgart, Appl. Opt., 19 (1980) 1921.
12 R. Gilbert and M. Gilbert, Appl. Opt., 19 (1980) 1930.
13 S. F. Pellicori, Appl. Opt., 19 (1980) 1913.
14 V. D. Miller and S. F. Pellicori, J. Biol. Photogr. Assoc., 49 (1981) 71.
15 F. Ratliff, Sci. Am., 226 (1972) 90.
16 P. Vignon, The Shroud of Christ, Reprinted by University Books, New Hyde Park, New York, 1970.
17 J. P. Jackson, E. J. Jumper, R. W. Mottern and K. Stevenson, in Ref. [6], p. 74.
18 J. D. German Jr., in Ref. [6], p. 234.
19 R. D. LaRue Jr., in Ref. [6], p. 219.
20 G. B. Judica Cordiglia, Ref. [5], p. 93.
21 T. M. McCown, in Ref. [6], p. 95.
22 D. Devan, in Ref. [6], p. 136.
23 D. H. Janney, in Ref. [6], p. 146.
24 J. J. Lorre and D. J. Lynn, in Ref. [6], p. 154.
25 J. P. Jackson, in Ref. [6], p. 190.
26 I. Wilson, Ref. [1], p. 230.
27 T. Humber, Ref. [2], p. 216.
28 I. Wilson, Ref. [1], p. 191.
29 N. Gabrielli, Ref. [5], p. 87.
30 J. Nickell, Humanist, 38 (1978) 20.
31 J. Nickell, Pop. Photogr., 85 (1979) 97.
32 R. A. Gorkin, Science, 201 (1978) 1080.
33 S. Curto, Ref. [5], p. 59.
34 M. Frei, Naturwiss. Rundsh., 32 (1979) 133.
35 W. C. McCrone and C. Skirius, Microscope, 28 (1980) 105.
36 W. C. McCrone, Microscope, 28 (1980) 115.
37 J. H. Heller and A. D. Adler, J. Forensic Sci., to be published.
38 D. V. Thompson, The Materials and Techniques of Medieval Painting, Reprinted by Dover, New York, 1956.
39 R. G. Gettens and G. L. Stout, Painting Materials: A Short Encyclopedia, Reprinted by Dover, New York, 1966.

40 J. H. Heller and A. D. Adler, Appl. Opt., 19 (1980) 2742.
41 P. Caramello, J. Cottino and E. Delorenzi, Ref. [5], p. 19.
42 W. C. McCrone, Microscope, 29 (1981) 19.
43 E. Ott, H. M. Spurlin and M. W. Grafflin, High Polymers, Vol. V, 2nd edn., Part I, Cellulose and Cellulose Derivatives, Wiley—Interscience, New York, 1954, p. 29.
44 N. M. Bikales and L. Segal, High Polymers, Vol. V, Part V, Cellulose and Cellulose Derivatives, Wiley—Interscience, New York, 1971, pp. 1015—1078.
45 J. A. T. Robinson, in Ref. [6], p. 23.
46 P. Barbet, A Doctor at Calvary, Image Books, New York, 1963.
47 G. Ashe, Sindon, 15 (1966) 15.
48 R. Drakoff, Science, 201 (1978) 774.
49 B. Graham, Science, 201 (1978) 774.
50 J. P. Jackson, in Ref. [6], p. 223.
51 G. G. Gubareff, J. E. Janssen and R. H. Torborg, Thermal Radiation Properties Survey, 2nd edn., Honeywell Research Center, Minneapolis—Honeywell Regulator Company, Minneapolis, 1960, pp. 16—19.
52 C. S. Smith, Science, 201 (1978) 572.
53 C. L. Eastlake, Methods and Materials of Painting of the Great Schools and Masters, Dover, New York, 1960, Chap. 5.
54 P. Vignon and E. A. Wuenschel, Sci. Am., 156 (1937) 162.
55 E. J. Jumper, in Ref. [6], p. 182.
56 T. Humber, Ref. [2], p. 185.
57 A. L. Lorincz, in S. Rothman (Ed.), The Human Integument Normal and Abnormal, Publication No. 54 of the AAAS, Washington DC, 1959, pp. 127—150.
58 R. N. Rogers, in Ref. [6], p. 131.
59 G. Frache, E. Mari Rizzatti and E. Mari, Ref. [5], p. 49.
60 G. Filogamo and A. Zina, Ref. [5], p. 55.
61 R. Lemberg and J. W. Legge, Hematin Compounds and Bile Pigments, Interscience, New York, 1949, pp. 207—229.
62 B. F. Cameron and P. George, Biochem. Biophys. Acta, 194 (1969) 16.
63 E. Delorenzi, Ref. [5], p. 107.
64 G. Raes, Ref. [5], p. 79.
65 A. Lucas and J. R. Harris, Ancient Egyptian Materials and Industries, 4th edn., Edward Arnold, London, 1962, p. 141.
66 K. H. Purser, A. E. Litherland and H. E. Gove, Nucl. Instrum. Methods, 162 (1979) 637.
67 H. E. Gove, D. Elmore, R. Ferraro, R. P. Beukens, K. H. Chang, L. R. Kilius, H. W. Lee, A. E. Litherland, K. H. Purser and M. Rubin, Radiocarbon, 22 (1980) 785.
68 A. Timossi, La S. Sindone nella sua Constituzione Tessile, Torino, 1933.
69 R. Bucklin, Medicine, Science, and the Law, 1970, pp. 14—26.

Analytica Chimica Acta, 135 (1982) 51—59
Elsevier Scientific Publishing Company, Amsterdam — Printed in The Netherlands

CRITICAL EVALUATION OF THE APPLICABILITY OF NEUTRAL CARRIER-BASED CALCIUM SELECTIVE MICROELECTRODES

F. LANTER, R. A. STEINER, D. AMMANN and W. SIMON*

Department of Organic Chemistry, Swiss Federal Institute of Technology, CH-8092 Zürich (Switzerland)

(Received 7th September 1981)

SUMMARY

The performance of calcium ion-selective microelectrodes based on a neutral carrier for extra- and intra-cellular measurements of free Ca^{2+} ions as reported in the recent literature is assessed. A novel membrane consisting of readily available components is presented which overcomes the technical problems associated with very fine electrode tips. Measured selectivity factors, log K^{pot}_{CaM}, for M^{z+} = Na^+, K^+, and Mg^{2+} are −5.5, −5.4, and < -4.9, respectively.

The recent literature documents the widespread use of ion-selective microelectrodes for the intra- as well as extra-cellular measurement of free Ca^{2+} [1—66] . With rare exceptions [1—4], intracellular studies of Ca^{2+} activities are being done with electrodes based on the neutral carrier (−)-(*R*,*R*)-*N*,*N*'-bis(11-ethoxycarbonyl)undecyl)-*N*,*N*',4,5-tetramethyl-3,6-dioxaoctane diamide [67, 68] (ETH 1001) [5—25]. The poor selectivities of electrodes based on esters of phosphoric acid, e.g., bis[*p*-(1,1,3,3-tetramethylbutyl(phenyl]-phosphoric acid (*t*-HDOPP [1—4, 69]), especially with respect to Mg^{2+} ions (selectivity factors log K^{pot}_{CaMg} −3.3 to −3.6 [70]), hinder their reliable use in intracellular environments [71, 72]. They therefore will not be discussed further in this report.

Until very recently, neutral carrier-based microelectrodes with tip diameters of $\geqslant 1$ μm, that did not lead to severe technical problems, have mainly been used. It has lately been shown that electrodes with tip diameters of <1 μm in a certain activity range often exhibit a response above the theoretical slope and a rather high detection limit (see Fig. 1) [14, 21]. In this report, different methods of electrode preparation are compared, and simple solutions are proposed for eliminating the problems encountered.

EXPERIMENTAL

Ion-selective ligand and electrode system

The synthesis of the ionophore ETH 1001 has been described [73]. The ligand (cat. no. 21192) and other necessary membrane components are commercially available (Fluka, CH-9470 Buchs).

0003-2670/82/0000-0000/$02.75

The ion-selective liquids used by Tsien and Rink [71] and O'Doherty et al. [24] were prepared exactly according to the prescriptions recommended by those authors. Our original membrane consists of 10% (w/w) ligand, 1% (w/w) sodium tetraphenylborate (NaTPB) and 89% (w/w) *o*-nitrophenyloctyl ether (*o*-NPOE) [67]. To obtain the PVC-containing Ca^{2+}-selective membrane, 14% (w/w) of poly(vinyl chloride) (PVC S704, hochmolekular, Lonza, CH-3930 Visp) was added to the ion-selective liquid mentioned above. The components were then dissolved in about 3 times their weight of freshly distilled tetrahydrofuran (THF) to give a viscous liquid.

Cells of the type Ag;AgCl, 3 M KCl/sample solution//membrane//Ca^{2+}-buffer solution/AgCl;Ag were used. The buffer solution (internal filling solution) contained 10^{-4} M calcium chloride, 1.1×10^{-3} M nitrilotriacetic acid (NTA), 4.7×10^{-2} M sodium tetraborate ($I = 0.1$, $[Na^+] = 9.4 \times 10^{-2}$ M, pCa 6.77). The external reference microelectrode had a tip diameter of about 3 μm.

Ion-selective microelectrodes

Glass micropipets were drawn from single-barreled pyrex capillary tubing (GC150T-15, Clark Electromedical Instruments, Pangbourne, Reading, England), which had been cleaned as described elsewhere [21]. The so-treated glass tubing was dried at 200° C for at least 24 h and stored over silica gel. The tips of the micropipets were broken on the polished surface of a pyrex glass rod advanced under microscopic observation by a micromanipulator. The resulting outer diameters of the tips were in the range 0.8—1.0 μm. To get even smaller tip diameters, the breaking procedure was omitted.

Silanization techniques. For tip diameters of $\geqslant 1$ μm, the technique introduced by Neher and Lux [74] was slightly modified. The micropipets, filled with the internal filling solution, were dipped into a solution of 5% (w/w) dichlorodimethylsilane in tetrachloromethane. A syringe was used to suck the silane solution up to a height of around 200 μm and then push it out. The sucking and blowing were repeated about 5 times. The microelectrodes were then ready to be filled with the ion-selective liquid.

A silanization treatment with hot silane vapor was chosen for tip diameters of <1 μm. The micropipets, placed in and covered with glass beakers, were pre-dried at 200° C for at least 30 min. Then a small amount (≈ 50 μl) of *N*-trimethylsilyldimethylamine (TMSDMA, purum, Fluka) was injected into the beaker. The hot vapor was allowed to react with the glass surface at 200° C for approximately 30 min. Then the covering glass beaker was removed and the micropipets were kept another 10 min at 200° C before use.

Filling methods. Microelectrodes with tip diameters in the range 0.8—2.0 μm were first filled with the internal filling solution and then dipped into the ion-selective liquid, which often spontaneously filled the siliconized part. If PVC-containing membrane material was used, suction was applied until there was a column of about 100 μm inside the tip. Finally, a silver/silver

chloride wire connected with a small silver plug was dipped into the internal filling solution. The electrode was sealed with wax (Deiberit 502; L. Böhme, D-3423 Bad Sachsa/Harz). This technique has been applied to electrodes with tip diameters of about 0.5 μm [21].

Microelectrodes with tip diameters $\leqslant$0.8 μm (non-broken) were filled by use of a syringe and as fine as possible plastic tubing. A small volume of the ion-selective liquid was injected into the top of the microelectrode shank (height $\approx$ 5 mm) and moved to the very tip by use of pressure. The micropipet was then back-filled with the internal filling solution and the preparation was completed as described above. For PVC-containing membranes, this method cannot be used.

E.m.f. measurements

The e.m.f. measurements were made at 22 ± 0.5°C (relative humidity $\approx$65%) with a FET operational amplifier (AD 515 L, Analog Devices, Norwood, MA; input impedance $10^{13}\Omega$/1.6 pF differential, $10^{15}\Omega$/0.8 pF common mode; input bias current <75 fA; capacity neutralization). The amplifier was mounted on top of the electrode. The electrode assembly and other high-impedance components were located inside a faraday cage.

The given selectivity factors for the microelectrode, log K^{pot}_{CaM}, were obtained by the fixed interference method [75]. The activity coefficients used have been described in detail [76, 77]. To obtain the e.m.f. response curves (e.m.f. vs. log a_{Ca}), the experimental e.m.f. values were corrected for changes in the liquid junction potential by using the Henderson formulae [76, 77].

Calcium buffer solutions

The compositions of the calcium ion buffer solutions containing K^+ and Na^+ ions, which were used as calibration solutions, were calculated as described by Tsien and Rink [21] and Růžička et al. [78], respectively. The stability constants used by Růžička et al. for the calculation of Na^+-containing Ca^{2+} buffer solutions were adapted to those used by Tsien and Rink [21]. The final activities of free calcium were checked [79] with a calcium-selective macroelectrode (see also Fig. 3). The solutions for the determination of the selectivity factor, log K^{pot}_{CaMg}, were not buffered.

All solutions were made with salts of high purity (Fluka or Merck) and water doubly-distilled from quartz apparatus.

RESULTS AND DISCUSSION

The performance of ion-selective microelectrodes highly depends not only on the membrane composition but on the geometry of the glass pipets used. The Ca^{2+}-selective liquid introduced by Oehme et al. [67] in 1976 became one of the most reliable tools for determining intra- as well as extra-cellular activities of free Ca^{2+} when it was used in electrodes with tip diameters of

$\geqslant 1$ μm [5—17, 26—66]. For such electrodes, the geometry (e.g., tip diameter, thickness of the glass wall at the very tip) and the silanization technique used did not influence the electrode performance significantly. In order to measure free Ca^{2+} in small cells, electrodes with tip diameters below 1 μm had to be produced. Because of this reduction in tip size, the behaviour of the microelectrode cell assembly often deviated from the behaviour observed for larger tips. A collection of e.m.f. response curves published in the recent literature is shown in Fig. 1. An over-Nernstian slope in the range 10^{-4}—10^{-6} M Ca^{2+} and a rather high detection limit were observed by Coray et al. [14] (curve 1) and Tsien and Rink [71] (curve 2), yet Lee et al. [10] reported extremely low detection limits (curve 5) with the original membrane material [67]. Because problems of over-Nernstian slope and/or high detection limit might be due to kinetic limitations in the diffusion of Ca^{2+} and interfering ions between membrane phase and sample solution [80, 81], the NaTPB in the membrane was replaced by other salts. By incorporating tetraphenylphosphonium bis(1,3-diethyl-2-thiobarbiturate)trimethineoxonol [21] (curve 3) or tetraphenylarsonium tetrakis(*p*-biphenylyl)borate [71] and calcium 3,5-dibromosalicylate curve 4 [24] respectively, over-Nernstian slopes were apparently eliminated. In agreement with Tsien and Rink [71], we were unable to reproduce fully the latter results [24] with our preparation and measuring technique. Unfortunately, the technique used by Tsien and Rink also deviates from the procedure described

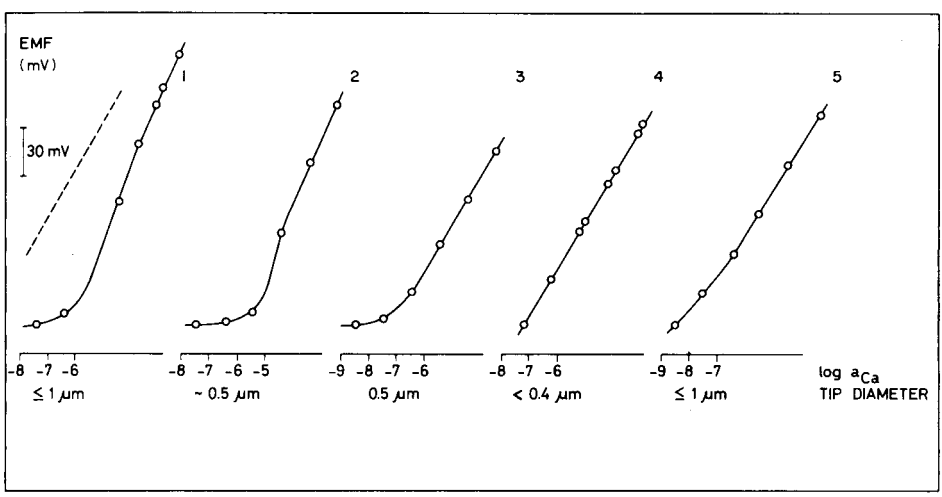

Fig. 1. Calcium-electrode functions of various liquid-membrane microelectrodes based on the synthetic neutral carrier ETH 1001, as published in the recent literature. Dashed line: theoretical slope of 29.3 mV at 22°C. Curves: (1) Coray et al. [14]; (2) Tsien and Rink [71]; (3) Tsien and Rink [21]; (4) O'Doherty et al. [24]; (5) Lee et al. [10]. Silanization is done by various gaseous techniques.

by O'Doherty et al. [24]. The deviation in the relative humidity during the preparation of the electrodes seems to be a major point [24].

Tsien and Rink [71] eliminated the over-Nernstian response by preparing PVC-containing membranes. Simultaneously they achieved very low detection limits (Fig. 2, curve 4). They described the improvement as being due to elimination of an electrical shunt through the hydrated glass wall at the very tip [71]. Similar behaviour has been observed by Lewis and Wills [82] and Armstrong and Garcia-Diaz [83]. With tip diameters well below 1 μm, slopes of up to 72 mV per decade of Ca^{2+} activity (10^{-6}—10^{-5} M) were obtained in the present work when the original membrane material [67] was used (curve 2, Fig. 2). Because extended conditioning of such freshly prepared microelectrodes with different Ca^{2+}-containing buffer solutions does not significantly influence the electrode response, diffusion phenomena at the phase boundary of the membrane are not the sole origin of the problems encountered. When the original membrane material is used in a PVC matrix, an electrode response is obtained which is almost identical to that reported by Tsien and Rink [71] (see curves 3 and 4, Fig. 2). This fact supports the hypothesis of electrical leakage in the absence of a PVC layer.

In conclusion, the use of the membrane composition based on easily available materials can be recommended for microelectrodes with tip diameters above 1 μm. If microelectrodes with tips of $\leqslant 1$ μm diameter have to be used, treatment of the original membrane material with PVC as described in the experimental section is to be recommended.

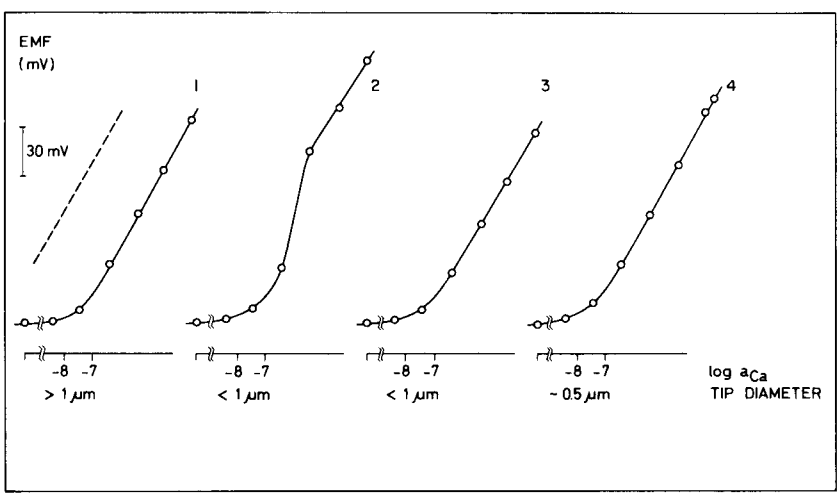

Fig. 2. Calcium-electrode functions of various liquid-membrane microelectrodes based on the synthetic neutral carrier ETH 1001. Comparison of the original liquid ion-exchanger [67] (curves 1 and 2) with membranes containing PVC (curves 3 and 4). Dashed line: theoretical slope of 29.3 mV at 22°C. Curves: (1) liquid silanization technique [67]; (2) gaseous silanization, this work; (3) gaseous silanization with PVC membrane, this work; (4) gaseous silanization with PVC membrane [71].

TABLE 1

Selectivity factors, log K^{pot}_{CaM}, for the Ca^{2+}-selective microelectrode based on a neutral carrier in a PVC membrane and the corresponding macroelectrode

Electrode	log K^{pot}_{CaM}		
	Na^+	K^+	Mg^{2+}
Micro	-5.5 ± 0.2 ($n = 3$)[a]	-5.4 ± 0.2 ($n = 7$)[a]	<-4.9[b]
Macro [68]	-6.1	~ -6.2	-5.1

[a]FIM with Ca^{2+} buffered solutions. [b]FIM with Ca^{2+} unbuffered solutions (1 M Mg^{2+}).

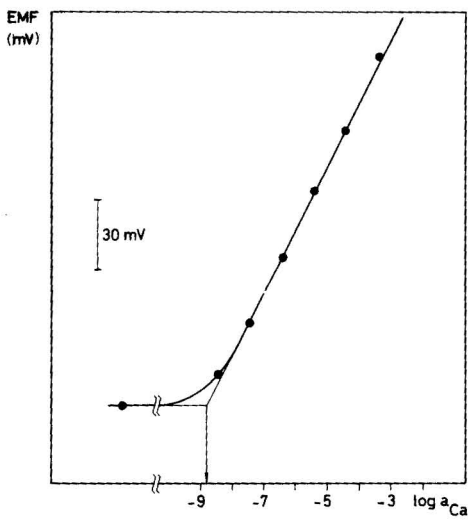

Fig. 3. E.m.f. response of the Ca^{2+}-selective macroelectrode cell assembly based on ETH 1001, potassium tetra(*p*-chlorophenyl)borate, *o*-NPOE and PVC in different Ca^{2+} buffer solutions as used by Tsien and Rink [21]. Trace: response computed at an ion background of 125 mM K^+ using the value K^{pot}_{CaK} of 2.2×10^{-7} found to best-fit the experimental results (points). Experimental data are corrected for changes in liquid junction potential and activity coefficients.

These microelectrodes give the selectivities listed in Table 1, which are comparable to the selectivities of the corresponding PVC-based macroelectrodes. As documented in Fig. 3, however, the detection limit of the macroelectrode is lower by about one order of magnitude.

We thank J. O'Doherty and W. McD. Armstrong, as well as R. Y. Tsien and T. J. Rink, for the supply of material and for stimulating exchange of information. This work was partly supported by the Swiss National Science Foundation.

REFERENCES

1 H. M. Brown, J. P. Pemberton and J. D. Owen, Anal. Chim. Acta, 85 (1976) 261.
2 J. D. Owen, H. M. Brown and J. P. Pemberton, Biophys. J., 16 (1976) 34a.
3 G. R. J. Christoffersen and L. Simonsen, Acta Physiol. Scand., 101 (1977) 492.
4 J. D. Owen, H. M. Brown and J. P. Pemberton, Anal. Chim. Acta, 90 (1977) 241.
5 C. O. Lee, A. Taylor and E. E. Windhager, Nature (London), 287 (1980) 859.
6 D. M. Bers and D. Ellis, J. Physiol. (London), 310 (1981) 73 P.
7 M. J. Berridge, Cell. Calc., 1 (1980) 217.
8 F. P. McGlone, I. J. Russel and O. Sand, J. Exp. Biol., 83 (1979) 123.
9 M. Moreau, J. P. Vilain and P. Guerrier, Dev. Biol., 78 (1980) 201.
10 C. O. Lee, D. Y. Uhm and K. Dresdner, Science, 209 (1980) 699.
11 H. D. Lux and G. Hofmeier, Pflügers Arch. Gesamte Physiol. Menschen Tiere, 373 (1978) R 47.
12 G. Hofmeier and H. D. Lux, Pflügers Arch. Gesamte Physiol. Menschen Tiere, 373 (1978) R 47.
13 G. Dahl and G. Isenberg, J. Membr. Biol., 53 (1980) 63.
14 A. Coray, C. H. Fry, P. Hess, J. A. S. McGuigan and R. Weingart, J. Physiol. (London), 305 (1980) 60 P.
15 J. H. Sokol, C. O. Lee and F. J. Lupo, Biophys. J., 25 (1979) 143a.
16 P. Hess and R. Weingart, J. Physiol. (London), 307 (1980) 60 P.
17 C. C. Ashley, T. J. Rink and R. Y. Tsien, J. Physiol. (London), 280 (1978) 27 P.
18 E. Marban, T. J. Rink, R. W. Tsien and R. Y. Tsien, Nature (London), 286 (1980) 845.
19 F. Alvarez-Leefmans, T. J. Rink and R. Y. Tsien, J. Physiol. (London), 315 (1981) 531.
20 E. Marban, T. J. Rink, R. W. Tsien and R. Y. Tsien, J. Physiol. (London), 305 (1980) 24 P.
21 R. Y. Tsien and T. J. Rink, Biochim. Biophys. Acta, 599 (1980) 623.
22 T. J. Rink, R. Y. Tsien and A. E. Warner, Nature (London), 283 (1980) 658.
23 F. J. Alvarez-Leefmans, T. J. Rink and R. Y. Tsien, J. Physiol. (London), 306 (1980) 24 P.
24 J. O'Doherty, S. J. Youmans, W. McD. Armstrong and R. J. Stark, Science, 209 (1980) 510.
25 J. O'Doherty and R. J. Stark, in E. Sykavá, P. Hník and L. Vyklický (Eds.), Ion-Selective Microelectrodes and Their Use in Excitable Tissues, Plenum Press, New York, 1981.
26 S. Yoshikami, J. S. George and W. A. Hagins, Nature (London), 286 (1980) 395.
27 S. Yoshikami, J. George and W. A. Hagins, Fed. Proc. Fed. Am. Soc. Exp. Biol., 39 (1980) 2066.
28 C. Nicholson, Trends Neurosci., 3 (1980) 216.
29 M. Galvan, G. ten Bruggencate and R. Senekowitsch, Brain Res., 160 (1979) 544.
30 C. Benninger, J. Kadis and D. A. Prince, Brain Res., 187 (1980) 165.
31 M. E. Morris, in E. Sykavá, P. Hník and L. Vyklický (Eds.), Ion-Selective Microelectrodes and Their Use in Excitable Tissues, Plenum Press, New York, 1981.
32 K. Krnjevič and M. E. Morris, in T. Zeuthen (Ed.), The Application of Ion-Selective Microelectrodes, Elsevier—North Holland, Amsterdam, 1982.
33 K. Krnjevič, M. E. Morris and R. J. Reiffenstein, Can. J. Physiol. Pharmacol., 58 (1980) 579.
34 F. Math and J. L. Davrainville, Experientia, 35 (1979) 1355.
35 F. Math and J. L. Davrainville, Brain Res., 190 (1980) 243.
36 G. G. Somjen, J. Neurophysiol., 44 (1980) 617.
37 M. Segal and J. Gutnick, Brain Res., 195 (1980) 389.
38 C. Nicholson, Fed. Proc. Fed. Am. Soc. Exp. Biol., 39 (1980) 1519.
39 H. Stöckle and G. ten Bruggencate, Neuroscience, 5 (1980) 893.

40 U. Heinemann and R. Pumain, Exp. Brain Res., 40 (1980) 247.
41 U. Heinemann and R. Pumain, Neurosci. Lett., 21 (1981) 87.
42 J. Louvel and U. Heinemann, C. R. Acad. Sci. Ser. D, 291 (1980) 997.
43 C. Nicholson, R. P. Kraig, G. ten Bruggencate, H. Stöckle and R. Steinberg, Arzneim. Forsch./Drug Res., 28 (1978) 874.
44 H. Stöckle and G. ten Bruggencate, Exp. Neurol., 61 (1978) 226.
45 U. Heinemann, A. Konnerth and H. D. Lux, Neurosci. Lett., 1 (1978) S 63.
46 U. Heinemann and A. Konnerth, in R. Canger, F. Angeleri and J. K. Penry (Eds.), Advances in Epileptology: XIth Epilepsy Int. Symp., Raven Press, New York, 1980.
47 M. Galvan, P. Grafe and G. ten Bruggencate, in M. Klee, H. D. Lux and E. Speckmann (Eds.), Physiology and Pharmacology of Epileptogenic Phenomena, Raven Press, New York, in press, 1980.
48 H. D. Lux and C. B. Heyer, in F. O. Schmitt and F. G. Worden (Eds.), The Neurosciences:4th Study Program, MIT Press, Cambridge, MA, USA, 1979.
49 U. Heinemann, H. D. Lux and M. J. Gutnick, Exp. Brain Res., 27 (1977) 237.
50 D. Heuser, J. Astrup, N. A. Lassen, B. Nilsson, K. Norberg and B. K. Siesjo, Acta Neurol. Scand., 56 (1977) 216.
51 D. Heuser, Cerebral Vascular Smooth Muscle and its Control, Ciba Foundation Symp. 56, Elsevier/Excerpta Medica, Amsterdam, 1978.
52 C. Nicholson, G. ten Bruggencate, R. Steinberg and H. Stöckle, Proc. Natl. Acad. Sci., 74 (1977) 1287.
53 C. Nicholson, R. Steinberg, H. Stöckle and G. ten Bruggencate, Neurosci. Lett., 3 (1976) 315.
54 S. K. Bosher and R. L. Warren, Nature (London), 273 (1978) 377.
55 C. Nicholson, in F. O. Schmitt and F. G. Worden (Eds.), The Neurosciences: 4th Study Program, MIT Press, Cambridge, MA, USA, 1979.
56 R. P. Kraig and C. Nicholson, Neuroscience, 3 (1978) 1045.
57 C. Nicholson, G. ten Bruggencate, H. Stöckle and R. Steinberg, J. Neurophysiol., 41 (1978) 1026.
58 U. Heinemann, H. D. Lux and M. J. Gutnick, in N. Chalazonitis and M. Boisson (Eds.), Abnormal Neuronal Discharges, Raven Press, New York, 1978.
59 A. R. Gardner-Medwin and C. Nicholson, J. Physiol. (London), 275 (1977) 66 P.
60 H. D. Lux and U. Heinemann, in W. A. Cobb and H. Van Duijn (Eds.), Contemporary Clinical Neurophysiology (EEG Suppl. No. 34), Elsevier, Amsterdam, 1978.
61 G. ten Bruggencate and R. Steinberg, Naunyn-Schmiedeberg's Arch. Exp. Pathol. Pharmakol., 302 (1978) R 55.
62 G. ten Bruggencate, R. Steinberg, H. Stöckle and C. Nicholson, in R. W. Ryall and J. S. Kelly (Eds.), Iontophoresis and Transmitter Mechanisms in the Mammalian Central Nervous System, Elsevier—North-Holland, Amsterdam, 1978.
63 M. Kessler, J. Höper, D. Schäfer and R. Strehlau, Bibl. Anat., 15 (1977) 237.
64 R. Steinberg and G. ten Bruggencate, Pflügers Arch. Gesamte Physiol. Menschen Tiere, 373 (1978) R 68.
65 H. Stöckle, G. ten Bruggencate, C. Nicholson and R. Steinberg, Plügers Arch. Gesamte Physiol. Menschen Tiere, 368 (1977) R 37.
66 C. B. Heyer and H. D. Lux, in N. Chalazonitis and M. Boisson (Eds.), Abnormal Neuronal Discharges, Raven Press, New York, 1978.
67 M. Oehme, M. Kessler and W. Simon, Chimia, 30 (1976) 204.
68 W. Simon, D. Ammann, M. Oehme and W. E. Morf, Ann. N. Y. Acad. Sci., 307 (1978) 52.
69 G. R. J. Christoffersen and E. S. Johansen, Anal. Chim. Acta, 81 (1976) 191.
70 H. M. Brown and J. D. Owen, Ion-Select. Elec. Rev., 1 (1979) 145.
71 R. Y. Tsien and T. J. Rink, J. Neurosci. Meth., 4 (1981) 73.
72 D. Ammann, P. C. Meier and W. Simon, in C. C. Ashley and A. K. Campbell (Eds.), Detection and Measurement of Free Ca^{2+} in Cells, Elsevier—North Holland, Amsterdam, 1979.

73 D. Ammann, R. Bissig, M. Guggi, E. Pretsch, W. Simon, I. J. Borowitz and L. Weiss, Helv. Chim. Acta, 58 (1975) 1535.
74 E. Neher and H. D. Lux, J. Gen. Physiol., 61 (1973) 385.
75 G. G. Guilbault, R. A. Durst, M. S. Frant, H. Freiser, E. H. Hansen, T. S. Light, E. Pungor, G. Rechnitz, N. M. Rice, T. J. Rohm, W. Simon and J. D. R. Thomas, Pure Appl. Chem., 48 (1976) 127.
76 P. C. Meier, D. Ammann, W. E. Morf and W. Simon, in J. Koryta (Ed.), Medical and Biological Applications of Electrochemical Devices, Wiley, Chichester, 1980.
77 P. C. Meier, D. Ammann, H. F. Osswald and W. Simon, Med. Prog. Technol., 5 (1977) 1.
78 J. Růžička, E. H. Hansen and J. Chr. Tjell, Anal. Chim. Acta, 67 (1973) 155.
79 O. Scharff, Anal. Chim. Acta, 109 (1979) 291.
80 A. Hulanicki and R. Lewandowski, Chem. Anal. (Warsaw), 19 (1974) 53.
81 H. Seto, A. Jyo and N. Ishibashi, Chem. Lett., (1975) 483.
82 S. A. Lewis and N. K. Wills, Biophys. J., 31 (1980) 127.
83 W. McD. Armstrong and J. F. Garcia-Diaz, Fed. Proc., Fed. Am. Soc. Exp. Biol., 39 (1980) 2851.

Analytica Chimica Acta, 135 (1982) 61—67
Elsevier Scientific Publishing Company, Amsterdam — Printed in The Netherlands

A METHANE GAS SENSOR BASED ON OXIDIZING BACTERIA

ISAO KARUBE*, TADASHI OKADA and SHUICHI SUZUKI

Research Laboratory of Resources Utilization, Tokyo Institute of Technology, Nagatsuta-cho, Midori-ku, Yokohama 227 (Japan)

(Received 14th April 1981)

SUMMARY

A bacterial sensor system based on *Methylomonas flagellata* AJ 3670 is described for methane determinations. The system consists of a bacterial reactor, a reference reactor and two oxygen sensors. The current decreases with time until a steady state is reached within 30 s at 30°C; the maximum current difference is obtained at 30°C and pH 7.2. The response time for the determination of methane is less than 1 min. A linear relationship is obtained between the current difference and the methane concentration below 6.6 mM; the lower limit of determination is 5 μM, and the current decrease is reproducible within 5%. The current output of the sensor is almost stable for more than 10 days and 250 assays.

Methane is an attractive energy source and a main component of natural gases. It is used as gaseous fuel in many fields, and it is well known that methane forms explosive mixtures with air (5—14%). Therefore, rapid methods for the determination of methane in air are required in various fields such as coal mining and gasification processes. Methane is also produced by methanogenic bacteria. The biological formation of methane is the result of a specific type of bacteria energy-yielding metabolism. World-wide interest has arisen in the production of methane by fermentation of biomass, renewable resources. Control of the fermentation process is needed for effective production of these useful materials. The determination of raw materials and products in the media is required for process control, spectrophotometric methods normally being applied. However, as molasses and other natural materials are used as the raw materials for fermentation, the media are not optically clear. Electrochemical monitoring of these compounds may have definite advantages.

For some time, the utilization of micro-organisms has not been restricted to the fermentation industries [1] and many valuable applications have been found, including new electrochemical uses. As previously reported, many microbial sensors have been developed for the determination of BOD [2—4], assimilable sugars (glucose, fructose and sucrose) [5], and volatile or gaseous compounds such as alcohols [6], acetic acid [7] and ammonia [8]. These electrodes consist of micro-organisms and oxygen electrodes. Assimilation of organic compounds by micro-organisms can be determined from the respiratory activity of the micro-organisms, which can be directly measured by an oxygen electrode.

0003-2670/82/0000-0000/$02.75

Whittenbury et al. [9, 10] isolated more than 100 gram-negative, strictly aerobic, methane-utilizing bacteria. More recently, an easily-grown methane-oxidizing bacterium was isolated in a pure culture from a natural source through studying the production of single cell protein [11]. This bacterium was identified as a new species *Methylomonas flagellata*, capable of growing by oxidizing methane as the main carbon and energy source.

In general, methane-oxidizing bacteria utilize methane, and oxygen is consumed by the respiration as follows [12, 13]

$$CH_4 + O_2 \xrightarrow{\text{methane-oxidizing bacteria}} CH_3OH + H_2O$$

In this study, the characteristics of a methane sensor system are described, and the sensor system is applied to the determination of methane in air.

EXPERIMENTAL

Materials and micro-organisms

Reagents were commercially available analytical-grade chemicals. Deionized water was used for all procedures.

The micro-organism used was *M. flagellata*, which was kindly provided by the Fermentation Research Institute, Ministry for Industrial Trade and Industry, Tsukuba. The *M. flagellata* was maintained on a gel (pH 7.2) containing 0.5 g $(NH_4)_2SO_4$, 0.3 g KH_2PO_4, 1.8 g $Na_2HPO_4 \cdot 12H_2O$, 0.2 g $MgSO_4 \cdot 7H_2O$, 10 mg $FeSO_4 \cdot 7H_2O$, 1.0 mg $CuSO_4 \cdot 5H_2O$ and 30 g of agar per liter of distilled water.

Cultivation. The *M. flagellata* was cultured under aerobic conditions for 48 h in the same medium (pH 7.2) as the above gel except for agar. Methane was provided as a growth substrate by incubating the culture under an atmosphere of 80% air—20% methane at 30°C in 500-ml suction flasks sealed with rubber stoppers and placed in a rotary shaker incubator. The cells were centrifuged at 5°C and 8000g, and washed twice with physiological saline solution.

Apparatus

Figure 1 shows a schematic diagram of the system. The system consisted of two oxygen electrodes (model U-1, Ishikawa Seisakujo, Tokyo), two reactors, an electrometer (Hokuto Denko model 0.55Z, Iwaki) and a recorder (Riken Denki model SP-J6C).

The reactors (55-ml capacity) contained 41 ml of the culture medium, one with and one without bacterial cells. The oxygen electrodes consisted of a teflon membrane (50-μm thick), a platinum cathode, a lead anode and sodium hydroxide electrolyte (30% w/v). These electrodes were fixed to custom-made teflon flow-through cells. The system was connected up with glass and teflon tubing (0.3 cm diameter).

The system contained two vacuum pumps, one to evacuate the gas sample tube (glass, diameter 0.4 cm, length 80 cm, volume 40 ml) and the other to

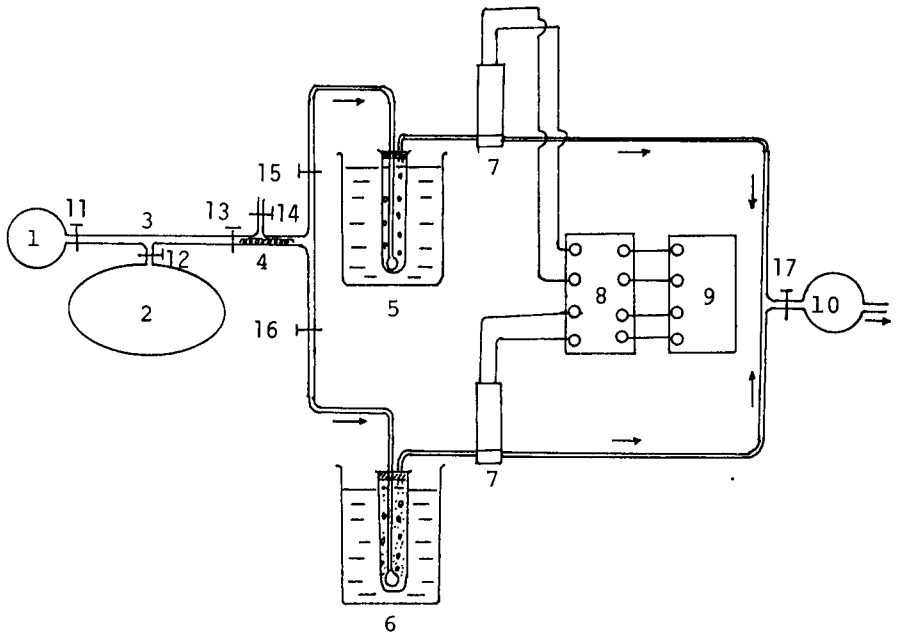

Fig. 1. Scheme of microbial sensor system for methane. 1, vacuum pump; 2, sample gas bag; 3, gas sample line; 4, cotton filter; 5, control reactor; 6, methane-oxidizing bacteria reactor; 7, oxygen electrode; 8, amplifier; 9, recorder; 10, vacuum pump; 11—17, glass stopcocks.

transport the sample gas through the system. The flow rate of the sample gas through the reactors was controlled with the glass valves at 80 ml min^{-1}. The cotton filter served to remove other micro-organisms in the sample gas and to prevent contamination of the two reactors and gas lines. The sample gas exiting from the system was passed into the laboratory extraction hoods via glass tubes.

All the lines were made gas-tight with teflon tubes and glass tubes, and careful checks were made for leakage. The lines were designed so as to maintain symmetry between the measuring and reference flow lines. The flow rates in each line were balanced by adjusting valves 15 and 16. The reactors were maintained at 30°C ± 0.1°C by a thermostatted bath.

Procedure for measurement

In a typical procedure, pump 10 was switched on and valves 14—17 were opened with valve 13 closed, so that air flowed through the system. A steady current was obtained within a few minutes, corresponding to the concentration of oxygen at the outer surface of the electrodes. During passage through the reactor containing micro-organisms, some oxygen was consumed but the oxygen concentration at the outlet of the reactor reached a constant level within a few minutes. Valves 12 and 13 were then closed, valve 11 was opened

and the gas sample line was evacuated by pump 1. Closing valve 11 and opening valve 12 allowed the sample gas containing methane to flow into the gas sample line. Vacuum pump 1 was then removed and valve 12 closed. Valves 11 and 13 were then opened and valve 14 was closed simultaneously, so that the sample gas was transferred to the measuring lines by pump 10. During the passage of the sample gas containing methane, the difference in current recorded for the two electrodes depended on the concentration of methane. Each sample was measured in duplicate by repeating the procedure.

Preparation of methane standards

The methane used was obtained commercially (99.99% purity). A known volume (V) of this methane was injected into a 2-1 gas bag (vinyl fluoride film), which was then filled with air from a gas-tight syringe. The molarity of methane (at 25°C, 1 atm.) in the gas bag was then calculated from x (mole) = $273\ V/(22.4 \times 298 \times 2)$.

Methane was determined by gas chromatography (Shimazu Seisakujo, model GC3BT) with 5A molecular sieve (60—80 mesh) in a 3 m × 0.3 cm i.d. column at 40° C, with argon as the carrier gas and thermal conductivity detection in the usual manner.

RESULTS AND DISCUSSION

Response and calibration of the electrode

Figure 2 shows typical response curves of the sensor system. When the sample gas containing methane entered the reactor, methane was assimilated by the micro-organisms with consumption of oxygen. The current decreased to a minimum, which indicated that the consumption of oxygen by the micro-organisms, and the supply of oxygen from the air was in equilibrium. As the system contained two oxygen electrodes, the maximum difference of current depended on the concentration of methane in the sample gas. When pure air was again passed through the reactors, the current of the sensor returned to its initial level within 1 min. The response time required for the determination of methane was within 1 min, and the total time required for an assay of methane was 2 min.

The calibration graphs for the system were strictly linear for concentrations of methane in the range 0—6.6 mM, the current difference ranging from 0 to 0.35 μA. The minimum concentration for determination was 5 μM. The current difference measured for the same sample (0.66 mM) was reproducible within 5%; the standard deviation was 9.40 nA in 25 experiments.

Effects of temperature, air flow and cell content on the current difference

Figure 3 shows the effect of temperature on the current difference of the microbial system. The current difference was determined after 30-min incubation of the reactors at various temperatures. The concentration of dissolved oxygen decreased with increasing temperature, and the results were

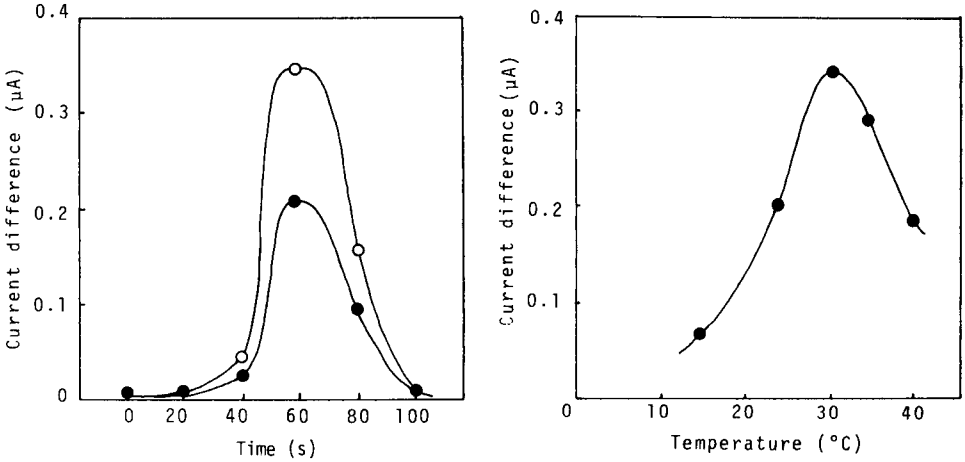

Fig. 2. Response curves of the microbial sensor for methane. The sample gas was transferred into the gas sampler at time 0: (○) 0.66 mM; (●) 0.39 mM methane. Conditions as in Experimental; 300 mg of wet cells per reactor.

Fig. 3. Effect of temperature on current difference of the microbial sensor. Other conditions as for Fig. 2.

corrected on the basis of the concentration of dissolved oxygen determined at various temperatures. As shown, the currents decreased above 35° C because the bacteria were inactivated by heat, but because the respiration activity of the bacteria decreased below 25° C, the current increased with decreasing temperature. The maximum current difference was observed at 30° C.

The effect of the air flow rate on the current difference of the sensor is shown in Fig. 4. The current difference was almost constant below flow rates of 80 ml min^{-1}, but above this flow rate the current difference decreased rapidly.

Insofar as the respiration activity of *M. flagellata* is measured in the system, the cell content in the reactor will obviously affect the current output. The wet cell content of each reactor was changed from 100 mg to 400 mg and the effects on the current difference were examined. Figure 5 shows that the current difference increased as the wet cell content increased up to 300 mg per reactor, and a wet cell content of 300 mg per reactor is recommended.

The long-term stability of the microbial sensor system was examined with sample gases containing 0.66 or 0.39 mM of methane. The current output was almost constant for more than 10 days and 250 assays, but showed better reproducibility at the higher concentration over that time.

Comparison with gas chromatography

The microbial sensor system was applied to the determination of methane in air samples that were also analyzed by conventional gas chromatography. Over the range 0.2—3.5 mM methane in air the correlation coefficient between the results of the two methods was 0.97.

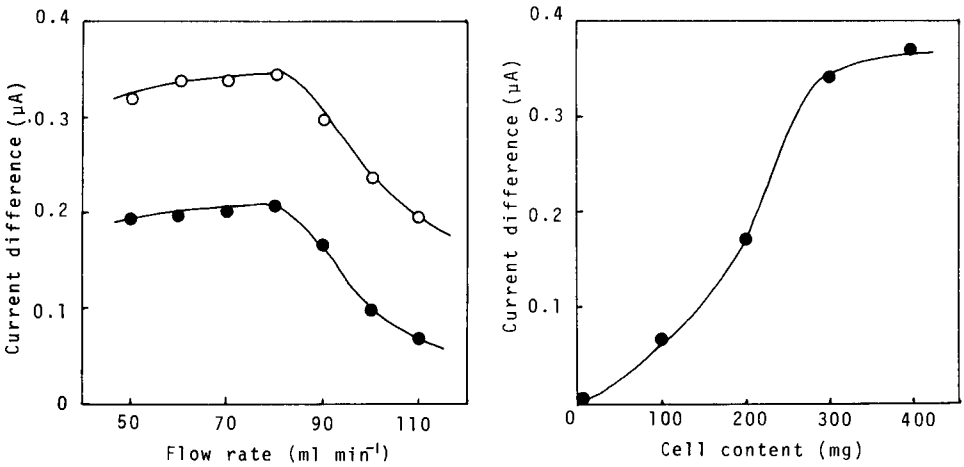

Fig. 4. Effect of sample gas flow rate on current difference of the microbial sensor for methane concentrations of 0.66 mM (○) and 0.39 mM (●). Other conditions as for Fig. 2.

Fig. 5. Effect of cell content on current difference of the microbial sensor. Other conditions as in Fig. 2.

Conclusions

A rapid and continuous method for the determination of methane is desirable in many fields, and on-line measurement of methane is required for its effective production by fermentation. Although gas chromatography can be used, it seems basically unsuitable for such on-line measurements. In the proposed method, the respiration of micro-organisms is converted immediately to a current signal. The sensitivity of this amperometric signal is almost the same as that of the gas chromatographic signal; the minimum measurable concentration is 3 μM by gas chromatography with a flame ionization detector, and 5 μM by the proposed microbial sensor. Accordingly, the microbial sensor system with *M. flagellata* seems promising for the rapid on-line determinations of methane.

REFERENCES

1 J. Levy, J. Campbell Jr. and T. H. Blackburn, Introductory Microbiology, J. Wiley, New York, 1973.
2 I. Karube, T. Matsunaga, S. Mitsuda and S. Suzuki, Biotechnol. Bioeng., 19 (1977) 1535.
3 I. Karube, S. Mitsuda, T. Matsunaga and S. Suzuki, J. Ferment. Technol., 55 (1977) 243.
4 M. Hikuma, H. Suzuki, T. Yasuda, I. Karube and S. Suzuki, Eur. J. Appl. Microbiol. Biotechnol., 8 (1979) 289.
5 M. Hikuma, H. Obana, T. Yasuda, I. Karube and S. Suzuki, Enzyme Microb. Technol., 2 (1980) 234.
6 M. Hikuma, T. Kubo, T. Yasuda, I. Karube and S. Suzuki, Biotechnol. Bioeng., 21 (1979) 1845.
7 M. Hikuma, H. Suzuki, T. Yasuda, I. Karube and S. Suzuki, Anal. Chim. Acta, 109 (1979) 33.

8 I. Karube, T. Okada and S. Suzuki, Anal. Chem., 53 (1981) 1852.
9 R. Whittenbury, K. C. Phillips and J. F. Wilkinson, J. Gen. Microbiol., 61 (1970) 205.
10 R. Whittenbury, S. L. Davies and J. F. Davy, J. Gen. Microbiol., 61 (1970) 219.
11 Y. Morinaga, S. Yamanaka, S. Otsuka and Y. Hirose, Agric. Biol. Chem., 40 (1976) 8.
12 D. W. Ribbons, J. Bacteriol., 122 (1975) 1351.
13 I. J. Higgins and J. R. Quayle, Biochem. J., 188 (1970) 201.

Analytica Chimica Acta, 135 (1982) 69—75
Elsevier Scientific Publishing Company, Amsterdam — Printed in The Netherlands

DETERMINATION OF CYANIDE ION BY HOMOGENEOUS CATALYSIS AND GAS CHROMATOGRAPHY

MAURI A. DITZLER* and FRANCIS L. KEOHAN

Department of Chemistry, College of the Holy Cross, Worcester, MA 01610 (U.S.A.)

W. F. GUTKNECHT

Systems and Measurements Division, Research Triangle Institute, Research Triangle Park, NC 27709 (U.S.A.)

(Received 3rd August 1981)

SUMMARY

A simple procedure for the determination of trace levels of cyanide ions is described and evaluated. The procedure is based on the cyanide-catalyzed cleavage of benzil in the presence of methanol to produce benzaldehyde and methyl benzoate. The concentrations of these products are determined by gas chromatography. Linearity between gas chromatographic response and cyanide concentration is observed from 0.05 to 3 ppm cyanide; a detection limit of 1 ppb is calculated. A series of anions is shown not to interfere.

At present, there are several widely accepted procedures for detecting trace levels of cyanide [1]. There is, however, a continuing interest in finding new methods to improve the capability of selectively determining this ion at extremely low levels, as is illustrated by the appearance of a number of new procedures in recent years [2—8]. Ion-selective electrodes responsive to cyanide ion [3, 5] have been used but are subject to interference by halides and sulfide. Indeed, isolation of cyanide by conversion to hydrocyanic acid in acid solution is often necessary [1, 4, 6, 8]; sulfide, which interferes with most methods for cyanide determination, is however, also readily converted to a volatile, weak acid under these conditions, so it is often present in the final sample along with cyanide. A procedure that overcomes this problem of sulfide interference is described by Canterford who measured cyanide and sulfide simultaneously with direct current polarography [2].

This paper describes an alternate, relatively simple procedure requiring only widely available instrumentation and reagents that exhibit a low detection limit and a high degree of selectivity, especially relative to sulfide. The technique involves first carrying out a chemical reaction catalyzed by the substance of interest and then separating and measuring a product of that reaction using gas chromatography with a flame ionization detector. Under controlled conditions, the gas chromatographic signal will be proportional to the concentration of the catalyst. Because of the catalytic nature of the ion of interest, the benefits of chemical amplification will be realized.

While catalytic methods are available for quantifying many ions, including cyanide [4, 7, 9], gas chromatography has not yet been widely exploited as a means of enhancing the selectivity of catalytic schemes. The utility of this type of detection scheme has been demonstrated recently for the catalytic determination of copper(I) [10] and iron(III) [11]. Gas chromatographic methods have been used previously for determining trace levels of cyanide. They are based on the formation and detection of the volatile cyanide-containing compounds, HCN [12], CNBr [13], or CNCl [14]. Because these procedures do not involve chemical amplification, it is necessary to use either a more sensitive instrument or some form of sample concentration step to obtain sensitivity comparable with the procedure described in this report.

The basis of this new procedure for the determination of cyanide is the gas chromatographic measurement of methyl benzoate, which is the product of the cyanide-catalyzed reaction between benzil and methanol in a basic, aqueous solution. The reaction is

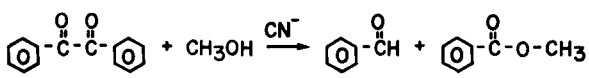

This reaction was selected for use in the determination of cyanide, partially on the basis of a study by Kwart and Baevsky [15]. These authors found that the reaction was specifically catalyzed by cyanide. The reaction was also found to be unaffected by the addition of as much as 30% water to the methanol solvent. This is important because many samples of interest contain water. The reaction is easily carried out, making it attractive for the development of a straightforward experimental procedure. Furthermore, both products, benzaldehyde and methyl benzoate, are amenable to isolation and quantitation by gas chromatography.

EXPERIMENTAL

Equipment and reagents

All gas chromatographic studies were performed with a Perkin-Elmer Sigma-4 gas chromatograph with a flame ionization detector. This instrument was equipped with a glass-lined injection port. A glass column (6 ft. × 1/8 in. o.d.) packed with 3% OV-17 on 100—120-mesh Chromosorb GAW was used in all determinations. The instrumental output was recorded on a Houston Instrument Omniscribe recorder at 1-mV full scale (25 cm). All reactions were run in sealed 50-ml Florence flasks at 20°C.

All reagents were analytical-reagent grade and used without further purification except benzil (Eastman), which was recrystallized from a 1:1 mixture of water and methanol. All solvents were of spectral quality. Water was deionized in a Continental deionization unit. Adjustment of pH was made with Fisher 1.000 ± 0.002 M NaOH. The cyanide solutions were diluted from an aqueous stock solution of 100 ppm cyanide prepared from

reagent-grade sodium cyanide. Concentrations of cyanide are reported relative to the aqueous samples, not the final reaction mixture. In the interference studies, all solutions of anions were prepared from either sodium or potassium salts and solutions of cations were prepared from their chloride salts.

Optimization procedure

The optimum experimental conditions were found by the sequential simplex optimization procedure [16—19]. The computations for this procedure were done with aid of a computer program similar to that described by Nedler and Mead [20], with the exception that the massive contraction rule was replaced. In the revised program, if a particular vertex still had the worst response after a contraction, the second-worst vertex was rejected rather than performing a massive contraction. Four parameters, hydroxide concentration, benzil concentration, volume ratio of sample (aqueous) to methanol in the reaction mixture, and reaction time were allowed to vary.

Analysis procedure

The following procedure produced optimum results and was used in all experiments unless indicated otherwise. Sufficient sodium hydroxide was added to the sample to give a concentration of 2.5×10^{-2} M. An aliquot (5 ml) of this solution was added to 6.5 ml of methanol and the solution was allowed to sit for 30 min to dissipate the heat generated as a result of mixing. Then 1 ml of 0.075 M benzil solution in methanol was added to this mixture, and the resulting solution was mixed by swirling. After a set reaction time (either 15 or 30 min), a 1.0-μl portion was injected for measurement of benzaldehyde and methyl benzoate with the chromatographic system described above. The column was operated at 60°C with a nitrogen flow of 20 ml min^{-1}. The solvent peak exhibited substantially less tailing if the injection ports were cleaned daily. Responses were determined from peak heights. The 0.075 M benzil solution was protected from light and kept refrigerated when it was stored for long periods.

RESULTS AND DISCUSSION

Optimization results

In determining the optimum experimental conditions, maximum permissible values for several of the variables were set. The hydroxide concentration of the reaction mixture was initially limited to values below 10^{-2} M to avoid salt build-up in the injection port of the gas chromatograph. For convenience, a maximum of 30 min was set for the reaction time. The maximum permissible benzil concentration was controlled by its solubility, which in turn was related to the ratio of water (from the aqueous sample) to methanol in the reaction mixture.

The hydroxide concentration found to produce optimum results was the maximum level allowed. This suggested that a greater sensitivity could be

obtained if solutions containing a higher sodium hydroxide concentration could be used. However, it was found that increasing the hydroxide concentration above 10^{-2} M resulted in a dramatic increase in the methyl benzoate blank. This was attributed to a non-cyanide-catalyzed production of this product.

As expected, the reaction time found to be the optimum was also the maximum permissible. In reality, the optimum reaction time will depend on the needs of the user. As was noted above, maximum sensitivity was achieved at an arbitrarily set maximum time which was selected on the basis of the need to complete the determination in a "reasonable" amount of time. If higher sensitivity is necessary, it can be obtained through the use of longer reaction times. However, at high cyanide concentrations, a long reaction time will result in a substantial consumption of the reactants which will cause a deviation from the desired linear relationship between the concentration of cyanide and the concentration of benzaldehyde or methyl benzoate.

Product detection

Figure 1 shows a chromatogram obtained from the analysis of a 1 ppm cyanide solution using the conditions found to be optimum. It can be seen that the signals from benzaldehyde and methyl benzoate are well resolved from the solvent peak and are easily measured. If the method is to be based on the methyl benzoate peak (it will be shown that this provides the best detection limit) rather than the benzaldehyde peak, adequate resolution can still be obtained at higher flow rates or temperatures. This will substantially shorten the time required.

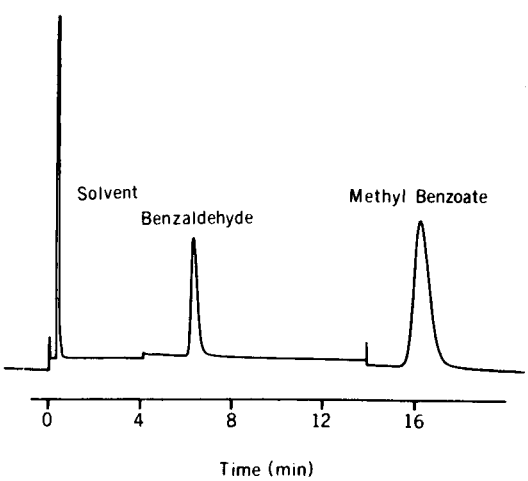

Fig. 1. A typical chromatogram representing the determination of 1 ppm cyanide. Relative instrumental sensitivities are 1 for solvent (methanol), 625 for benzaldehyde, and 2500 for methyl benzoate. A 30-min reaction time was used.

Linearity, sensitivity, and detection limit

Calibration curves based on the response of both benzaldehyde and methyl benzoate vs. the concentration of cyanide were prepared. For a 15-min reaction, correlation coefficients of 0.998 were found for the range of 0—3 ppm for both curves. (Data points were taken at 0, 0.05, 0.25, 0.50, 1.00, 1.50, 2.00 and 3.00 ppm cyanide.) Thus, under these experimental conditions, the reaction is apparently first order with respect to the cyanide catalyst and pseudo-zero order with respect to all other reactants.

The sensitivity of the procedure is partially determined by the amplification factor (molecules of either benzaldehyde or methyl benzoate produced per cyanide ion). This factor was determined by measuring the instrumental response to dilute samples of benzaldehyde, thereby determining how much of this product was produced from a cyanide-containing sample. An amplification factor of about 70 molecules of benzaldehyde per cyanide ion was found for a 1 ppm cyanide sample with a reaction time of 15 min. An amplification factor of about 140 was found for a 30-min reaction.

It was observed that even in the absence of an added catalyst, the reaction occurs to some extent. This is of interest because the uncertainty in this blank value will ultimately set the detection limit of the procedure. A commonly accepted definition of the detection limit of a procedure is the concentration of analyte giving a signal that is twice the standard deviation in the blank. Using this definition, a series of determinations of the blank for a reaction time of 30 min (see Table 1), and the measured sensitivity of the procedure to cyanide, a detection limit of 1 ppb was determined. This detection limit was based on the response to methyl benzoate. The uncertainty in the blank value for benzaldehyde was much higher and thus unsuitable for the detection of low levels of cyanide. The large benzaldehyde blank was not present if the products were extracted from the reaction mixture into *n*-butyl benzoate prior to the chromatographic separation. Apparently, benzaldehyde is formed in a non-cyanide-catalyzed reaction when the entire reaction mixture is injected into the hot injection port of the gas chromatograph.

Interferences

The possibility of ions other than cyanide catalyzing the reaction is of considerable concern. This would result in an uncertainty in the origin of a response. In addition to the possibility of catalysis, another concern was the extent to which any of these ions might inhibit the reaction. Thus, the effects of a variety of potentially interfering ions on both blanks and 1 ppm cyanide samples were measured. While a complete study of all possible ions was not made, several anions and cations were tested. The responses were determined from the methyl benzoate signals. The levels of interfering ions and the results of the interference tests are shown in Table 1. The signals obtained from the blank and 1 ppm cyanide for several replicate samples, without interfering ions present, are included for comparison and to demon-

TABLE 1

Response[a] for a blank and 1 ppm cyanide in the presence of various ions

Ion tested	Conc. (ppm)	Response (cm)		Ion tested	Conc. (ppm)	Response (cm)	
		Blank	1.0 ppm CN^-			Blank	1.0 ppm CN^-
None		1.63 ± 0.08[b]	151 ± 9[b]	S^{2-}	20	1.65	153
Br^-	40	1.70	162	$Fe(CN)_6^{3-}$	2	1.90	—
Cl^-	600	1.70	156	Cu^{2+}	4	—	6.0
F^-	40	1.75	166	Ni^{2+}	4	—	8.0
PO_4^{3-}	40	1.75	156	Fe^{3+}	4	—	142
SO_4^{2-}	40	1.90	164	Mn^{2+}	4	—	148
CO_3^{2-}	40	1.70	166	Zn^{2+}	4	—	120
$C_2H_3O_2^-$	40	1.60	162	Mg^{2+}	4	—	148
NO_3^-	200	1.60	160	Na^+	400	—	156

[a]Response is based on methyl benzoate peak height with an instrumental attenuation of 2. Reaction time is 30 min. [b]Average of 5 results with standard deviation (±1s).

strate the precision of the procedure at these levels. Except for Cu^{2+}, Ni^{2+}, and Zn^{2+}, the cyanide response in the presence of the interfering ions was within two standard deviations of the cyanide response without potentially interfering ions present. Also, it can be seen that the signal from the blank was virtually unaffected by the presence of relatively high concentrations of the interfering ions.

As noted previously, the response to sulfide is of particular interest because sulfide interferes with many of the present methods for cyanide detection. Table 1 shows that 20 ppm sulfide does not give a signal significantly different than the blank. Because 1 ppb cyanide has been shown to be detectable under these conditions, the response of the system to cyanide is at least 2×10^4 times as great as the response to sulfide. Another ion of interest is hexacyanoferrate(III). The system did not respond to this ion which is undissociated in alkaline solutions [21]. It can be seen that the transition metal ions copper(II) and nickel(II) significantly inhibit the reaction. This inhibition can be readily explained by the formation of inactive metal-cyanide complexes. The addition of iron(III) ions to a 1 ppm cyanide solution has, at most, a slight inhibiting effect, apparently because of the formation of hydrated iron(III) oxide species. The relatively large concentration of hydroxide with respect to the concentration of cyanide in the solution ensures that the iron(III) will be masked and so will not significantly lower the cyanide concentration. This is not in conflict with the earlier observation that hexacyanoferrate(III) does not release cyanide CN^- to the solutions, because it is kinetically inert.

The inability of the system to respond to metal-cyanide complexes is not a serious drawback. Frequently, only free cyanide is of interest [5]. Several procedures for isolating the cyanide from the metal before quantitation are available if total cyanide is desired [1, 4, 6, 22, 23].

The authors acknowledge the contributions of S. L. Morgan (University of South Carolina) for providing the computer program used in the simplex optimization procedure and C. H. Lochmüller (Duke University) for offering helpful suggestions. This work was supported, in part, by National Institute of Environmental Health Sciences (NIEHS) Grant 5 P01 ES01581-02, NIEHS Environmental Trainee Grant IT32ES07031-01-A1, an ACS Analytical Division Fellowship (awarded to M.A.D.) sponsored by the Society for Analytical Chemists of Pittsburgh, and the Department of Chemistry, Duke University, where much of this work was performed. This work was presented, in part, at the National ACS Meeting in Washington, DC, September 1979.

REFERENCES

1 American Public Health Association, American Water Works Association and Water Pollution Control Federation. Standard Methods for the Examination of Water and Wastewater, 14th edn., American Public Health Assoc., Washington, DC, 1976, pp. 361—386.
2 D. R. Canterford, Anal. Chem., 47 (1975) 88.
3 H. Clysters, F. Adams and F. Verbeek, Anal. Chim. Acta, 83 (1976) 27.
4 M. Brebec, G. Delarue, B. Santoni and P. Sarrat, Analusis, 4 (1976) 127.
5 M. Hofton, Environ. Sci. Technol., 10 (1976) 277.
6 I. Sekerka and J. F. Lechner, Water Res., 10 (1976) 479.
7 T. Okutani, H. Kotani and S. Utsumi, Bunseki Kagaku, 26 (1977) 166.
8 R. A. Durst, Anal. Lett., 10 (1977) 961.
9 G. G. Guilbault and D. N. Kramer, Anal. Chem., 38 (1966) 834.
10 M. A. Ditzler and W. F. Gutknecht, Anal. Lett., A(11) (1978) 611.
11 M. A. Ditzler and W. F. Gutknecht, Anal. Chem., 52 (1980) 614.
12 C. R. Schneider and H. Freund, Anal. Chem., 34 (1962) 69.
13 G. Nota and R. Palombari, J. Chromatogr., 84 (1973) 37.
14 J. C. Valentour, V. Agarwal and I. Sunshine, Anal. Chem., 46 (1974) 924.
15 H. Kwart and M. M. Baevsky, J. Am. Chem. Soc., 80 (1958) 580.
16 D. E. Long, Anal. Chim. Acta, 46 (1969) 193.
17 S. N. Deming, S. L. Morgan and M. R. Willcott, Am. Lab., 8 (1976) 13.
18 S. N. Deming and S. L. Morgan, Anal. Chem., 45 (1973) 278A.
19 W. Spendley, G. R. Hext and F. R. Himsworth, Technometrics, 4 (1962) 441.
20 J. A. Nedler and R. Mead, Comput. J., 7 (1965) 308.
21 E. de Barry Barnett and C. L. Wilson, Inorganic Chemistry, Longmans Green, London, 1953, p. 203.
22 M. S. Frant, J. W. Ross, Jr. and J. H. Riseman, Anal. Chem., 44 (1972) 2227.
23 P. D. Goulden, B. K. Afghan and P. Brookshank, Anal. Chem., 44 (1972) 1845.

Analytica Chimica Acta, 135 (1982) 77—84
Elsevier Scientific Publishing Company, Amsterdam — Printed in The Netherlands

DETERMINATION OF MONOMETHYLARSONIC ACID AND DIMETHYLARSINIC ACID BY DERIVATIZATION WITH THIOGLYCOLIC ACID METHYLESTER AND GAS—LIQUID CHROMATOGRAPHIC SEPARATION

BERNHARD BECKERMANN

Department of Pharmacology and Toxicology, University of Münster, 4400 Münster (W. Germany)

(Received 24th August 1981)

SUMMARY

An elegant method for the determination of monomethylarsonic acid and dimethylarsinic acid in biological materials is described. The methylarsenic acids are derivatized with thioglycolic acid methylester to yield lipophilic species, which can be determined by gas chromatography using a flame ionization detector or the more selective thermionic specific detector. The method permits the quick determination of methylarsenic acids in concentrations as low as 10 ng ml^{-1} in urine or blood.

Since the original demonstration by Braman and Foreback [1] in 1973 of the occurrence of monomethylarsonic acid (MMAA) and dimethylarsinic acid (DMAA) in human urine, several investigations have revealed that all studied mammalian species are capable of converting inorganic arsenic into these methylated forms [2—4]. It is assumed that at least 50% of the ingested or administered dose of arsenic undergoes biomethylation, but little is known about the underlying mechanism. The methylated forms of arsenic are much less toxic than their inorganic parent compounds [5]. Thus the biomethylation of inorganic arsenic constitutes an efficient mode of detoxification. For this reason there is considerable interest in suitable methods for the determination of methylated forms of arsenic in blood, urine, and tissues [6]. While the determination of "total arsenic" by atomic absorption spectrometry (a.a.s.) nowadays is a matter of routine, the separation and quantification of nanogram amounts of methylarsenic acids is still laborious, troublesome, and time-consuming.

Most methods are based on conversion to the corresponding methylarsine compounds by sodium borohydride. The generated arsines are trapped by means of liquid nitrogen and after fractional evaporation introduced into an a.a.s. system [7—8]. In other variants, the arsines are selected by liberation at different pH, pre-separated by ion-exchange chromatography or separated by gas—liquid chromatography [9—11]. The disadvantages of these methods

0003-2670/82/0000-0000/$02.75

are the volatility of the arsines at room temperature, the possibility of molecular rearrangements between monomethyl- and dimethyl-arsine, and the sensitivity of the arsines to atmospheric oxygen.

Because of these difficulties, there has been no dearth of efforts to convert DMAA and MMAA into stable derivatives, which then could be determined by gas—liquid chromatography. Henry and Thorpe [12], for instance, experimented with silylation reagents. The obtained silylethers, however, proved to be extremely sensitive to hydrolysis. The method was not applicable to biological materials. Soderquist et al. [13] converted DMAA to dimethylarsine iodide by means of hydriodic acid and in this way determined DMAA in soils and waters. It is true that the derivative decomposed in diluted solutions within 30 min, a circumstance that precludes the routine usage of this method. Daughterey et al. [14] extracted inorganic arsenic, MMAA and DMAA into an organic solvent by diethylammonium dithiocarbamate and separated the obtained arsenic complexes by gas—liquid chromatography. These authors also had to cope with the problem of insufficient stability of the derivatives, which necessitated the periodical extensive silanization of the packing and column wall.

In the present paper, a simple but sensitive method is reported for the determination of these methylarsenic acids in biological materials, based on the conversion with thioglycolic acid methylester into stable derivatives which can be separated by gas chromatography.

EXPERIMENTAL

Materials and equipment

The commercial MMAA (95%; Ferak) and DMAA (98%; Merck) had to be purified by chromatography on an ion-exchange resin as described by Dietz and Perez [15]. Thioglycolic acid methylester (TGM; 98%; Merck) was used. Buffer pH 5.5 consisted of 0.3 M citric acid and 0.91 M disodium hydrogenphosphate with 5% (w/w) ethylenediaminetetraacetic acid (EDTA). All other chemicals were reagent grade.

A Varian Model 3700 gas chromatograph equipped with a flame ionization detector and a thermionic specific detector was used. Glass columns (1.8 m × 2 mm i.d.) packed with Chromosorb G AW-DMCS coated with 2.5% XE-60 for flame ionization detection and with GasChrom Q (100—120 mesh) coated with 2.5% silicone QF-1 for thermionic specific detection were used. Injection port and detector temperatures were maintained at 150°C and 300°C, respectively. A linear temperature program with an initial time of 2 min at 100°C, a program rate of 20°C min^{-1} up to 200°C with a final time of 10 min was used. Nitrogen served as carrier gas at a flow rate of 30 ml min^{-1}. The detectors were operated with air and hydrogen at the flow rates recommended by the manufacturer. The thermionic specific detector was run with a bead current of 4.0 A and a bias voltage of 4.2 V.

The gas chromatography—mass spectrometry (g.c—m.s.) system used for identification of the derivatives consisted of a Varian Model 1400 gas chromatograph interfaced with a Varian MAT 112 mass spectrometer. Recording and evaluation of the mass spectra were done with Finnigan Instruments INCOS Data Systems.

Procedure

Take 5.0 ml of the sample (water, urine or whole blood), add 2 ml of concentrated nitric acid and evaporate the sample to a volume of about 1 ml (sand bath, 90° C). Dilute with distilled water to a volume of 10 ml. Take an aliquot of 2.0 ml into a capped vial, adjust with 1 ml of buffer solution to pH 3—5, add 50 μl of TGM, and 2.0 ml of cyclohexane. Shake the vial vigorously for at least 3 min and wait for complete phase separation. Inject 1—5 μl of the upper phase into the gas chromatograph and measure the peak heights. Calibration is done with the method of external standards.

RESULTS AND DISCUSSION

Derivatization

The derivatization of DMAA and MMAA is based on the long known affinity of arsenic compounds for the —SH group, which has been used historically to determine inorganic arsenic by hydrogen sulphide. The reaction of thiols with DMAA to yield thioarsenites was studied intensively during the 1930s [16]. The thioarsenites with cysteine and glutathione have been reported to be easily obtained under mild conditions. The reaction course is demonstrated by the reaction of DMAA with TGM

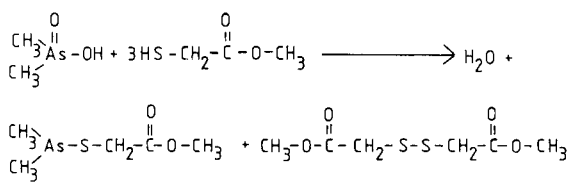

First, the reduction of the pentavalent arsenical to the trivalent form takes place under formation of a disulphide. This is followed by the reaction of a third mole of thiol to yield the thioarsinite. Such thioarsinites are known to be stable in acidic or slightly alkaline solution, but are readily hydrolysed in sodium hydroxide solution [17].

TGM seemed to be a promising agent for the derivatization of the methylarsenic acids because of the volatility and lipophilicity of the reaction product. To check this hypothesis, 10 mmol of TGM and 3 mmol of DMAA and MMAA were reacted in a semi-preparative experiment as described above. The subsequent separation by gas chromatography showed three major products (Fig. 1). Mass spectra of these compounds were obtained by g.c—m.s.,

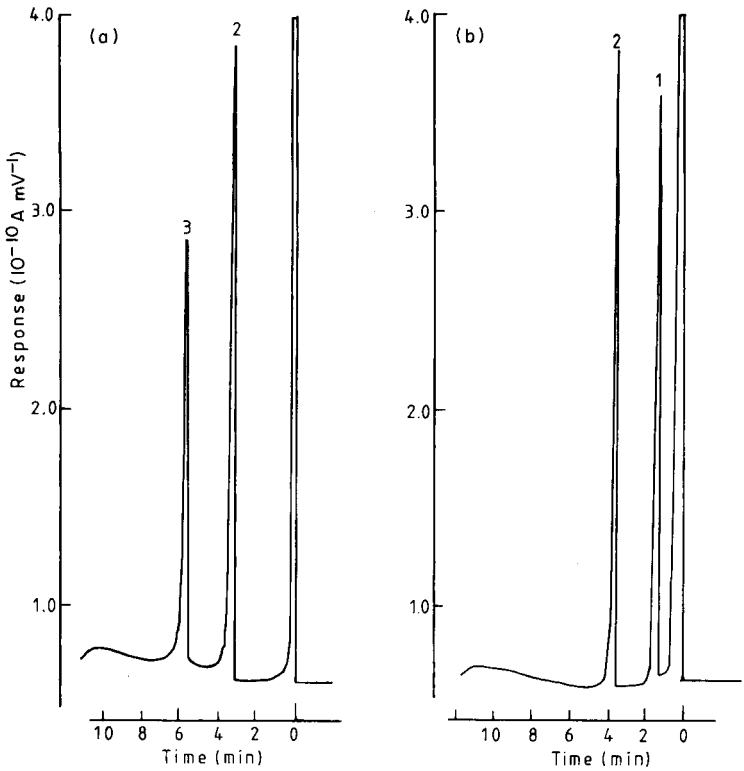

Fig. 1. Chromatogram of the reaction products of (a) MMAA with TGM, and (b) DMAA with TGM. Peaks: (1) DMAA derivative; (2) TGM disulphide; (3) MMAA derivative. Column: 1% OV-17 on Chromosorb G, 100—120 mesh. Conditions: initial temperature 160°C, 20°C min^{-1} to 240°C; flame ionization.

which identified the peaks as *S*-(dimethylarsino)thioglycolic acid methylester (peak 1 in Fig. 1), dithiodiglycolic acid methylester (peak 2) and *S*-(monomethylarsino)-bis-thioglycolic acid methylester (peak 3). The corresponding mass spectra are shown in Figs. 2 and 3.

Gas chromatographic behaviour

Separation of the TGM-arsenicals was evaluated on a variety of liquid phases, at different column temperatures, and with two different detectors. A linear temperature program as described above was chosen because it enables both methylarsenic acids to be determined simultaneously. Besides, with isothermal operation the separate determination of DMAA at 120°C and of MMAA at 200°C is possible. The rather polar cyanopropyl-containing silicone XE-60 is an efficient liquid phase. Carbowax can also be used, whereas the use of the less polar silicone OV-17 leads to tailing of the MMAA peak and decomposition on the column, when nanogram amounts are determined. When the thermionic specific detector is used, the nitrogen-free liquid phase QF-1, a middle polar fluorine-containing silicone was used.

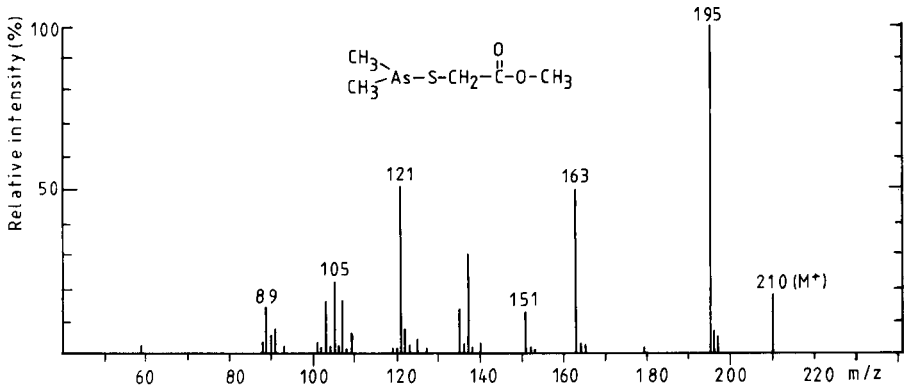

Fig. 2. Mass spectrum of peak 1 in Fig. 1(b) (DMAA derivative).

The thermionic detector, which is generally used for specific detection of nitrogen and phosphorus-bearing compounds, was supposed to be responsive to arsenic also, because arsenic, like nitrogen, belongs to the fifth main group of the Periodic Table. As shown in Fig. 4, the arsenic derivatives are in fact detectable with the thermionic detector, but the sensitivity is distinctly less

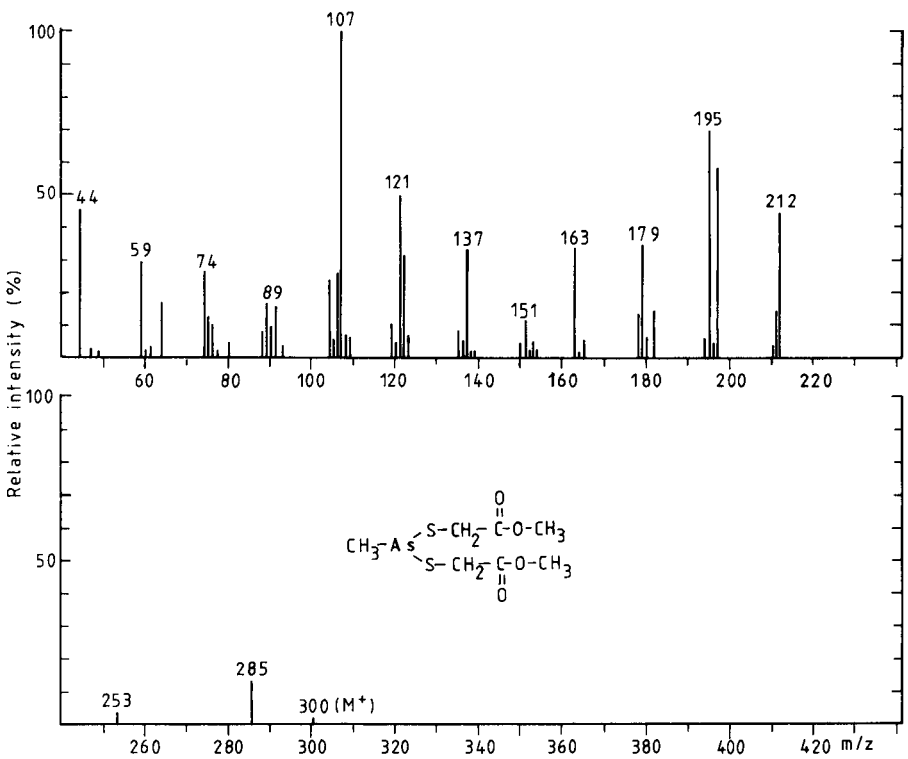

Fig. 3. Mass spectrum of peak 3 in Fig. 1(a) (MMAA derivative).

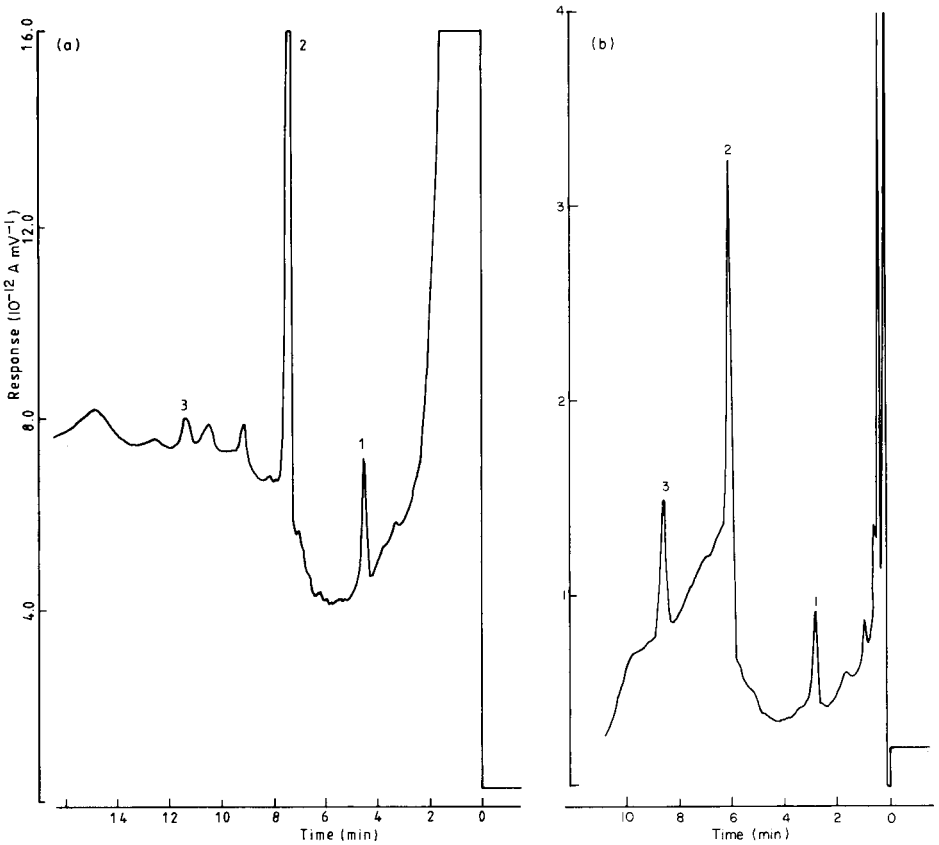

Fig. 4. Chromatograms of a urine sample spiked with 10 μg As in the form of DMAA and MMAA after injection of 10 ng of each species in 2 μl. (a) Flame ionization detector and XE-60 column; (b) thermionic specific detector and QF-1 column. Peaks: (1) DMAA derivative; (2) TGM disulphide; (3) MMAA derivative.

than that for nitrogen. In order to quantify the difference, the area under the peak of DMAA was compared with that for biphenyl and for quinoline. It was found that, on a molar basis, the sensitivity of the thermionic detector for quinoline was 94-fold higher than that for DMAA, whereas the signal of DMAA was 173-fold higher than that for biphenyl. The employment of the thermionic detector has the advantage that the base-line drift and the width of interfering peaks is reduced as demonstrated for the solvent peak and the disulphide peak in Fig. 4. The possibility of using both detectors in combination with different liquid phases means a considerable improvement of analytical validity.

Application to the analysis of biological materials

In order to verify the feasibility of the determination of methylarsenic acids by means of the proposed derivatization, an additional examination

was performed on the following criteria: reproducibility, interferences, chemical stability of the derivative, linearity of the detector response, and obtainable detection limit.

Interferences by ions like Fe^{3+} or Cu^{2+}, which could reduce the concentration of TGM by oxidation or direct reaction are conceivable. In order to eliminate these ions, the chelating agent EDTA was added to the buffer and an excess of TGM was used. Under these conditions, no interferences were seen for the blood and urine matrices (Table 1). Good reproducibility was confirmed by further examination of five urine samples, which were spiked with 1.0 mg of arsenic as DMAA and run through the procedure; 2-μl portions containing 50 ng As were injected. The mean response was 2.29×10^{-10} A mV^{-1}, the standard deviation being 0.091 and the relative standard deviation 4.0%.

Variations in the reaction pH conditions showed no difference in the signals in the pH range 2.0—6.0; a wider range was not studied. The derivatization of DMAA and MMAA at different temperatures resulted in no improvement; results were the same when the reaction was done at 100°C for 10 min instead of at room temperature. Evidently, the extraction of the derivatives into the organic solvent promotes complete conversion. The amount of the derivative did not decrease significantly after storage at room temperature for several days (Fig. 5).

Calibration curves were drawn up using urine samples and blood samples, which were spiked with DMAA and MMAA. The curves obtained (Fig. 6) show reasonable linearity in the range 5—200 ng of arsenic. With the XE-60 column, the flame ionization detector, and isothermal operation, the minimal detection limit is 0.2 ng of DMAA and 0.4 ng of MMAA. The relative limit of detection depends on the volumes of the sample and the extraction solvent. With a sample volume of 5 ml and extraction with 0.5 ml of cyclohexane, it is possible to determine the methylarsenic acids at concentrations as low as 10 ng ml^{-1}. Further lowering of the relative detection limit could be achieved by preliminary concentration of the sample. Evaporation after derivatization leads to losses. The number of peaks resulting from the matrix can be drastically reduced if the sample is extracted with a large amount of cyclohexane before derivatization.

TABLE 1

Recovery of DMAA from different matrices

Sample (n = 3)	Dist. water	Urine	Blood
DMAA added (μg)	100.0	100.0	100.0
Response (10^{-11} A mV^{-1})	4.24	4.14	4.22
Standard deviation	0.15	0.22	0.08
Recovery (%)[a]	—	97.6	99.5

[a] Recovery from distilled water is set to 100%.

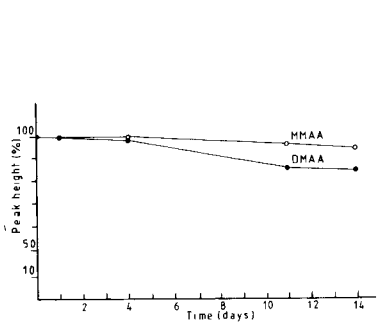

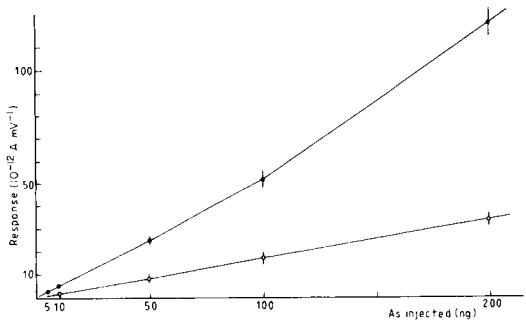

Fig. 5. Detector response (flame ionization) to DMAA after storage at room temperature for several days. Response on the day of derivatization is set to 100%. Injection: 10 ng As in 2 μl.

Fig. 6. Working curves for TGM-arsenicals with external standards in urine samples: (•) DMAA; (○) MMAA. n = 4; 2 μl injected.

The method described has been successfully applied in the analysis of blood and urine of animals after arsenic ingestion. Application to other biological matrices should be possible. Current investigations are concerned with inorganic arsenic, which also forms a TGM derivative.

I thank Dr. R. Eckard for obtaining the mass spectra and Prof. Dr. K. Opitz for his helpful suggestions and review of the manuscript.

REFERENCES

1 R. S. Braman and C. C. Foreback, Science, 182 (1973) 1247.
2 Y. Odanaka, O. Matano and S. Goto, Bull. Environ. Contam. Toxicol., 24 (1980) 452.
3 E. A. Crecelius, Environ. Health Perspect., 19 (1977) 147.
4 K. H. Tam, S. M. Charbonneau, F. Bryce and G. Lacrois, Anal. Biochem., 86 (1978) 505.
5 I. Simon, Arch. Int. Pharmacodyn. Ther., 45 (1933) 142.
6 F. E. Brinckman, G. E. Parris, W. R. Blair, K. L. Jewett, W. P. Iverson and J. M. Bellama, Environ. Health Perspect., 19 (1977) 11.
7 J. S. Edmonds and K. A. Francesconi, Anal. Chem., 48 (1976) 2019.
8 J. P. Buchet, R. Lauwerys and H. Roels, Int. Arch. Occup. Environ. Health, 46 (1980) 11.
9 A. G. Howard and M. H. Arab-Zavar, Analyst, 106 (1981) 213.
10 W. A. Maher, Anal. Chim. Acta, 126 (1981) 157.
11 M. O. Andreae, Anal. Chem., 49 (1977) 820.
12 F. T. Henry and T. M. Thorpe, J. Chromatogr., 166 (1978) 577.
13 C. J. Soderquist, D. G. Crosby and J. B. Bowers, Anal. Chem., 46 (1974) 155.
14 E. H. Daughterey, A. W. Fitchett and P. Mushak, Anal. Chim. Acta, 79 (1975) 199.
15 E. A. Dietz and M. E. Perez, Anal. Chem., 48 (1976) 1088.
16 G. O. Doak and L. D. Freedman, Organometallic Compounds of Arsenic, Antimony, and Bismuth. Interscience—Wiley, New York, 1977, p. 81.
17 H. J. Barber, J. Chem. Soc., (1931/I) 1365.

Analytica Chimica Acta, 135 (1982) 85—98
Elsevier Scientific Publishing Company, Amsterdam — Printed in The Netherlands

ION-PAIR EXTRACTION OF SOME SYMPATHOMIMETICS
Description of an Extraction Model for Terbutaline and Investigation of some Factors Influencing the Recovery of Sympathomimetics

P. M. BRANDTS, R. A. A. MAES and J. G. LEFERINK*

Centre for Human Toxicology, University of Utrecht, Vondellaan 14, 3521 GE Utrecht (The Netherlands)

C. L. DE LIGNY* and G. H. E. NIEUWDORP

Laboratory for Analytical Chemistry, University of Utrecht, Croesestraat 77a, 3522 AD Utrecht (The Netherlands)

(Received 25th January 1981)

SUMMARY

The ion-pair formation of terbutaline, a resorcinolamine, was studied during extraction into ethyl acetate, a slightly polar organic solvent. Factors influencing the extraction, e.g., the concentration of various ions in the aqueous phase, are considered. Terbutaline is extracted as a simple ion-pair without the formation of higher adducts. The extraction of some sympathomimetics is also described with respect to the nature of the organic solvent, the drug and the extracting anion. Factor analysis is applied to the data, and the reliability of predicted values is discussed. A search for a correlation between the factor analysis parameters characterizing the aqueous—organic phase systems and their physical properties led to a correlation between these parameters and interfacial tension; this result is explained by the macroscopic model of a solid surface (i.e., of the extracted compound) in contact with two fluids.

Much attention has been paid to the development of analytical procedures for catecholamines and their synthetic congeners. Straightforward analytical methods used for their identification in pharmaceutical preparations are unsuitable for the determination of the low concentrations encountered in biological materials. Accurate extraction and detection procedures are needed for measuring therapeutic blood levels, e.g., for pharmacokinetic studies. The large variation in the hydrophilic character of various catechol- and resorcinol- amines limits the effectiveness of general extraction procedures. While some compounds may be separated with moderate efficiency by plain liquid/liquid extraction, others can be recovered from biological or aqueous media only via the formation of a hydrophobic ion pair. A frequently used method involves sample clean-up by column chromatography with ion-exchange resins [1—3] or aluminium oxide [4]. In most of these procedures, only large amounts ($>0.5\ \mu g\ ml^{-1}$) of the drugs can be treated because of partial irreversible adsorption to the resin. These adsorption phenomena do not occur with liquid ion-exchangers that form highly soluble

0003-2670/82/0000-0000/$02.75

salts in organic solvents. Complexing substances such as methyl orange [5, 6], methylene blue [7], *p*-toluenesulphonic acid [6, 8], bromothymol blue [6, 9, 10] and bis(2-ethylhexyl)phosphoric acid [11, 12] have been extensively used. The last compound has proved to be exceptionally good for the extraction of some of the modern sympathomimetics [13, 14]. However, only low concentrations of this acid can be used because of its interference in subsequent gas chromatographic procedures. Optimization of the extraction procedure for the expected concentration range of a sympathomimetic amine may minimize such interferences. Modin and Johansson [12] described an extraction procedure for high concentrations of the amines, but extrapolations to low therapeutic concentrations proved impossible with their mathematical model.

The first part of this paper describes a model which is useful at these low concentrations and which includes factors such as pH, sodium ion concentration and the concentrations of the amine and the anion. The model substances used are terbutaline, as a representative of modern β_2-sympathomimetics, bis(2-ethylhexyl)phosphate as the anion and ethyl acetate as the organic phase. In the second part, the extraction of a variety of amines as ion-pairs with several anions into organic solvents is described.

EXPERIMENTAL

Samples, reagents and apparatus

The drugs investigated, arranged in order of increasing estimated polarity, were as follows

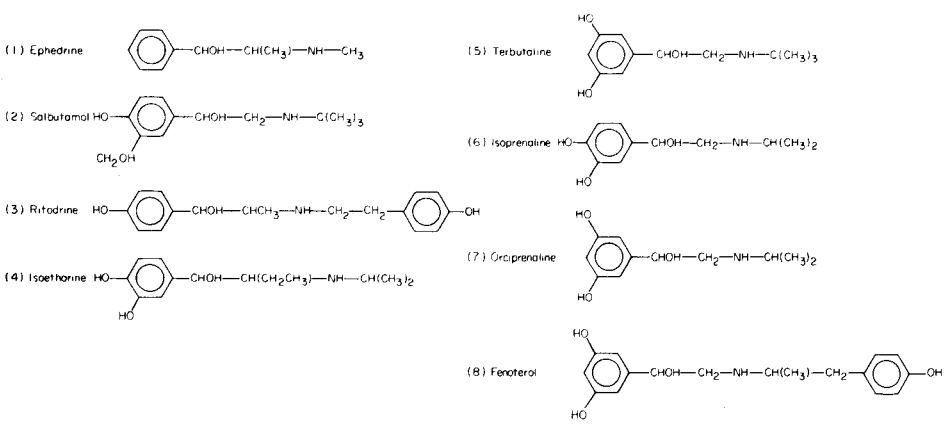

The anions examined for ion-pair formation, arranged in order of increasing polarity, were: bis(2-ethylhexyl)phosphate, triisopropylnaphthalenesulphonate, lauryl sulphate, *p*-toluenesulphonate, hexylsulphonate and perchlorate.

The solvents (all from Merck, analytical purity) examined for extraction are listed in Table 1. The buffers used consisted of 0.1 M NaH_2PO_4, 0.05 M

TABLE 1

Recovery (%) of some sympathomimetics[a] in ion-pair extraction with bis(2-ethylhexyl)-phosphate ion into various organic solvents

Solvent[b]	E	S	R	I_e	T	I_p	O	F
Hexane	28	1	2	4	2	0	0	0
Diisobutyl ether	—	3	2	5	4	0	0	0
Benzene	59	7	17	10	7	0	0	1
Toluene	72	9	21	10	6	0	0	1
Tetrachloromethane	72	10	13	15	11	0	4	0
Tetrachloroethene	—	—	—	—	4	—	0	—
Dichloromethane	99	63	68	57	44	30	41	29
Trichloromethane	99	64	73	66	46	45	46	35
1,2-Dichloroethane	89	32	43	34	21	8	15	6
1,1,2-Trichloroethane	73	38	47	36	24	8	14	7
Ethyl acetate	89	63	100	75	87	64	79	99
Butyl acetate	82	53	97	59	82	46	74	98
Hexyl acetate	—	26	—	16	48	—	28	33
Methyl ethyl ketone	11	21	47	15	27	5	10	39
Diethyl ketone	71	38	—	46	66	21	63	69
2-Heptanone	—	60	97	55	79	—	67	95
1-Butanol	2	33	80	30	52	14	31	72
1-Pentanol	36	61	85	44	69	—	76	83
3-Methylbutan-1-ol	41	70	96	54	83	42	82	90

[a]E = ephedrine, S = salbutamol, R = ritodrine, I_e = isoetharine, T = terbutaline, I_p = isoprenaline, O = orciprenaline, F = fenoterol. [b]Solvents listed in order of increasing polarity.

Na_2HPO_4 and 0.033 M Na_3PO_4 so that the combination required for a particular pH always resulted in a fixed sodium ion concentration.

A Varian 2100 gas chromatograph was equipped with a flame ionization detector and a 1.8 m × 3 mm glass column packed with 3% OV-1 on Gas-Chrom Q (60—80 mesh), which was operated at 200°C with a carrier gas flow of 30 ml min^{-1}. This system was used for concentrations larger than 10^{-6} M. A gas chromatography/mass spectrometry (g.c.—m.s.) combination [15] was used for lower concentrations. All extractions and measurements were made at least in duplicate.

Extractions

The drugs were extracted with bis(2-ethylhexyl)phosphate at pH 7.60. Extractions of terbutaline with the other anions were done at pH 6.90. These pH values were the optimal values for extraction except for ephedrine where a higher pH was required. In the first part of the study, the concentrations of terbutaline, bis(2-ethylhexyl)phosphate and the sodium ion were varied as indicated. In the second part of the study, the concentrations of the drugs, the extracting anions and the sodium ions were kept constant at 8.66×10^{-6} M, 10^{-3} M, and 5×10^{-2} M respectively.

The extraction procedure was as follows. To 1 ml of the buffered aqueous sympathomimetic solution, 1 ml of the organic solvent containing the reagent forming the ion pair was added. After thorough mixing for 5 min on a Vortex mixer, the phases were separated by centrifugation at 1500g. From the organic layer, 0.5 ml was transferred to a Reacti-Vial (Pierce) and the internal standard in appropriate concentration was added (*n*-octadecane for the gas chromatographic procedure or d_6-terbutaline for gas chromatography/mass spectrometry). The organic phase was evaporated under a nitrogen stream at 55°C. The residue was treated with 20 μl of a silylating reagent (BSTFA + 1% TMCS) for 15 min at 80°C. Subsequently 1-μl portions were injected into the gas chromatograph.

Symbols and definitions

The following symbols and definitions are used to describe the processes in the ion-pair extraction of terbutaline (T) and bis(2-ethylhexyl)phosphate (HD) into ethyl acetate: the protonation constant K_{H1} for $H^+ + T \rightleftharpoons HT^+$; the acidity constant K_a for $HD \rightleftharpoons H^+ + D^-$; the ionization constant K_s for $NaD \rightleftharpoons Na^+ + D^-$; the distribution constants $(K_D)_{HD}$ for $HD_w \rightleftharpoons HD_o$ and $(K_D)_{NaD}$ for $NaD_w \rightleftharpoons NaD_o$; and the extraction constant K_{ex} for $T_w + (n + 1)\ HD_w \rightleftharpoons HTD(HD)_{no}$.

RESULTS

Data on the extraction of terbutaline by HD into ethyl acetate are given in Figs. 1 and 2. Data on the extraction of the various drugs with several anions and organic solvents are given in Tables 1 and 2. The recovery of free terbutaline was determined by using equal volumes of aqueous and organic phases without HD present. At pH 7, only 2% of the terbutaline was extracted, with 3% extraction at pH 7.6, 6% at pH 8.2 and 13% at pH 8.8 A maximum recovery of 14% was obtained at pH 9.4.

An indication of the effect of the sodium ions on the extraction of terbutaline was obtained by the following experiment: terbutaline (8.7×10^{-7} M) was extracted at pH 7.6 and an HD concentration of 5×10^{-4} M at two sodium ion concentrations, 0.092 M and 0.050 M. The observed recoveries were 50% and 62%, respectively. The reproducibility of all measurements was 3% for recoveries higher than 10% and 1% for recoveries between 1 and 5%. Some data could not be obtained because impurities in the solvent interfered with the gas chromatographic determination of the drug.

DISCUSSION

Extraction of terbutaline by bis(2-ethylhexyl)phosphate into ethyl acetate

Figure 1 indicates that a variation in the terbutaline concentration of more than 2 decades does not influence the recovery of the terbutaline ion-pair. The HD concentration strongly influences the recovery, high concentrations

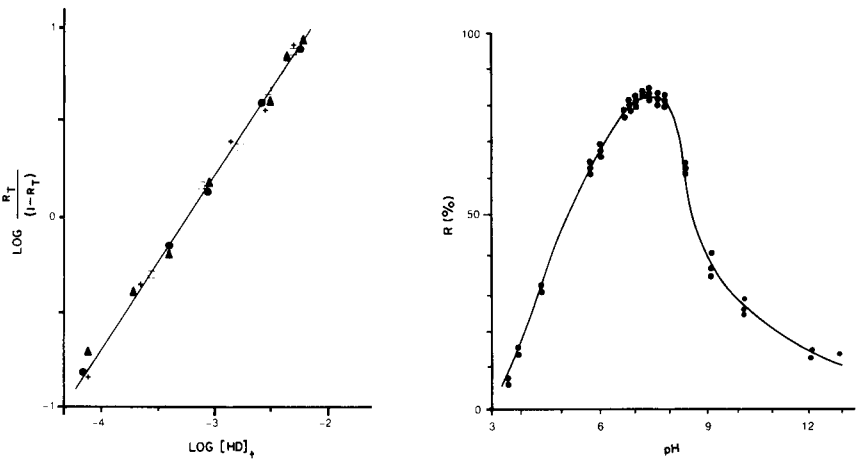

Fig. 1. Relation between the concentration (M) of $[HD]_t$ and the recovery (R_T) at different terbutaline concentrations: (□) 3.5×10^{-7} M; (•) 1.78×10^{-6} M; (+) 8.89×10^{-6} M; (▲) 4.44×10^{-5} M. Conditions: pH 7.6, $[Na^+] = 0.092$ M.

Fig. 2. Recovery of terbutaline as a function of pH. The values for the duplicate or triplicate measurements are indicated. Conditions: $[Na^+] = 0.082$ M, $[HD] = 4.0 \times 10^{-3}$ M, [terbutaline] $= 1.78 \times 10^{-6}$ M.

of HD being favourable. Figure 1 also provides information on the process of ion-pair formation. Assuming that the amount of terbutaline, extracted as such, can be neglected at pH 7.5 when equal volumes of organic and aqueous phases are used, and assuming that at this pH terbutaline is mainly protonated, the recovery of terbutaline (R_T) can be expressed in terms of K_{ex}, K_{HI}, [HD] and $[H^+]$ as follows

$$R_T/(1-R_T) = [HTD(HD)_n]_o/[HT^+] = K_{ex}[HD]_w^{n+1}/K_{HI}[H^+] \quad (1)$$

At constant pH and constant sodium ion concentration, $[HD]_w$ depends only on the initial concentration of HD ($[HD]_i$), thus $[HD]_w = K[HD]_i$, in which K is a combination of $[H^+]$ and $[Na^+]$ and the constants K_a, K_s, $(K_D)_{HD}$ and $(K_D)_{NaD}$. Substitution of this simplification into Eqn. (1) and transformation yields the logarithmic equation

$$\log [R_T/(1-R_T)] = (n+1) \log [HD]_i + \text{constant} \quad (2)$$

The slope of the line in Fig. 1 is calculated to be 0.98, consequently from Eqn. (2), n equals 0. Therefore terbutaline is extracted into ethyl acetate only in the form of an ion pair (HTD) without the formation of adducts. This is in contrast to the work of Modin and Johansson [12] where values for n up to 2 were observed during extraction into trichloromethane, indicating the formation of HTD·HD and HTD·$(HD)_2$. This discrepancy can be explained by the lower concentration of HD used in the present experiments and by the higher polarity of ethyl acetate versus trichloromethane.

TABLE 2

Recovery (%) of terbutaline in ion-pair extraction with some anions[a] into various organic solvents

Solvent	HD	TS	LS	PS	HS	PC
Hexane	2		0	—	—	—
Diisobutyl ether	4	0	0	—	—	—
Benzene	7	0	1	—	—	—
Toluene	6	0	1	0	—	—
Tetrachloromethane	11	0	—	—	—	—
Dichloromethane	44	—	—	0	0	—
Trichloromethane	46	8	34	—	0	—
1,2-Dichloroethane	21	0	1	—	—	—
1,1,2-Trichloroethane	24	0	2	—	—	—
Ethyl acetate	87	73	60	1	2	4
Butyl acetate	82	67	44	1	1	2
Hexyl acetate	48	49	20	—	—	—
Methyl ethyl ketone	27	27	24	1	—	—
Diethyl ketone	66	65	90	2	—	—
2-Heptanone	79	73	70	—	—	—
1-Butanol	52	49	—	—	—	—
1-Pentanol	69	69	—	19	—	—
3-Methylbutan-1-ol	83	78	—	15	—	—

[a]HD = bis(2-ethylhexyl)phosphate, TS = triisopropylnaphthalenesulphonate, LS = laurylsulphate, PS = *p*-toluenesulphonate, HS = hexylsulphonate, PC = perchlorate.

The influence of pH on the recovery of the terbutaline—HD complex is shown in Fig. 2. The maximum between pH 7.1 and 7.9 allows easy extraction from serum or plasma with a normal pH of around 7.4 and a slight buffering capacity. Above pH 9, the accuracy of the measurements decreases because of instability of the terbutaline and reactions in the organic phase (saponification of the ethyl acetate). Another factor that may influence the extraction process is the presence of metal ions which form a complex with HD. When sodium ions are present the following reaction occurs: $D^- + Na^+ \rightleftharpoons NaD_w \rightleftharpoons NaD_o$. Although simple mathematical relations can be derived [16] for the influence of the sodium ion concentration on the distribution of HD between organic and aqueous phases, it is not readily possible to give a relation between the sodium ion concentration and the recovery of terbutaline. Qualitatively, as indicated under Results, increasing sodium ion concentrations decrease the available amount of D^- in the aqueous phase, depending on the dissociation constants K_a and K_s, and thus lower the extraction efficiency for terbutaline.

Extraction of various drugs with several anions and organic solvents

The drugs were listed above in order of increasing estimated polarity, i.e., first in order of increasing number of phenolic hydroxyl groups, then in order of decreasing number of carbon atoms. Likewise, the anions were

arranged in order of decreasing number of carbon atoms. The solvents were arranged in the order: hexane, diisobutyl ether, aromatic hydrocarbons, tetrachloromethane, tetrachloroethane, partially substituted chloroalkanes, esters, ketones, and alcohols.

Table 1 shows that a high recovery is obtained only when the polarities of the drug and the solvent are matched. The apolar solvent, hexane, gives a recovery of only 28% with the least polar drug, ephedrine, recoveries of 1—4% with salbutamol, ritodrine and isoetharine, and virtually no recovery with the most polar drugs isoprenaline, orciprenaline and fenoterol. Diisobutyl ether shows analogous behaviour. The ether group is apparently completely shielded. Somewhat higher recoveries are obtained with benzene, toluene, tetrachloromethane and tetrachloroethene: 60—70% with ephedrine, and 5—20% with salbutamol, ritodrine, isoetharine and terbutaline, but again, the three most polar drugs are scarcely extracted. At the other end of the polarity scale are methyl ethyl ketone and butanol. These solvents are too polar to give good recoveries, especially with the least polar drug, ephedrine. With ephedrine, recoveries exceeding 80% are obtained with partially substituted chloroalkanes and esters. With the most polar drug, fenoterol, extraction by esters, ketones or alcohols is advisable. Esters are thus generally useful solvents.

Table 2 shows that nothing is gained by choosing a more polar anion than bis(2-ethylhexyl)phosphate (HD), though in polar solvents triisopropylnaphthalene sulphonate (TS) gives nearly the same recoveries. This is in agreement with Schill's results [17].

Factor analysis of extraction data with bis(2-ethylhexylphosphate (Table 1)

The appropriate mathematical—statistical technique to correlate a data set like that in Table 1, which can be classified according to the drug or to the solvent, is factor analysis [18]. In its classic form, factor analysis can cope with complete data sets only, but procedures have been developed that can still be applied when half the data are missing [19].

The object of applying factor analysis to the data $y_{d,s}$ in Table 1, where d denotes the drug and s the solvent under consideration, is to describe them by the equation

$$y_{d,s} = \sum_{j=1}^{n} D_j S_j \tag{3}$$

where D and S are adjustable parameters, characterizing the drugs and the solvents, respectively. The number of terms n on the right-hand side of Eqn. (3) is made as large as seems necessary to reduce to residuals

$$y_{d,s} - \sum_{j=1}^{n} D_j S_j = r_{d,s,n} \tag{4}$$

to an acceptably small level.

In the methodology developed for incomplete data sets [18], the successive terms $D_j S_j$ are calculated one-by-one by an iterative procedure ("misfac"),

according to the least-squares criterion, so that $\Sigma_{d,s} r^2_{d,s,n}$ is minimal. The number of terms n is next established, and these n terms are recalculated simultaneously by an iterative procedure ("newfac"), again with the above-mentioned least-squares criterion. The missing data are thus estimated and factor analysis is applied to the completed data set.

In the application of this method to the data in Table 1, it appeared impossible to obtained both a description of the data by Eqn. (3) within the experimental error of 3%, and plausible values for the missing data. This seemed to happen because the data for ephedrine were not well correlated with the data for the other drugs. Ephedrine was the only drug tested that did not contain a phenolic hydroxyl group, and consequently the pH during the extraction (7.60) was lower than the optimal pH for this drug. (The decrease in the recovery of the other drugs at pH >7.60 is due to the onset of ionization of their phenolic groups.) The analysis was therefore repeated without the data on ephedrine, and on tetrachloroethene, for which only two data were available.

The reduction of the mean squared error $(1/m)\Sigma_{d,s} r^2_{d,s,n}$ (where m is the number of data points) in the successive steps of the misfac procedure is given in Table 3. It appears that three terms in the right-hand side of Eqn. (3) suffice to reduce the mean squared error to the value of 9, expected from the experimental error. In other words, the precision of the data does not warrant the calculation of a fourth term. Moreover, the rough experimental estimates that were obtained afterwards for some of the missing data in Table 1 agreed better with values calculated using three terms than those obtained with four terms. Therefore, data calculated by the newfac procedure with three terms was used to complete the matrix, and factor analysis was applied to the completed data set. The results are given in Tables 4 and 5.

Regression analysis of extraction data for terbutaline (Table 2)

The results from the factor analysis can be applied to describe the data on ephedrine in Table 1 and the data in Table 2 by regression analysis, using the equation

$$y_s = \sum_{j=1}^{3} D_j S_j \qquad (5)$$

TABLE 3

Values of the mean squared error in the successive steps of the misfac and factor analysis procedures

m	Misfac	Factor analysis
1	97.2	106.2
2	31.5	39.1
3	10.2	9.7
4	4.6	4.5
5	1.1	1.0

TABLE 4

Values of the parameters D_j, characterizing the drug (in combination with the anion HD), found by factor analysis of the data in Table 1

Drug[a]	D_1	D_2	D_3	Drug[a]	D_1	D_2	D_3
S	1.78	3.96	−0.76	I_p	1.16	2.31	3.20
R	2.82	−0.08	−3.70	O	1.93	0.12	3.25
I_e	1.69	4.57	−0.27	F	2.45	−6.18	0.55
T	2.18	−1.06	0.40				

[a]See footnote to Table 1.

Here, S_j is an independent variable, the values of which are given in Table 5, and D_j is an adjustable parameter. The results (Table 6) show that predictions on drugs, anions (and presumably solvents) that do not occur in the data set of Table 1 must be considered with some reserve: whereas the reliability of predictions for the missing data in Table 1 is 3%, the reliability of predictions for missing data on the extraction of ephedrine, or of the extraction of terbutaline with laurylsulphate, is much worse.

Physical interpretation of the data

Inspection of Table 5 shows that the values of D_j are not related to the polarity of the drugs. However, Table 6 shows a different picture: the values of S_1 are clearly related to the polarity of the solvents. The values of S_2 and S_3 are orthogonal to those of S_1, i.e., they are not linearly related. However, Fig. 3 suggests that S_2 and S_1 are linearly related, if the apolar and polar solvents are considered separately. Further, a quadratic relationship appears to exist between S_3 and S_1.

This suggests that S_1, S_2 and S_3 are all governed by one physical property of the solvents, which is related to their polarity. Therefore, the regression on S_j was investigated for the following physical properties y_s of the solvents:

TABLE 5

Values of the solvent parameters S_j found by factor analysis of the data in Table 1

Solvent[a]	S_1	S_2	S_3	Solvent[a]	S_1	S_2	S_3
HEX	0.59	0.24	−0.16	TCE	39.61	0.46	3.18
DIE	0.76	0.09	−0.17	EAC	36.34	−1.31	1.64
BEN	3.20	0.75	−1.84	BAC	22.22	−4.82	−4.62
TOL	3.65	0.86	−2.28	HAC	12.57	−1.34	−3.17
TCM	3.80	1.15	−1.13	MEK	27.38	−1.08	0.43
TEE	22.89	4.35	−1.45	DEK	35.35	−1.12	0.23
DCM	25.42	4.85	−0.14	HEP	23.55	−2.47	−3.46
CHL	11.22	2.95	−2.98	BUT	32.75	−0.50	2.62
DCE	12.30	3.22	−3.54	MBU	36.71	−0.26	1.71

[a]Listed in the order given in Table 1, without 1-pentanol.

TABLE 6

Values of parameters D_j, characterizing drug—anion combinations, found by regression analysis of the data on ephedrine (Table 1), and of the data in columns 3—5 of Table 2

Drug[a]	Anion[b]	D_1	D_2	D_3	σ[c]
E	HD	2.09 ± 0.33	13.3 ± 3.6	−4.8 ± 3.5	29.0
T	TS	1.80 ± 0.05	−5.5 ± 0.6	2.0 ± 0.5	5.6
T	LS	0.19 ± 0.06	−0.4 ± 0.5	0.8 ± 0.5	5.0
T	PS	1.63 ± 0.20	−1.7 ± 1.9	2.5 ± 1.9	16.7

[a]E = ephedrine; T = terbutaline. [b]See footnote to Table 2. [c]Standard deviation of the regression.

molecular mass, density, dielectric constant, refractive index, diamagnetic susceptibility, boiling point, heat of vaporization, Hildebrand's solubility parameter, solubility in water, solubility of water in the solvent, surface tension, and interfacial tension vs. water. Only the last property (γ) appeared to be well correlated with S_j

$$\gamma = (48 \pm 3) - (1.30 \pm 0.12)S_1 + (3.2 \pm 0.6)S_2 + (3.2 \pm 1.0)S_3$$

the standard deviation of the regression being 4 dyne cm^{-1}.

For a macroscopic model, the dependence of the recovery on the interfacial tension can be made plausible as follows. When the surface of a solid D is in contact with a drop of a liquid O, the remaining part of the surface being covered with another liquid A, the following relation holds [20] between the free enthalpies of the surface of D in contact with A and O ($G_{D/A}$ and $G_{D/O}$, respectively), the interfacial tension of A and O ($\gamma_{A/O}$), and the contact angle of O with D ($\theta_{O/D}$)

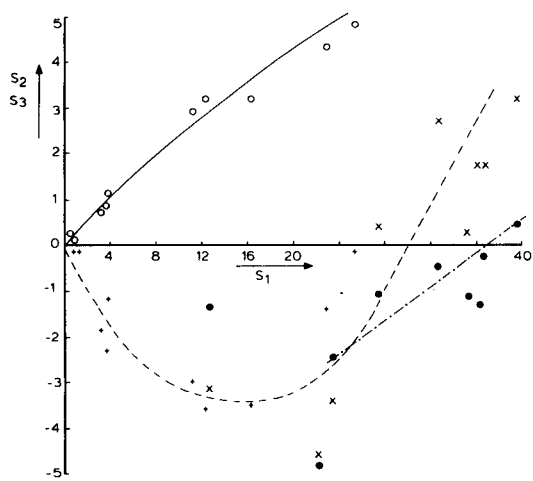

Fig. 3. S_2 and S_3 as a function of S_1. (○) S_2 (polar solvents); (●) S_2 (apolar solvents); (+) S_3 (polar solvents); (×) S_3 (apolar solvents); (——) relationship between $S_2$and S_1 for polar solvents; (—·—) relationship between S_2 and S_1 for apolar solvents; (---) relationship between S_3 and S_1.

$$G_{D/O} - G_{D/A} = -\gamma_{A/O} \cos \theta_{O/D} \quad (6)$$

The free enthalpy for the transfer of a particle of the solid D with surface area Q from the interior of the liquid A to that of the liquid O is then equal to

$$\Delta G_{tr} = -Q\gamma_{A/O} \cos \theta_{O/D} \quad (7)$$

In the present microscopic case, the left-hand side of Eqn. (7) must be replaced by $\Delta \bar{G}^{\circ}_{tr}$, the partial molar standard free enthalpy for the transfer of the drug—anion pair from the aqueous phase A to the organic phase O. $\Delta \bar{G}^{\circ}_{tr}$ cannot be deduced separately from the present measurements, but only in combination with the partial molar standard free enthalpy for ion-pair formation, $\Delta \bar{G}^{\circ}_{pair}$. For example, if drug a and anion α are extracted as an ion-pair in the reaction $a^{+}_{w} + \alpha^{-}_{w} \rightleftharpoons a\alpha_{o}$, then

$$-\mathrm{RTln}\, K = \Delta \bar{G}^{\circ}_{pair} + \Delta \bar{G}^{\circ}_{tr} \quad (8)$$

where $K = [a\alpha]_o/([a^+]_w[\alpha^-]_w) = ([\alpha a]_o[a\alpha]_w)/([a^+]_w[\alpha^-]_w[a\alpha]_w)$

At pH 7.60, $[a\alpha]_o$ and $[a^+]_w$ are virtually equal to the total concentrations of the drug in the organic and aqueous phases, respectively. The concentration of the anion $[\alpha^-]_w$ is smaller than the initial concentration $[\alpha^-]_i$, because of the formation and extraction of ion-pairs with sodium ions. For the ion-pair formation between Na^+ and α^- ions

$$([\alpha^-]_w + [Na\alpha]_w)/[\alpha^-]_w = 1 + [Na^+]_w/K_s \quad (9)$$

For the extraction of $Na\alpha$

$$([\alpha^-]_w + [Na\alpha]_w)/[\alpha^-]_i = 1 - R' \quad (10)$$

where R' is the extracted fraction. From Eqns. (9) and (10) it follows that

$$[\alpha^-]_w = [\alpha^-]_i (1 - R')/(1 + [Na^+]_w/K_s) \quad (11)$$

which, in combination with Eqn. (8), yields

$$\mathrm{RTln}\, \{R/(1-R)\}\{1 + [Na^+]_w/K_s\}/\{(1-R')[\alpha^-]_i\} = -(\Delta \bar{G}^{\circ}_{pair} + \Delta \bar{G}^{\circ}_{tr})$$
$$= Q\gamma \cos \theta_{O/D} - \Delta \bar{G}^{\circ}_{pair} \quad (12)$$

For sodium bis(2-ethylhexyl)phosphate, $K_s = 29 \pm 3$ M, and values of R' are given in Table 7. For the sodium salts of other anions, the formation and extraction of ion-pairs can be neglected.

From the values of R, calculated from Eqn. (3), the above-mentioned values of K_s and R' and the known values of $[Na^+]_w$ and of the original concentration of the extracting anions, values of $\Delta \bar{G}^{\circ}_{pair} + \Delta \bar{G}^{\circ}_{tr}$ were calculated. Two examples of the relationship between $\Delta \bar{G}^{\circ}_{pair} + \Delta \bar{G}^{\circ}_{tr}$ and γ are given in Fig. 4 for the least and most polar drugs. The shapes of the curves in Fig. 4 can be explained as follows. For a given ion-pair, ΔG°_{pair} is constant. Small values of γ occur when the aqueous and organic phases are very alike. In that case, the contact angle $\theta_{O/D}$ of the organic phase O with the solid D will be little different from 90°, and $\cos \theta_{O/D} \simeq 0$. When γ increases, the right-hand

TABLE 7

Recovery (%) of sodium bis(2-ethylhexyl)phosphate in ion-pair extraction with various organic solvents

Solvent	Recovery (%)	Solvent	Recovery (%)	Solvent	Recovery (%)
HEX	2	CHL	31	MEK	40
DIE	4	DCE	3	DEK	40
BEN	4	TCE	4	HEP	35
TOL	5	EAC	34	BUT	60
TCM	3	BAC	8	PEN	30
DCM	20	HAC	8	MBU	30

side of Eqn. 12 increases rapidly, partly because of the increase of γ, but mostly because $\theta_{O/D}$ decreases from 90°, i.e., the solid is wetted better by a polar organic than by the aqueous phase. The maximum in the left-hand side occurs in those solvents that wet the solid best, i.e., it corresponds to the minimum value of $\theta_{O/D}$. When γ increases beyond the value corresponding with the maxima in the graphs in Fig. 4, i.e., when the organic phase becomes less and less polar, the solid is wetted increasingly poorly and $\theta_{O/D}$ increases again. The largest conceivable value of γ is 72 dyne cm^{-1}, occurring when the fluid O is the vapour phase. Clearly, the left-hand side of Eqn. (12) then has a very large negative value which means that cos $\theta_{O/D}$ is now negative, or $\theta_{O/D} > 90°$, or $\theta_{A/D} < 90°$, which is plausible. This variation of θ with γ is illustrated in Fig. 5.

A correlation of liquid—liquid partition coefficients with the interfacial tension of the two-phase system has been observed before [21, 22], for uncharged organic solutes. In these investigations, extreme values of the partition coefficients at γ values of 10—25 dyne cm^{-1}, like those shown in Fig. 4, were found, but the authors were not able to give an explanation for

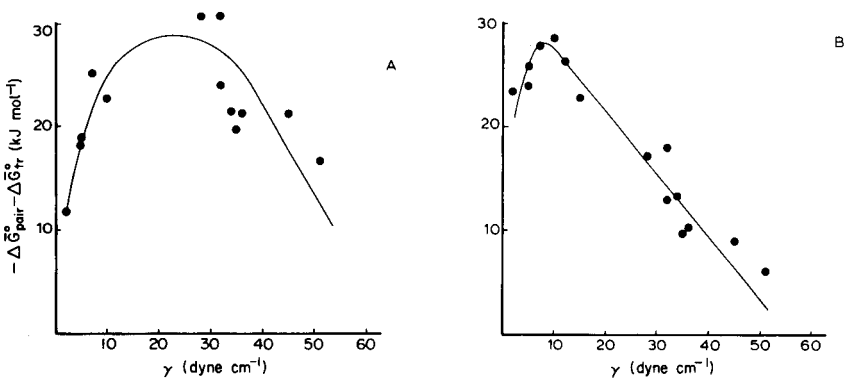

Fig. 4. $-\Delta\bar{G}^{\circ}_{pair} - \Delta\bar{G}^{\circ}_{tr}$ as a function of the interfacial tension γ of the aqueous and organic solvent phases, for the extraction of ephedrine (A) and fenoterol (B) with bis(2-ethylhexyl)phosphate. Values of γ are taken from refs. 23—26.

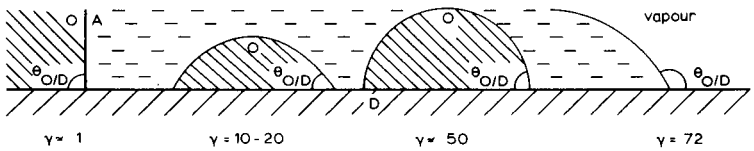

Fig. 5. A solid D in contact with two fluids A and O, an aqueous phase and an organic (or the vapour) phase, respectively. The magnitude of the contact angle between the solid and fluid O, $\theta_{O/D}$, as a function of the interfacial tension between the two fluids, $\gamma_{A/O}$, is shown.

the phenomenon. They interpreted the slopes of their graphs at higher values of γ in terms of the molar surface area of the solute. It follows from the present model and from Eqn. (12) (which are correct for the macroscopic case) that this is not justified, because of the occurrence of the unknown factor $\cos\theta$ in the right-hand side of this equation.

CONCLUSIONS

Terbutaline is only extracted as HTD into ethyl acetate in the concentration range 10^{-2}—10^{-4} M. The processes involved in the extraction procedure with ethyl acetate are: (1) formation of the ion pair, $H^+ + D^- + T_w \rightleftharpoons HTD_w \rightleftharpoons HTD_o$, which is dependent on the hydrogen ion concentration and the HD_w or D^- concentration; (2) decrease of the D^- concentration by ion-pair formation with Na^+ ions, $Na^+ + D^- \rightleftharpoons NaD_w \rightleftharpoons NaD_o$; and (3) extraction of the free terbutaline, $T_w \rightleftharpoons T_o$, which depends on the pH (at low pH terbutaline is protonated and so not extracted).

The recovery of seven sympathomimetics with a common extracting anion and eighteen organic solvents can be described by factor analysis. Three factors are required to describe the data with a precision corresponding to the experimental error. A linear relationship appears to exist between the interfacial tension of the aqueous and organic phases and the three factor analysis parameters that characterize the phase systems. The influence of the interfacial tension on the recovery can be explained by a macroscopic model of a solid surface in contact with two fluids. A high recovery is obtained by using a large apolar anion and solvents of intermediate polarity such as esters.

The authors thank the following companies for providing the sympathomimetics: Astra Pharmaceuticals, Boehringer Ingelheim, Glaxo and Philips Duphar.

REFERENCES

1 Y. Kakimoto and M. D. Armstrong, J. Biol. Chem., 237 (1962) 208.
2 S. L. Tripp, E. Williams, W. J. Roth, W. E. Wagner and G. Lucas, Anal. Lett., B11 (1978) 741.
3 T. L. Perry and W. A. Schroeder, J. Chromatogr., 12 (1963) 358.
4 M. G. Bigdeli and M. A. Collins, Biochem. Med., 12 (1975) 55.

5 B. B. Brodie, S. Udenfriend and W. Dill, J. Biol. Chem., 168 (1947) 335.
6 R. Modin and G. Schill, Acta Pharm. Suec., 4 (1967) 301.
7 G. J. Divatia and J. Biles, J. Pharm. Sci., 50 (1961) 916.
8 J. Levine and R. T. Ottes, J. Assoc. Off. Anal. Chem., 44 (1961) 291.
9 K. O. Borg, H. Holgersson and P. O. Lagerström, J. Pharm. Pharmacol., 22 (1970) 507.
10 G. Schill, Acta Pharm. Suec., 2 (1965) 13.
11 D. M. Temple and R. Gillespie, Nature, 209 (1966) 714.
12 R. Modin and M. Johansson, Acta Pharm. Suec., 8 (1971) 561.
13 J. G. Leferink, I. Wagemaker-Engels, W. M. Arendse, R. A. A. Maes and M. van der Straeten, Biomed. Mass Spectrom., 3 (1976) 184.
14 J. G. Leferink, Ph.D. Thesis, University of Utrecht, 1979.
15 J. G. Leferink, I. Wagemaker-Engels, R. A. A. Maes, H. Lamont, R. Pauwels and M. van der Straeten, J. Chromatogr., 143 (1977) 399.
16 P. Brandts, Graduation Report, State University Utrecht, 1980.
17 G. Schill, Acta Pharm. Suec., 8 (1971) 561.
18 H. H. Harman, Modern Factor Analysis, University of Chicago Press, Chicago, 1970.
19 C. L. de Ligny, G. H. E. Nieuwdorp, W. K. Brederode, W. E. Hammers and J. C. van Houwelingen, Technometrics, 23 (1981) 91.
20 J. T. Davies and E. K. Rideal, Interfacial Phenomena, Academic Press, New York, 1961, equation 1.42, and p. 16.
21 A. Vignes, J. Chim. Phys. Phys. Chim. Biol., 57 (1960) 966.
22 C. Eon, B. Novosel and G. Guichon, J. Chromatogr., 83 (1973) 77.
23 R. C. Weast (Ed.), Handbook of Chemistry and Physics, CRC Press, Cleveland, 1978—1979, F 45 pp.
24 Landolt-Börnstein, Zahlenwerte und Funktionen, 11. Band, 3. Teil, Springer-Verlag, Berlin, 1956, 462 pp.
25 P. C. Hiemenz, Principles of Colloid and Surface Chemistry, M. Dekker, New York, 1977, 406 pp.
26 J. van Alphen, Tabellenboekje, D. B. Centen, Amsterdam, 1962, 187 pp.

Analytica Chimica Acta, 135 (1982) 99—110
Elsevier Scientific Publishing Company, Amsterdam — Printed in The Netherlands

TRACE METAL SPECIATION IN SEA WATER — A PAPER ELECTROPHORETIC APPROACH

RAIMUND RÖHL[a]
P. M. Gross Chemical Laboratory, Duke University, Durham, NC 27706 (U.S.A.)
(Received 1st June 1981)

SUMMARY

Stability constants of individual trace metal complexes form the basis for calculations predicting the distribution of trace metal species in complexing media, such as sea water. In this study, the electrophoretic mobility of radiotracer ^{210}Pb is measured as a function of ligand concentration in chloride and sulfate solutions of constant ionic strength and temperature. A theoretically-derived expression, relating mobility to ligand concentration and complex stability constants, is fitted by the method of least squares to the experimental data to obtain estimates of the conditional stability constants of lead(II) chloro and sulfato complexes at 23°C and ionic strength 0.7 i.e., under conditions resembling those of ocean water. The values obtained are: $\log \beta_1 = 0.999 \pm 0.014$, $\log \beta_2 = 1.037 \pm 0.032$, $\log \beta_3 = 1.250 \pm 0.015$ for lead(II) chloro complexes, and $\log \beta_1 = 1.048 \pm 0.015$ and $\log \beta_2 = 1.183 \pm 0.025$ for lead(II) sulfato complexes. Experiments with eight other metal ions [Au(III), Bi(III), Cd(II), Co(II), Cu(II), Hg(II), Ni(II), and Po(IV)] and with sea water as electrolyte indicate the general applicability of the method.

The chemical speciation of trace metals in complexing media is of considerable interest to several fields of scientific study. In environmental systems, such as sea water, speciation is considered to be the main factor controlling the distribution and transport of metals. Chemical speciation studies in sea water are usually hampered by the low metal concentrations and the high ionic strength and chemical complexity of the medium. Most techniques presently available that have the potential to cope with these problems are based on anodic stripping voltammetry. This work explores the potential utility of paper electrophoresis as a tool for studying metal speciation in high ionic strength electrolytes, particularly sea water.

Electrophoresis separates charged particles according to their differential migration under the influence of an electric field. Although it is most often applied to complex organic molecules, the method was originally developed for inorganic ions [1]. Much attention has been devoted to applying electrophoresis to the separation of radioisotopes [2, 3] and metastable complexes of platinum group metals [4, 5]. Few studies are found in the literature in which electrophoresis was used to gain quantitative information about the speciation of an element [5—8].

[a]Present address: Tennenloher Str. 14, 8521 Uttenreuth, W. Germany.

Because of the continued interest in the speciation of heavy metals in sea water, the complexation reactions of lead(II) with chloride and sulfate in synthetic electrolytes of ionic strength 0.7 were chosen as model systems for this study. A small number of experiments was also carried out with other metals [Au(III), Bi(III), Cd(II), Co(II), Cu(II), Hg(II), Ni(II), and Po(IV)] and with sea water as electrolyte.

THEORY

When a metal ion M^i forms complexes with an anionic ligand L^-

$$M^i \overset{L^-}{\rightleftharpoons} ML^{i-1} \overset{L^-}{\rightleftharpoons} ML_2^{i-2} \cdots ML_j^{i-j} \tag{1}$$

in an electrophoretic experiment, its attraction by the cathode is decreased in the presence of L^-, because of a reduction in charge n ($n = i - j$). At equilibrium, these reactions can be described by a series of stability constants. Total conditional stability constants, β_j, of complexes ML_j^{i-j} are then given by $\beta_j = [ML_j^{i-j}]/[M^i][L^-]^j$. If conversion of ionic species is rapid on the time scale of an electrophoretic experiment, the metal migrates in a single zone, at a rate which is determined by the mobilities of the individual species and their time-averaged abundances [3, 6, 7]. All other factors being equal, the mobility of the composite zone, u_z, can be expressed as a function of ligand concentration by

$$u_z([L]) = \sum_{j=0}^{J} u_{ML_j}\beta_j[L]^j \Big/ \sum_{j=0}^{J} \beta_j[L]^j \tag{2}$$

With a knowledge of individual mobilities u_{ML_j}, this relation provides a basis for estimating stability constants, β_j, from measurements of u_z at different ligand concentrations. If conversion is relatively slow, however, different ionic species are separated from each other and migrate in isolated zones. This has been observed for the halogeno complexes of Rh(III), Ir(III), Os(IV), Pt(IV), and Re(IV) [5] and under certain conditions for those of Cd(II) [9]. Therefore, electrophoresis yields information on the thermodynamic stability and the kinetic behavior of metal complexes.

EXPERIMENTAL

The electrophoresis apparatus (Warner Chilcott E8002B) consisted of a 40 × 21 cm water-cooled plexiglas plate and two electrolyte vessels fitted with graphite electrodes. Voltage of the Warner Chilcott 1910 power supply could be controlled to better than ±2 V. Cooling of the paper was achieved by circulating water of 22°C from a refrigerated water bath through the plexiglas plate and a 45 × 21 cm polyethylene bag placed on top of the paper strips. The bag was sealed with weather-stripping adhesive and fitted with two pieces of Tygon tubing at diagonally opposite corners for water

inlet and outlet. This structurally flexible design was chosen to provide for even pressure on the paper and to avoid shifts in the distribution of electrolyte. Whatman No. 1 paper was cut into 4 × 57 cm strips and used without further pretreatment. All experiments were done with paper from the same batch. The final temperature in the paper strips was 23 ± 0.1°C. A Varian Aerograph LB 2722 radiogram scanner served to determine the position of radionuclides in developed electrophoregrams.

Reagents were ACS certified except for sodium perchlorate, which was of purified grade. Chemical tests showed that the salt contained negligible amounts of chloride and sulfate ions. Double deionized water was used to prepare all synthetic electrolytes. A solution of lead-210 nitrate (Amersham-Searle) was diluted to give a lead concentration of 1.6×10^{-7} M in 0.03 M nitric acid; it also contained small amounts of the radioactive daughter nuclides ^{210}Bi and ^{210}Po. Sea water was collected off the North Carolina continental shelf at 1200 m depth and stored at 5°C. Before use, the water was brought to room temperature and filtered through 0.2-μm Nuclepore membranes to remove any suspended material; its pH was measured to be 8.2. A few milligrams of gold were dissolved in aqua regia to obtain a solution of "gold chloride". Test solutions of other metals were prepared by dissolving cadmium nitrate, nickel sulfate, and the chlorides of cobalt, copper and mercury in sea water to give concentrations of approximately 0.1 M. A 3% solution of hydrogen peroxide served as an indicator for electro-osmotic flow.

Synthetic electrolyte solutions were prepared from 0.697 M sodium perchlorate, 0.697 M sodium chloride, 0.232 M sodium sulfate and 1.00 M perchloric acid which was 5.00×10^{-4} M in (stable) lead nitrate. In the two main experiments, perchlorate was gradually replaced by chloride and sulfate to give chloride concentrations in the range 0—0.690 M and sulfate concentrations of 0—0.232 M. All solutions were made 1.00×10^{-2} M in perchloric acid and 5.0×10^{-6} M in lead nitrate to give a formal ionic strength of 0.700 and a pH of 2.0—2.6. Low pH was chosen to avoid interference from complexation of lead with hydroxide and carbonate and to decrease adsorption of lead by the paper.

Paper strips were soaked in supporting electrolyte for about 2 min. After removal of excess of solution by pulling the strips over a glass rod, they were sandwiched between two polyethylene sheets which prevented radioactive contamination of the electrophoresis apparatus. Half of the remaining electrolyte was filled into each of the two electrode vessels. Before addition of the test solutions, a potential of 400 V was applied to the system for 5 min to allow the temperature of the paper strips to attain steady state. The cooling bag and cover sheets were then briefly removed and 25 μl of hydrogen peroxide or metal solution was applied in a line at half distance between the electrodes. After reassembly, electrophoresis was allowed to proceed for 60 min at 400 V. The field strength was measured to be 8.16 V cm^{-1}. Developed electrophoregrams were blotted with filter paper and air-dried.

Radioactivity scans for lead were performed 30 days after experiments. This time lag was necessary to let the weak β-emitting ^{210}Pb decay to its hard β-emitting daughter nuclide ^{210}Bi. Migration of ^{210}Bi and ^{210}Po originally present in test solutions was measured by scanning within three days of electrophoretic separations. The α-radiation of ^{210}Po could be excluded from detection by placing a 4.3×10^{-3} g cm^{-2} aluminum diaphragm in front of the counter window. Thus, the time dependence of nuclide concentrations and the widely different energies of radiation made it possible to determine the position of all three nuclides on the electrophoregrams.

RESULTS AND DISCUSSION

The narrow and symmetrical shapes of scanning peaks (Fig. 1) indicated that diffusional spreading of radioactive zones was small and that adsorption of cationic lead(II) species was negligible. From ten measurements at different ligand concentrations, an average width at half height of 0.87 ± 0.09 cm was calculated for lead peaks. Migration distances measured for lead(II) at different chloride and sulfate concentrations are plotted versus ligand concentration in Fig. 2. The data shown represent averages from two different paper strips and are corrected for electro-osmotic flow. Replicate electro-osmotic flow measurements with hydrogen peroxide yielded an average of 0.30 ± 0.03 cm h^{-1} (n = 6) for synthetic electrolyte solutions, and 0.39 ± 0.03 cm h^{-1} for sea water (n = 4).

Scanning curves for bismuth and polonium showed no significant mobility of these elements in any of the sulfate-containing solutions or in chloride solutions up to 0.1 M. At higher chloride concentrations, both ^{210}Bi and ^{210}Po migrated at increasing rates towards the anode, reaching −5.3 cm h^{-1} at 0.69 M. The broadness of scanning peaks made quantitative evaluation of

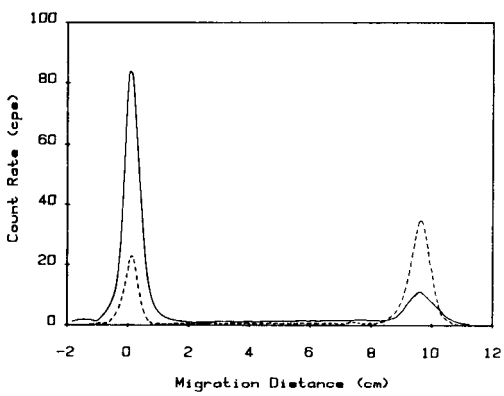

Fig. 1. Scanning curves of an electrophoregram obtained without the aluminum window after 3 days (—) and 30 days (---). The peak near the origin is caused by ^{210}Bi and ^{210}Po, which did not migrate under the experimental conditions (0.69 M $NaClO_4$, E = 8.16 V cm^{-1}, pH 2).

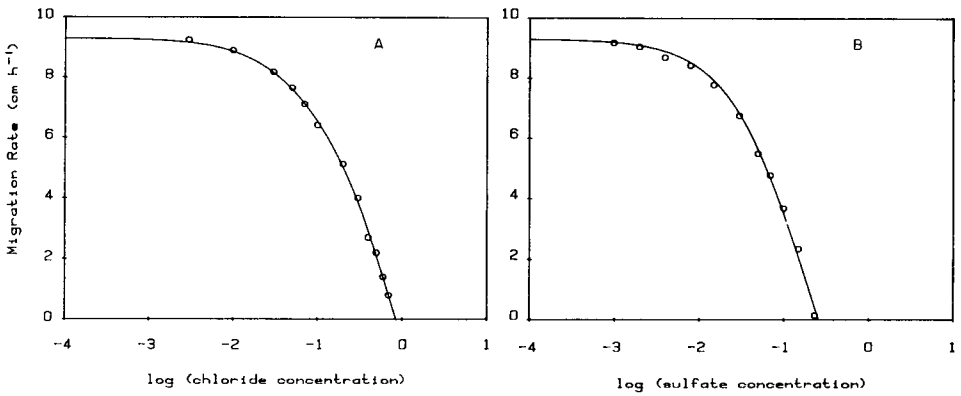

Fig. 2. Migration distance of lead(II) as (A) a function of chloride concentration and (B) a function of total sulfate concentration, after 1 h at 8.16 V cm^{-1} and 23°C. Circles represent means of experimental data corrected for electro-osmotic flow; the line is a least-squares fit of Eqn. (2) to these points.

results difficult. Migration distances measured for nine metals in sea water are summarized in Table 1. Cationic migration was observed for Cd(II), Co(II), Cu(II), Pb(II) and Ni(II), zero mobility for Bi(III) and Po(IV), and anionic migration for Au(III) and Hg(II).

To obtain conditional stability constants for lead chloro and sulfato complexes from the migration data, appropriate forms of Eqn. (2) were fitted to the experimental results, by using an iterative least-squares procedure with the logarithms of the stability constants as fitting parameters. Correlation analysis showed that the standard deviation of individual experiments was independent of migration distance. Therefore, all data points

TABLE 1

Migration of nine metals in sea water at 23°C after 1 h at 8.16 V cm^{-1}

Metal	Migration distance ± std. dev. (cm h^{-1})	No. of detns.	Compound in test solution	Zone detection
Au(III)	−3.86 ± 0.08	4	$HAuCl_4$	H_2O_2/NaOH
Bi(III)	0.00 ± 0.00	2	Ra DEF[a]	Scanning
Cd(II)	0.80 ± 0.04	4	$Cd(NO_3)_2$	NaHS
Co(II)	5.78 ± 0.11	2	$CoCl_2$	NaHS
Cu(II)	4.85 ± 0.07	2	$CuCl_2$	NaHS
Hg(II)	−9.49 ± 0.06	4	$HgCl_2$	NaHS
Ni(II)	5.38 ± 0.11	2	$NiSO_4$	NaHS
Pb(II)	1.18 ± 0.11	2	Ra DEF	Scanning
Po(IV)	0.00 ± 0.00	2	Ra DEF	Scanning

[a]Ra DEF = solution containing a mixture of ^{210}Pb, ^{210}Bi and ^{210}Po.

within one set were assumed to have the same statistical weight. The standard deviations of the fitted parameters were calculated by the method described by Bevington [10], i.e., by parabolic extrapolation of three points on the χ^2 hypersurface near its minimum.

Formation of chloro complexes is among the most intensively studied reactions of lead. The existence of complexes $PbCl_j$ for $1 \leqslant j \leqslant 6$ has been reported in the literature. Most stability constants compiled by Sillén and Martell [11] are thermodynamic constants, i.e., extrapolated to zero ionic strength. Because of the uncertainty in activity coefficients, it is difficult to back-extrapolate such values to high ionic strength conditions. To avoid this problem, the concept of conditional stability constants is commonly employed [12]. In this study, activity coefficients of unity were assumed for all ions in electrolytes of ionic strength 0.7, thus yielding conditional stability constants for lead(II) complexes in the media specified.

From Sillén and Martell's compilations, it can be concluded that the highly substituted complexes $PbCl_5^{3-}$ and $PbCl_6^{4-}$ are formed only at chloride concentrations exceeding those used in this work. Interpretation of migration distances in chloride solutions therefore considered only the formation of complexes up to $PbCl_4^{2-}$. Comparative calculations with $j = 3$ and $j = 4$ showed that the experimental data could be explained on the basis of the first three lead(II) chloro complexes alone. Migration rates of lead in sulfate solutions were adequately fitted by an equation taking into account the formation of $PbSO_4$ and $Pb(SO_4)_2^{2-}$.

With regard to the mobility of lead(II) in different ionic forms, it must be pointed out that only the mobility of uncomplexed Pb^{2+} could be measured directly. In the initial phase of curve-fitting calculations, it was assumed that mobilities of lead(II) complexes were determined by charge alone, i.e., that mobilities of singly-charged complexes were half those of doubly-charged species. Table 2 lists the results obtained with this simplifying assumption. More refined calculations for the chloride data-set included the mobilities of $PbCl^+$ and $PbCl_3^-$ as fitting parameters and produced the values given in Table 3. The latter results were used to plot the fitted mobility curves in

TABLE 2

Stability constants of lead(II) chloro and sulfato complexes at 23°C and I = 0.7 derived from electrophoresis data assuming that complex mobilities are proportional to charge

Complexing ion	Coordination number, j	Fitting parameter $\log \beta_j$	Total stability constant, β_j	Individual stability constant, K_j
Cl^-	1	1.004 ± 0.014	10.1 ± 1.03	10.1 ± 1.03
	2	1.054 ± 0.031	11.3 ± 1.07	1.12 ± 0.16
	3	1.240 ± 0.015	17.4 ± 1.04	1.53 ± 0.17
SO_4^{2-}	1	1.048 ± 0.015	11.2 ± 1.04	11.2 ± 1.04
	2	1.183 ± 0.025	15.3 ± 1.06	1.36 ± 0.16

TABLE 3

Stability constants and mobilities of lead(II) chloro complexes at 23°C and I = 0.7 derived from electrophoresis data. The mobilities of $PbCl^+$ and $PbCl_3^-$ were included as fitting variables in the calculations

Fitting parameter	Total stability constant	Individual stability constant
$\log \beta_1 = 0.999 \pm 0.014$	$\beta_1 = 9.98 \pm 1.03$	$K_1 = 9.98 \pm 1.03$
$\log \beta_2 = 1.037 \pm 0.032$	$\beta_2 = 10.9 \pm 1.08$	$K_2 = 1.09 \pm 0.17$
$\log \beta_3 = 1.250 \pm 0.015$	$\beta_3 = 17.8 \pm 1.04$	$K_3 = 1.63 \pm 0.19$
$u_{PbCl^+} = 4.61 \pm 0.07$ cm h^{-1}		
$u_{PbCl_3^-} = -4.45 \pm 0.21$ cm h^{-1}		

Fig. 2 and the distribution of lead(II) chloro complexes as a function of ligand concentration in Fig. 3. Although the refined fitting calculations (Table 3) yielded somewhat lower mobilities than those based on charge alone (Table 2), the stability constants obtained by both methods were identical within the calculated error limits.

Two sea-water speciation models frequently referred to in the literature [13, 14] used the following values for stability constants of lead(II) chloro complexes:

Reference	$\log \beta_1$	$\log \beta_2$	$\log \beta_3$	$\log \beta_4$
Zirino and Yamamoto [13]	1.07	0.92	0.76	0.61
Dyrssen and Wedborg [14]	0.88	1.49	1.09	0.94

The wide discrepancy between these models is a good example of the uncertainty in the speciation of many trace metals in sea water. Using the results of the present study as a basis, it was calculated that at the chloride concentration of sea water of about 0.54 M [15], the relative abundance of

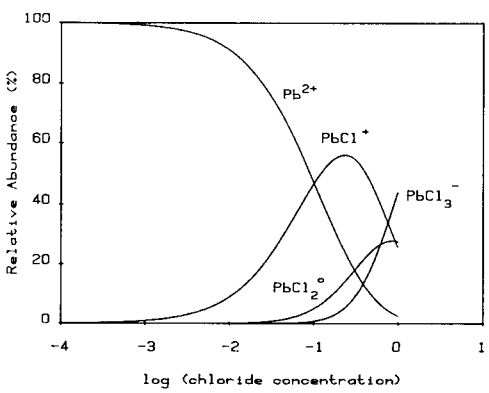

Fig. 3. Distribution of lead(II) chloro complexes as a function of chloride concentration.

lead(II) chloro complexes decreases in the sequence $PbCl^+$ (44 ± 5%), $PbCl_2$ (26 ± 3%), and $PbCl_3^-$ (22 ± 2%) with 8 ± 1% remaining as free Pb^{2+} ions.

An attempt was also made to refine the fitting calculations for the sulfate data-set by allowing the mobility of $Pb(SO_4)_2^{2-}$ to vary freely. However, a unique solution, i.e., an absolute χ^2 minimum could not be identified unambiguously. This was probably due to the disposition of experimental data points with very few measurements in the sulfate concentration range in which $Pb(SO_4)_2^{2-}$ is formed. The results listed in Table 2 were therefore taken as best estimates of stability constants for sulfato complexes of Pb(II) at ionic strength 0.7 and 23°C and were used to calculate the curves plotted in Figs. 2B and 4. At the average oceanic sulfate concentration of 0.029 M [15], the predominant species in the series of lead(II) sulfato complexes is the free Pb^{2+} ion (75 ± 7%), followed by $PbSO_4$ (24 ± 3%) and $Pb(SO_4)_2^{2-}$ (1 ± 0.1%). Considering both chloride and sulfate complexation, the distribution of major Pb(II) species is: $PbCl^+$ (42 ± 9%), $PbCl_2$ (25 ± 5%), $PbCl_3^-$ (22 ± 4%), Pb^{2+} (8 ± 1%), and $PbSO_4$ (3 ± 0.5%). The stability constants obtained for $PbSO_4$ and $Pb(SO_4)_2^{2-}$ (Table 2) agree well with values given by Goleva et al. [16]. These authors used $\log \beta_1 = 2.22$ and $\log \beta_2 = 2.46$ (for $I = 0$) in their study of lead(II) migration in ground waters. Extrapolation of their constants to $I = 0.7$ with the activity coefficients employed by Zirino and Yamamoto [13], yields $\log \beta_1 = 1.08$ and $\log \beta_2 = 1.10$, respectively.

The results of paper electrophoresis experiments with Au(III), Bi(III), Cd(II), Co(II), Cu(II), Hg(II), Ni(II), Pb(II) and Po(IV) in sea water are given in Table 1. These experiments were intended to give information about the suitability of natural sea water as a background electrolyte and about the applicability of the method to speciation studies of metals other than lead. As neither pH nor any of the major ion concentrations were varied, the results primarily provide an indication of the average charge of the different complex species formed by each element under sea-water conditions.

If one assumes that the free metal ions have mobilities similar to Pb^{2+} in 0.69 M sodium perchlorate at pH 2 (taking into account the effect of

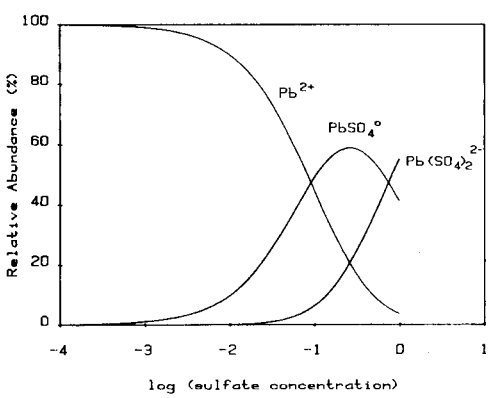

Fig. 4. Distribution of lead(II) sulfato complexes as a function of total sulfate concentration.

charge), all of the metals tested showed a certain degree of complexation in sea water. It was lowest for the transition metals Co(II), Ni(II) and Cu(II), and highest for Au(III) and Hg(II), which were the only metals exhibiting anodic migration. Interestingly, the order in which the migration rates decreased from Co(II) to Ni(II) and Cu(II) coincides with the sequence of increasing tendency of transition elements to form complexes given by the Irving–Williams series [17].

Several sea-water speciation models for seven of the metals tested are compiled in Table 4. Since this study focussed on the speciation of lead, the table includes six published models for this element. No detailed information on the chemical speciation of bismuth(III) and polonium(IV) seems to be presently available. The following observations are based on a comparison of Tables 1 and 4.

The migration rate measured for mercury(II) is in agreement with most speciation models for this element [12, 14, 24], giving $HgCl_4^{2-}$ as the predominant species at the chloride concentration of sea water. The electrophoresis result for gold indicates an average charge of −1, which is in accord with the predominance of $AuCl_4^-$ or $AuCl_2^-$ [18]. The electrophoretic migration rates measured for cobalt(II) and nickel(II) qualitatively agree with Ahrland's report [19], indicating that the major species of these elements in sea water are the free cations M^{2+} and monovalent chloride complexes MCl^+.

Both speciation models cited in Table 4 for Cd(II) give uncharged $CdCl_2$ as the principal form of cadmium, but differ widely in their estimates of the relative abundances of $CdCl^+$ and $CdCl_3^-$. Assuming $u_{CdCl^+} = u_{PbCl^+}$ and $u_{CdCl_3^-} = u_{PbCl_3^-}$, and taking into account the correction for electro-osmotic flow, a

TABLE 4

Major inorganic species of seven metals in sea water according to several published models

Metal	Major species	Reference
Au	$AuCl_2^-$ (66%), $AuClBr^-$ (12%)	18
Cd	$CdCl_2$ (50%), $CdCl^+$ (40%), $CdCl_3^-$ (6%)	13
Cd	$CdCl_2$ (38%), $CdCl^+$ (29%), $CdCl_3^-$ (28%)	14
Co	Co^{2+} (54%), $CoCl^+$ (31%), $CoCO_3$ (7%), $CoSO_4$ (7%)	19
Cu	$Cu(OH)_2$ (83%), $CuCO_3$ (11%)	13
Cu	CuOHCl (65%), $CuCO_3$ (22%), $CuCl^+$ (6%), $CuOH^+$ (4%)	14
Hg	$HgCl_4^{2-}$ (66%), $HgCl_3Br^{2-}$ (12%), $HgCl_3^-$ (12%)	14
Ni	Ni^{2+} (53%), $NiCl^+$(31%), $NiCO_3$ (9%), $NiSO_4$ (6%)	19
Pb	$PbCl^+$ (30%), $PbHCO_3^+$ (25%), Pb^{2+} (20%), $PbCO_3$ (15%)	20
Pb	$PbCO_3$ (76%), $PbCl^+$ (11%), $PbCl_2$ (5%)	13
Pb	$PbOH^+$ (42%), $PbCO_3$ (32%), $PbCl^+$ (12%)	21
Pb	$PbCl_2$ (42%), $PbCl^+$ (19%), $PbOH^+$ (10%), PbOHCl (9%)	14
Pb	$PbOH^+$ (90%), Pb^{2+} (7%), $PbCO_3$ (3%)	22
Pb	$PbCO_3$ (48%), $PbCl_2$ (25%), $PbCl^+$ (12%), $PbCl_3^-$ (8%), Pb^{2+} (2%), $PbCl_4^{2-}$ (2%), $PbOH^+$ (2%)	23

concentration ratio $[CdCl^+]:[CdCl_3^-]$ of 1.38 can be calculated from the measured migration rate of cadmium in sea water. This is rather close to the value (1.04) obtained from Dyrssen and Wedborg's model [14]. Of course, this calculation is only valid if cadmium does not complex with ligands other than chloride. Baric and Branica [25] reported that hydrolysis of Cd(II) does not occur below pH 9.5, and that $CdCl^+$ is the predominant cadmium species in sea water.

A wide discrepancy exists between ionic abundances predicted by the referenced models [13, 14] and the average electrophoretic mobility determined for copper(II) complexes in sea water. While the latter indicates an average charge of +1, the models predict that between 87 and 94% of all Cu(II) in sea water is in the form of uncharged complexes (CuOHCl, $Cu(OH)_2$, and $CuCO_3$). It is conceivable that the relatively high copper concentration of 0.1 M in the test solution "swamped" the small amounts of hydroxide and carbonate ions in the background electrolyte, so that the major portion of copper ions was not complexed by these ligands, but was present as aquated Cu^{2+} and in the form of Cu(II) chloro complexes.

Based on results from electrophoresis experiments in sodium perchlorate/chloride mixtures, one would expect a lead migration rate of 1.76 cm h^{-1} at the oceanic chloride concentration of about 0.54 M if only chloro complexes were formed. Taking into account sulfate complexation, this value is reduced to 1.70 cm h^{-1}. The remaining difference to the migration rate measured in sea water (1.18 cm h^{-1}) is most probably due to complexation of lead with hydroxide and carbonate. Unfortunately, it is generally difficult to study reactions of metals with these ligands independently from each other, because the speciation of carbonate itself is pH-dependent. One electrophoresis experiment done with 0.01 M sodium hydrogencarbonate in 0.69 M perchlorate (pH 8.2) resulted in zero net migration of ^{210}Pb, giving no indication of the formation of $Pb(CO_3)_2^{2-}$ ions [21]. The average hydrogencarbonate concentration of sea water is 2.4×10^{-3} M [15].

There are two critical points in the present approach to studying metal speciation. The first is the necessity to avoid all interferences which alter zone mobilities aside from the effect of complexation; the second is to obtain good estimates of mobilities which are not accessible to direct determination. Interferences can be reduced by exclusion through proper design, by careful control of experimental conditions, and by correction. Complicating factors which were eliminated were evaporation of solvent and variable distribution of electrolyte in the paper caused by uneven pressure. Parameters kept constant were electric field strength, duration of experiments, temperature, type, size and batch of paper, and formal ionic strength. Electro-osmotic flow was measured and results were used to correct metal zone mobilities.

Judging from the shape of radio-scanning peaks, adsorption did not significantly influence the migration of lead(II), presumably because of the high electrolyte content of background solutions. As lead is one of the metals most strongly held by paper [26], this conclusion can probably be extended to other metals as well.

When a series of metal complexes ML_j^{i-j} is subjected to electrophoresis, varying j changes several important properties of the migrating ions, namely size, mass, charge and polarizability. Although the effects of increasing mass and size partially cancel out, the extent of this cancellation is difficult to predict, especially when complex ions have non-spherical shape. Jokl [27] has reviewed several reported attempts to quantify the effects of ionic radius and mass on electrophoretic mobilities. For practical purposes, the best approach seems to be to estimate mobilities of complex species from a series of composite zone migration rate measurements taken at different ligand concentrations. The reliability of these estimates increases with the difference between stability constants, and the number and precision of individual data points. With respect to the electrophoretic system under investigation, the relative precision of individual data points could be improved by extending the distance travelled by the mixture of trace metal ions and by increasing the number of replicate determinations.

Adoption of these refinements should make the proposed method a valuable tool for investigating metal speciation in sea water. Its particular advantages are simple basic equipment and procedures, and the applicability to test solutions with high ionic strength and extremely low metal concentrations. For marine chemical work, the significance of the latter point cannot be overestimated. Most methods for studying (trace) metal speciation fail for sea-water conditions because they require metal concentrations which result in the precipitation of sparingly soluble salts or disturb other equilibria in this complex electrolyte system.

The author thanks Dr. R. W. Baier for his advice and for providing funding for this work through NSF grant OCE-74-12831. He also thanks Dr. C. H. Lochmüller for his helpful comments regarding the original manuscript. Financial support from a Fulbright-Hays scholarship is gratefully acknowledged.

REFERENCES

1 G. Zweig and J. R. Whitaker, Paper Chromatography and Electrophoresis, Vol. 1, Academic Press, New York, 1967.
2 S. K. Shukla and J. P. Adloff, J. Chromatogr., 8 (1962) 501.
3 R. W. Henkens and D. R. Kalkwarf, Anal. Chem., 34 (1962) 830.
4 J. P. Majumdar and M. M. Chakrabartty, Anal. Chim. Acta, 17 (1957) 228.
5 E. Blasius and W. Preetz, Chromatogr. Rev., 6 (1964) 191.
6 R. A. Alberty and E. L. King, J. Am. Chem. Soc., 73 (1951) 517.
7 V. Jokl, J. Chromatogr., 14 (1964) 71.
8 V. Vajgand and T. Suranyi-Mihajlovic, Talanta, 22 (1975) 803.
9 Z. Pucar, Anal. Chim. Acta, 17 (1957) 485.
10 P. R. Bevington, Data Reduction and Error Analysis for the Physical Sciences, McGraw-Hill, New York, 1969.
11 L. G. Sillén and A. E. Martell, Stability Constants, Chemical Society, London, Special Publication No. 17 (1964) and No. 25 (1971).

12 W. Stumm and P. A. Brauner, in J. P. Riley and G. Skirrow (Eds.), Chemical Oceanography, Vol. 1, Academic Press, London, 1975.
13 A. Zirino and S. Yamamoto, Limnol. Oceanogr., 17 (1972) 661.
14 D. Dyrssen and M. Wedborg, in E. D. Goldberg (Ed.), The Sea, Vol. 5, Wiley—Interscience, New York, 1974.
15 J. P. Riley and G. Skirrow (Eds.), Chemical Oceanography, Vol. 1, Appendix, Table 2, Academic Press, London, 1975.
16 G. A. Goleva, V. A. Polyakov and T. P. Nechayeva, Geokhimiya, 3 (1970) 344.
17 H. Irving and R. J. P. Williams, J. Chem. Soc., (1953) 3192.
18 B. I. Peshchevitskiy, G. N. Anoshin and A. M. Yereburg, Dokl. Akad. Sci. USSR Earth Sci. Sect., 162 (1965) 205.
19 S. Ahrland, in E. D. Goldberg (Ed.), The Nature of Seawater, Dahlem Konferenzen, Berlin, 1975.
20 R. W. Baier, Ph.D. Dissertation, University of Washington, Seattle, 1971.
21 H. Bilinski, R. Huston and W. Stumm, Anal. Chim. Acta, 84 (1976) 157.
22 L. M. Petrie, Ph.D. Dissertation, Duke University, Durham, 1977.
23 C. H. van der Weijden, M. J. H. L. Arnoldus and C. J. Meurs, Neth. J. Sea Res., 11 (1977) 130.
24 L. G. Sillén, Acta Chem. Scand., 3 (1949) 539.
25 A. Baric and M. Branica, J. Polarogr. Soc., 13 (1967) 4.
26 A. J. Ultee and J. Hartel, Anal. Chem., 27 (1955) 557.
27 V. Jokl, J. Chromatogr., 13 (1964) 451.

Analytica Chimica Acta, 135 (1982) 111—119
Elsevier Scientific Publishing Company, Amsterdam — Printed in The Netherlands

THE PREPARATIVE SCALE SEPARATION AND THE IDENTIFICATION OF CONSTITUENTS OF ANTHRAQUINONE-DERIVED DYE MIXTURES Part 1. 1-Methylaminoanthraquinone, 1,4-Diamino-2,3-dihydroanthraquinone and 1,4-Diaminoanthraquinone

I. B. RUBIN*, M. V. BUCHANAN and G. OLERICH

Bio/Organic Analysis Section, Analytical Chemistry Division, Oak Ridge National Laboratory, P.O. Box X, Oak Ridge, TN 37830 (U.S.A.)

(Received 1st September 1981)

SUMMARY

Two colored smoke mixes, red and violet, were separated to isolate the major dye components from their impurities for both chemical characterization and biological testing. The red smoke mix was separated into three fractions by vacuum sublimation. The major dye component, 1-methylaminoanthraquinone (MAA) was isolated in fraction 2 at about 98% purity. Fraction 1 contained a number of impurities, including aminoanthraquinone, azobenzene, azoxybenzene, aminobiphenyl, and phenyldiazobenzene. The third fraction was a non-volatile black powder containing only C, H, and O with hydroxyl groups. The violet smoke mix was separated into four fractions by using differential solubilities, taking advantage of the solubility differences of the two main components, MAA and 1,4-diamino-2,3-dihydroanthraquinone (DDA) in chloroform. Fraction 1 contained primarily MAA, with trace amounts of anthraquinone, DDA, aminonaphthalene, aminoanthraquinone, phenyldiazobenzene and 1,4-diaminoanthraquinone (DAA). Fraction 2 contained mostly DDA, along with some DAA and small amounts of MAA, aminoanthraquinone, aminonaphthalene and anthraquinone. Fraction 3 contained both DDA and DAA with a trace of aminonaphthalene. Fraction 4 was a gray chloroform-insoluble residue.

Dyes derived from anthraquinone are commonly used in industry as coloring agents in food, drugs, hair dyes, cosmetics, and textiles [1, 2]. Anthraquinone-derived dyes are also used in colored dye mixes prepared for signal smoke grenades [3]. Because of the structural similarity of these anthraquinone derivatives to several polycyclic aromatic hydrocarbons which exhibit bacterial mutagenic activity as well as carcinogenic activity, studies have been conducted on the biological activity of these dye materials. Results have shown that several of these anthraquinone-derived dyes exhibit bacterial mutagenic activity [2]. Owens and Ward [3] have reviewed the biological effects of some of the dyes used in the smoke mixes, as well as of the whole smoke mixes. However, the dye materials used in formulating the smoke mixes are used as received from the manufacturer and typically contain a number of impurities from unreacted starting materials or reaction by-products. Because these impurities could be responsible for all or part of the

biological activity of the smoke mixes, it was desirable to separate the major smoke mix components from their impurities prior to the biological testing of these smoke mixes.

Anthraquinone derivatives form a large category of dyestuffs, and their chemistry has been reviewed by Venkataraman [1]. Separation, quantitation, and identification procedures for dyestuffs in general, including anthraquinone dyes, have been discussed [1, 4]. Mixtures of various types of anthraquinone dyes can be separated readily by means of thin-layer chromatography (t.l.c.) on silica gel, alumina, and acetylated cellulose layers with a variety of solvent systems [5—9]. Passarelli and Jacobs [10] have separated a series of anilino- and toluidino-substituted anthraquinones by high-performance liquid chromatography.

Although various chromatographic procedures are workable for the analytical-scale separation of anthraquinone dyes, the present requirement to separate enough of the major components for biological tests necessitated the preparative-scale separation of the colored smoke-mix components. Effort was made to achieve the greatest possible recovery of the total starting material. A constraint was frequently imposed by solubility problems with some of the materials; this caused difficulties in the chromatographic methods. In this paper, the preparative-scale separation of two smoke dye mixes, red and violet, for biological testing and chemical characterization is outlined. Various techniques were used to monitor the course of the separation processes and to characterize the various dye mix fractions.

EXPERIMENTAL

Samples and reagents

The colored smoke mixes were provided by the Pine Bluff Arsenal and included a red smoke mix (RSM) and a violet smoke mix (VSM). Two standard dyes, 1-methylaminoanthraquinone [I; MAA; 1-(methylamino)-9,10-anthracenedione; CAS Registry No. 82-38-2; CI Disperse Red 9, CI Solvent Red 111, CI No. 60505] and 1,4-diamino-2,3-dihydroanthraquinone [III; DDA; 1,4-diamino-2,3-dihydro-9,10-anthracenedione; CAS 81-63-0] were obtained from the U.S. Army Armament Research Development Command, Aberdeen Proving Ground, Maryland. The 1,4-diaminoanthraquinone [II; DAA; 1,4-diamino-9,10-anthracenedione, CAS 128-95-0; CI Disperse Violet 1, CI Solvent Violet 11, CI No. 61100] was converted from DDA by heating a solution of the latter in dimethylsulfoxide overnight at 90°C. Also, the DAA was separated from a chloroform solution of DDA by t.l.c.

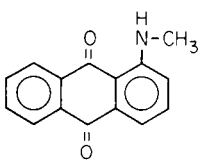

I

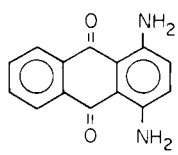

II

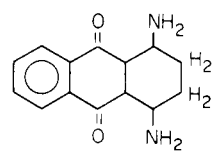

III

Tetramethylsilane (TMS), deuterated chloroform ($CDCl_3$) and deuterated dimethylsulfoxide (DMSO-d_6) for the nuclear magnetic resonance (n.m.r.) studies were obtained from Aldrich. Spectrophotometric-grade DMSO was purchased from Schwartz/Mann. All other organic reagents were redistilled from glass prior to use, except that reagent-grade solvents were used for spectrophotometric measurements and for analytical-scale t.l.c.

Procedures

Soxhlet extractions were performed with Schleicher and Schuell No. 603 extraction thimbles. The thimbles were extracted overnight with hot chloroform prior to use for sample extraction. For separation by vacuum sublimation, a standard glass vacuum sublimation apparatus was immersed in a heated oil bath. A moderate vacuum (0.075—0.1 torr) was maintained by a rotary vacuum pump. The volatile fractions were collected on a water-cooled condenser at the indicated temperature for 5 h, and were washed off the condenser with distilled chloroform.

Analytical-scale t.l.c. was the primary method used for monitoring the effectiveness of the separatory procedures. Both Polygram SIL-G (0.25 mm) and SIL-N-HR (0.20 mm) silica plates (Brinkmann Instruments) were used, with equivalent results. For preparative-scale t.l.c. separations, SIL-G-200 UV254 (2 mm) silica plates (Brinkmann Instruments) were used. The red and violet smoke mixes and their individual components were chromatographed with a methyl ethyl ketone/chloroform/acetic acid (80:60:1) developing solution [5].

A Perkin-Elmer Model 3920 gas chromatograph with a flame ionization detector was used to separate and detect the dye fraction components. The chromatograph was equipped with a 12 ft. by 1/8 in. o.d. glass column packed with 3% Dexsil 400 on 80/100 mesh Chromosorb W. Various temperature programs were applied, depending on the circumstances.

Visible and ultraviolet spectra were obtained using a Carey Model 14 double beam spectrophotometer with a 1-cm cell. Chloroform was used as the solvent in all cases, although DDA and DAA were also studied in DMSO. All samples were run at concentrations of 0.02 mg ml^{-1} for visible spectra and 0.005—0.01 mg ml^{-1} for ultraviolet spectra. Fluorescence spectra were run using a Perkin-Elmer Model MPF-44A fluorescence spectrophotometer with sample concentrations of 0.01 mg ml^{-1} in chloroform. Infrared spectra were obtained using a Digilab FTS-20C Fourier-transform spectrometer. Samples were prepared as potassium bromide pellets using about 1 mg of sample per 300-mg pellet. A blank potassium bromide pellet was used as the reference, and spectra were accumulated for 100 scans.

Proton (^1H) and carbon (^{13}C) n.m.r. spectra were obtained at 89.56 MHz and 22.50 MHz, respectively, using a JEOL FX90Q Fourier-transform spectrometer with a broad band synthesizer. The spectra were run at an ambient probe temperature of 23°C, and with an internal deuterium lock. The samples were dissolved in deuterated chloroform or dimethylsulfoxide

with tetramethylsilane added as an internal reference. The proton spectra were obtained using a 28 μs (90°) pulse, a 2.5 s pulse delay, and a 4 pulse accumulation. The ^{13}C spectra were generally collected using a 12 μs (45°) pulse and 15 s pulse delay. The number of scans accumulated for the ^{13}C spectra varied with each sample, but most spectra were run overnight (about 4500 scans) because of the low solubilities of the compounds.

Mass spectra were obtained with a Hewlett-Packard 5985A gas chromatograph/mass spectrometer (g.c.—m.s.), with the electron impact source at 70 eV. The non-volatile samples were introduced into the mass spectrometer via a direct insertion probe which was temperature-programmed from room temperature to 200°C. Volatile samples were introduced via a gas chromatograph interfaced to the mass spectrometer. The gas chromatograph was equipped with a fused silica open tubular column coated with OV-101 (SGE, Austin, TX) or SE-52 (J & W Scientific, Orangval, CA). Helium was used as the carrier gas at 30 lbs. head pressure. The inlet and g.c.—m.s. transfer lines were maintained at 280°C and the oven temperature was programmed from 80 to 280°C at 3°C min^{-1}. A splitless injector was used to introduce the sample.

RESULTS AND DISCUSSION

Red smoke mix (RSM)

The RSM is formulated to contain only one dye component, 1-methylaminoanthraquinone [3]. However, preliminary solubility studies revealed the presence of a significant quantity of a black, chloroform-insoluble material. Thin-layer chromatographic investigations with silica, alumina, and cellulose layers and using a variety of solvent mixtures [5—9] resulted in the use of silica plates with a methyl ethyl ketone/chloroform/glacial acetic acid (80:60:1) solvent system. The t.l.c. separation of whole RSM resulted in a single visible red spot at R_f 0.68, which corresponds to MAA, with no other visible spots. Under u.v. irradiation, the red spot was essentially non-fluorescent. However, an orange fluorescent spot appeared just below and apparently overlapping the major spot and other fluorescent spots appeared at R_f 0.39 and at the origin. When a more concentrated sample was applied to a plate, several other fluorescent spots were detected. The packed-column g.c. profile of the RSM revealed two significant peaks which eluted prior to the major component, along with a number of very minor peaks. The g.c.—m.s. examination of the whole RSM suggested that these two major contaminants were azobenzene and anthraquinone. The g.c. retention times of these two compounds corresponded to the two peaks noted in the whole sample. Additionally, the t.l.c. R_f values of these two compounds were found to be almost identical to MAA.

The RSM was separated into three fractions by vacuum sublimation, as shown in Fig. 1. The major components identified in the three fractions are given, as well as the percent of the original material recovered in each fraction.

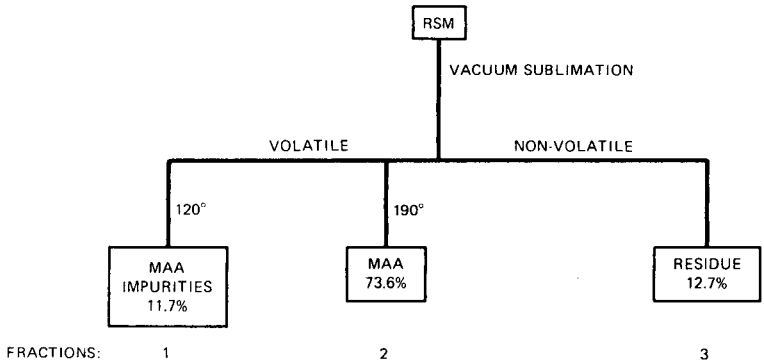

Fig. 1. Separation scheme for red smoke mix.

The third fraction was a black, involatile powder. The separation scheme outlined in Fig. 1 was used to concentrate the volatile impurities in fraction 1 and the least amount of MAA in fraction 3. As will be shown later, some impurities were retained in fraction 2, although this fraction was found to be almost 98% pure MAA.

Thin-layer chromatography of the first vacuum sublimation fraction (up to 120°C at 0.075 torr) indicated that it was composed primarily of MAA with at least five impurities. Gas chromatography showed the presence of nearly 25 impurities, although most of these were present in trace amounts. Combined g.c.—m.s. identified the largest impurity in fraction 1 as anthraquinone (about 20—30% of the MAA by area). Other peaks identified at the 1% or lower level included compounds with molecular weights of 223 (aminoanthraquinone), 182 (azobenzene), 198 (azoxybenzene), 169 (aminobiphenyl), 258 (phenyldiazobenzene) and 284 (a diketone of a condensed ring compound with a molecular weight of 254, such as dibenzoacenaphthylene or phenylanthracene).

Fraction 2 (74%, 120—190°C) was found to contain mostly MAA, with a small amount of anthraquinone and trace amounts of several other impurities. The u.v., visible and fluorescence spectra of fraction 2 were identical to the corresponding spectra of the MAA standard. The infrared, ^{1}H-, and ^{13}C-n.m.r. spectra of fraction 2 and the MAA standard were also identical.

Fraction 3 (13%) was a black powder which was involatile at 190°C and 0.075 torr. When it was equilibrated with chloroform, about 13% of this fraction dissolved, yielding a red solution. This color was apparently caused by a small amount of residual MAA. To test if the sublimation residue was present in the original RSM or if it was a thermal degradation product, the RSM was dissolved in chloroform and the insoluble material was filtered, dried, and weighed. The insoluble material (retained by a 5-μm filter) was found to represent 13.3% of the original RSM. Both the insoluble material and the sublimation residue were tested by elemental quantitation and i.r. spectroscopy. The elemental compositions are given in Table 1. The infrared spectrum of fraction 3 indicated that the residue contained oxygen present

TABLE 1

Elemental composition of RSM residues

	Composition (%)				Total (%)
	C	H	N	O	
RSM insolubles	40.6	6.0	0.49	49.8	96.9
RSM residue	41.3	5.9	0.68	46.5	94.4

as hydrogen-bonded hydroxyl groups. The infrared of fraction 3 was found to be very similar to that of the RSM insolubles. These data confirm the idea that the vacuum sublimation residue is not a thermal decomposition product, but is a component of the original smoke mix.

Violet smoke mix (VSM)

The VSM is formulated to contain 80% DDA and 20% MAA [3]. However, initial t.l.c. studies revealed the presence of a third major component. A t.l.c. study of the DDA standard showed two major spots, one purple and one yellow—brown, instead of the single expected spot. Only one peak was observed in the DDA standard when studied by packed-column g.c. However, capillary-column g.c.—m.s. revealed two peaks with molecular weights of 240 and 238, corresponding to DDA and diaminoanthraquinone (DAA), respectively. The ^{13}C-n.m.r. (in DMSO-d_6) spectrum of DDA standard was consistent with that of DDA. However, when this solution was inadvertently allowed to heat up in the n.m.r. probe overnight, the solution color changed from yellow—brown to purple. The ^{13}C-n.m.r. spectrum of the purple solution indicated that it was DAA, with the saturated carbon at 27.5 ppm in the DDA spectrum shifting to the aromatic region.

The conversion of DDA was studied further by t.l.c. Approximately 25 mg of the DDA was streaked on a silica preparative scale plate and developed with a 80:60:1 solution of methyl ethyl ketone, chloroform, and acetic acid. A narrow purple band was readily separated from the broad yellow—brown band which is characteristic of DDA. The purple band was removed, subjected to capillary-column g.c.—m.s. (OV-101) and visible spectrophotometry, and identified as almost pure DAA. The second band was observed to change to a purple color as it was developed on the t.l.c. plate. When the plate was dried however, the color changed to brown. Analysis of this band showed that it was a mixture of DDA and DAA. The visible spectra of DDA and DAA are shown in Fig. 2. The spectra are similar in shape and intensity but differ by about 100 nm in λ_{max}. A spectral shift, evidently caused by the oxidation of DDA to DAA was noted by Owens and Ward in their spectrophotometric studies of VSM before and after ignition [3].

The preparative-scale t.l.c. separation also revealed the presence of several impurities in the DDA standard sample. A light blue visible band, with no fluorescence, at R_f 0.76 was followed by an adjoining orange visible and fluorescent band at R_f 0.71. The next constituent at R_f 0.63, was tentatively

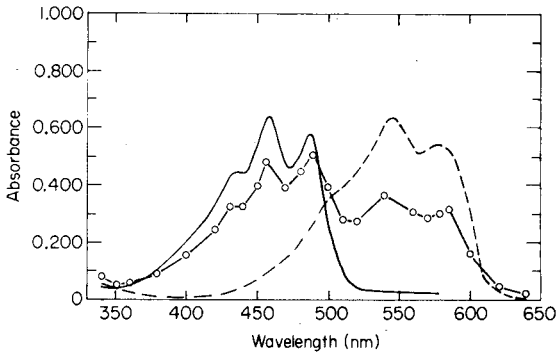

Fig. 2. Visible spectra of 1,4-diamino-2,3-dihydroanthraquinone (—), 1,4-dihydroanthraquinone (---), and violet smoke mix, fraction 3 (—o—).

identified as MAA and was followed by the purple DAA streak (deep red fluorescence) of R_f 0.56. A narrow yellow visible and fluorescent streak was observed at R_f 0.38. The broad DDA band extended from R_f 0.28 almost to the origin. This compound is initially yellow with a brilliant yellow fluorescence, but the leading edge starts to turn purple almost as soon as any separation is effected. The fluorescence slowly turns to a brownish—orange color. The results of these studies indicate that there was a small amount of DAA present in the DDA sample initially, and that the DDA is fairly readily oxidized to DAA. The presence of DAA was also observed in the Soxhlet extraction of DDA where the extract was initially purple, but became yellow as the extraction continued.

The separation of the VSM into four fractions, as shown in Fig. 3, was based upon the difference in solubilities of the two major components in chloroform, with MAA being nearly 70 times more soluble than DDA. The sample was first equilibrated in chloroform for 1 h and then filtered through a 4.5—5.5 μm glass frit. The solvent was removed from the material in solution and the recovered material was weighed and then transferred to another fine-fritted glass funnel. This material was then washed through the funnel with two 10-ml aliquots of chloroform. The soluble material was labelled as fraction 1 and the insolubles as fraction 2. The dried solids from the initial separation in chloroform (77.3% of the starting material) were transferred to an extraction thimble and extracted continuously with hot chloroform until no further color was observed in the extract. This extract was initially deep purple, but gradually became light yellow. The soluble material was labeled as fraction 3 and the insolubles as fraction 4.

The t.l.c. of fraction 1 indicated that the major component was MAA, but there was also a purple streak at a lower R_f value which was identified as DAA; g.c.—m.s. showed that the major component of fraction 1 was MAA, with several components present at less than 1%. The minor impurities identified include anthraquinone (molecular weight of 208), DDA (240), aminonaphthalene (143), aminoanthraquinone (223), phenyldiazobenzene (258), and DAA (238). Fraction 2, which represents only 3.6% of VSM, was found to contain mostly DDA, with varying amounts of DAA (depending

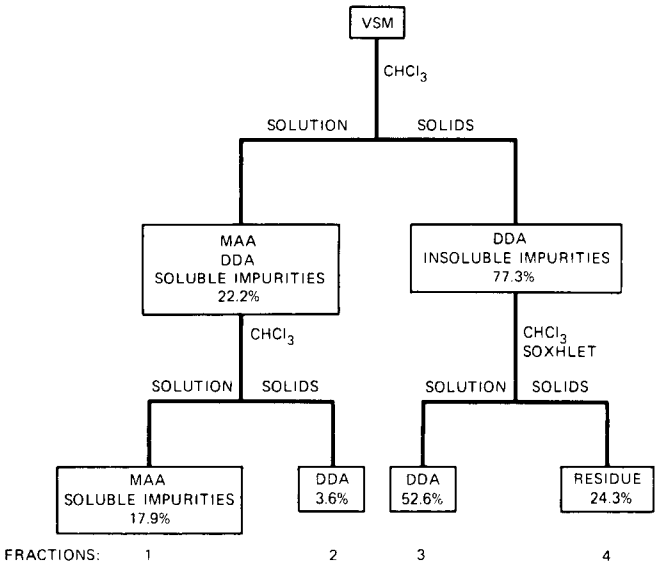

Fig. 3. Separation scheme for violet smoke mix.

upon sample treatment), small amounts (<1%) of MAA (237), aminoanthraquinone, aminonaphthalene, and anthraquinone. Fraction 3 (52.6%), when examined by t.l.c. and visible, u.v., and fluorescence spectrophotometry, was found to contain both DDA and DAA. Combined capillary g.c.—m.s. showed aminonaphthalene (present at less than 1%) as the only impurity. The amounts of DDA and DAA present in the g.c.—m.s. of this fraction were also found to vary with sample treatment. The visible spectrum of VSM fraction 3 is also shown in Fig. 2. The insoluble residue, fraction 4, is a gray powder that represents 24% of the original sample. The direct probe mass spectra obtained on this sample were too complex to allow the identification of specific compounds, but a very small amount of DAA was detected.

The authors thank Ms. Sara Harmon for carrying out the infrared spectrophotometry. This research was sponsored by the U.S. Army Medical Research and Development Command, Fort Detrick, MD 21701, under Army Project Orders 9600 and 0027 under interagency Agreement No. 40-1016-79 with Union Carbide Corporation.

REFERENCES

1 K. Venkataraman, The Chemistry of Synthetic Dyes, Vol. 2, Academic Press, New York, 1952.
2 J. P. Brown and R. J. Brown, Mutat. Res., 40 (1976) 203.
3 E. J. Owens and D. M. Ward, Report AD/A-003827 (Dec. 1974) NTIS, U.S. Dept. of Commerce, Springfield, VA.

4 R. W. Horobin, Histochem. J., 1 (1969) 231.
5 A. M. Arsov, B. K. Mesrob and A. B. Gateva, J. Chromatogr., 81 (1973) 181.
6 P. P. Rai and T. D. Turner, J. Chromatogr., 104 (1975) 196.
7 G. S. Egerton, J. M. Gleadle and N. N. Uffindell, J. Chromatogr., 26 (1967) 62.
8 J. Franc and M. Hajkova, J. Chromatogr., 16 (1964) 345.
9 P. Wollenweber, J. Chromatogr., 7 (1962) 557.
10 R. J. Passarelli and E. J. Jacobs, J. Chromatogr. Sci., 13 (1975) 153.

Analytica Chimica Acta, 135 (1982) 121—128
Elsevier Scientific Publishing Company, Amsterdam — Printed in The Netherlands

THE PREPARATIVE SCALE SEPARATION AND THE IDENTIFICATION OF CONSTITUENTS OF ANTHRAQUINONE-DERIVED DYE MIXTURES
Part 2. Benzanthrone, Dibenzochrysenedione, and 1,4-di-*p*-Toluidinoanthraquinone

I. B. RUBIN* and M. V. BUCHANAN

Bio/Organic Analysis Section, Analytical Chemistry Division, Oak Ridge National Laboratory, P.O. Box X, Oak Ridge, TN 37830 (U.S.A.)

(Received 1st September 1981)

SUMMARY

Two colored smoke mixes, yellow and green, which contain anthraquinone-derived dyes, were separated for chemical characterization and biological testing. The yellow smoke mix was separated by vacuum sublimation, Soxhlet extraction, and differential solubility. The compounds identified in this mix included the major dye components, benzanthrone and dibenzochrysenedione as well as anthraquinone, a diketone with a molecular weight of 366, a number of high-molecular-weight hydrocarbons, and a nonvolatile residue. The green smoke mix contained 1,4-di-*p*-toluidinoanthraquinone as the major component along with benzanthrone and dibenzochrysenedione. The bulk of the toluidino derivative was separated from the other two components by chromatography on a basic alumina column. The benzanthrone and dibenzochrysenedione were then separated by vacuum sublimation, although some residual toluidino accompanied the benzanthrone.

Continued interest in the biological activity of anthraquinone-derived dyes in colored smoke mixes has prompted the preparative-scale separation of two more colored smoke mixes for biological testing and chemical characterization. The separation of two smoke mixes, red and violet, into their components and the identification of the major components and impurities, were discussed in Part 1 of this series [1]. In this paper, the results of similar work on two colored smoke mixes, yellow and green, is reported.

The yellow smoke mix is formulated to contain 64% benzanthrone and 36% dibenzochrysenedione; the green smoke mix contains 70% 1,4-di-*p*-toluidinoanthraquinone, 20% benzanthrone, and 10% dibenzochrysenedione [2]. Various methods for separating anthraquinone derivatives have been reported [1, 3, 4]. However, the need to prepare sufficient quantities of the separated materials for biological testing required that larger-scale separation techniques be employed. The low solubility of these dyes often precluded the use of these established separation methods on a larger scale. Thus, several techniques were investigated for use in the separation of the yellow and green smoke mixes. The separated fractions were then characterized by using a variety of chemical techniques prior to biological testing.

EXPERIMENTAL

The yellow smoke mix (YSM) and the green smoke mix (GSM) were obtained from Pine Bluff Arsenal. Benzanthrone [I; BZA; 7-*H*-benz(d,e)-anthracen-7-one, CAS No. 82-05-3], dibenzochrysenedione [II; DBC; dibenzo(b,def)chrysene-7,14-dione, CAS No. 128-66-5; CI Vat Yellow 4, CI Constitution No. 59100], and 1,4-di-*p*-toluidinoanthraquinone [III; PTA; 1,4-bis-[4-(methylphenyl)-amino]-9,10-anthracenedione; CAS No. 128-80-3; CI Solvent Green 3, CI No. 61565] were provided by the U.S. Army Armament Research and Development Command, Aberdeen Proving Ground,

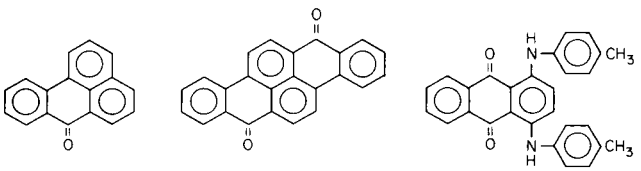

I II III

Maryland. Column chromatography was done on BioRad AG10 basic alumina with no pretreatment. Other reagents were the same as reported previously [1]. The chromatographic and spectroscopic methods described in the earlier report [1] were also used for this study, except that the silica thin-layer chromatographic plates were developed with cyclohexane/diethylether (1:1) [3].

RESULTS AND DISCUSSION

Vacuum sublimation and differential solubility methods were shown to be effective in the separation of the red and violet smoke mixes [1]. These methods were also found to be useful in the separation of the YSM and GSM. The BZA and DBC standard dyes were found to contain substantial impurities. Thus, the separations of these standard dyes from their impurities were investigated first and were incorporated later into the separation schemes of the GSM and YSM.

The BZA standard was stated to be nearly 99% pure. However, it was found to contain a substantial amount (19.7%) of chloroform-insoluble material. When the BZA was separated into four fractions by vacuum sublimation, as outlined in Fig. 1, a non-volatile material representing 19.3% of the starting material was isolated. The elemental compositions of the chloroform-insoluble material and the sublimation residue (Table 1) showed that these materials were virtually identical. There appear to be other elements present in both samples. The infrared spectra of both materials were complex, but similar, with both containing a strong hydroxyl absorption band. By thin-layer chromatography (t.l.c.), all three volatile fractions appeared to be nearly pure BZA with only traces of impurities in fractions 1 and 3. The R_f value of BZA on silica plates (with cyclohexane/diethyl ether, 1:1)

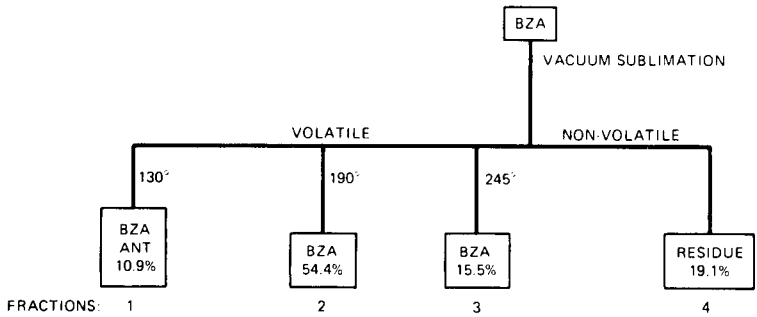

Fig. 1. Separation scheme for benzanthrone.

TABLE 1

Elemental composition of BZA residues

	Composition (%)				
	C	H	O	N	Total (%)
BZA-E insolubles	43.2	4.0	39.4	0.2	86.8
BZA-E non-volatiles	48.5	3.5	35.2	0.1	87.4

was 0.48. The BZA yielded a visible yellow spot with an intense light blue fluorescence. Combined gas chromatography/mass spectrometry (g.c.—m.s.) of these three volatile fractions revealed the presence of anthraquinone in each. Anthraquinone was also observed in the ^{13}C-nuclear magnetic resonance (n.m.r.) spectrum of the chloroform-soluble portion of the BZA standard dye. However, the amount of anthraquinone detected by g.c.—m.s. decreased from fraction 1 to fraction 3. Fraction 2 was thought to be the purest sample of BZA because fraction 3 contained a small amount of the black sublimation residue. The ^{1}H-n.m.r. spectrum of fraction 2 was consistent with that of benzanthrone.

The DBC standard received was stated to be about 80% pure. The DBC was first separated by vacuum sublimation into volatiles (fraction 1) and non-volatiles. The non-volatile fraction was extracted in a Soxhlet apparatus using chloroform. This yielded a soluble portion and an insoluble residue, which was labeled fraction 4. The soluble portion was dried, weighed and then washed through a 5-μm filter with two 20-ml aliquots of chloroform. This latter soluble portion was identified as fraction 2 and the residual solids as fraction 3. The separation of DBC is summarized in Fig. 2, along with the percentage of the starting material isolated in each fraction. Thin-layer chromatography of fraction 1 of the DBC standard revealed the presence of at least six compounds, including DBC and BZA, which is a starting material in the manufacture of DBC [5]. The DBC, which is not displaced

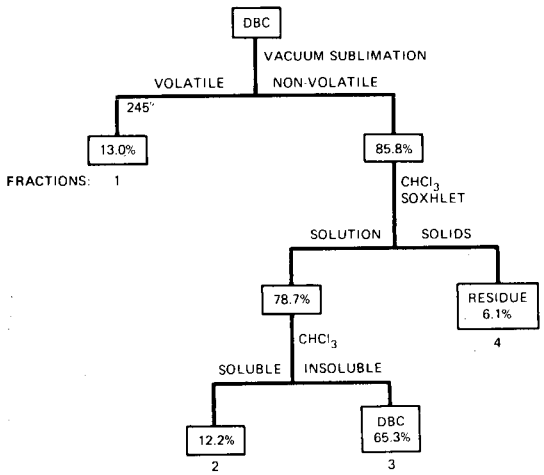

Fig. 2. Separation scheme for dibenzochrysenedione.

from the origin, was yellow—orange, with a dark orange fluorescence. Direct-probe mass spectral investigation of this fraction indicated the presence of BZA, DBC, three diketones with molecular weights of 334, 336, 366 and several other compounds which could not be unambiguously identified. The compounds with molecular weights 334 and 336 may be 3-benzoylbenzanthrone and 1,5-dibenzoylnaphthalene, respectively, both of which may be intermediates in the manufacture of DBC [5].

During the Soxhlet extraction studies with DBC, it was noted that the initial part of the extract was dark brown, and that the extract after two or three cycles was a light yellow, characteristic of DBC. Thus, it was apparent that the soluble, non-volatile portion of the DBC contained at least one component that was considerably more soluble than the DBC itself, which has a solubility of about 0.05 mg ml^{-1} in chloroform. Consequently, the chloroform extract was divided into fraction 2 which was the relatively soluble brown portion, and fraction 3 which was predominantly the DBC portion. Fraction 2 was found to contain fewer constituents than fraction 1 by t.l.c. The direct probe mass spectra of fraction 2 revealed the presence of a number of compounds, including DBC, and the same 336 and 366 molecular weight compounds found in fraction 1. Fraction 3 contained only two t.l.c. bands, one of which corresponded to DBC. Both DBC and dibenzochrysene were identified by direct-probe mass spectrometry in this fraction. The residue was found to contain DBC, the 366 diketone, and a large amount of high-molecular-weight material, which was not volatilized.

Investigation of the yellow smoke mix

The yellow smoke mix (YSM) is formulated to contain BZA and DBC. The BZA is substantially more soluble and more volatile than DBC, so either

differential solubility or vacuum sublimation would seem to be suitable methods to separate this mixture. However, the discovery that a relatively soluble compound was present as an impurity in the DBC made differential solubility less useful. Therefore, vacuum sublimation was used to separate the YSM into four volatile fractions and one non-volatile fraction. This last fraction was separated further, as shown in Fig. 3, which outlines the separation of the YSM. Both fractions 1 and 2 appeared to contain only BZA when examined by t.l.c. A number of hydrocarbon impurities in fraction 1 were identified by capillary-column g.c.—m.s., however. These hydrocarbons are thought to be from the antidusting agent Marcol 52 (R) added to the YSM [2]. Fraction 2 was also found to contain a small impurity (<1%), which was identified as anthraquinone by g.c.—m.s. The visible spectrum of fraction 2 was found to be identical to that of the BZA standard.

Fractions 3 and 4 were found by g.c.—m.s. to contain only BZA. However, t.l.c. revealed several other small impurities which were probably non-volatile. For example, direct-probe mass spectrometry of fraction 4 revealed the presence of some DBC, whereas fraction 5, which was brown, was found to contain BZA, DBC, and an unidentified diketone with a molecular weight of 366. These spectra were too complex, however, to identify minor components. In g.c.—m.s., BZA was the only compound in fraction 5 volatile enough to be chromatographed. Fraction 6 was found to contain mostly DBC by direct-probe mass spectrometry, plus the impurity with a molecular

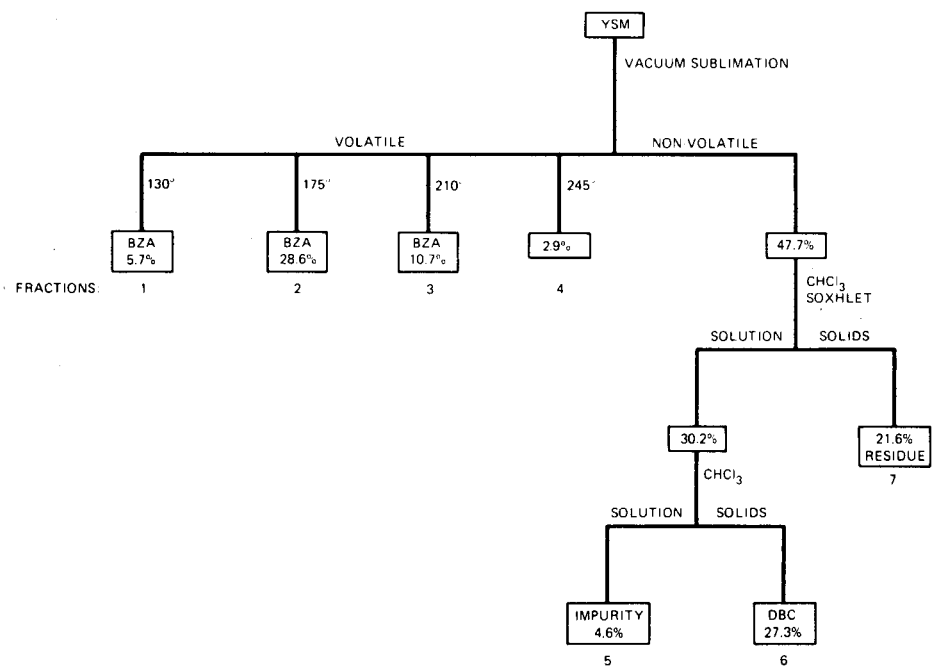

Fig. 3. Separation scheme for yellow smoke mix.

weight of 366, which was also observed in fraction 5. Only two compounds were observed by t.l.c. in this fraction. The visible and ultraviolet spectra of fraction 6 are essentially the same as the corresponding spectra of fraction 3 of the DBC standard. Thus, it can be assumed that fraction 6 is relatively pure DBC. The direct probe mass spectra of fraction 7 were very complex, with only DBC being clearly identified. Also, after the direct probe analysis was completed, a substantial amount of non-volatilized material remained in the sample cup, indicating that this fraction contains a large proportion of high-molecular-weight material. The infrared spectrum of this fraction was very complex, but exhibited substantial hydroxyl content.

Investigation of the green smoke mix

The GSM is formulated to contain PTA, BZA, and DBC in a ratio of 70:20:10 [2]. The BZA and PTA can be readily separated from DBC by either vacuum sublimation or differential solubility. However, BZA and PTA sublime together throughout a wide temperature range (up to 245°C at 0.075 torr) and thus cannot be separated by vacuum sublimation. The two compounds have similar solubilities in a wide range of solvents and, thus do not allow separation on a solubility basis. Although BZA, PTA, and DBC can be resolved on analytical-scale silica t.l.c. plates, the separation of whole GSM on preparative-scale t.l.c. plates was very poor. Column chromatography on alumina had been shown to be successful in separating some anthraquinone derivatives [3], and this method proved to be successful in the separation of the GSM.

The GSM was separated into five fractions as shown in Fig. 4. The GSM was first extracted in a Soxhlet apparatus with hot chloroform until the extract was colorless. The insoluble material was labeled fraction 1. The soluble material was dried and weighed and then separated on a 3.8 cm o.d. × 90 cm column packed with approximately 750 g of basic alumina in cyclohexane. A 0.6—0.8 g portion of the soluble material was dissolved in chloroform and mixed with 25—30 g of the basic alumina. The solvent was removed and the treated alumina was poured onto the head of the column. The column was then developed in chloroform. The collection of fraction 2 began when the first noticeable color appeared in the eluate and continued until the color changed from blue to green. This required approximately 2.7 l of chloroform. Another portion (18.5%) was eluted with additional chloroform (about 350 ml) until no further yellow coloration was detected. This portion was later separated by using vacuum sublimation into volatiles (fraction 3) and non-volatiles (fraction 4). After the second cut, the column was washed with 2—4 l of methanol. This eluate was labeled fraction 5. A bright blue band along with some pink material was retained at the head of the column and the entire column remained light blue even after elution with 4 l of methanol. This material could not be desorbed by volatilization (up to 245°C at 0.1 torr). Recovery of the GSM was only 93%, compared to 98% or better for the other colored smoke mixes.

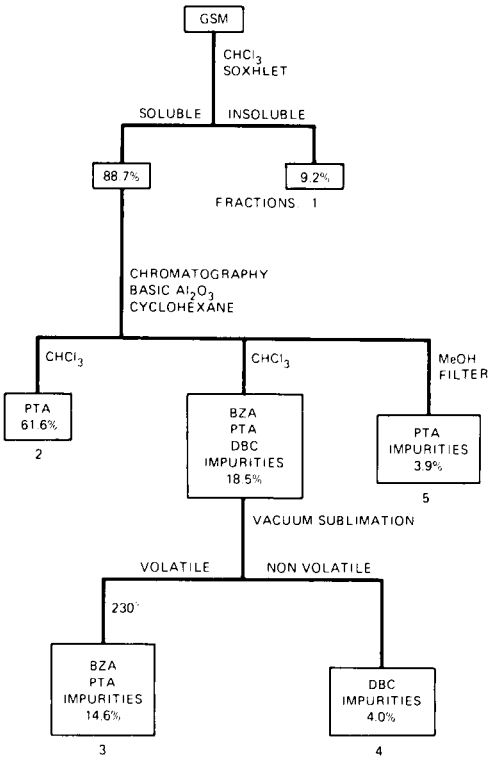

Fig. 4. Separation scheme for green smoke mix.

Fraction 1 of the GSM, the Soxhlet extraction residue, was examined by direct-probe mass spectrometry. Most of this material did not volatilize, however, and only high-molecular-weight hydrocarbon-type fragmentations were observed in the resulting mass spectra. This hydrocarbon material probably originated from the antidusting agent which was also observed in the YSM. Fraction 2 revealed only one spot when studied by t.l.c. This spot corresponded to PTA, being a visible blue color at R_f 0.56 and having no fluorescence. Direct-probe mass spectrometry of fraction 2 revealed the presence of some BZA, also. The u.v., visible, infrared and ^{13}C-n.m.r. spectra of this fraction are identical to those of the PTA standard.

The major component in fraction 3 was found by t.l.c. to be BZA, along with small amounts of PTA, DBC, and three other impurities. The mass spectra for this fraction showed only BZA and PTA to be present. The t.l.c. of fraction 4 showed one large band corresponding to DBC and traces of two impurities. Only DBC was observed in this fraction by mass spectrometry. Fraction 5 was found to contain mostly PTA by t.l.c., along with four smaller bands. Direct-probe mass spectrometry of fraction 5 revealed PTA, BZA, and DBC to be present.

Because it was not necessary to effect a complete separation of all of the components for the purposes of this study, the fact that a small amount of PTA accompanied the BZA in fraction 3 was not critical, as each could be readily identified. However, these two compounds could be completely separated by preparative-scale t.l.c. When whole GSM was chromatographed, the PTA tailed badly and overlapped the BZA zone completely. However, when fraction 3 was chromatographed, there was a good separation between PTA and BZA, as well as from the impurities present in this fraction. This would also open the possibility of a larger scale separation by chromatography on a silica column. It is also feasible to quantify the amounts of BZA and PTA in the presence of each other by dual-wavelength spectrophotometric measurements at 392 and 645 nm.

The authors thank Ms. Sara Harmon for the infrared spectrophotometry and Ms. G. Olerich for the mass spectrometry. This research was sponsored by the U.S. Army Medical Research and Development Command, Fort Detrick, MD. 21701, under Army Project Orders 9600 and 0027 under Interagency Agreement No. 40-1016-79 with Union Carbide Corporation.

REFERENCES

1 I. N. Rubin, M. V. Buchanan and G. Olerich, Anal. Chim. Acta, 135 (1982) 111.
2 E. J. Owens and D. M. Ward, Report AD/A-003827, Dec. 1974, NTIS, U.S. Dept. of Commerce, Springfield, VA.
3 J. Franc and M. Hajkova, J. Chromatogr., 16 (1964) 345.
4 G. S. Egerton, J. M. Gleadle and N. D. Uffindell, J. Chromatogr., 26 (1967) 62.
5 K. Venkataraman, The Chemistry of Synthetic Dyes, Vol. 2, Academic Press, New York, 1952, p. 953.

Analytica Chimica Acta, 135 (1982) 129—135
Elsevier Scientific Publishing Company, Amsterdam — Printed in The Netherlands

DETERMINATION OF SELECTED ELEMENTS IN BONE SAMPLES BY NEUTRON ACTIVATION AND γ-SPECTROMETRY

HENRYK BEM[a] and DOUGLAS EARL RYAN*

Trace Analysis Research Centre, Chemistry Department, Dalhousie University, Halifax, Nova Scotia B3H 4J1 (Canada)

(Received 27th April 1981)

SUMMARY

A non-destructive method for the quantification of eleven elements in bone samples is described. The analytical scheme is based on short (30 s) irradiation with thermal neutrons followed immediately (decay time 10 s) by counting fluorine-20 for 30 s and, after a total waiting time of 150 s, by 10-min γ-spectrometry counting, which give data for Ca, Cl, Mg, Mn, Na, and V. Use of a boron carbide shield for a second set of irradiations with epithermal neutrons permits the additional determination of bromine and strontium and calculation of the contribution of aluminium and phosphorus to the total activity of ^{28}Al.

The determination of bone mineral content is of considerable medical interest because bones serve as important storage areas for calcium, phosphorus, magnesium, sodium, fluorine and other essential elements for the body. Interest in the role of these elements in the development of bone diseases, and in monitoring of changes in their concentrations after various treatments, has grown in recent years.

Although neutron activation followed by γ-spectrometry is a rapid and sensitive technique for quantifying components of biological samples [1], it has been seldom used for multi-elemental determinations in bone because of the high concentrations of calcium, phosphorus, and sodium. These elements induce macro-activities of corresponding nuclides, which considerably increase background in all regions of the spectrum and consequently increase the detection limits of other elements. Fast neutron activation has been used in bone analysis for the determination of fluorine, calcium, phosphorus and potassium only [2—9]. Fluorine and the main components of bone can also be quantified by very short (ca. 1 min) thermal neutron irradiation [2, 10, 11] or cyclic activation [12].

A complex thermal neutron activation method for quantifying elements in bone samples has been proposed by Bratter et al. [13]; fluorine, calcium and sodium were quantified after irradiation for 20 s. The determination

[a]On leave from the Institute of Applied Radiation Chemistry, Technical University, Lodz, Poland.

0003-2670/82/0000-0000/$02.75

of other elements (total of 24) required irradiations for 1.5 h and 10 days, but, after the 10-day irradiation, a decay period of about three months was necessary to reduce sufficiently the bremsstrahlung radiation from ^{32}P β-rays. Later, Erasmus et al. [14] recommended a combination of 5-min thermal neutron irradiation for determination of main bone components and 36-h epithermal irradiation with a cadmium shield, followed by radiochemical removal of sodium-24, for multi-element determination of essential biological elements in bone tissue. Such a combination of thermal and epithermal irradiations has also been applied for the determination of aluminium and phosphorus in bone [15, 16]. After activation with the entire reactor spectrum, the radionuclide ^{28}Al is produced via the thermal neutron reaction $^{27}Al(n,\gamma)^{28}Al$ and via the fast neutron reactions $^{28}Si(n,p)^{28}Al$ and $^{31}P(n,\alpha)^{28}Al$. Silicon is present in bone in trace amounts but the physiological phosphorus to aluminium ratio in bone is about 2500; in spite of the low cross-section for the $^{31}P(n,\alpha)^{28}Al$ reaction, the phosphorus contribution to the total activity of ^{28}Al must be taken into account or aluminium must be chemically separated before irradiation [17, 18]. A neutron filter screens the thermal part of the neutron flux and, after two irradiations with and without a shield, the contribution of both elements can be simply calculated.

The aim of the present study was to investigate the suitability of boron carbide shields [19] for fast non-destructive multi-elemental determinations in bone. The cut-off energy of neutrons for this shield is about 12 eV compared to 0.5 eV for cadmium and the activities of ^{24}Na, ^{27}Mg and ^{49}Ca are considerably lowered; other elements, especially those with high values of the ratio of resonance integral to thermal cross-section, can then be detected.

EXPERIMENTAL

Samples (500 mg) of the International Atomic Energy Agency standard material Calcined Animal Bone A3-74 were used. In selecting proper standards, matrix effects must be considered: calcium hydrogenphosphate ($CaHPO_4 \cdot 2H_2O$; Analar grade) was therefore chosen as a matrix. This compound contains 23% Ca and 18% P compared to 30% Ca and 15% P in bone. All standards were prepared by mixing 400 mg of powdered calcium hydrogenphosphate with powders of appropriate compounds (Analar grade) or by addition of standard solutions (Alpha, for Atomic Absorption) to 400 mg of calcium hydrogenphosphate followed by evaporation of water. The homogeneity of standards was checked by comparing the results for five parallel samples and was found to be satisfactory (relative standard deviations were below 5%). Samples and standards were weighed directly into small polyethylene irrradiation vials. In the first experiments, these vials were placed in typical 7-dram polyethylene vials and then irradiated for 30 s in the outer site of the research reactor (SLOWPOKE) at a flux of 5×10^{11} n

cm^{-2} s^{-1}. After a decay time of 10 s, the samples were counted for 30 s in order to determine fluorine. These conditions were chosen on the basis of previous experiments with fluorine [20]. After a total decay time of 150 s, the samples were recounted for 10 min.

In the epithermal experiments, the vials with bone samples and standards were inserted, before irradiation, into the shielding containers with boron carbide (surface density of boron was about 440 mg cm^{-2}); they were then irradiated for 10 min in an outer site. These samples were counted twice for 10 min after decay times of 1 min and 15 min, respectively, using a 60-cm^3 Canberra Ge(Li) detector (full width at half maximum of 1.88 keV at the 1332 MeV photopeak of ^{60}Co, peak-to-Compton ratio 35:1, and an efficiency of 9.5%) in conjunction with a Tracor Northern TN-11 4096 channel pulse-height analyzer. To decrease the dead time induced in the analyzer by high-energy β-rays after thermal neutron irradiations, a 1-cm aluminium absorber was placed between detector and samples.

The irradiation conditions shown in Table 1 for activation were chosen on the basis of preliminary experiments.

RESULTS AND DISCUSSION

Figure 1 shows the typical γ-ray spectra of bone samples irradiated by thermal neutrons (decay time 150 s, counting time 10 min) and by epithermal neutrons (decay time 15 min, counting time 10 min). It is evident that, after thermal neutron activation, the trace elements manganese and vanadium can be detected as well as fluorine and the major bone components (calcium, magnesium, sodium and chlorine).

For epithermal irradiation, because of high values of shield ratios (the ratio of the activity obtained without the shield to that observed with the shield) of 180 for ^{49}Ca, 160 for ^{27}Mg and 145 for ^{24}Na, background and dead time are reduced significantly. A longer irradiation of 10 min is therefore possible and strontium and bromine are detected in addition to Ca, Na, Mg, Cl and Mn. With the exception of bromine and strontium, standard deviations and detection limits for the epithermal method are obviously higher because of high boron ratios for all measured nuclides. The detection limits shown in Table 2 were calculated from Currie's criterion [22]. Results

TABLE 1

Irradiation conditions for activation of bone

Irradiation	Decay time	Counting time	Element quantified
Thermal neutrons	10 s	30 s	F
30 s	150 s	10 min	Ca, Na, Mg, Cl, Mn, V, (P + Al)
Epithermal neutrons	1 min	10 min	Ca, Na, Mg, Cl, Mn, (P + Al)
10 min	15 min	10 min	Ca, Na, Cl, Mn, Sr, Br

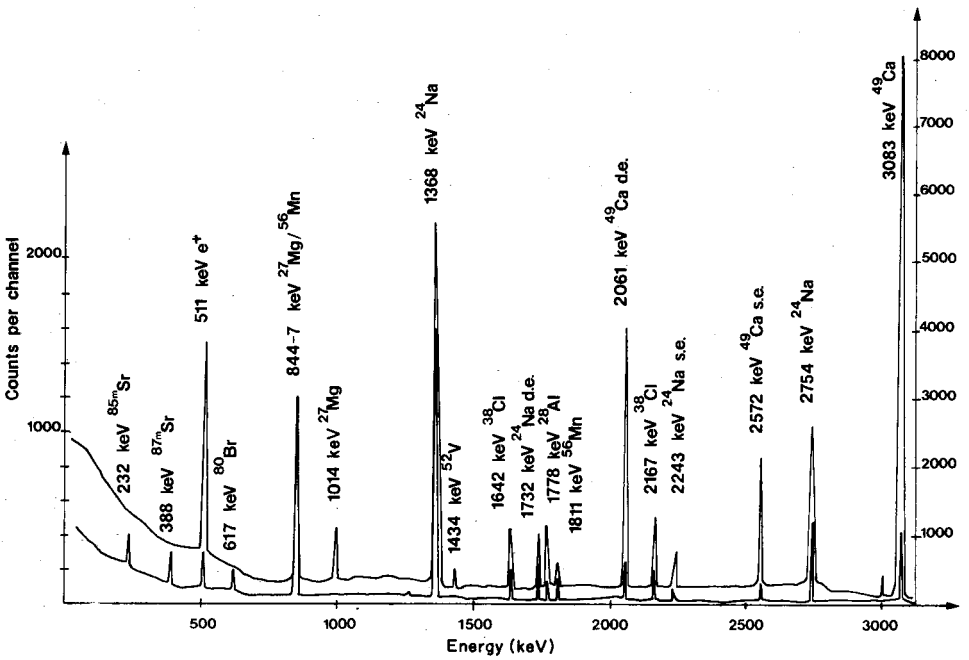

Fig. 1. A comparison of the γ-ray spectra of the IAEA Calcined Animal Bone sample after epithermal neutron activation (lower spectrum and left scale) and thermal neutron activation (upper spectrum and right scale).

TABLE 2

Determination of elements in the IAEA standard material, Calcined Animal Bone A3-74.

Element	Nuclide measured	Thermal neutrons		Epithermal neutrons		Literature value
		Conc. (mg g^{-1})	Detection limit (mg)	Conc. (mg g^{-1})	Detection limit (mg)	
Ca	^{49}Ca	320 ± 1.1	0.50	319 ± 3	1.3	313 [9]
Mg	^{27}Mg	6.50 ± 0.05	0.030	6.5 ± 0.3	1.5	—
Na	^{24}Na	11.0 ± 0.2	0.055	11.1 ± 0.4	0.25	11.5 [12], 13.3 [26]
Cl	^{38}Cl	2.20 ± 0.15	0.067	2.25 ± 0.8	0.35	—
F	^{20}F	0.590 ± 0.01	0.040	—	—	0.613 [9], 0.566 [12]
Mn	^{56}Mn	0.033 ± 0.001	0.004	0.033 ± 0.001	0.005	0.032 [21]
V	^{52}V	0.0011 ± 0.0002	0.0002	—	0.001	—
Br	^{80}Br	—	0.004	0.0029 ± 0.0001	0.0005	
Sr	^{87m}Sr	—	0.1	0.232 ± 0.008	0.023	—
Al	^{28}Al	0.0463 ± 0.002				0.0435 [15]
P	^{28}Al	154.0 ± 1				155 ± 5 [9]

for fluorine were corrected for sodium interference from the $^{23}Na(n,\alpha)^{20}F$ reaction.

A combination of thermal and epithermal activation enables a mathematical separation of the aluminium and phosphorus contribution to the

total activity of the ^{28}Al nuclide. This method is very attractive when the outer site of a SLOWPOKE reactor is used. The ratio of the thermal-to-fast flux for this site is about 27 [23] and the ratio of ^{28}Al specific activities for aluminium and phosphorus is 2500 [19]. This means that for thermal activation of bone, the contribution of aluminium and phosphorus to the total activity of ^{28}Al is approximately equal. When a boron carbide shield is used, the aluminium contribution is reduced by a factor of 143 (the value of the boron ratio for aluminium [19]), while the activity of ^{28}Al produced from phosphorus by fast neutron reaction is almost unchanged (boron ratio 1.05). This allows determination of phosphorus very precisely by epithermal activation and simultaneously decreases the error of the aluminium determination.

For two irradiations

$$I_t = A_a m_p + A_p m_p \text{ and } I_e = A_{ea} m_a + A_{ep} m_p$$

where I_t is the total activity of ^{28}Al after thermal activation, I_e is the total activity of ^{28}Al after epithermal activation, A_a and A_{ea} are the specific activities of aluminium standards, A_p and A_{ep} are the specific activities of phosphorus standards, and m_a and m_p are the weights of aluminium and phosphorus in bone samples. The solution of these equations gives

$$m_a = [I_t A_{ep} - I_e A_p]/[A_a A_{ep} - A_{ea} A_p] \quad (1)$$

and

$$m_p = [I_e A_a - I_t A_{ea}]/[A_a A_{ep} - A_{ea} A_p] \quad (2)$$

From these equations, the relative standard deviations, δm_p and δm_a can be derived from counting statistics for the phosphorus and aluminium masses. If S_p and S_a are standard deviations from counting statistics, then $\delta m_p = S_p/m_p$ and $\delta m_a = S_a/m_a$, and

$$S_p^2 = S_{I_t}^2(\delta m_p/\delta I_t)^2 + S_{I_e}^2(\delta m_p/\delta I_e)^2 \quad (3)$$

$$S_a^2 = S_{I_t}^2(\delta m_a/\delta I_t)^2 + S_{I_e}^2(\delta m_a/\delta I_e)^2 \quad (4)$$

After differentiating and substituting $S_{I_t}^2 = I_t$ and $S_{I_e}^2 = I_e$

$$S_p = [I_t A_{ea}^2 + I_e A_a^2]^{1/2}/[A_a A_{ep} - A_{ea} A_p] \quad (5)$$

and

$$S_a = [I_t A_{ep}^2 + I_e A_p^2]^{1/2}/[A_a A_{ep} - A_{ea} A_p] \quad (6)$$

Substituting the values of m_a, m_p, S_p and S_a into the above expressions for δm_p and δm_a gives

$$\delta m_p = [I_t A_{ea}^2 + I_e A_a^2]^{1/2}/[I_e A_a - I_t A_{ea}] \quad (7)$$

$$\delta m_a - [I_t A_{ep}^2 + I_e A_p^2]^{1/2}/[I_t A_{ep} - I_e A_p] \quad (8)$$

TABLE 3

Analysis of NBS SRM 1571 Orchard Leaves

Element	Experimental value ($mg\ g^{-1}$)	Certified value ($mg\ g^{-1}$)
Calcium	20.0	20.9
Magnesium	6.3	6.2
Chlorine	0.78	0.72
Manganese	0.092	0.091
Bromine	0.0105	0.010
Aluminium	0.380	0.410 [24], 0.359 [25]

On substitution of numerical values into Eqns. (7) and (8), quite satisfactory values of $\delta m_p = 0.6\%$ and $\delta m_a = 4.5\%$ were obtained. The data for aluminium and phosphorus content calculated by using base Eqns. (1) and (2) are given in Table 2. It should be pointed out that even 20 ppm of aluminium in 0.5-g bone samples can be determined by this method with a relative standard deviation not exceeding 10%.

Agreement of these results with available literature data for IAEA Calcined Animal Bone confirms the suitability of this method for multi-element determinations in bone; it also confirms that standards prepared on calcium hydrogenphosphate are useful for bone. Nadkarni and Morrison [24] obtained good results using the standard reference material Orchard Leaves (SRM 1571) as a multi-element standard for neutron activation of different biological samples. In Table 3 are listed the present data for this SRM which also confirms its use but with one restriction. This standard contains about 0.2% silicon [25] and cannot be used for the simultaneous determination of aluminium and phosphorus because of the interfering reaction $^{28}Si(n,p)^{28}Al$.

This work was supported by a grant from the Natural Sciences and Engineering Research Council of Canada.

REFERENCES

1 H. J. M. Bowen, CRC Crit. Rev. Anal. Chem., 10 (1980) 127.
2 G. C. Goode, C. M. Howard, A. R. Wilson and V. Parsons, Anal. Chim. Acta, 58 (1972) 363.
3 W. Van der Mark and H. A. Das, J. Radioanal. Chem., 13 (1973) 107.
4 F. J. Batra and D. K. Bewley, J. Radioanal. Chem., 16 (1973) 275.
5 P. Eisenbarth and P. Hille, J. Radioanal. Chem., 40 (1977) 203.
6 P. Holmberg, M. Hyvönen and M. Tarvainen, J. Radioanal. Chem., 42 (1978) 169.
7 J. L. Irigaray, J. C. Capelani, B. Sauvezie and J. L. Chabard, Nuclear Activation in the Life Sciences, IAEA-SM-227/93, Vienna, 1979, p. 433.
8 M. A. Chaudri, Int. J. Appl. Radiat. Isot., 30 (1979) 179.
9 J. R. W. Woittiez and H. A. Das, J. Radioanal. Chem., 59 (1980) 213.
10 H. Conaway, G. W. Leddicotte and A. D. Kenny, Anal. Biochem., 39 (1971) 218.

11 J. R. Mernagh, J. E. Harrison, R. Hancock and K. G. McNeill, Int. J. Appl. Radiat. Isot., 28 (1977) 581.
12 S. A. Kerr and N. M. Spyrou, J. Radioanal. Chem., 44 (1978) 159.
13 P. Bratter, D. Gawlik, J. Lausch and U. Rösick, J. Radioanal. Chem., 37 (1977) 393.
14 C. S. Erasmus, K. Hoffman and A. C. Kennedy, Nuclear Activation in the Life Sciences, IAEA-SM-227/4, Vienna, 1979, p. 419.
15 G. C. Goode, J. Herrington and P. O. Goddard, Radiochem. Radioanal. Lett., 31 (1977) 87.
16 W. Gatschke and D. Gawlik, J. Radioanal. Chem., 56 (1980) 203.
17 G. R. Gilmore and B. L. Goodwin, Radiochem. Radioanal. Lett., 10 (1972) 217.
18 A. J. Blotcky, E. P. Rack, R. R. Recker, J. A. Leffler and S. Teitelbaum, J. Radioanal. Chem., 43 (1978) 381.
19 H. Bem and D. E. Ryan, Anal. Chim. Acta, 124 (1981) 373.
20 H. Bem and D. E. Ryan, J. Radioanal. Chem., 63 (1981) 405.
21 Final Report, IAEA No. RL/25, 1974, Vienna.
22 L. A. Currie, Anal. Chem., 40 (1968) 586.
23 D. E. Ryan, D. C. Stuart and A. Chattopadhyay, Anal. Chim. Acta, 100 (1978) 87.
24 R. A. Nadkarni and G. H. Morrison, J. Radioanal. Chem., 43 (1978) 347.
25 J. D. Jones, P. B. Kaufman and W. L. Rigot, J. Radioanal. Chem., 50 (1978) 261.
26 M. Ördögh, J. Radioanal. Chem., 46 (1978) 27.

Analytica Chimica Acta, 135 (1982) 137—143
Elsevier Scientific Publishing Company, Amsterdam — Printed in The Netherlands

SOME OBSERVATIONS ON SULFURIC ACID REACTIONS IN ELECTROTHERMAL ATOMIC ABSORPTION SPECTROSCOPY WITH GRAPHITE FURNACES

I. MARTINSEN and F. J. LANGMYHR*
Department of Chemistry, University of Oslo, Oslo 3 (Norway)
(Received 3rd September 1981)

SUMMARY

Interferences were found when mixtures of sulfuric acid with either nitric or perchloric acid were atomized in the graphite furnace of an atomic absorption spectrometer. The mixtures apparently formed thermally stable compounds with the graphite, which were not removed by pyrolysis at temperatures up to 1100°C. During the subsequent atomization, volatile species were released and their absorption could not be compensated by the conventional deuterium lamp system. The absorption and emission spectra of the species formed in the furnace showed the presence of CS and probably COS, as well as bands appropriate to S_2, SO_2 and NS. The uncorrectable absorptions detected at the 303.8-nm nickel line, the 303.94-nm indium line, and the 304.40-nm cobalt line are thought to be caused by the fine-structure of an unknown molecular compound.

In electrothermal atomic absorption spectroscopy (a.a.s.) with graphite furnaces, nitric, sulfuric and perchloric acids are often present in the sample and standard solutions. They may also be added as matrix-modifying or wet-ashing agents to solid or liquid samples deposited in the graphite tube.

A recent paper [1] reports on the chemical interference of perchloric acid on the a.a.s. determination of aluminum, gallium and thallium. The acid severely suppressed the peak absorbances, and it was found impossible to remove the acid in the normal pyrolyzing step. The acid, or its decomposition products, apparently interacted with the graphite to form thermally stable compounds which were released during the atomization step, in which they formed molecular species with the analyte atoms. Heating to about 1700°C was required to remove this chemical interference.

The present paper describes cases of interferences resulting from the interaction of graphite with mixtures of sulfuric acid and nitric or perchloric acid, and the release of volatile, absorbing compounds during the atomization step. The absorptions observed at the 303.8-nm nickel line, the 303.94-nm indium line, and the 304.40-nm cobalt line could not be compensated for by the conventional method of background correction.

EXPERIMENTAL

Apparatus, reagents and solutions

The Perkin—Elmer 400S spectrometer used was equipped with two lamps for background correction, a Pye-Unicam SP9-01 atomizer and graphite tubes of the standard and profile types without pyrolytic coating. The atomizer was modified by installing silica windows in both ends, and by introducing two streams of the purging gas, one exterior stream enveloping the graphite tube, and two interior streams passing from the ends of the tube and out at the sample introduction port in the middle.

The above equipment was also used to record absorption spectra; in these instances the hollow-cathode lamp was replaced by a deuterium lamp connected to a separate power supply.

Emission spectra from the graphite furnace were recorded with a Hilger Medium Quartz spectrograph and Kodak spectrum analysis plates, No. 1. The spectra were plotted with a micro densitometer.

The concentrated nitric, sulfuric, perchloric, hydrochloric and hydrofluoric acids were of Suprapur quality (Merck). The acids were diluted with water to a concentration of 1.0 mol l^{-1}. The argon was of 99.9% purity.

Preliminary experiments

During some attempts at the a.a.s. determination of indium in synovial fluid, it was found that the original sample did not give any signal; however, after a wet-ashing step in the graphite tube with sulfuric acid, a signal was recorded which corresponded to a concentration of 90 ng ml^{-1} indium. Wet-ashings of the sample in the furnace with mixtures of nitric and sulfuric acids gave still higher values.

The following series of measurements and observations were then made with the use of the deuterium background corrector lamp and the instrumental parameters listed in Table 1: (a) blank measurements of the empty furnace, which provided no signals at all; (b) atomization of separate 10-μl portions of the five acids, none of which gave a signal; (c) atomization of 10-μl portions of two acids together, of which the mixtures of nitric and sulfuric acids, and perchloric and sulfuric acids, exhibited distinct signals; (d)

TABLE 1

Instrumental parameters

Lamp current (mA)	20	Heating program:	
Wavelength (nm)	303.94	Drying	40 s, 100°C
Spectral bandwidth (nm)	0.7	Evaporation	40 s, 300°C
Argon flow rate l min^{-1}		Pyrolysis	40 s, 850°C
Interior	0.34	Atomization	5 s, 2350°C
Exterior	3.0	Tube cleaning	5 s, 2500°C

blank measurements of the empty furnace, which again gave no signals. Some typical signals from these measurements are reproduced in Fig. 1.

The effect of varying the pyrolysis temperature on the atomization signal from mixtures of sulfuric and nitric acid was then studied; the other parameters in Table 1 were unchanged. As is apparent from Fig. 2, the signal is not removed at pyrolysis temperatures up to 1100° C. Likewise, the effect of varying the atomization temperature on the signal from the sulfuric/nitric acid mixture was studied, the other settings in Table 1 being unchanged. Figure 2 shows that the peak height increased in the temperature range 2000—2600° C.

With the use of the indium hollow-cathode lamp as the radiation source and the deuterium lamp as the background corrector, the effects of a change of the slit width on the absorption of 10 μl of 100 ng ml^{-1} indium solution, and of a mixture of 10 μl of 1.0 mol l^{-1} nitric acid and 10 μl of 1.0 mol l^{-1} sulfuric acid were measured. The absorbances at 0.2, 0.7 and 2.0-nm slit widths were practically the same.

These preliminary experiments indicated that sulfuric acid in mixture with nitric or perchloric acid interact with graphite to form thermally stable compounds; during the atomization step, absorbing species are released, and these are not compensated for by the deuterium background corrector lamp.

Recording of absorption spectra

The unknown absorbing species may be detected from their absorption spectra. With the use of graphite tubes of the standard type, a deuterium

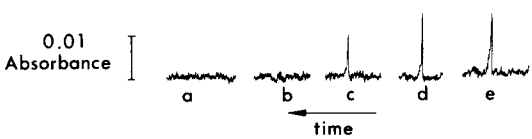

Fig. 1. Signals as recorded from: (a) the empty furnace; (b) 10 μl of 1.0 mol l^{-1} sulfuric acid; (c) 10 μl of 1.0 mol l^{-1} sulfuric acid and 10 μl of 1.0 mol l^{-1} nitric acid; (d) as (c) but without background corrector; (e) 10 μl of 1.0 mol l^{-1} sulfuric acid and 10 μl of 1.0 mol l^{-1} perchloric acid.

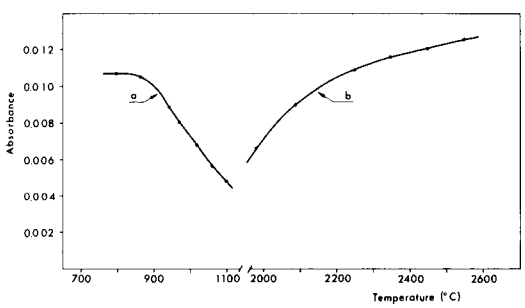

Fig. 2. The effect of varying the temperature of pyrolysis (curve a) and atomization (curve b) on the signal from a mixture of 10 μl of 1.0 mol l^{-1} sulfuric acid and 10 μl of 1.0 mol l^{-1} nitric acid.

lamp as the radiation source, and the instrumental parameters given in Table 1, absorption curves were plotted at 10-nm intervals in the wavelength range 220—350 nm. First, 10-μl portions of the 1.0 mol l^{-1} solutions of nitric, sulfuric and perchloric acids were atomized separately, and then mixtures of 10 μl of sulfuric acid and 10 μl of either nitric or perchloric acid were atomized. The sulfuric/nitric acid mixture was atomized in both new and used graphite tubes. The curves showing the total absorbance as a function of the wavelength are given in Fig. 3.

The three acids, when atomized separately, did not exhibit any signal in the wavelength range studied. However, the two binary mixtures gave similar absorption curves with bands at about 260 and 280 nm, as well as a shoulder at approximately 310 nm. Compared to measurements with a new graphite tube, the absorbances were considerably higher with a used tube. A more detailed plot of the absorption of the sulfuric/nitric acid mixture was then recorded for the range 250—290 nm. From Fig. 4, it can be seen that two relatively sharp peaks appear at two of the maxima in Fig. 3.

Some absorption measurements for acid mixtures were also made around the 303.94-nm indium line. In these measurements the slit width was reduced to 0.2 nm, and the wavelength settings were adjusted by means of the indium, nickel and cobalt lines at 303.94, 303.8 and 304.40 nm, respectively. Concentrated nitric and sulfuric acids (2-μl portions) were transferred to the graphite tube, and atomized according to the usual program (Table 1). The absorption curve (Fig. 5) exhibits a maximum at 303.90 nm.

Finally, some absorption measurements were made at the 303-94-nm indium line, and with the use of the deuterium background corrector. A tantalum scoop was placed in the middle of a graphite tube of the standard type, and with the instrumental parameters of Table 1, the following experiments were done. Measurement of the empty scoop gave no signal. Separate measurements of 10 μl of 1.0 mole l^{-1} nitric or sulfuric acid gave no signals, nor did a mixture of these acids. When the mixture of the two acids was

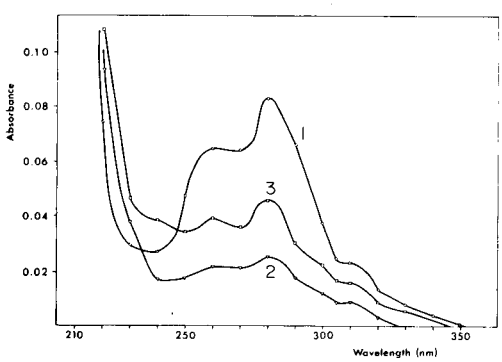

Fig. 3. Absorption spectra of mixtures of 10 μl of each of the following 1.0 mol l^{-1} acids: (1) sulfuric/nitric acid in a used graphite tube; (2) the same acids in a new graphite tube; (3) sulfuric/perchloric acid in a new graphite tube.

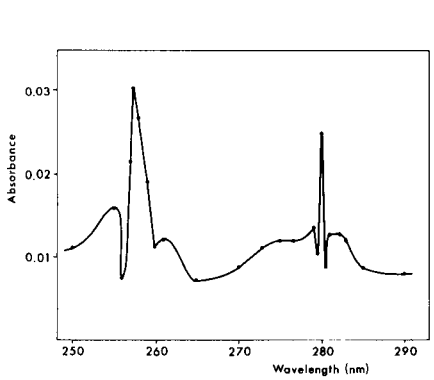

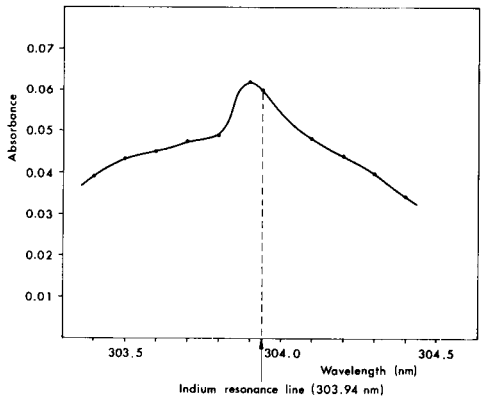

Fig. 4. The absorption spectrum of the mixture of 10 μl each of sulfuric and nitric acids (both 1.0 mol l^{-1}).

Fig. 5. The absorption band near 304 nm for a mixture of 2 μl of concentrated sulfuric acid and 2 μl of concentrated nitric acid. Slit width 0.2 nm.

deposited on pulverized graphite from an unused tube, no signal was recorded; but when the mixture was deposited on a solid piece of graphite cut from the wall of a new tube under otherwise identical conditions, a signal was obtained.

Recording of emission spectra

Information about the species released from the graphite tube during atomization may also be obtained by recording emission spectra. To increase the intensity of the emission, high-temperature graphite tubes of the profile type were used, the acids were added in the concentrated form, and atomizations were made at about 3000°C with a heating period of 8 s (the other steps on the heating program were as listed in Table 1). Following calibration of the wavelength scale of the spectrograph by recording of the emission spectrum of indium, the following emission spectra were recorded: (a) from a new empty graphite tube; (b) from nitric, sulfuric and perchloric acid atomized separately; (c) from a mixture of 2 μl of sulfuric acid and 2 μl of either nitric or perchloric acid; and (d) from the graphite tube employed in the above experiments.

In the spectra from experiments (a) and (b) only CN bands were detected; in the spectrum from experiment (d) a few faint bands were seen in addition to these bands. The spectra from experiment (c) were similar, and exhibited the bands listed in Table 2.

DISCUSSION

From a comparison of the absorption spectra reproduced in Figs. 3—5 with the literature on molecular spectra [2], the following conclusions were

TABLE 2

The bands observed in the emission spectra of mixtures of 2 μl of concentrated sulfuric acid and 2 μl of either concentrated nitric or perchloric acid, compared with the band heads reported in the literature [2]. The bands observed above 285 nm are weak.

Bands observed (nm)	Band heads reported (nm)	Bands observed (nm)	Band heads reported (nm)
246.1	CS 246.02; NS 246.07	278.5	CS 278.57
247.7	CS 247.70	280.0	CS 280.15; S_2 279.88
248.3	Not identified	282.0	CS 281.95
249.4	CS 249.37	283.7	CS 283.68; S_2 282.91
251.0—251.6	CS 250.73, 251.12; NS 250.67	285.0	CS 285.23; C_2 285.5
251.9	NS 251.85	288.0	COS 288.0; S_2 288.79; 289.23
252.4	CS 252.32	291.2	COS 291.1
254.0	CS 253.87	292.1	S_2 292.02
255.6	CS 255.58	294.3	COS 294.3
257.6	CS 257.56	295.0	S_2 295.40
258.1	Not identified	298.0	COS 297.6
259.2	CS 258.96	299.1	S_2 298.95; C_2 298.7
260.5	CS 260.59	299.9	Not identified
262.1	CS 262.16	300.9	COS 300.9
266.3	CS 266.26	302.6	S_2 302.46
267.9	CS 267.70	303.5	Not identified
269.3	CS 269.32	304.7—305.4	COS 304.3; S_2 305.47
270.9	CS 270.89	307.7	COS 307.7
272.7	CS 272.67	308.8	S_2 309.15
274.4	CS 274.39	309.7	Not identified
275.5	CS 275.47	312.0	C_2 312.9
277.2	CS 276.92; S_2 276.94	313.9	S_2 313.22

drawn. The maximum at about 255 nm (Figs. 3 and 4) probably originates from COS, which is reported to have an absorption band extending from a sharp edge at 255 nm towards shorter wavelengths. The broad absorption band observed at 257 nm (Fig. 3) and the peak at 257 nm (Fig. 4) compare well with the maximum at 257.56 nm reported for CS. The observed predominating band at about 280 nm (Figs. 3 and 4) may be explained by the presence of S_2 and/or SO_2 which exhibit absorption maxima at 279.88 nm and 279.7 nm, respectively. No species was found which could explain the observed absorption at 303.90 nm (Fig. 5); it was assumed to result from the presence of an unknown molecular compound, the fine-structure of which introduces the observed uncorrectable interference experienced at the 303.94-nm indium line.

The comparison in Table 2 between the observed and reported bands clearly demonstrates the presence of CS, and also indicates that COS is present. Other species which may be present are NS, S_2 and C_2, in addition to the CN bands already mentioned.

From the literature [3], it appears that sulfuric acid, in the presence of such oxidizing agents as nitric or perchloric acid, penetrates into graphite forming graphite hydrogensulfate of the type $C_m^+HSO_4^- \cdot 4H_2SO_4$. These compounds apparently do not decompose completely at the temperatures of the drying and pyrolysis steps; during atomization the remaining substances produce the volatile species detected in the present study. These compounds are likely to result from a series of reactions involving carbon and SO_2, SO, S_2 and COS.

In those instances where the absorption bands of volatile molecules overlap the emission/absorption line of the analyte atom, the fine-structure of the molecular band may introduce an interference which cannot be compensated for by the conventional deuterium or tungsten lamp background correction systems. The interference experienced in the present study at the 303.94-nm indium line was assumed to result from the fine-structure of an unknown molecule; this interference was also observed at the 303.8-nm nickel line and the 304.40-nm cobalt line.

REFERENCES

1 S. R. Koirtyohann, E. D. Glass and F. E. Lichte, Appl. Spectrosc., 35 (1981) 22.
2 R. W. B. Pearse and A. G. Gaydon, The Identification of Molecular Spectra, 3rd edn., Chapman and Hall, London, 1963.
3 See, e.g., Gmelins Handb. d. anorg. Chem., 8th edn., Kohlenstoff, Teil B, Lieferung 3, Verlag Chemie, Weinheim, 1968, p. 869.

Analytica Chimica Acta, 135 (1982) 145—152
Elsevier Scientific Publishing Company, Amsterdam — Printed in The Netherlands

EFFECT OF THE ORGANIC LIGAND ON THE RESPONSE FOR VANADIUM IN FLAME ATOMIC EMISSION SPECTROMETRY

BEVERLY J. WOOD[a], J. F. GALOBARDES and L. B. ROGERS*
Department of Chemistry, University of Georgia, Athens, GA 30602 (U.S.A.)
(Received 7th August 1981)

SUMMARY

Flame emission intensities from vanadium in the forms of chelates with *N*-nitrosophenylhydroxylamine and 8-quinolinol in methyl isobutyl ketone were measured. Although differences in atomic absorption characteristics for vanadium bound by different ligands have been reported, significant differences were not found in the emission intensities of these two chelates after signals for the appropriate blanks had been subtracted.

Most petroleum crudes contain measurable quantities of many metals though they are usually in low concentrations. Nickel and vanadium are most abundant and their presence causes many problems. The removal of these metals from crude has been the subject of much research over the years [1, 2]. Venezuelan crude oils contain relatively large amounts of vanadium, as much as 4000 ppm; thus, the problems associated with its presence are most evident in the refining of those oils. Vanadium causes corrosion of refinery machinery and stability problems in products of crude oil. The major problem, however, arises from the ability of vanadium to poison the cracking catalysts. The metal increases the dehydrogenation activity of the catalyst so that more hydrogen and coke are produced at the expense of gasoline [2]. Vanadium is present as the vanadyl ion which Selbin [3] states is very stable. A large fraction of the vanadium is present as porphyrins, in which four nitrogen atoms are bound to each vanadyl ion. In the non-porphyrin fraction, the vanadyl ion can also be bound to oxygen and sulfur atoms [1].

Many methods have been used for the determination of vanadium in crudes, including flame spectrometric methods [1, 2]. The long-range goal of the present study was to explore the feasibility of using flame emission as an on-line detector in liquid chromatography. The direct determination of vanadium-containing species in fractions separated by high-performance liquid chromatography has been described recently [4, 5]. Making direct measurements on effluents while maintaining relative insensitivity to changes in organic species present, is an important aspect of the application. Flame

[a]Present address: Eastman Kodak Company, Rochester, New York, NY 14650, U.S.A.

0003-2670/82/0000-0000/$02.75

spectrometric methods are not as sensitive as non-flame techniques, especially in determinations of refractory oxide-forming metals such as vanadium [6].

Several studies of vanadium have been made utilizing atomic absorption spectrometry (a.a.s.) [7—9]. Recently, differences in sensitivity in a.a.s. depending on the organic ligand bound to vanadium or nickel in the sample have been reported [10—12]. Absorbances were compared from vanadyl tetraphenylporphyrin and bis-1-phenyl(1,3)-butadione, as were those of nickel(II) tetraphenylporphyrin and nickel(II) cyclohexylbutyrate. Results showed that the porphyrins gave higher absorbances. Lang et al. [12] observed differences in absorption signals from solutions of eight organometallic compounds of nickel. Takeuchi et al. [13] extracted nickel using several complexing agents; they also observed a dependence of the nickel absorbance on the type of ligand present in the sample.

Because many different ligands are undoubtedly combined with vanadium in crude oil, this raises the question of whether or not quantitative measurements can be made with a single calibration curve. Some authors [14] have gone as far as to say that a.a.s. should not be used for the determination of vanadium because of the strong matrix effects. Crump-Wiesner and Purdy [15] and Chau and Lum-Shue-Chan [16] extracted vanadium using several reagents and compared the atomic absorbances of the extracted vanadium. They determined which of the complexing agents best extracted vanadium in terms of the highest absorbance signal. However, the effects of suitable blanks were not reported to the extent necessary to show effects of various parameters in the extraction of vanadium.

Atomic emission spectrometry was chosen here for the vanadium determination because of its availability in this laboratory. Atomic emission has a reported detection limit of 0.3 ppm [6]. However, the effects of ligand and/or bond type on emission intensities for vanadium complexes have not been reported. To test the latter, ligands were chosen for their abilities to extract vanadium quantitatively. Hence, known concentrations of vanadium in a nonaqueous solvent could be prepared conveniently by quantitative extraction from an aqueous solution into a known volume of organic solvent. After each extraction, both the aqueous and organic phases were subjected to spectrometry so as to calculate a material balance. In addition, back-extraction into alkaline aqueous solution was used as a further check.

The solvents normally used for the extraction of vanadium include chloroform and methyl isobutyl ketone (MIBK). Although chlorinated solvents are excellent extraction media, their use in flame spectrometric methods produces toxic by-products such as phosgene. Some success has been found in the extraction of a chelate into chloroform, evaporation, and redissolution in a more suitable solvent, such as methyl isobutyl ketone. However, because of the probable volatility of the vanadium complex, serious loss of vanadium may occur during the evaporation process.

Several variables were examined in the present study. The major variable, the ligand, was explored using the ammonium salt of *N*-nitrosophenyl-

hydroxylamine (cupferron) and 8-quinolinol (8-hydroxyquinoline, oxine). An attempt was made to minimize the flame effects encountered with chloroform by employing pulse nebulization [17, 18] and by evaporating the chloroform and replacing it with MIBK. However, most of the quantitative studies were completed with the MIBK.

EXPERIMENTAL

Apparatus

Emission intensities were measured using a Heath Model EU-703 spectrometer equipped with a Varian-Techtron burner fed with premixed nitrous oxide—acetylene. A Varian A-25 recorder was used for read-out of spectral intensities. The experimental conditions were as follows: analytical line, 437.8 nm; slit width, 50 μm; air pressure, 20 psi; nitrous oxide, 17 psi; acetylene, 10 psi; rate of aspiration of solution, 2.1 ml min^{-1}. Gas flow rates were controlled using arbitrary flow control levers.

A Corning Model 130 pH meter and a Coleman 124 spectrophotometer fitted with 1-cm quartz cells were used for pH and u.v. absorption measurements, respectively.

Reagents and solutions

The vanadium reference solution (Fisher Scientific, Pittsburg, PA) contained vanadium pentoxide dissolved in dilute hydrochloric acid. The cupferron (Mallinckrodt Chemical, St. Louis, MO) which included a preservative for stability, and the oxine (Matheson, Coleman & Bell, Cincinnati, OH) were used as received. The solvents were methyl isobutyl ketone (Fisher Scientific) and chloroform (J. T. Baker Chemical Co., Phillipsburg, NJ). For pH adjustment, the buffer consisted of 50 ml of 0.02 M sodium acetate and 950 ml of 0.2 M acetic acid. The pH was adjusted with dilute sodium hydroxide or sulfuric acid, as needed.

Solutions of the ligands were made as follows. The cupferron was dissolved in water at 20°C before extraction into MIBK or chloroform. Oxine was dissolved directly in both organic solvents to make 5% solutions; both reagent solutions were stored in a refrigerator. Cupferron decomposed readily and fresh solutions were prepared daily. All chemicals were analytical grade.

Procedures

For "simple" extractions, a 10-ml sample of a 50 ppm vanadium solution was made from the vanadium standard by pipetting a 0.5-ml portion of the reference solution into a 10-ml volumetric flask, followed by 1.0 ml of the buffer solution and dilute acid and/or base for pH adjustment before diluting to volume. This solution was transferred quantitatively to a separatory funnel by rinsing with three 0.5-ml portions of the buffer, and a 5-ml portion of the organic ligand solution was pipetted into it. After shaking for two 1-min intervals, the phases were allowed to separate and then transferred to separate

beakers. The heavier aqueous phase was then returned to the separatory funnel and another 5-ml portion of the ligand solution added. After that extraction process had been completed, the extracts were combined. Two additional 5-ml portions were added, the extractions completed and all of the extracts combined. Both the aqueous and the organic phases were retained for spectrometry.

Blanks were prepared by making solutions of the exact volume and composition as the sample solutions but without the vanadium. The solution was then taken through the entire extraction process. Additional blanks were prepared to represent the aqueous phase after extraction. Duplicates of the original sample blank were prepared so that other blanks could be made to show the effect on the aqueous phase signal of solvent alone and of the excess of ligand in the solvent. The solvent blank was prepared by placing one of the original sample blank solutions in contact with an equal volume of MIBK and shaking for two 1-min intervals; the aqueous phase was then separated and retained as the blank. The ligand in the solvent blank was prepared by taking another portion of the original blank solution and contacting it with an equal volume of ligand in MIBK. It was then shaken and the final aqueous phase used as the blank. Aqueous phase blanks were prepared for both ligand solutions.

Blanks were also prepared for the organic phase. Volumes of solvent equal to that in the extraction process were placed in contact with buffer solution and agitated for two 1-min intervals. The organic phase was retained to evaluate the effect of the aqueous buffer on the organic phase signal. Another blank was prepared by placing the appropriate volume of ligand in MIBK in contact with the buffer, repeating the shaking, and then retaining the organic phase so as to evaluate the effect of the aqueous buffer on the ligand solution. Again, blanks were made for both ligand solutions. All samples and blanks were prepared and measured in triplicate.

Calibration curves were prepared at pH 2 using different concentrations of the standard reference solution. Calibration curves were also prepared by diluting the organic phases after quantitative extraction of a known amount of vanadium from an aqueous solution using either cupferron or oxine. These calibration curves were used to compare the results from the "simple" extractions employing the ligands.

Back-extractions were done to check the concentration of vanadium in the extracts. After a sample had been processed through the simple extraction step and measured, it was returned to the separatory funnel. A 10-ml portion of aqueous pH 11 solution was pipetted into the separatory funnel and shaken for two 1-min intervals. The phases were separated and measured.

The blanks for the back-extracts were prepared using an aqueous solution at pH 11 without vanadium. The first blank was obtained directly on a portion of that solution. Another blank was obtained from a portion of the aqueous phase that had been shaken with MIBK alone; the final blank was obtained on a portion that had been shaken with a solution of the ligand in MIBK. Thus, the effect of pH, solvent, and ligand on emission from an

aqueous phase could be found and compared to the simple extraction done at pH 2. All samples and blanks were prepared in triplicate.

Calibration curves were also prepared at pH 11 using suitable aqueous dilutions of the standard reference solution. Appropriate blanks were again prepared.

Volatility losses of chelated vanadium were examined as follows. The primary extraction step was completed with the ligand dissolved in chloroform. After phase separation, 3 ml of the organic phase was pipetted into a 5-ml volumetric flask and the volume brought to the mark with chloroform. Approximately 2 ml of this solution was quantitatively transferred to a 1-cm quartz cell and its absorption spectrum was scanned over the range 350—700 nm against a blank consisting of the ligand in chloroform; the wavelength and the absorbance at the maximum were noted. The solution in the cell was returned to the original 5-ml flask by washing 3 times with 0.5-ml portions of chloroform. The flask was then placed in a vacuum oven at 25° C and half of the solvent was evaporated off. The volume was then brought back to 5 ml and the maximum absorbance was determined as before. This entire evaporation procedure was repeated twice, including the absorbance measurements. Three samples were measured from which a relative standard deviation $\leqslant 5\%$ was found between runs using calibration curves prepared by direct extraction of known amounts of vanadium.

Whether an organic or an aqueous vanadium solution was used, the wavelength for emission measurement was chosen by scanning the range 437—439 nm, for each series of measurements; consistently, the peak was found at 437.8 nm. The samples and blanks were measured as both aqueous and organic solutions. A 10-ml portion of an aqueous sample was measured by nebulizing it for a 5-s period and then substituting water so as to allow the signal to return to background level and to minimize the noise in the flame resulting from deposits on the burner. Each sample was measured 3 times. The organic samples were measured in the same manner with adjustment of the flame necessary for the solvents. Appropriately, the organic solvents were nebulized between their samples to allow for minimization of burner noise just as water was used for the aqueous samples.

The average signal was determined for each sample and blank. The signals used for comparisons were averages of the intensities for three separate measurements. The difference between the averages for the sample and the blank was then taken and attributed to the emission of the vanadium. The relative standard deviations for the intensities obtained were $\leqslant 5\%$.

RESULTS AND DISCUSSION

The calibration curve for the aqueous standard at pH 2 gave values of concentration having a standard deviation of ± 2 ppm. Both of the calibration curves for the chelated vanadium gave standard deviations of ± 3 ppm as did the calibration curves for the back-extraction at pH 11. Small non-zero intercepts in all of these calibrations corresponded to the blanks.

Typical results for samples and blanks are shown in Table 1 for both the cupferron and the oxine systems. The consistent values for the starting aqueous solution of 50 ppm at pH 2 and its blanks for both series of runs should be noted. It is also clear that vanadium had been completely extracted by each ligand. Although the signals obtained from the MIBK phase were lower than those for the aqueous solution at pH 2, the concentrations were also lower due to dilution to volume. The results were 25.2 ppm for oxinate and 24.4 ppm for cupferrate as compared to the expected 25 ppm. The important conclusion is that both of the chelates gave the same net signal value within experimental error (r.s.d. $\leqslant 5\%$) in the organic phase.

After back-extraction of the vanadium to the original volume of the aqueous phase, the concentrations were again close to the expected value of 50 ppm. Concentrations of 45 ppm and 48 ppm were obtained for the cupferrate and oxinate, respectively. Although the signals of the back-extracts were higher, the blanks were also higher because of the increased amount of sodium present as a result of the pH adjustment. Thus, net signals were only slightly higher than at pH 2. Again, both chelates gave the same signal intensity within experimental error.

From the above data, it was concluded that no significant differences in intensities occur for the cupferron and oxine chelates; although the vanadyl ion is bound through two oxygen atoms in the former and through an oxygen and a nitrogen in the latter, the stabilities of these molecules, apparently, were similar in the flame.

These findings are contrary to the earlier results [10—12] obtained by atomic absorption spectrometry in which the absorption signal for cupferrate was found to be 20% higher than that for the oxinate, and absorption differences as much as 75% were seen between other ligands. In those earlier studies, it was not clear whether appropriate blanks had been employed in comparing the different chelates in the organic phase or in the aqueous phase that remained.

The importance of blanks became obvious in preliminary studies. Extractions of 50 ppm vanadium with oxine at pH 4 showed that 55 ppm was present in the aqueous phase and 10 ppm remained in the organic phase after an extraction. Obviously, other factors were affecting the signal. Table 1 and Fig. 1 show that a significant signal was obtained for the blanks in the aqueous and organic phases for both ligand systems.

Other preliminary studies included extractions with chloroform. As shown in Table 2, the evaporation of half the chloroform led to significant losses of vanadium. Hence, the possibility of evaporating the chloroform and replacing it with MIBK for nebulization was unsuitable for quantitative work. Attempts at pulse nebulization of chloroform were also unsuccessful. Repeated clogging of the burner head and problems with erratic behavior of the pulses made quantitative measurements impossible.

In summary, flame methods as a means of quantifying the amounts of vanadium present are independent of the ligand for the two species studied here. However, other ligands must be studied to test the generality of these

TABLE 1

Comparison of emission signals for cupferron and oxine systems

Conditions	Signal (V)	
	Cupferron	Oxine
Simple extraction, pH 2		
Original solution before extraction (50 ppm)		
1. With vanadium	2.82	2.78
2. Without vanadium	0.26	0.29
3. Net signal	2.56	2.49
Aqueous phase after extraction		
1. Aqueous phase	0.34	0.38
2. Blanks		
a. Aqueous phase after contact with MIBK	0.31	0.33
b. Aqueous phase after contact with ligand/MIBK	0.36	0.41
3. Net signal	0.0	0.0
Organic phase after extraction (25 ppm)		
1. Organic phase	1.95	2.04
2. Blanks		
a. MIBK after contact with buffer	0.12	0.18
b. Ligand/MIBK after contact with buffer	0.15	0.27
3. Net signal	1.80	1.77
Back-extraction, pH 11		
Aqueous phase after extraction (50 ppm)		
1. Aqueous phase	3.30	3.50
2. Blanks		
a. Aqueous phase	0.36	0.38
b. Aqueous phase after contact with MIBK	0.40	0.41
c. Aqueous phase after contact with ligand/MIBK	0.44	0.45
3. Net signal	2.86	3.05

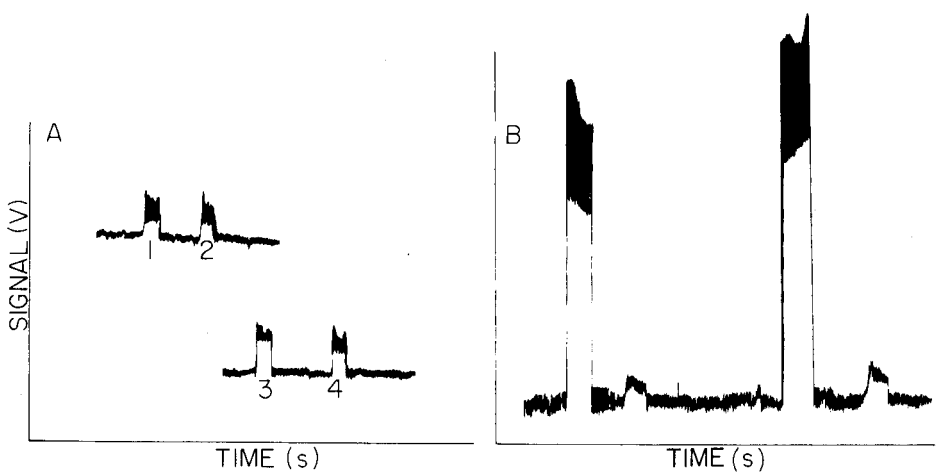

Fig. 1. Emission intensities for (A) the aqueous phase and (B) the organic phase, after the extraction; cupferron (1) and blank (2); oxine (3) and blank (4).

TABLE 2

Absorbances of vanadium chelates before and after evaporation of some chloroform

Chelate	Wavelength (nm)	Absorbance		Loss (%)
Cupferrate	401	Initial	0.78	
		Evaporation 1	0.67	13.8
		Evaporation 2	0.59	12.2
Oxinate	381	Initial	0.70	
		Evaporation 1	0.61	12.6
		Evaporation 2	0.56	7.7

results. In any case, the agreement found here suggests that the ligand effect needs further study before flame emission can be dismissed as a viable quantitative method for these determinations.

The authors thank William Spencer for helpful discussions. This research was supported in part by the Department of Energy, under contract number DE-AS09-76ER00854.

REFERENCES

1 T. F. Yen, The Role of Trace Metals in Petroleum, Ann Arbor, Ann Arbor, MI, 1975.
2 G. D. Hobson and W. Pohl, Modern Petroleum Technology, Applied Science Publishers, London, 1975.
3 J. Selbin, Chem. Rev., 65 (1965) 153.
4 S. K. Hajibrahim, P. J. C. Tibbetts, C. D. Watts, J. R. Maxwell, G. Eglinton, H. Colin and G. Guiochon, Anal. Chem., 50 (1978) 549.
5 D. Jones IV and S. E. Manahan, Anal. Chem., 48 (1976) 1897.
6 C. T. J. Alkemade, Analytical Flame Spectroscopy, Macmillan, London, 1970.
7 S. L. Sachdev, J. W. Robinson and P. W. West, Anal. Chim. Acta, 37 (1967) 12.
8 H. J. Crump-Wiesner and R. Feltz, Anal. Chim. Acta, 55 (1971) 29.
9 D. C. G. Pearton, J. D. Taylor, P. K. Fawe and T. W. Steele, Anal. Chim. Acta, 44 (1969) 353.
10 G. Sebor, I. Lang, P. Vavrecka, V. Sychra and O. Weisser, Anal. Chim. Acta, 78 (1975) 99.
11 P. Vavrecka, G. Sebor, I. Lang and O. Weisser, Riv. Combust., 9 (1975) 375.
12 I. Lang, G. Sebor, V. Sychra, D. Kolihova and O. Weisser, Anal. Chim. Acta, 84 (1976) 299.
13 T. Takeuchi, M. Suzuki and M. Yanagisawa, Anal. Chim. Acta, 36 (1966) 258.
14 J. M. Sugihara, Am. Pet. Inst. Res. Proj., 60 (1972) 35.
15 J. J. Crump-Wiesner and W. C. Purdy, Talanta, 16 (1969) 126.
16 Y. K. Chau and L. Lum-Shue-Chan, Anal. Chim. Acta, 50 (1970) 210.
17 H. Berndt and W. Slavin, At. Absorpt. Newsl., 5 (1978) 109.
18 D. L. Tsalev and I. I. Petrov, Anal. Chim. Acta, 111 (1978) 155.

Analytica Chimica Acta, 135 (1982) 153—158
Elsevier Scientific Publishing Company, Amsterdam — Printed in The Netherlands

Short Communication

THE GRAPHITE SPRAY ELECTRODE AND ITS APPLICATION IN THE ANODIC STRIPPING VOLTAMMETRY OF BISMUTH

J.-M. KAUFFMANN, A. LAUDET and G.-J. PATRIARCHE*

Institut de Pharmacie, Université Libre de Bruxelles, Campus Plaine 205/6, Boulevard du Triomphe, B-1050 Bruxelles (Belgium)

G. D. CHRISTIAN

Department of Chemistry, University of Washington, Seattle, WA 98195 (U.S.A.)

(Received 15th June 1981)

Summary. The surface characteristics of carbon-paste electrodes are greatly improved by spraying the surface with graphite from an aerosol. Significant differences are shown by scanning electron microscopy. The available potential range in different electrolytes is narrower but background currents are decreased and reproducibility is improved, compared to the carbon-paste electrode. With a mercury film and 10-min deposition times, the detection limit for bismuth(III) is 2×10^{-9} M by the differential pulse technique.

Solid electrodes have become widely used in analytical electrochemistry [1, 1a], largely because of the interesting properties of carbon materials compared to platinum and gold surfaces, particularly their low background currents. Modified carbon electrodes have been the subject of many investigations [2, 3]. A very easy and rapid way of preparing a reproducible graphite surface is described in this paper. The graphite spray electrode was prepared on a carbon-paste electrode and on a glassy carbon electrode.

Bismuth determination was made on the mercury-covered graphite surface [4]; this technique was reported by Matson et al. [5] and further studied by Seitz [6].

Experimental

Apparatus. Voltammetric measurements were made on a Bruker E100 polarograph with a Hewlett-Packard type 7004B recorder. A three-electrode cell was used, with a saturated calomel reference electrode and a platinum auxiliary electrode. Nitrogen was passed over the solutions during all measurements.

Two different working electrodes were tested: (1) a rotating disc electrode which was a Tacussel type EDI electrode with a glassy carbon disk (7.07-mm^2 geometric area); and (2) a stationary carbon-paste electrode (Metrohm EA267; 1.2-cm diameter) prepared from a standard paste (Metrohm EA207C) of spectroscopic-grade carbon powder and Uvasol liquid paraffin.

Reagents and solutions. Reagent-grade sulfuric acid and potassium chloride were found to have very low bismuth contents and were used without further purification. Water was demineralized and then distilled twice, first from permanganate, and stored in polyethene bottles.

Stock solutions of 5×10^{-3} M bismuth chloride in 1 M HCl were diluted with 0.25 M HCl to prepare standard solutions with lower concentrations for use: the solutions were deaerated by bubbling nitrogen for 15 min. Metal solutions were transferred with Eppendorf micropipettes having disposable plastic tips.

Preparation of the graphite spray electrodes. Glassy carbon electrodes were cleaned before the graphite spray was applied, by polishing on metallographic paper (Carbinet 600, Buchler, Evanston, IL). A uniform layer of graphite particles was applied to the disc by spraying from a can of Kontakt Chemie Graphite 33 (Rastatt, Germany) available in electronic stores. The spray was applied in short (2 s) spurts from the can held at a distance of approximately 50 cm until complete coating of the disk and teflon ring surrounding it was observed. Then the outer edge of the electrode body was polished to give a graphite spray disk covering only the glassy carbon disk plus the teflon ring surrounding the disk. The total surface area (disk and teflon ring) of the electrode was 95.0 mm^2 (11-mm diameter). After each measurement, the electrode was cleaned and resprayed.

When carbon-paste electrodes were used, the carbon-paste surface was renewed, before the spraying, and before each run, by extruding a small portion of the paste from the electrode followed by polishing on a smooth paper surface.

In both cases, the coated electrodes were heated under ventilation for a short time in order to remove any traces of organic solvents.

Surface observation of the electrodes. Comparison of the physical properties of the carbon-paste electrode and the graphite spray electrodes was done by optical and scanning electron microscopy (s.e.m.). The s.e.m. observations were made without prior metallic vapor coating.

Results and discussion

Surface properties of the electrodes. Optical microscopy at different magnifications revealed very different granular textures of the carbon-paste and graphite spray electrodes (Fig. 1). With the carbon-paste electrode (Fig. 1a, b), the grain size is non-uniform and the shape is irregular; the grains are separated, with paraffin cementing them together. The surface of the carbon-paste electrode is also characterized by the presence of pits and channels between the grains, associated with the mosaic structure. In contrast, the graphite spray electrode (Fig. 1c) has much more finely divided and uniform, perhaps more amorphic, particles more evenly distributed. There is a notable absence of cavities or canyons between particles. The s.e.m. observations confirm these interpretations (Fig. 2).

Electrochemical properties of the graphite spray electrode. Table 1

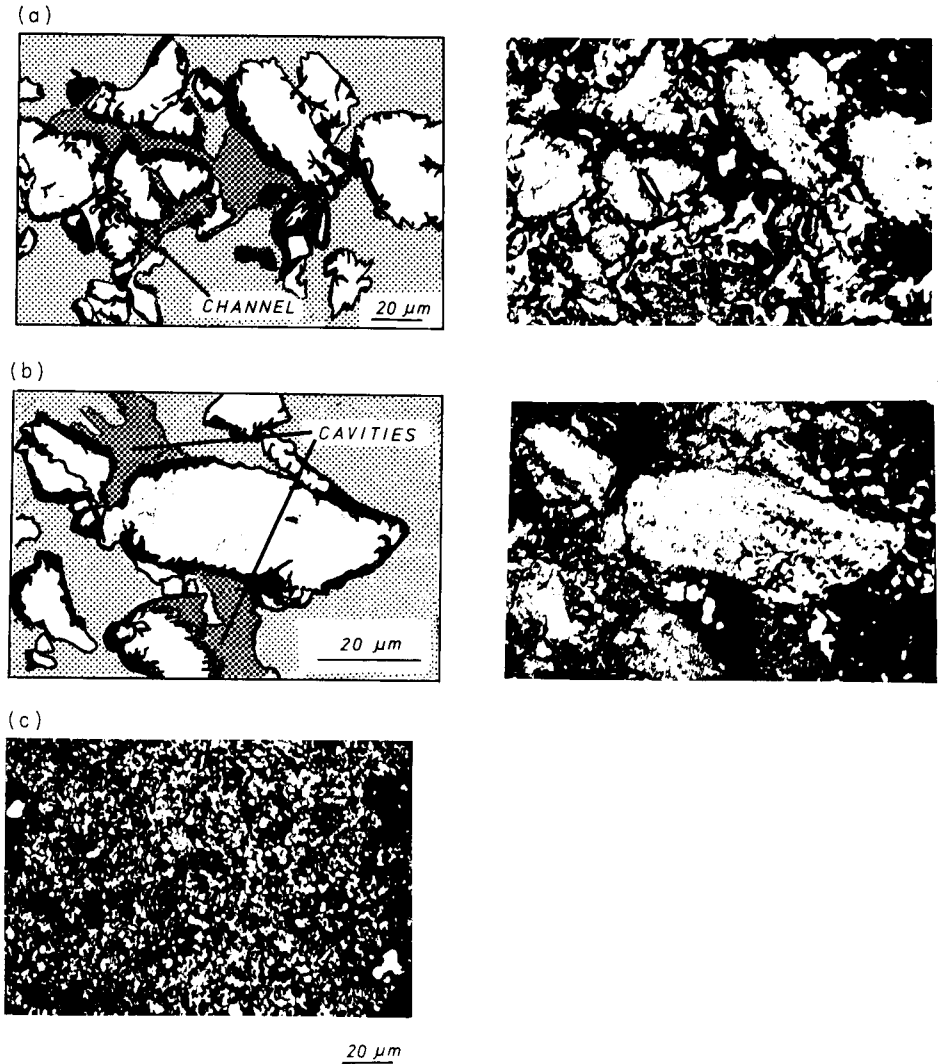

Fig. 1. Optical micrographs of the electrodes: (a) and (b) carbon-paste electrodes; (c) graphite spray electrode.

reports the cathodic and anodic potential limits observed in different media for the carbon-paste and graphite spray electrodes; a 1-μA deviation from the residual current was used as the cut-off limit under conventional voltammetric conditions.

Differential pulse anodic stripping voltammetry at the graphite-covered carbon-paste electrode was examined. Mercury film electrodes prepared in situ were employed, for which purpose various volumes of the 5×10^{-3} M mercury(II) chloride solution were added to 25 ml of test solution to obtain

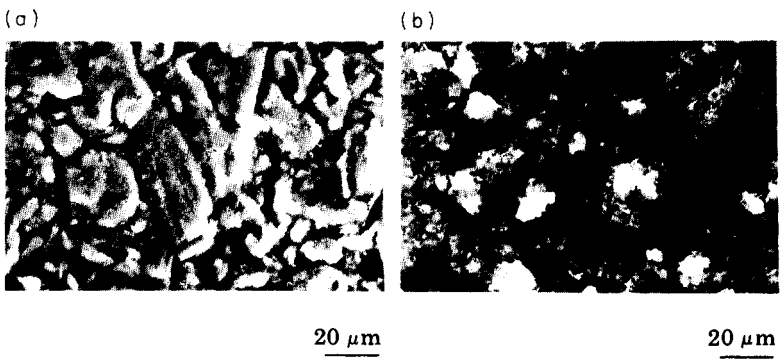

Fig. 2. Scanning electron micrographs: (a) carbon paste (350×); (b) graphite spray (350×).

TABLE 1

Potential limits for the carbon-paste and the graphite spray electrodes

Medium	Cathodic potential (V)		Anodic potential (V)	
	Carbon paste	Graphite spray	Carbon paste	Graphite spray
0.25 M HCl	−0.550	−0.250	+1.100	+0.850
1 M H_2SO_4	−0.450	−0.200	+1.250	+0.975
1 M H_2SO_4 + 0.1 M KCl	−0.520	−0.225	+1.200	+0.900
PO_4^{3-} buffer, pH 2.0	−0.425	−0.300	+1.250	+0.900
PO_4^{3-} buffer, pH 6.5	−0.650	−0.350	+1.200	+0.700

a 5×10^{-6}—2×10^{-4} M mercury(II) ion concentration. The tested ion was bismuth(III) in a 1 M sulfuric acid solution containing potassium chloride [4]; bismuth was chosen because it is toxicologically interesting and is known not to form intermetallic compounds with other metals [7, 8]. The presence of chloride is necessary in order to obtain high sensitivities for bismuth [8]. An electrodeposition potential of −0.300 V vs. SCE was employed for up to 20 min, with a waiting period of 30 s before the stripping scan was initiated. The stripping peak current observed at the graphite-covered electrode became independent of the mercury concentration at about 10^{-4} M mercury(II) and this concentration was employed in subsequent studies. Figure 3 shows the high reproducibility from run-to-run on seven freshly prepared graphite-covered carbon-paste surfaces in 1 M sulfuric acid solutions containing 0.1 M potassium chloride and 10^{-4} M mercury(II) chloride. The coefficient of variation was 2%; the carbon-paste electrode under the same conditions gave a coefficient of variation of 11%.

The peak current for 2×10^{-8} M bismuth at the graphite-covered electrode was a linear function of the electrodeposition time up to at least 15 min.

Differential pulse anodic stripping voltammetry at the graphite-covered

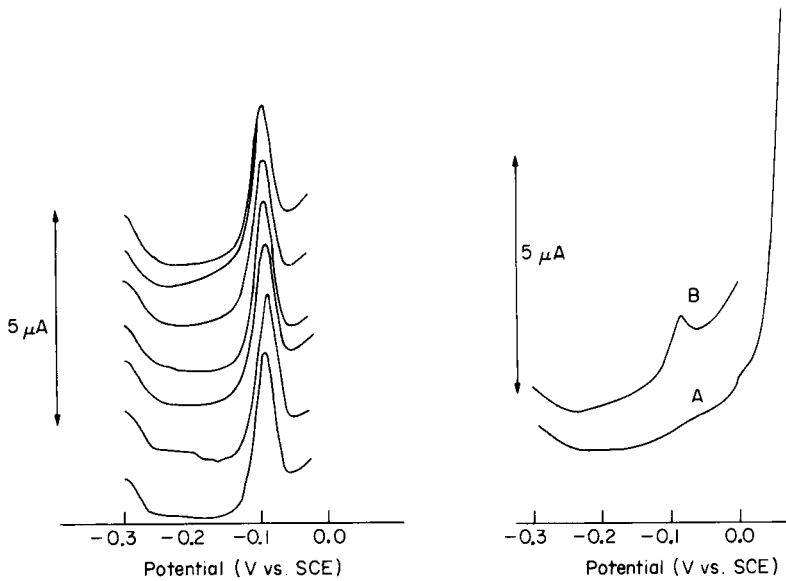

Fig. 3. Anodic stripping peaks of bismuth (2×10^{-8} M) on seven different graphite spray surfaces from 1 M H_2SO_4—0.1 M KCl, after deposition for 10 min. Scan rate 2 mV s^{-1}; measurements on first scan.

Fig. 4. Differential pulse stripping voltammetry of bismuth(III): (A) background current of the 1 M H_2SO_4—0.1 M KCl supporting electrolyte; (B) detection of 2×10^{-9} M bismuth(III) after deposition for 10 min.

glassy carbon electrode was also tested; the experimental conditions were the same as above. Seven determinations on fresh surfaces for the glassy carbon electrode and the graphite-covered glassy carbon electrode (scan rate 2 mV s^{-1}; rotation speed = 1,500 rpm; deposition time 10 min) gave coefficients of variation of 5% and 4%, respectively. The bismuth peak currents at the graphite-covered glassy carbon electrode were proportional to the square root of the rotation speed up to 3500 rpm. A linear calibration graph was obtained for 10^{-8}—10^{-7} M bismuth. The dependence of the bismuth peak current on the electrodeposition time was linear up to 15 min.

Figure 4 shows the peak current observed with the carbon-paste graphite-covered electrode for a bismuth solution. The detection limits for the different electrodes used in this study, with 10-min deposition times, are reported in Table 2. Further experimental data on copper, selenium, cadmium, thallium, lead and zinc ions will be presented in a future publication.

This paper was presented in part at the Journées Européennes d'Electrochimie de la Société Chimique de France et de Belgique, Brussels, June, 1981. Thanks are expressed to the Fonds National de la Recherche Scientifique, Belgium (G.-J.P.) and the National Institutes of Health (GM 22311-05)

TABLE 2

Limits of detection ($\mu g\ l^{-1}$) with 10-min deposition times

Carbon paste	Carbon-paste graphite covered	Glassy carbon	Glassy-carbon graphite covered
0.5	0.1	1	1

(G.D.C.) for support of this work, and Prof. Bouillon and Prof. Vereecken (V.U.B.) for use of their laboratory facilities.

REFERENCES

1 R. Adams, Electrochemistry at Solid Electrodes, M. Dekker, New York, 1969.
1 a W. E. van der Linden and J. W. Dieker, Anal. Chim. Acta, 119 (1980) 1.
2 See, e.g., G. J. Patriarche, J.-M. Kauffmann and G. D. Christian, Microtechniques in Drug Sciences, M. Dekker, New York, New York, 1982.
3 Adsorptive attachment and chemical bonding to electrodes, U.S.—France seminar, Bender, June, 1980.
4 J.-M. Kauffmann and G. J. Patriarche, Anal. Lett., 14 (1981) B15.
5 W. R. Matson, D. K. Roe and D. E. Carrit, Anal. Chem., 37 (1965) 1594.
6 W. R. Seitz, R. Jones, L. N. Klatt and W. D. Mason, Anal. Chem., 45 (1974) 840.
7 T. M. Florence, J. Electroanal. Chem., 49 (1974) 255.
8 G. Gillain, G. Duyckaerts and A. Disteche, Anal. Chim. Acta, 106 (1979) 23.

Analytica Chimica Acta, 135 (1982) 159—163
Elsevier Scientific Publishing Company, Amsterdam — Printed in The Netherlands

Short Communication

AMMONIUM ION SENSOR BASED ON IMMOBILIZED NITRIFYING BACTERIA AND A CATION-EXCHANGE MEMBRANE

TADASHI OKADA, ISAO KARUBE* and SCHUICHI SUZUKI

Research Laboratory of Resources Utilization, Tokyo Institute of Technology, Nagatsuta-cho, Midori-ku, Yokohama 227 (Japan)

(Received 1st July 1981)

Summary. The ammonium ion sensor is based on nitrifying bacteria isolated from activated sludge. The sensor comprises a cation-exchange membrane, an alkaline solution layer (pH 10), a gas-permeable membrane, an immobilized microbial membrane, and an oxygen electrode. This novel combination provides accurate amperometric determinations of ammonium ions in aqueous solutions within 7 min in the range 10^{-4}—4.5×10^{-2} M. Volatile amines or other ions do not interfere. The relative error is within 4% and the sensor can be used continually for more than 10 days.

Ammonium ions are usually determined spectrophotometrically, but the procedures are sometimes quite complicated. Recently, several new ammonium ion electrodes of reasonable selectivity have been developed, based on potentiometric ammonia determination [1, 2]. Also techniques for immobilization of living micro-organisms have been developed for the determination of alcohols [3], microbial populations [4], glutamic acid [5], glutamine [6], and for preliminary screening of mutagens [7].

A microbial amperometric electrode for ammonia gas has been developed by the authors [8, 9]. It consists of a gas-permeable membrane, immobilized nitrifying bacteria and an oxygen electrode. Nitrifying bacteria utilize ammonia as their sole source of energy, and oxygen is consumed. The selectivity of this electrode is satisfactory. However, the pH of the sample solution has to be kept sufficiently above the pK value for ammonia (9.1 at 30°C) because ammonium ions cannot pass through the gas-permeable membrane. In this communication, an improved ammonium ion sensor is described and applied to the determination of ammonium ions in urine.

Experimental

The materials used, including the micro-organism culture, and the immobilization of the bacteria were as described previously [9].

Assembly of the microbial electrode. A diagram of the microbial electrode assembly is shown in Fig. 1. The basic electrode was constructed as described previously [9]. An alkaline solution layer (glycine—NaCl—NaOH, pH 10) and a cation-exchange membrane (Asahi Glass Co., Selemion Type CMV) were fixed onto the electrode, as shown in Fig. 1. Thus the bacteria were

0003-2670/82/0000-0000/$02.75

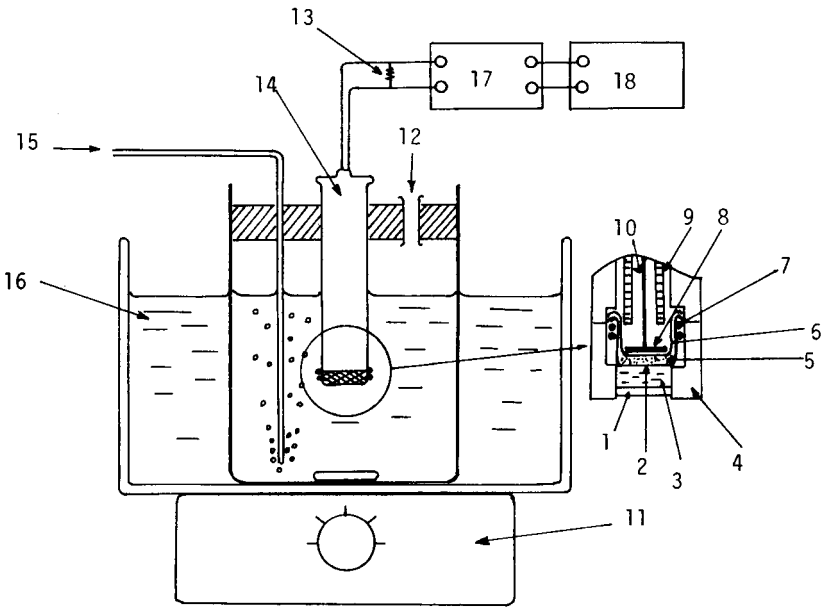

Fig. 1. The microbial sensor system for ammonium ions: (1) cation-exchange membrane (diameter 20 mm, thickness 0.11 mm); (2) gas-permeable teflon membrane (diameter 35 mm, thickness 0.15 mm, pore size 0.45 μm); (3) alkaline solution layer (pH 10) (diameter 18 mm, thickness 1.0 mm); (4) holder; (5) immobilized bacterial layer (diameter, 8 mm, thickness 0.25 mm); (6) teflon membrane; (7) rubber O-rings; (8) cathode (Pt); (9) anode (Pb); (10) electrolyte (30% KOH); (11) magnetic stirrer; (12) sample solution inlet; (13) resistance (2 kΩ); (14) oxygen electrode; (15) air; (16) water bath; (17) amplifier; (18) recorder.

immobilized between the two porous membranes (teflon membrane and acetylcellulose membrane). The procedure for use was as described earlier [9].

Results

Principle of ammonium ion determination. When the microbial electrode was inserted into a sample solution, ammonium ions passed through the cation-exchange membrane, and were converted to ammonia in the alkaline layer. The ammonia passed through the gas-permeable membrane and was utilized by the nitrifying bacteria. Oxygen was thus consumed by the respiration of the bacteria, and was determined by the oxygen electrode. The concentration of the ammonium ions was proportional to the decrease in current from the oxygen electrode.

Response of the sensor. Figure 2 shows typical current—time responses of the microbial sensor after addition of ammonium ions. Previously a steady output current had been obtained, corresponding to the endogeneous respiration activity of the immobilized bacteria in pH 8 (glycine—NaCl—NaOH) buffer. In the presence of ammonium ions, the current decreased because of

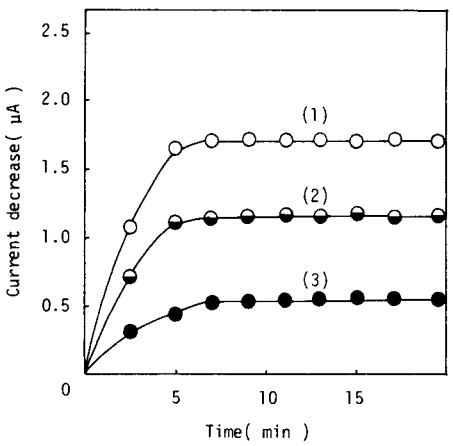

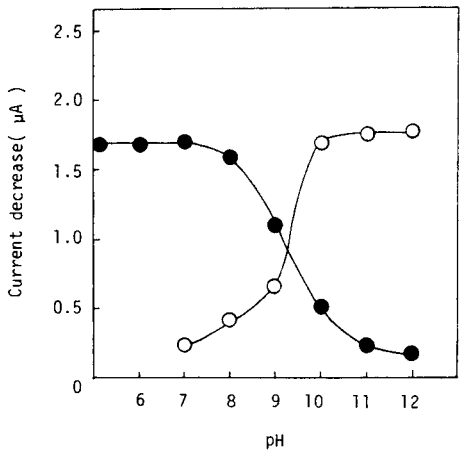

Fig. 2. Current—time responses of the microbial sensor. At zero time, the sample solution was injected into the buffer solution (pH 7.0) to give concentrations of (1) 30; (2) 20; (3) 10 mM ammonium chloride (30°C; wet cell content, 0.96 mg mm^{-3}).

Fig. 3. Effect of the pH of the sample solution and the alkaline solution on the current decrease. Conditions as in Fig. 2 except for pH of (•) buffer solution; (○) alkaline bed. Final concentration was 30 mM NH_4Cl.

oxygen consumption by the bacteria, and became steady within 7 min. This steady-state current was proportional to the concentration of the ammonium ions. When the sensor was placed in tap water, the current returned to its initial level within 2 min. Thus the total time required for determination was 9 min.

Inhibition of nitrifying bacteria with nitrite formed by the micro-organisms was not observed during the experiments. Therefore, the nitrifying bacteria isolated from activated sludges could be used for determining ammonium ion. The response to ammonium ions did not change with the harvesting time of the bacteria.

The maximum current decrease was linearly dependent on the ammonium chloride concentration in the range 5 mg—2.4 g l^{-1}. When a sample solution containing 1.6 g l^{-1} of ammonium chloride was analyzed 20 times the standard deviation was 55 mg l^{-1}.

Effect of pH. Figure 3 shows that the current decrease increased as the pH decreased, and reached a maximum at pH 7.0. This is because ammonium ions change to ammonia in alkaline conditions, and ammonia cannot permeate through the cation-exchange membrane. Sample solutions at pH 7.0 were employed for further work.

Figure 3 also shows the effect of the pH of the alkaline layer. The response increased as the pH of the layer was increased, reaching a maximum at pH 10. Under these conditions, most of the ammonium ions are changed to ammonia, which easily permeates through the gas-permeable membrane. However, the

stability of the sensor was decreased above pH 11. Therefore, the internal solution was kept at pH 10 in further experiments.

Microbial cell content. The number of bacteria immobilized on the membrane affects the output current. Figure 4 shows the effect of cell concentration on the current decrease. The response was greatest for bacteria contents of 1 mg mm^{-3} and this level was therefore employed in further work.

Selectivity. The sensor did not respond to metal ions (K^+, Mg^{2+}, Ca^{2+}, Mn^{2+}, Fe^{2+}, Co^{2+}, Cu^{2+}, Ni^{2+}), volatile nutrients such as acetic acid ethanol, and involatile nutrients such as glucose and glutamic acid. Conventional ammonia electrodes respond to volatile amines (such as diethylamine, propylamine and butylamine), but the microbial sensor was unaffected, because the amines were not assimilated by immobilized bacteria.

Application and stability. The sensor was applied to the determination of ammonium ions in human urine (pH 6.7—7.0). The urine was diluted (1:50) with the glycine—NaCl—NaOH buffer. The ammonium ion concentration was also determined spectrophotometrically by the Japanese Industrial Standard method based on indophenol blue [10]. Good agreement was obtained between the two procedures (correlation coefficient 0.99).

The long-term stability of the sensor was examined with a sample solution containing ammonium chloride (1.6 g l^{-1}). The current was almost constant for more than 10 days and 200 assays.

Discussion

A number of bacteria can use inorganic compounds as a source of energy for autotrophic growth. A microbial sensor consisting of immobilized *Nitrosomonas europeae* and oxygen electrodes has been constructed for the determination of ammonia [8]. However, its stability was poor, possibly

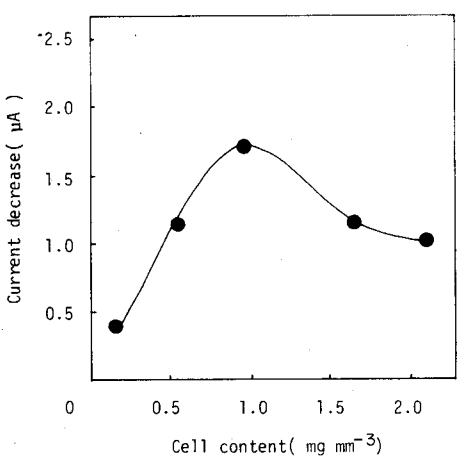

Fig. 4. Effect of cell concentration on the current decrease. Conditions as in Fig. 2 except for the cell content.

because of the inactivation of bacteria with the nitrite formed. Stable nitrifying bacteria were required for the microbial sensor. The nitrifying bacteria isolated from activated sludges were therefore cultured and employed. Inactivation of bacteria with nitrite formed was not observed. Previous work has shown that such a microbial sensor very gradually responded to nutrients such as glucose and acetic acid [8]. This was caused by the growth of contaminated bacteria in the membrane. The construction of the microbial sensor now proposed seems promising and attractive for amperometric determinations of ammonium ion.

REFERENCES

1 P. L. Bailey, Analysis with Ion-Selective Electrodes, Heyden, London, 1978, Chap. 7.
2 M. E. Meyerhoff, Anal. Chem., 52 (1980) 1532, 2383.
3 M. Hikuma, T. Kubo, T. Yasuda, I. Karube and S. Suzuki, Biotechnol. Bioeng., 21 (1979) 1845.
4 T. Matsunaga, I. Karube and S. Suzuki, Appl. Environ. Microbiol., 37 (1979) 117.
5 M. Hikuma, H. Obana, T. Yasuda, I. Karube and S. Suzuki, Anal. Chim. Acta, 116 (1980) 61.
6 M. A. Arnord and G. A. Rechnitz, Anal. Chem., 52 (1980) 1170.
7 I. Karube, T. Matsunaga, T. Nakahara and S. Suzuki, Anal. Chem., 53 (1981) 1026.
8 M. Hikuma, T. Kubo, T. Yasuda, I. Karube and S. Suzuki, Anal. Chem., 52 (1980) 1020.
9 I. Karube, T. Okada and S. Suzuki, Anal. Chem., 53 (1981) 53 (1981) 1852.
10 M. Tabara, Testing Methods for Ammonium Ion (JIS K 0101), Japanese Industrial Standard Committee, Tokyo, 1979, pp. 116—122.

Analytica Chimica Acta, 135 (1982) 165—168
Elsevier Scientific Publishing Company, Amsterdam — Printed in The Netherlands

Short Communication

A SIMPLE SALT-ENHANCED SURFACE-TENSION TECHNIQUE FOR DETECTION OF TRACE SURFACTANTS IN WATER

D. W. ARMSTRONG,* F. LAFRANCHISE and D. YOUNG
Department of Chemistry, Georgetown University, Washington, DC 20057 (U.S.A.)
(Received 30th July 1981)

Summary. A simple, relatively inexpensive DuNoy tensiometer can be used to detect small amounts of surfactants in water (at the $\mu g\ l^{-1}$ level in many cases). The surfactant must be salted-out to produce the desired effect. Addition of salt to pure water produces a reproducible increase in surface tension, whereas addition of salt to a water sample containing traces of surfactant produces a distinct, reproducible decrease. For pure surfactant solutions, calibration curves can be constructed for quantitative work.

The detection and/or quantitation of surfactants in aqueous solution is an important and in some cases difficult analytical problems. Several methods can be used in analyses for specific classes of surfactants, including spectrophotometric [1—6], titrimetric [7, 8], atomic absorption spectrometric [9, 10], ion-selective electrode [11, 12], and other [13] techniques. These methods are frequently selective for certain types of hydrophilic head groups (e.g., complexation of sulfonate and/or sulfate functional groups by methylene blue). While these techniques may have adequate sensitivity and accuracy for dealing with relatively pure solutions containing a single surfactant component, they often suffer shortcomings in the analysis of more complicated and/or dilute samples. For example, in environmental samples, the total surfactant concentration may be at the $mg\ l^{-1}$ level (or less); however, the concentration of any single surfactant (or surfactant type) would be much lower. There is also the well known "neutralization effect" when cationic and anionic surfactants are present in the same solution [14]. Furthermore, both commercial and naturally occurring surfactants are usually mixtures of isomeric and homologous compounds. To analyze such complex mixtures properly, chromatographic separation is often employed [13—20]. The task of analyzing a water sample which contains very low levels of several different classes of surfactants and hundreds of different individual compounds (most of which are nonvolatile without derivatization) can be expensive and time-consuming. Alternatives to exhaustive chromatographic separations of surfactant-containing samples include other physicochemical techniques [21], which do not distinguish between different types of surfactants but provide information concerning the total surfactant load in a sample. The presence of surfactants can often be detected down to the $\mu g\ l^{-1}$ level. These techniques

0003-2670/82/0000-0000/$02.75

are rapid, inexpensive, and can also be used to obtain quantitative results if well defined solutions are concerned.

In this work a simple, rapid, and economical surface-tension technique is described for the detection of aqueous trace surfactant contaminants. This method utilizes salt effects to enhance the surface activity of surfactants in dilute solutions. Most surface or interfacial tension measuring devices can be used.

Experimental

Materials. Sodium dodecylsulfate (SDS; electrophoresis purity, BioRad) was recrystallized from high-purity ethanol. Triton X-100 (BioRad) was used as received. Cetyltrimethylammonium chloride (CTACl; Sigma) and cetylpyridinium chloride (CPCl; Sigma) were recrystallized three times each from ethanol. Sodium laurate (NaL) and dodecylbenzene sulfonate (DBS), both from Pfaltz & Bauer, were recrystallized three times from ethanol. Igepol CO-630 (GAF) and Polyfon-H (Westvãco) were used as received. Triton X-100 and Igepol CO-630 are nonionic surfactants with polyoxyethylene head groups. Polyfon-H is a lignosulfonate which is often produced in paper pulping operations. All solid surfactants were dried in vacuum over P_2O_5 before use. Anhydrous sodium chloride and sodium sulfate (Baker) were extracted with diethyl ether for 48 h (with a Soxhlet apparatus) to insure that they were surfactant-free; unpurified salts often gave anomalous results. Acetone, methanol, and benzene (Baker) were fractionally distilled in clean surfactant-free apparatus.

Methods. All glassware must be surfactant-free. Soaking in hot chromic acid for 24 h and rinsing with pure water is often necessary to insure the absence of surface-active agents. Cleaned glassware should not be dried with paper towels or other similar materials; these were found often to contain traces of surface-active agents. These traces of surfactant are easily detected and thus interfere with the enhanced surface-tension measurements.

A typical experiment which demonstrates the decrease in surface tension with increasing ionic strength (in an aqueous surfactant solution) is as follows. A portion (5 ml) of 100 $\mu g\ l^{-1}$ (ppb) Igepal CO-630 solution was pipetted into a clean watch glass. The uncorrected surface tension of this solution was measured at 21°C with a Fisher Model 20 Surface Tensiometer. Several 0.020-ml increments of surfactant-free 4.0 M NaCl were then added to the solution and the uncorrected surface tension was recorded each time after a wait of several minutes for the system to equilibrate. For some solutions of very low surfactant concentration, it took as much as 60 min for a reading to stabilize. In this type of experiment, lower surface tension readings are obtained after addition of salt. If there is no surfactant present in the sample, an increase in the surface tension reading is observed upon addition of salt.

Data for a typical standard curve of surface tension versus surfactant concentration were obtained as follows. A stock solution of 100 mg l^{-1} CPCl was prepared. Standards of lower concentration were prepared by dilution of this solution in Grade A volumetric glassware. A stock solution of 0.08 M

NaCl was prepared and 5 ml of the NaCl solution was mixed with 5 ml of each of the surfactant standards. The surface tension was measured as reported above.

To avoid diluting aqueous samples, a pre-measured quantity of salt can be added directly to a known volume of sample. In testing for the presence of surfactant in purified water, fresh-water environmental samples, or pulp mill effluent, it was found that the addition of solid salt or injection of a small amount of a concentrated solution was the most efficient and sensitive procedure. By comparing the change in the sample surface tension with that of a nonsurfactant-containing blank, the presence or absence of surfactants can be detected down to 1 $\mu g\ l^{-1}$ in some cases.

Results and discussion

Figure 1 illustrates the salt effect on the surface tension of a surfactant-free aqueous solution and solutions containing trace amounts of surfactant. It is well-known that the addition of salt to water causes modest increases in the surface tension as a result of the electrostriction of water around the salt ions [22]. However, the addition of a trace amount of virtually any surface-active agent will mask the usual electrostriction effect at the air—water interface. Instead, a dramatic lowering of the surface tension is observed because of the increased concentration of surfactant at the air—water interface (Fig. 1). Small amounts of most common organic solvents did not interfere with the detection of surfactants by this technique. For example, aqueous solutions saturated with benzene or containing 25 mg l^{-1} methanol or acetone all gave increased surface tension readings with added salt.

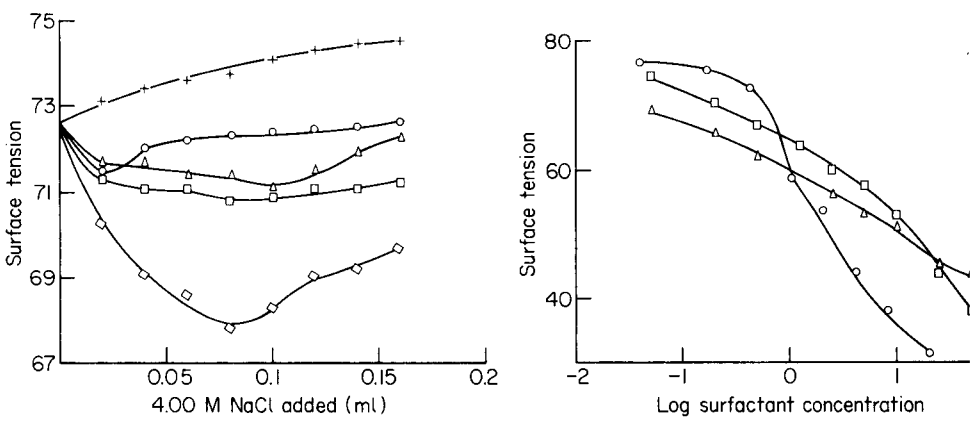

Fig. 1. Plots of the variation in surface tension (given in dyne cm^{-1}) of different aqueous solutions as a function of added salt. All surface tension values are uncorrected and normalized (at zero salt concentration) to 72.6 dyne cm^{-1}. (+) Pure water; (○) 0.5 mg l^{-1} CTACl; (△) 50 $\mu g\ l^{-1}$ Igepol CO-630; (□) 1.0 mg l^{-1} NaL; (◇) 50 mg l^{-1} Polyfon H (lignosulfonate).

Fig. 2. Calibration curves (21° C) of salt-enhanced surface tension (dyne cm^{-1}) versus surfactant concentration (mg l^{-1}): (○) SDS, [NaCl] = 1.75 M; (□) Triton X-100, [NaCl] = 0.08 M; (△) CPCl, [NaCl] = 0.04 M.

This technique can be used to quantify surfactants in single-component or well characterized multi-component solutions. Calibration curves of surface tensions versus surfactant concentrations (at constant ionic strength) are illustrated in Fig. 2. A range of over three orders of magnitude of surfactant concentrations (from about 10 $\mu g\ l^{-1}$ to 100 $mg\ l^{-1}$) is covered. The shape of the calibration curve depends on the surfactant standard used, the temperature, and the nature and concentration of the salt used to increase the ionic strength of the solution. Surface tension readings are precise and accurate to within ± 0.1 dyne cm^{-1} provided that experimental conditions such as temperature and sample size are kept constant.

It was found that the salt-enhanced surface tension technique is useful for monitoring surfactant content in pulp mill effluents and treated sewage effluents. Furthermore, surfactants have been detected via this technique (in rivers, lakes, groundwater, and "pure" laboratory water) which were undetectable by traditional spectroscopic, titrimetric, electrode, and chromatographic techniques.

Acknowledgement is made to the donors of the Petroleum Research Fund (American Chemical Society) and the Research Corporation for support of this research.

REFERENCES

1 L. K. Wang and D. F. Langley, N. Engl. Water Works Assoc., 89 (1975) 301.
2 L. K. Wang and R. G. Ross, Int. J. Environ. Anal. Chem., 4 (1976) 285.
3 S. L. Boyer, K. F. Guin, R. M. Kelley, M. L. Mausner, H. F. Robinson, T. M. Schmitt, C. R. Stahl and E. A. Setzkorn, Environ. Sci. Technol., 11 (1977) 1167.
4 L. K. Wang and D. F. Langley, Arch. Environ. Contam. Toxicol., 5 (1977) 447.
5 K. Higuchi, Y. Shimoishi, H. Miyata, K. Tôei and T. Yayami, Analyst, 105 (1980) 768.
6 Y. Ambe and T. Hanya, Bunseki Kagaku, 21 (1972) 252.
7 L. K. Wang, J. Am. Oil Chem. Soc., 52 (1975) 339.
8 K. Vytras, M. Dajkova and V. Mach, Anal. Chim. Acta, 127 (1981) 165 (and references therein).
9 P. T. Crisp, J. M. Eckert, N. A. Gibson, G. F. Kirkbright and T. S. West, Anal. Chim. Acta, 87 (1976) 97.
10 A. Lebiham and J. Courtot-Coupey, Anal. Lett., 10 (1977) 759.
11 B. J. Kirch and D. E. Clarke, Anal. Chim. Acta, 67 (1973) 387.
12 H. M. Rendall, J. Chem. Soc. Faraday Trans., 72 (1976) 481.
13 R. A. Llenado and R. A. Jamieson, Anal. Chem., 53 (1981) 174 R (and references therein).
14 L. K. Wang and D. F. Langley, N. Engl. Water Works Assoc., 90 (1976) 354.
15 R. D. Swisher, J. Am. Oil Chem. Soc., 43 (1966) 137.
16 W. T. Sullivan and R. D. Swisher, Environ. Sci. Technol., 3 (1969) 481.
17 F. H. M. Nestler and D. F. Zinkel, Anal. Chem., 39 (1967) 1118.
18 J. F. K. Huber, F. F. M. Kolder and J. M. Miller, Anal. Chem., 44 (1972) 105.
19 A. Nakae and K. Kunihira, J. Chromatogr., 152 (1978) 137.
20 A. Nakae, K. Tsuji and M. Yamanaka, Anal. Chem., 52 (1980) 2275.
21 R. Cini, A. Ficalbi and G. Loglio, Mikrochim. Acta, (1974) 203.
22 J. J. Bikerman, Surface Chemistry, Theory and Applications, Academic Press, New York, 1958.

Analytica Chimica Acta, 135 (1982) 169—172
Elsevier Scientific Publishing Company, Amsterdam — Printed in The Netherlands

Short Communication

DETERMINATION OF BORON IN GEOLOGICAL MATERIALS BY INDUCTIVELY-COUPLED PLASMA EMISSION SPECTROMETRY

JAMES W. OWENS[a], ERNEST S. GLADNEY* and DARYL KNAB

University of California, Los Alamos National Laboratory, P.O. Box 1663, MS 490, Los Alamos, NM 87545 (U.S.A.)

(Received 27th July 1981)

Summary. Determination of boron in international silicate reference materials with an argon plasma is demonstrated. Detection limits are about 5 ppm for rock samples.

Geochemical interest in boron centers around the complexing abilities of clay minerals and studies of paleoclimate and erosion [1—3]. Environmentally, boron is an important element in plant metabolism. The tolerance range between deficiency and toxicity is rather narrow [4, 5]. Boron is a major constituent of geothermal waters from power and steam production (6), and its discharge into environmentally-sensitive areas requires monitoring for toxic effects.

There are many methods for the determination of boron in environmental materials (soils, rocks, biological, and waters). Several of these have been reviewed [7]. Newer methods for boron in silicates have included emission spectroscopy with an inductively-coupled plasma (i.c.p.e.s.) [8—13]. Of these, only Nadkarni [13] presents any data on reference materials to demonstrate that the measurement is potentially quantitative (two determinations on NBS 1633 Fly Ash). The subject of this communication is to demonstrate the determination of boron in a variety of silicate reference materials at ppm levels using a sequential i.c.p. optical emission spectrometer.

Experimental

A Perkin-Elmer ICP/5000 inductively-coupled argon plasma atomic absorption spectrophotometer system with a Perkin-Elmer Model 10 data station including the Perkin-Elmer ICP multielement and graphics software packages, was used for all determinations. A Perkin-Elmer auto-sampler with peristaltic pump was used for sample introduction. Liquid argon provided the plasma torch gas supply. The plasma was operated at 1250 W and viewed at 15 mm above the load coil. Sample flow rates of 1.6 ml min^{-1} and signal integration times of 1.0 s were employed. The 249.8-nm emission line was found to have minimal interferences and was used exclusively. Background correction was done by observing regions 0.05 nm above and 0.15 nm below

[a]Present address: Green Country Orchards, P.O. Box 87, Colcord, OK 74338, U.S.A.

the 249.8 nm line. The ICP/5000 system is computer-controlled in the sequential mode, to focus on a small region of the emission spectrum (1.0 nm) rather than in a fixed multielement configuration, focusing on the full emission spectrum.

Sample preparation. Fifteen silicate reference materials from the U.S. National Bureau of Standards (NBS), U.S. Geological Survey (USGS), and the Canadian Certified Reference Materials Project (CCRMP) were selected for study. Several 100—400 mg aliquots of these materials were weighed into platinum crucibles, 1.0 g of analytical reagent-grade sodium carbonate was added, and the contents were mixed thoroughly. This mixture was carefully covered with 1.0 g of sodium carbonate and then fused first for 15 min at 850°C followed immediately by 15 min at 950°C. These melts were allowed to cool and then dissolved in hot water. These solutions were filtered to remove insoluble residue, neutralized with perchloric acid, and diluted to 100 ml with distilled, deionized water. The diluted melts were left overnight to allow removal of dissolved CO_2.

Working standards were prepared by dissolving 2.0 g of sodium carbonate in water, adding a known amount of high-purity boric acid, and neutralizing and aging as above. Fusion blanks and unfused sodium carbonate blanks were also prepared.

TABLE 1

Boron concentrations in silicate reference materials determined by inductively-coupled argon plasma emission spectrometry

Reference material	Concentration (ppm)		Ratio (i.c.p./lit.)
	I.c.p.e.s.	Literature	
NBS 610 glass	368 ± 12 (3)[a]	351 [14]	1.05
NBS 612 glass	40 ± 4 (3)	32 [14]	1.25
NBS 1633 Fly Ash	450 ± 20 (3)	480 ± 40 [15]	0.94
NBS 1633A Fly Ash	39 ± 1 (6)	39.2 [16]	1.00
USGS BHVO-1	<5	2.3 ± 0.2 [17]	—
USGS BIR-1	<5	0.24 ± 0.08 [18]	—
USGS DNC-1	<5	1.0 ± 0.2 [18]	—
USGS GXR-2	40 ± 4 (6)	44 ± 1 [19]	0.91
USGS GXR-3	207 ± 5 (3)	180 ± 20 [19]	1.15
USGS GXR-5	24 ± 4 (6)	25 ± 2 [19]	0.96
USGS GXR-6	9.8 ± 1.8 (6)	11 ± 1 [19]	0.89
USGS MAG-1	138 ± 12 (3)	138 ± 15 [17]	1.00
USGS QLO-1	36 ± 2 (3)	38 ± 4 [17]	0.95
USGS RGM-1	26 ± 2 (3)	29 ± 2 [17]	0.90
CCRMP SO-3	21 ± 1 (5)	22 ± 7 [20]	0.95
CCRMP SO-4	41 ± 3 (12)	43 ± 10 [20]	0.95
CCRMP SY-2	87 ± 14 (3)	86 [21]	1.01
CCRMP SY-3	110 ± 10 (3)	100 [21]	1.10
Overall mean ratio ± one standard deviation			1.00 ± 0.10

[a]Numbers in parentheses are number of determinations included in mean.

Results and discussion

The results for boron determinations in silicate reference materials are given in Table 1. The best available boron concentration values for most of these silicates were selected from literature compilations. These represent a "consensus" approach to recommended concentration values and are subject to a number of uncertainties, especially because of the limited number of available boron measurements in silicates. The data on NBS SRM glasses are uncertified NBS values. Some evidence for boron inhomogeneity in these SRMs has been reported [7]. Data in Table 1 represent the mean ± one standard deviation among the number of measurements indicated in the table. The ratios of the means to the best available boron concentration data are shown. The overall mean of these 15 ratios is 1.00 with a standard deviation of 0.10. This demonstrates the overall accuracy of the i.c.p. procedure, despite the 10% relative standard deviation.

The solution detection limit is similar to the 5 ppb reported by Nadkarni [13] which translates to approximately 1.2 ppm detection limit in the original rock. This value was not approached in this work for two reasons. The boron blank in the sodium carbonate ranged from 5 to 15 ppm depending upon the manufacturer and it has not been possible to purify this material effectively. Secondly, the instrument has shown severe calibration drift, necessitating restandardization at least every five samples. More frequent standardization would improve the overall precision, but is impractical for routine laboratory use.

REFERENCES

1 F. J. Dervis, A. A. Levinson and P. Bayliss, Geochim. Cosmochim. Acta, 36 (1972) 1359.
2 O. Brockamp, Geochim. Cosmochim. Acta, 37 (1973) 1339.
3 M. M. Ashry, Geochim. Cosmochim. Acta, 37 (1973) 2449.
4 S. C. Allen, H. M. Grunshaw, J. A. Parkmoon and C. Quarmby, Chemical Analysis of Ecological Materials, 1974, J. Wiley, New York, pp. 127.
5 F. T. Bingham, Trace Elements in the Environment, 1973, American Chemical Society, Washington, DC, pp. 130.
6 A. J. Ellis and W. A. J. Mahon, Chemistry and Geothermal Systems, 1977, Academic Press, New York.
7 E. S. Gladney, E. T. Jurney and D. B. Curtis, Anal. Chem., 48 (1976) 2139.
8 M. A. Floyd, V. A. Fassel and A. P. D'Silva, Anal. Chem., 52 (1980) 2168.
9 N. R. McQuaker, P. D. Knuckner and G. N. Chang, Anal. Chem., 51 (1979) 888.
10 G. F. Kirkbright and R. D. Snook, Anal. Chem., 51 (1979) 1938.
11 A. Montaser and J. Mortazavi, Anal. Chem., 52 (1980) 255.
12 M. A. Floyd, V. A. Fassel, R. W. Winge, J. M. Katzenberger and A. P. D'Silva, Anal. Chem., 52 (1980) 431.
13 R. A. Nadkarni, Anal. Chem., 52 (1980) 929.
14 Office of Standard Reference Materials, NBS, Certificates of Analysis, SRM 610 and 612, 1972.
15 E. S. Gladney, Anal. Chim. Acta, 118 (1980) 385.
16 M. P. Failey, D. L. Anderson, W. H. Zoller, G. E. Gordon and R. M. Linstrom, Anal. Chem., 51 (1979) 2209.

17 E. S. Gladney and W. E. Goode, Geostandards Newsl., 5 (1981) 31.
18 M. P. Failey, Ph.D. Dissertation, Dept. of Chemistry, University of Maryland, MD, 1979, p. 238.
19 E. S. Gladney, D. R. Perrin, J. W. Owens and D. Knab, Anal. Chem., 51 (1979) 1557.
20 W. S. Bowman, G. H. Faye, R. Sutarno, J. A. McKeague and H. Kodama, Geostandards Newsl., 3 (1979) 109.
21 S. Abbey, Reference Materials, Rock Samples SY-2, SY-3, and MRG-1, Canadian Centre for Mineral and Energy Technology Report 79-35, 1979.

Analytica Chimica Acta, 135 (1982) 173—178
Elsevier Scientific Publishing Company, Amsterdam — Printed in The Netherlands

Short Communication

SPECTROPHOTOMETRIC STUDY OF THE MOLYBDENUM(VI) CHELATE OF FLAVON-3-OL-2'-SULFONIC ACID IN STRONG ACID SOLUTIONS

KATSUMI YAMAMOTO, JUNKO HARA and KOUSABURO OHASHI*
Department of Chemistry, Faculty of Science, Ibaraki University, Mito 310 (Japan)
(Received 3rd December 1980)

Summary. Molybdenum(VI) reacts with flavon-3-ol-2'-sulfonic acid (HL) in strong acid solutions to form a 1:1 chelate which has a stability constant (log K) of 3.04 at 25°C and ionic strength (I) of 1.0. Beer's law is obeyed in the range 0.69—8.20 μg Mo ml^{-1} in 0.3 M perchloric acid; the molar absorptivity at 370 nm is 1.4×10^4 l mol^{-1} cm^{-1}.

Reactions of molybdenum(VI) with chelating reagents have often been studied but the chemical species of molybdenum(VI) that participate in the complex formation have rarely been considered. Species of molybdenum(VI) in strong acid and alkaline solutions have been investigated in detail; at pH >7, molybdenum(VI) is present as tetrahedral MoO_4^{2-} [1] and the addition of acid yields the protonated species $HMoO_4^-$ and H_2MoO_4 followed by polymeric species [2]. Monomer—dimer equilibrium constants were determined spectrophotometrically by Krumenacker [3] and Ojo et al. [4].

In the work described here, the reaction of molybdenum(VI) with water soluble sodium flavon-3-ol-2'-sulfonate, which has two functional groups available for complex formation, was studied in aqueous solution, full consideration being given to the molybdenum(VI) species involved. This reaction was applied to the spectrophotometric determination of molybdenum(VI).

The related reagents quercetin [5] and morin [6] have also been used for sensitive spectrophotometric determinations of molybdenum(VI) but the color must be developed in an organic medium, otherwise solvent extraction is required because the reagents and molybdenum(VI) complexes are not water-soluble.

Experimental

Reagents and apparatus. A 0.100 M molybdenum(VI) solution was prepared by dissolving 24.196 g of sodium molybdate dihydrate (Merck) in 1 l of sodium hydroxide solution (pH 9).

Sodium flavon-3-ol-2'-sulfonate was synthesized by a method similar to that of Oka et al. [7]. Sodium *o*-benzaldehyde sulfonate (21.0 g) in 60 ml of 50% (v/v) methanol and 12.4 ml of 0.1 M *o*-oxyacetophenone were added to 30 g of 50% (w/w) sodium hydroxide solution, and the solution

0003-2670/82/0000-0000/$02.75

was heated for 3 h at 50—60°C with stirring. The solution gradually turned red, and orange crystals precipitated. These were filtered off and a little ethanol was added to the filtrate, followed by acetic acid in small portions to neutralize the solution. The yellow crystals obtained were recrystallized twice from hot water, and dried in air. A 22.0-g sample of this intermediate in 400 ml of water was added to 4.1 g of sodium hydroxide in 33 ml of water, and 22 ml of 30% hydrogen peroxide was added dropwise, with ice-cooling. The solution was kept in a refrigerator for 3 days, and neutralized with 25 ml of 3 M HCl. Separate portions of the solution were evaporated under vacuum. The crystals obtained were washed three times with ethanol, and then recrystallized three times from hot water, followed by washing with ethanol and diethyl ether. [Elemental analysis: found 48.85 C, 2.9% H; calc. for $C_{15}H_9O_6NaS \cdot 1.5\ H_2O$ 49.05% C, 3.3% H.]

All other chemicals used were of analytical grade. Ionic strength was adjusted to 1.0 M with sodium perchlorate.

A Hitachi EPS-3 type spectrophotometer was used.

Procedure for the determination of the stability constant. In each experiment, portions of molybdenum(VI), flavon-3-ol-2′-sulfonic acid (in large excess) and perchloric acid solutions were pipetted into 25-ml volumetric flasks. The absorbance was measured in 1-cm cells at a given wavelength at 25°C.

Determination of molybdenum(VI). A 7-ml portion of 1.5 M perchloric acid, 5 ml of 2.00×10^{-2} M sodium flavon-3-ol-2′-sulfonate, and volumes of molybdenum(VI) solution containing 17—100 μg of molybdenum were pipetted with 25-ml volumetric flasks. After dilution to 25 ml with distilled water, the solution was allowed to stand at room temperature for 5 min. The absorbances were measured at 370 nm against a reagent blank.

Results and discussion

The chromogenic system obeys Beer's law over a range of 0.69—8.2 μg Mo ml^{-1}. Based on the molybdenum(VI) concentration, the apparent molar absorptivity at 370 nm in 0.30 M $HClO_4$ is 1.4×10^4 l mol^{-1} cm^{-1}. The relative standard deviation for the determination of 3.84 μg Mo ml^{-1} was 1.3% (n = 7) and for 1.92 μg Mo ml^{-1} was 1.6% (n = 8). The effect of other ions on the proposed procedure was examined for the determination of 3.0 μg ml^{-1} molybdenum(VI). Nickel, Co, Zn, Cd, Fe(III), Cr(III), Al, Ti(IV) and U(VI) (20 μg ml^{-1}) did not interfere, but the presence of an equimolar amount of Sn(IV), Zr(IV), Tl(III), T(IV) or V(V) interfered strongly.

Absorption spectra and complex formation. The change in the absorption spectrum of sodium flavon-3-ol-2′-sulfonate solution with pH is shown in Fig. 1; the isosbestic point is at 344 nm. The change in the absorption spectra may be ascribed to acid dissociation at the hydroxyl group rather than the sulfonic acid group. The acidity constant of the hydroxyl group of flavon-3-ol-2′-sulfonic acid is 5.01×10^{-9} M at 25°C and I = 1.0 M. In strongly acidic media, sodium flavon-3-ol-2′-sulfonate may exist in the uncharged

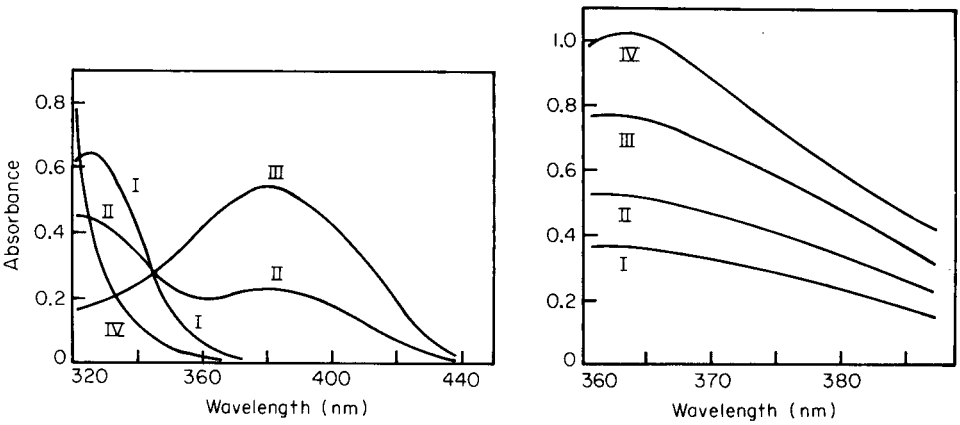

Fig. 1. Absorption spectra of 5.71×10^{-5} M sodium flavon-3-ol-2'-sulfonate at different pH values: (I) 0.30 M $HClO_4$; (II) pH 9.0; (III) pH 10.0; (IV) spectrum of 4.00×10^{-3} M molybdenum(VI) in 0.10 M $HClO_4$.

Fig. 2. Absorption spectra of 7.20×10^{-5} M molybdenum(VI) in 1.0 M $HClO_4$ at different sodium flavon-3-ol-2'-sulfonate concentrations: (I) 6.00×10^{-4} M; (II) 1.00×10^{-3} M; (III) 1.80×10^{-3} M; (IV) 4.00×10^{-3} M.

form. The absorption spectrum of 4.00×10^{-3} M molybdenum(VI) in 0.10 $HClO_4$ is also shown in Fig. 1.

Molybdenum(VI) exhibits a monomer—dimer equilibrium within the hydrogen-ion concentration range 0.2 to 3.0 M [4]. Therefore, complex formation between molybdenum(VI) and flavon-3-ol-2'-sulfonate was investigated in alkaline solution and in 0.3—1.0 M perchloric acid to eliminate complications caused by polymerization of molybdenum(VI). Above pH 7, complexation between molybdenum(VI) and flavon-3-ol-2'-sulfonate was not observed. The change in the absorption spectrum of 7.20×10^{-5} M molybdenum(VI) in 1.0 M $HClO_4$ on addition of sodium flavon-3-ol-2'-sulfonate solution is shown in Fig. 2. The absorbance increases with the increase in concentration of flavon-3-ol-2'-sulfonate. The color, after development, is stable at room temperature for at least 5 h under these experimental conditions.

The absorbance of the chelate decreases by about one third with increase in the concentration of perchloric acid from 0.30 to 1.0 M. The changes may be attributed to the hydrogen-ion dependence of the formation of the molybdenum(VI) chelate, and not to the dissociation of flavon-3-ol-2'-sulfonic acid.

The monomer—dimer equilibrium of molybdenum(VI) can be described as follows [4]

$$\begin{array}{ccc} 2\,HMoO_3^+ + H^+ & \xrightleftharpoons{K_1} & H_2Mo_2O_6^{2+} + H^+ \\ K_{MH} \Big\downarrow\Big\uparrow & & K_{DH} \Big\downarrow\Big\uparrow \\ H_2MoO_3^{2+} + HMoO_3^+ & \xrightleftharpoons{K_2} & H_3Mo_2O_6^{3+} \end{array}$$

The values of the equilibrium constants K_{DH}, K_{MH} and K_1 are 8 M^{-1}, 0.52 M^{-1}, and 55 M^{-1}, respectively, at 25°C and I = 1.0 M. Calculation of the concentrations of the various molybdenum(VI) species which exist in 0.3—1.0 M perchloric acid containing 7.20 × 10^{-5} M molybdenum(VI) indicates that most of the molybdenum(VI) exists as the monomer, $HMoO_3^+$. The decrease in absorbance with increasing acidity may be explained by considering the equilibrium between $HMoO_3^+$ and $H_2MoO_3^{2+}$. It seems probable that the $HMoO_3^+$ species forms the chelate; thus a decrease in the concentration of $HMoO_3^+$ will cause decreased absorbance. The mole ratio method indicated the formation of a moderately stable 1:1 molybdenum(VI)—flavon-3-ol-2′-sulfonate chelate in the strong acid medium.

Determination of the stability constant. As mentioned above, sodium flavon-3-ol-2′-sulfonate exists as the neutral form, HL, in strong acid medium. Therefore chelate formation with HL will occur through the reaction of $HMoO_3^+$ (or $H_3MoO_4^+$ [8])

$$H_3MoO_4^+ + HL \overset{K}{\rightleftharpoons} MoO_2(H_2O)_2(L)^+$$

where K is the stability constant. The equilibrium constant for protonation of monomeric molybdenum(VI) is $K_{MH} = [H_2MoO_3^{2+}]/[HMoO_3^+][H^+]$. The total concentration of molybdenum(VI) can be represented by

$$[Mo(VI)]_T = [HMoO_3^+] + [H_2MoO_3^{2+}] + [MoO_2(H_2O)_2(L)^+] = [HMoO_3^+](\alpha + K[HL])$$

where $\alpha = 1 + K_{MH}[H^+]$. The absorbance (A) at a given wavelength is given by

$$A = \epsilon_1[MoO_2(H_2O)_2(L)^+] + \epsilon_2[HL] + \epsilon_3[HMoO_3^+] + \epsilon_4[H_2MoO_3^{2+}]$$

where ϵ_1, ϵ_2, ϵ_3, and ϵ_4 are the molar absorptivities of the molybdenum(VI) chelate, flavon-3-ol-2′-sulfonic acid, $HMoO_3^+$ and $H_2MoO_3^{2+}$, respectively. Under the relevant experimental conditions, ϵ_3 and ϵ_4 are negligible compared to ϵ_1, thus A' (= $A - \epsilon_2[HL]$) is given by

$$A' = \epsilon_1 K[HMoO_3^+][HL] = [Mo(VI)]_T \epsilon_1 K[HL]/(\alpha + K[HL])$$

The apparent molar absorptivity can be represented by $\bar{\epsilon} = A'/[Mo(VI)]_T$. These two relationships for A', with appropriate manipulation, give the relationship $\bar{\epsilon}^{-1} = \epsilon_1^{-1} + \alpha([HL]\epsilon_1 K)^{-1}$.

Figure 3 shows plots of $\bar{\epsilon}^{-1}$ vs. $[HL]^{-1}$ for 7.20 × 10^{-5} M Mo(VI) and 1.0 M $HClO_4$. Values of ϵ_1^{-1} and $\alpha(K\epsilon_1)^{-1}$ can be determined from the intercept and slope, respectively. The relationship between αK^{-1} and $[H^+]$ is given by $\alpha K^{-1} = K^{-1} + K_{MH}[H^+]\,K^{-1}$. The plot of αK^{-1} and $[H^+]$ was found to be linear. The values of K and K_{MH}, determined graphically, were 1.1 × 10^3 and 0.99 M^{-1}, respectively, at 25°C and ionic strength 1.0 M. The value of K_{MH} is twice as great as that reported previously [8], possibly because of the different experimental conditions.

The reaction of 8-quinolinol (and its 5-sulphonic acid) with molybdenum(VI) in an alkaline medium provides an octahedral product in each case [9].

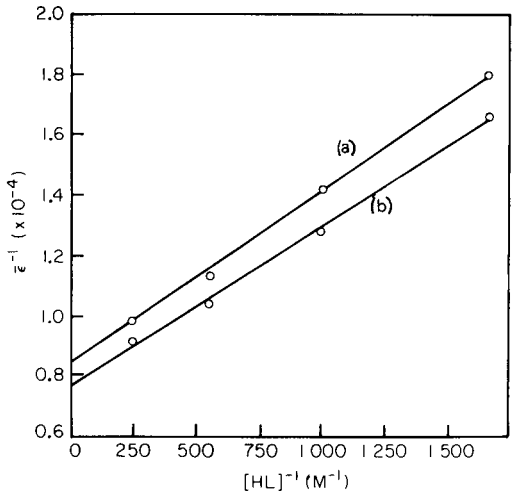

Fig. 3. Relation between $\bar{\epsilon}^{-1}$ and $[HL]^{-1}$ (duplicate runs). 7.20×10^{-5} M molybdenum(VI); 1.0 M $HClO_4$; I = 1.0 M; 25°C, 370 nm; (b) 375 nm.

As mentioned above, molybdenum(VI) is present as tetrahedral MoO_4^{2-} in alkaline solution, thus the transformation from tetrahedral to octahedral structure must take place during chelate formation. $HMoO_3^+$ (i.e. $H_3MoO_4^+$) may also have a tetrahedral structure.

When polymerization of $HMoO_4^-$ occurs, the coordination number of molybdenum(VI) may change from four to six [10]. Octahedral coordination of the central molybdenum(VI) in $HMoO_4^-$ or H_2MoO_4 may be attained by the addition of two monodentate ligands or one bidentate ligand. The complexes of molybdenum(VI) formed in an acid medium usually involve a *cis*-MoO_2^{2+} structure [10]. Flavon-3-ol-2′-sulfonic acid can coordinate to molybdenum(VI) as a bidentate ligand. Thus, the structure of the 1:1 chelate formed from $HMoO_3^+$ is likely to be *cis* (O,O)—$MoO_2(H_2O)_2(L)^+$.

Flavon-3-ol-2′-sulfonic acid reacts with tin(IV) in 0.3 M HCl [7], thorium-(IV) in 0.1 M HNO_3 [11] and thallium(III) at pH 3.3—4.3 [12] to yield a 1:1 chelate in each case. But 1:2 chelates were obtained for zirconium(IV) in 1.0 M $HClO_4$ [13], thorium(IV) at pH 6.0—7.0 [11] and thallium(III) at pH 6.0—7.6 [12]. Thus it may be suggested that flavon-3-ol-2′-sulfonic acid forms 1:1 chelates only in more acidic media.

The authors express their thanks to the Ministry of Education for financial support and to Miss K. Shikina for her assistance in this work.

REFERENCES

1 P. C. H. Mitchell, Q. Rev., 20 (1966) 103.
2 Y. Sasaki and L. G. Sillen, Ark. Kemi., 29 (1968) 253.
3 L. Krumenacker, Ann. Chim. (Paris), 7 (1972) 425.
4 J. F. Ojo, R. S. Taylor and A. G. Sykes, J. Chem. Soc. Dalton Trans., (1975) 500.

5 G. Goldstein, D. L. Manning and O. Menis, Anal. Chem., 30 (1958) 539.
6 A. Murata and F. Yamanouchi, Research Report of Technology, Shizuoka University, 9 (1958) 97.
7 Y. Oka, R. Tanaka and M. Umehara, Nippon Kagaku Zasshi, 83 (1962) 699.
8 J. Chojnacka, Rocz. Chem., 39 (1965) 161.
9 H. Diebler and R. E. Timms, J. Chem. Soc., (1971) 273.
10 K. H. Tytlo and O. Glemser, Adv. Inorg. Chem. Radiochem., 19 (1976) 239.
11 Y. Oka, K. Yamamoto and T. Aoki, Nippon Kagaku Zasshi, 85 (1964) 430.
12 K. Yamamoto and N. Takamizawa, Nippon Kagaku Zasshi, 88 (1967) 345.
13 Y. Oka and M. Yanai, Bunseki Kagaku, 13 (1964) 207.

More and more primary literature? Less and less time to read it?

take TrAC

trends in analytical chemistry

A monthly publication of short, critical reviews and news on trends and developments in analytical chemistry

How much better informed you could be if only you had the time to keep up with the latest developments.

Time we cannot give you, but we can give you concise, critical information on what is going on in the analytical sciences. Every month, as it happens.

It's all in TrAC – Trends in Analytical Chemistry – new for the 1980's from Elsevier and yours now at a low introductory rate.

Introductory Offer
SIXTEEN ISSUES FOR THE PRICE OF TWELVE!

Volume 1 – 1981/82 – of **Trends in Analytical Chemistry** will have sixteen issues: March 1981 and monthly from October 1981 to December 1982. Order the **Personal Edition** before December 1981 and receive all sixteen issues for US $42.50 (USA and Canada), £20.00 (UK), 91.50 Dutch guilders (Europe), 95.50 Dutch guilders (elsewhere). Or order the **Library Edition** for US $133.25 or 260.00 Dutch guilders throughout the world.

All issues of both editions are sent by air worldwide.

*) *The Dutch guilder price is definitive.*

Take just a minute to order either edition now – you will enjoy the time it saves you later.

ELSEVIER

TrAC is your opportunity to learn from researchers in related fields, to get first-hand, detailed reports on important developments in methodology and instrumentation. **TrAC** brings you current information on trends and techniques from laboratories all over the world.

Lab managers will find in **TrAC** evaluations of new methods and techniques which will enable them to make better-informed purchasing decisions. As a training aid **TrAC** is more up-to-date than any textbook.

TrAC is written in clear, jargon-free language, avoiding highly specialized terminology and provides you with a working knowledge of related methodology and techniques.

In every issue you will find:

- short critical reviews written for an interdisciplinary audience
- feature articles
- insights into the function, organization and operation of industrial, government or research laboratories
- news on topics of general interest
- teaching aids – TrAC is more up-to-date than any textbook
- articles on the history of analytical chemistry
- reports on meetings and book reviews

Trends in Analytical Chemistry comes in either the monthly **Personal Edition** or the special **Library Edition** which includes the monthly issues plus a hardbound volume containing all the review articles published over the year and indexed for easy retrieval.

Order Form

Special Introductory Offer for the Personal Edition valid until December 31, 1981

To **ELSEVIER Dept. TrAC. AB**
P.O. Box 330
1000 AH Amsterdam
The Netherlands

52 Vanderbilt Avenue
New York, NY 10017

US residents may call (212) 867-9040 and charge their American Express, Master Charge or Visa/Bankamericard account.

Yes! Please enter my subscription now – Volume 1 – 1981/82
☐ Personal Edition ☐ Library Edition
I enclose my ☐ personal cheque ☐ bankcheque

Orders from individual subscribers must be prepaid.

☐ Please send me a free sample copy first.

Name: _____ Position: _____ Date: _____

Address: _____

_____

City: _____ State: _____ Postal Code _____

Electron Capture – Theory and Practice in Chromatography

dited by A. ZLATKIS, *ouston, TX, USA and* F. POOLE, *Detroit, MI, SA*

OURNAL OF HROMATOGRAPHY BRARY – Volume 20

ept. 1981 xii + 418 pages
rice: US $76.50/
fl. 180.00
BN 0-444-41954-3

his book provides the first omprehensive coverage of l aspects of the theory, esign, operation and applica- ons of the electron capture tector (ECD) from the romatographer's point of ew. In addition, an up-to-date ok at the ancillary techniques selective electron-capture nsitization, atmospheric essure ionization and asma chromatography has en included. ECD users will d the solutions to instru- ental and technical oblems which arise during actice particularly valuable. hese have been derived from the experiences of the internationally distinguished team of authors.

Each chapter has been prepared by experts in their field and provides an in-depth coverage of its topic. The basic theory of the mechanisms of electron capture detection is included. Practical sections form the bulk of the book and are devoted to such topics as the construction and operating principles of the detector, including the establishment of instrument design criteria, and the different methods of derivatization. A more personal touch is provided by the inventor of the ECD, J.E. Lovelock, in his review of the development of the technique. Other chapters illustrate the importance of ECD in trace analysis in environmental and biomedical research. A unique feature is the extensive tabulation of all the pertinent data concerning the use of ECD in gas and liquid chromatography.

For those analytical chemists who use chromatography in their research, this book should become a standard text.

CONTENTS: Chapter 1. The electron-capture detector – A per sonal odyssey *(J.E. Lovelock).* 2. The design and operation of the electron-capture detector *(C.F. Poole and A. Zlatkis).* 3. Theory of electron capture *(W.E. Wentworth and E.C.M. Chen).* 4. Selective electron-capture sensitization *(F.C. Fehsenfeld, P.D. Goldan, M.P. Phillips and R.E. Sievers).* 5. Oxygen-doping of the carrier gas in electron-capture detection *(E.P. Grimsrud).* 6. Wide-range calibration of electron-capture detectors *(R.E. Kaiser and R.I. Rieder).* 7. Response of the electron-capture detector to compounds with natural electrophores *(J. Vessman).* 8. Sensitive derivatives for the determination of organic compounds by electron-capture gas chromatography *(C.F. Poole and A. Zlatkis).* 9. The detection of inorganic and organometallic compounds by electron-capture gas chromatography *(C.F. Poole and A. Zlatkis).* 10. Environmenta applications of the electron-capture detector – pesticides *(W.P. Cochrane and R.B. Maybury).* 11. Environmenta applications of the electron-capture detector – dioxins *(F. Bruner).* 12. The electron-capture detector as a monitor of halocarbons in the atmosphere *(P.G. Simmonds).* 13. Biomedical applications of the electron-capture detector *(J. Vessman).* 14. Negative ion atmospheric pressure ionization mass spectro metry and the electron-capture detector *(E.C. Horning, D.I. Carroll, I. Dzidic and R.N. Stillwell).* 15. Electron-capture process and ion mobility spectra in plasma chromatography *(F.W. Karasek and G.E. Spangler).* 16. The electron-capture detector as a detector in liquid chromatography *(U.A. Th. Brinkman).* Subject index.

ELSEVIER

P.O. Box 211, 1000 AE Amsterdam The Netherlands

52 Vanderbilt Ave. New York, N.Y. 10017

The Dutch guilder price is definitive. US $ prices are subject to exchange rate fluctuations.

CONTENTS